# HEAT AND MASS TRANSFER

A.V. Lykov and B.M. Smol'skii, Editors

## VOLUME I

# CONVECTIVE HEAT EXCHANGE IN A HOMOGENEOUS MEDIUM

TRANSLATED FROM RUSSIAN

Published for the National Aeronautics and Space Administration
and the National Science Foundation, Washington, D.C.
by the Israel Program for Scientific Translations

# HEAT AND MASS TRANSFER

(Teplo- i massoperenos)

A. V. Lykov and B. M. Smol'skii, Editors

VOLUME I

# CONVECTIVE HEAT EXCHANGE IN A HOMOGENEOUS MEDIUM

(Konvektivnyi teploobmen v odnorodnoi srede)

Volume edited by: B. S. Petukhov, I. P. Ginzburg, and A. S. Kasperovich

Nauka i Tekhnika
Minsk, 1965

Translated from Russian

Israel Program for Scientific Translations
Jerusalem 1967

NASA TT F-431
TT 67-51367

Published Pursuant to an Agreement with
THE NATIONAL AERONAUTICS AND SPACE ADMINISTRATION
and
THE NATIONAL SCIENCE FOUNDATION, WASHINGTON, D.C.


IPST Cat. No. 1842

Translated by A. Aladjem, M. Sc. (Chem. Eng., Mech. Eng.)
Edited by R. Kondor, Dipl. Ing.

Printed in Jerusalem by S. Monson
Binding: Wiener Bindery Ltd., Jerusalem

Available from the
U.S. DEPARTMENT OF COMMERCE
Clearinghouse for Federal Scientific and Technical Information
Springfield, Va. 22151

VIII/13/5

TABLE OF CONTENTS

This book comprises reports and communications dealing with the problems of convective heat transfer in a homogeneous medium, and with the heat and mass transfer during the interaction of bodies with liquid and gas streams. Most papers deal with studies based on the boundary layer theory. The papers include theoretical and experimental works on unsteady-state heat transfer, on heat transfer at variable physical properties of liquids and gases, and heat transfer during supersonic flows in dense and rarefied media.

Editors of this volume:
Professor B. S. Petukhov,
Professor I. P. Ginzburg,
Candidate of Tech. Sciences* A. S. Kasperovich

* [Equivalent to Ph. D.]

B.S. Petukhov

# CONVECTIVE HEAT TRANSFER IN A HOMOGENEOUS MEDIUM

The following main subjects may be singled out from the reports presented:

heat transfer and friction resistance under conditions of substantial changes in the physical properties of the liquid and the gas as a function of the temperature, with special emphasis on their flow in pipes;

heat transfer and resistance in systems of various geometrical shapes, mainly pipes and channels;

convective heat transfer under unsteady-state conditions;

hydrodynamics and heat transfer in jets;

intensification of convective heat transfer processes.

Many of the reports deal with the problems of heat transfer and friction resistance in the case of liquids and gases of variable physical properties. This includes reports on the heat transfer and resistance in turbulent gas streams at large temperature gradients, and in trickling fluid streams at large heat loads. Of great interest are reports on heat transfer in the supercritical region (parameters characterizing the state of the substances), both during forced turbulent flow in pipes and during free convection. In that region, the physical properties of the substances change very markedly and uniquely as a function of temperature and pressure. For this reason the supercritical region is especially interesting for the study of heat transfer at variable critical properties.

One of the reports presents the development of a theoretical method for the calculation of the boundary layer characteristics, the resistance and the heat transfer during turbulent flow of a compressible gas in the inlet sections of flat widening channels symmetrical to the axis, and with a zero pressure gradient. It would be of interest to compare the results of such a calculation with experimental results, and also to generalize this method of calculation for the case of a longitudinal pressure gradient.

In another report, a recently developed method is used as the basis for a theoretical calculation of the heat transfer and friction resistance in the case of carbon dioxide in the supercritical region. The results of the theoretical calculation (and the interpolation equation based on them) are in good agreement with experimental data. The above papers, as well as a number of other papers published in recent years, show the advantages of applying the semiempirical theory of turbulence in conjunction with appropriate computation methods to the solution of the complex problems of heat transfer during turbulent flow.

Nevertheless, the results of theoretical analyses of turbulent flows should not be regarded as reliable as those of laminar flow. This is not

only because the theory of turbulence is semiempirical, but also because the theory has been developed (and, to some extent, verified by experiment) only for the case of the simplest types of isothermal flow of noncompressible liquids. Nonetheless, it should be applied if there is a marked change in the physical properties of the fluid over the flow cross section, or if the gas compressibility has a marked effect, or if a chemical reaction occurs in the flow, or if other complex conditions exist. In such cases we usually resort to various hypotheses about the effect of the variable physical properties (the compressibility, etc.) on the turbulent transfer process. Thus, for example, it is assumed that turbulent transfer in the case of variable properties obeys the same rules as in the case of constant properties. The effect of variable physical properties on turbulent transfer is often allowed for by the introduction of some generalized independent variables, or by averaging the physical properties over the thickness of the laminar sublayer. Occasionally, the thickness of the laminar sublayer is taken as a function of the temperature factor, the Mach number, etc. A priori, none of those hypotheses could be substantiated. Often they lead to contradictory results. The validity or applicability of any of those hypotheses may be determined only by comparing the results of the theoretical calculations with experimental results. Of course, this reduces the value of the theoretical calculation, and makes it necessary to carry out complicated and expensive experiments. The study of the effect of variable physical properties (compressibility, etc.) on the characteristics of turbulent transfer should be regarded as an urgent problem.

The experimental data reported in one of the papers on heat transfer during the flow of gases in pipes show that in the case of heated mono-, di-, and triatomic gases, the heat transfer is inversely proportional to the square root of the temperature factor $\frac{T_w}{T_f}$. This conclusion is in agreement with the results of the theoretical analysis and of previously published experimental data. However, more recent papers show conclusively that the above relationship is valid only at $T_w/T_f \leqslant 2.5$. At $T_w/T_f > 2.5$ the temperature factor exerts a stronger influence. Moreover, the different influence of the temperature factor on local heat transfer at different points over the length of the pipe may be established as a fact.

The reports contain very interesting experimental data on the heat transfer in the supercritical region for carbon dioxide, water, and ethanol. The experiments extended over a wide range of pressures, temperatures, and heat loads. Empirical equations, generalizing a large amount of experimental data are proposed. However, of special interest are the experimentally observed physical phenomena that have not as yet received a satisfactory interpretation or a mathematical description. The first phenomenon is the rather sharp decrease in heat transfer and the corresponding increase in the wall temperature in the pipe sections in which the fluid temperature is lower, while the wall temperature is higher than the temperature corresponding to the maximum heat capacity. In that case, the wall temperature increases, reaches a maximum, and then decreases. The increase in the wall temperature at the maximum point reaches 100-200°C and becomes more pronounced as the heat load is increased and the pressure approaches the critical level. This is usually observed at moderate mass velocities of the liquid (in the case of water at $w_g < 1000\ \text{kg/m}^2 \cdot \text{sec}$) and at heat fluxes (on the walls) greater than a certain value (in the case of water at $q_e > 290 \cdot 10^3\ \text{w/m}^2$).

The deterioration in heat transfer is sometimes interpreted as resembling the heat transfer crisis in boiling, assuming that a kind of vapor film is formed in the pipe sections with a relatively poor heat transfer and high wall temperature. This approach is motivated by the natural desire to interpret this phenomenon by conventional concepts. It is, however, doubtful whether such an approach is useful.

There are reasons to believe that the deterioration of the heat transfer and the increase in wall temperature in certain sections of the pipe should be attributed to some specific changes in the physical properties of the fluid at a given specific combination of conditions. The above approach is supported by the fact that a deterioration of the heat transfer conditions, i.e., an increase in the wall temperature in some sections of the pipe is observed (though to a smaller extent) also at higher mass velocities of the fluid ($Re > 10^5$). These conditions, unlike those existing at low mass velocities, may be explained and described with the aid of the existing theory. Evidently, further advances in the theory are required before it can be used to describe the deteriorated conditions at low velocities. Such advances might require that pulsations in density and heat capacity, as well as some other effects not accounted for by the existing theory, be taken into account.

The second phenomenon observed during studies of the heat transfer in the supercritical range is known as "pseudoboiling." It was first observed by Goldman in experiments with water, and, as reported in one of the papers presented here, in experiments with ethanol. Pseudoboiling is observed at wall temperatures higher than the temperature corresponding to the maximum heat capacity and at fluid temperatures lower than this temperature. It occurs only at high heat flux densities and, correspondingly, at large Reynolds numbers (Re). In such cases a higher rate of the heat transfer is observed at certain sections of the pipe; at the same time the curve representing $t_w$ as a function of $q_w$ is of a shape such that when the heat flux is increased, the wall temperature changes negligibly (e. g., as in the case of nucleate boiling). Pseudoboiling is often accompanied by a strong whistling sound.

The mechanism of the process known as "pseudoboiling" is not completely clear. It appears that under the effect of turbulent pulsations in the velocity, the "cold" and "dense" liquid particles pass from the mainstream to the wall. On the "hot" wall, these particles are heated rapidly and expand explosively, forming low-density cavities in the layer adjacent to the wall. The growth and collapse of these cavities causes vigorous agitation of the layer adjacent to the walls and increases the heat transfer rate. Studies of the mechanism of the above phenomena and formulation of a quantitative theory for them are of great interest.

A number of reports deal with problems that, somewhat arbitrarily, may be described as studies of the flow and heat exchange in systems (mainly channels) of various geometrical shapes.

Other theoretical and experimental papers deal with heat exchange during laminar and turbulent flow in the inlet sections of pipes in the case of simultaneous development of the velocity and temperature profiles over the length; with heat exchange and liquid flow in curved channels, in particular as applied to the flow of fluids in gas turbines, between rotating cylinders, etc. Some new theoretical and experimental data on these subjects are reported.

Several reports contain new theoretical and experimental data on the heat exchange and hydraulic resistance during flow in pipes with an annular cross section and during longitudinal flow round pipe bundles. Even though the practical importance of the above problems is well known, until recently the problem of heat transfer during turbulent flow through annular pipes was not clear enough. There exist many empirical equations which yield markedly different results. A reliable basis for practical calculations was established only recently, as a result of studies that were carried out in the USSR and the U.S.A. This was achieved by an adequate combination of theoretical analyses of the problem with experiments carried out in accordance with a reliable procedure over a wide range of variations of the geometrical parameter. Most experimental studies of heat transfer in annular pipes have been carried out with gases. There is a marked lack of experimental data for liquid metals and especially for trickling fluids at Prandtl numbers higher than unity. The collection of such data would make it possible to reveal more clearly the effect of the channel geometry on the heat transfer at different Prandtl numbers. It is important to carry out exhaustive experimentation over a wide range of the geometrical parameter, in order to take into account the theory of the problem when setting up the experiment and processing the experimental results. The problem of heat transfer in annular pipes has been the subject of theoretical analyses in which a constant heat flux was assumed to exist on the walls. The study of this problem for other types of boundary conditions would certainly be of interest.

Although a number of papers have dealt with the problems of heat transfer and hydrodynamics in pipes with a rectangular cross section, pipe bundles with the fluid flowing along the bundle, and other similar systems, the results obtained so far are insufficient for the development of well-substantiated calculation methods. Here systematic studies must be carried out (both theoretical and experimental). At the same time it is very important that the experiments be carried out in such a way that the specific characteristics of the flow and heat transfer in such systems would be taken into account. For instance, it is very important that the changes in the heat transfer coefficient be studied not only over the length, but also on the perimeter of the pipe. It is necessary to carry out studies over a wide range of Prandtl numbers since a different influence of the geometry is observed at different Prandtl numbers.

The problem of convective heat transfer under unsteady-state conditions is one of the new problems insufficiently studied. A number of papers dealing with the above problem have been presented. Some of these papers consist of theoretical analyses of certain heat transfer problems during laminar flow in pipes or flow around the bodies, while others report the results of experimental studies of heat transfer and hydraulic resistance during turbulent flow in pipes.

As in the case of unsteady laminar flow, the study of unsteady heat transfer during laminar flow is a mathematical rather than physical problem. Definite calculation schemes have been derived and some approximate mathematical methods (e.g., the method of characteristics) have been used with success. Such methods have been used to solve a number of problems on the heat transfer in pipes, and during fluid flow around bodies. These results are familar both to Soviet and foreign literature.

Nevertheless, understanding of the problem of unsteady convective heat transfer during laminar flow falls far short of that, for example, of the theory of thermal conductivity. For instance, coupling problems have hardly been studied. Such problems involve a simultaneous investigation of the unsteady heat transfer between a solid surface and a fluid flow, and the unsteady thermal conductivity in the solid body. The solution of such problems is very complicated, and the difficulties have not yet been overcome.

Much more complex is the problem of unsteady heat transfer during turbulent flow. The possibilities of a theoretical analysis of the above problem are more limited, especially in the case of rapid processes. Indeed, if the time needed for a substantial change in the flow parameters is of the same order as the pulsation time of the velocity, temperature, and other variables, the possibility of using averaged motion and energy equations becomes doubtful or may even be out of the question. As a result, the semiempirical theory of turbulence cannot be used in the above case. Hence, experimental studies become of great importance in the study of unsteady convective heat transfer during turbulent flow. Only a few papers dealing with this problem have been published to date.

Some of the reports present results obtained in hydrodynamic and heat transfer studies in jets.* They contain data on free-stream jets, jets in an accessory flow, and jets propagating along the wall.

Experimental results on the turbulent transfer of the momentum and the heat in a free-stream jet are of great interest. On the basis of a large amount of experimental data, it is shown that the turbulence Prandtl number for such a jet is independent of the Reynolds number and the molecular Prandtl number over a wide range of values (from 0.02 to 300). Some interesting results have been obtained on the momentum and heat transfer in non-isothermic jets.

One of the central problems in the investigation of jets is the study of turbulent high-temperature jets of various types at large temperature gradients when chemical reactions occur in the jet (e. g. , dissociation, combustion), and when the heat transfer by radiation has a strong effect. Evidently, this concerns both subsonic and supersonic jet streams. Problems of this type are directly related to the problem of mixing of jets having different physicochemical properties, including those cases in which the media being mixed participate in chemical reactions, or when the mixing is accompanied by phase transformations. The study of these important problems is at present still in the initial stages, but that such a study is of great practical and scientific value is undoubted.

Many of the reports presented here deal with the intensification of convective heat transfer processes and are of great practical importance. They are directly concerned with the design of effective and at the same time rugged heat exchange equipment, leading to savings in the metal used for its construction.

As a rule, problems relating to heat transfer intensification are solved experimentally, since the flow and heat exchange in such systems are not subject to theoretical analysis. In many cases, an increase in the heat transfer rate is achieved as the result of an ordering of the flow with the detachment of the boundary layer from some of the surface elements. The

* The reports dealing with the above subject are included in Section 2.

eddies formed as a result of the above process are suppressed as they move along subsequent sections of the surface. The reports contain a large amount of experimental data on the heat transfer and hydraulic resistance on various types of finned heating surfaces, with a flow swirled by means of a trip wire or by pipes with a screw thread, on artificially roughed surfaces, etc.

A more thorough and detailed study of the flow and heat transfer in the eddying zones and the surface sections at which the eddies are suppressed would be of great value for the creation of more general methods for the calculation of such heat exchange systems.

It is desirable that the studies on the intensification of heat transfer problems be carried out directly by the design companies and plant laboratories, or in close collaboration with the design engineers. Only then could such studies be of real value and contribute to the design of highly effective heat exchange systems.

# *1. HEAT EXCHANGE AND FRICTION RESISTANCE DURING SUBSTANTIAL CHANGES IN THE PHYSICAL PROPERTIES OF LIQUIDS AND GASES AS A FUNCTION OF TEMPERATURE AND PRESSURE*

A. A. Gukhman, A. F. Gandel'sman, V. V. Usanov, and G. N. Shorin

## NEW DATA ON THE PROPERTIES OF TRANS-SONIC FLOWS

It has been firmly established /1-6/ that in the immediate vicinity of the speed of sound a degeneration of the turbulence occurs under certain conditions, in which cases the hydrodynamic theory of heat transfer cannot be used in its conventional form. The main factor affecting these phenomena is the effect of large negative pressure gradients.

The experimental procedure used by us in the study of the heat and momentum transfer in the region of disturbance of the Reynolds analogy /5/ was based on independent plotting of the curves showing the variations in the static pressure and the heat flux density over the length of the channel. The measurement technique developed by us made it possible to obtain values of the heat flux density (by sectional withdrawal of the condensate) and the static pressure (by means of an axial probe) at sufficiently small distances over the length. A high degree of accuracy may be achieved by the above method; the error in the measurement of the heat flux density is ±1% and of the static pressure ±1.5%. The possibility of establishing a virtually continuous distribution pattern of the primary parameters with a sufficient degree of accuracy is of decisive importance for the whole experiment (see table).

The above procedure is used to determine the local values of the hydraulic resistance coefficient $\zeta$ and its computation analog $\zeta_p \equiv 8\,\mathrm{St}$. The ratio $\varphi = \frac{\zeta}{\zeta_p}$ serves as a quantitative measure of the disturbance of the Reynolds analogy. A characteristic curve showing the distribution of $\varphi$ over the length of the channel (and, correspondingly, over $M$) is shown in Figure 1, which contains also the corresponding values of $\frac{T_w}{T_0}$. The curves representing the variations in $\zeta$ and $\zeta_p$ are shown in the lower section of the figure. At velocities substantially different from the speed of sound, the variations in $\zeta$ and $\zeta_p$ are roughly similar, but at trans-sonic velocities the shapes of the curves differ sharply; $\zeta$ decreases rapidly while $\zeta_p$ increases rapidly. These shapes of the curves are reflected in the curve representing the variation in $\varphi$. The disturbance of the Reynolds analogy in the trans-sonic region is clearly evident.

Curves representing the heat flux distribution over the length at different Reynolds numbers are shown in Figure 2. The resulting curves can be divided into two groups.

At fairly large values of the Reynolds number, $q_w$ is a monotonously decreasing function of the velocity, which is natural for the turbulent

boundary layer. At the same time, the sharp decrease in $q_w$ in the vicinity of the throat becomes gradually less pronounced with the transition from the throat to the nozzle edge.

Values of the parameters which control the conditions

| Conditions | $T_{00}$, °K | $p \cdot 10^{-5}$ n/m$^2$ | $G$, kg/sec | $Re_{T_0} \cdot 10^{-3}$ |
|---|---|---|---|---|
| I | 547.0 — 548.5 | 5.097 — 5.133 | 0.526 — 0.528 | 7.54 |
| II | 629.5 — 630.5 | 5.248 — 5.270 | 0.503 — 0.505 | 7.35 |
| III | 698.5 — 699.0 | 5.214 — 5.242 | 0.476 — 0.478 | 6.50 |
| V | 627.5 | 2.138 | 0.205 | 3.00 |
| VI | 687.6 | 1.707 | 0.157 | 2.15 |
| IX | 438.6 | 1.164 | 0.113 | 2.50 |

The decrease in the Reynolds number leads to a decrease in $q_w$ in the throat and to the appearance of a section in which the upward slope of the curve representing $q_w$ increases as the velocity is increased. Naturally, all those specific features in the shape of the curves are maintained (and even enhanced to a certain extent) in the transition to the heat transfer rate distribution over the length $St = St(x)$. The experimental data do not disagree with earlier results. They reveal some new characteristics of the heat transfer during trans-sonic flow, since the earlier and the more recent data supplement one another. We believe that a physical model describing the observed phenomena could be constructed.

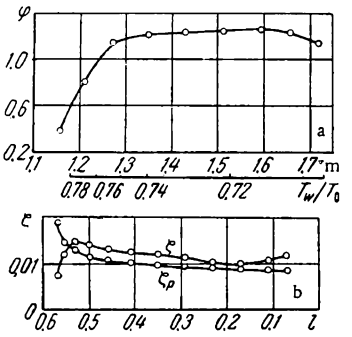


FIGURE 1. Distribution of $\varphi$, $\zeta$, and $\zeta_\rho$ (set of conditions II /5/).

At large Reynolds numbers the boundary layer formed at subsonic flow velocities is a turbulent one. Hence, the profile rearrangement (its elongation) observed as the speed of sound is approached should be accompanied by an increase in the dissipation, i. e., by an effect which is in contradiction to the experimental data. Hence, the profile rearrangement (and the accompanying increase in the heat transfer rate) is associated with a degeneration of the turbulence. Correspondingly, the region of most pronounced increase in the heat transfer rate shifts downward with the flow, in the direction of higher velocities. Subsequently, the rate decreases because of the growth of the boundary layer. At low Reynolds numbers the flow in the boundary layer is laminar; hence, the elongation of the profile (and all associated phenomena) should be observed earlier. The supersonic range comprises a set of conditions resembling conventional laminar flow (which is characterized by relatively low heat transfer rates), with a substantial increase of the heat transfer rate as a result of subsequent formation of turbulence.

The above results were obtained on the basis of a one-dimensional model. Nevertheless, despite the arbitrary nature of such a calculation, it has value at least for a qualitative evaluation. However, the amount of data available to us is not sufficient to allow determination of the flow conditions in the

boundary layer. Hence, two variants of the calculation shall be used, assuming that the flow is at first laminary and then turbulent. The calculation for the laminar flow was carried out by the method described in /7/; in our case, the use of the above method is more justified than the use of any other known approximate method. The calculations for the turbulent flow were carried out by the method of Kalikhman /8/, assuming the flow to be turbulent over the whole length of the channel. The calculated and experimental results are shown in Figure 3. It is evident that the results calculated by assuming a laminar flow contradict the experimental data (even the order of magnitude differs). On the other hand, the results calculated by assuming a turbulent flow are in much better agreement with the experimental data. Naturally, this does not mean that the flow is turbulent over the whole length of the channel, including the throat. The agreement between the experimental and calculated curves may be regarded as an indication of the turbulent nature of the flow in the boundary layer only for a channel section at a sufficient distance from the throat, where the arbitrary nature of the calculations is not of great importance. This is supported also by the shape of the velocity profile obtained by us in the vicinity of the nozzle edge.

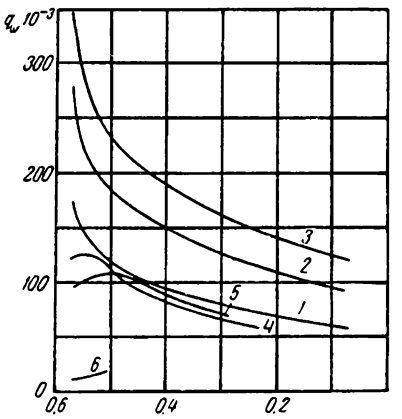


FIGURE 2. Distribution of the specific heat fluxes $q_w \left(\frac{w}{m^2}\right)$ over the length of the nozzle. 1, 2, 3, 4, 5, 6 — sets of conditions I, II, III, V, VI, and IX, respectively.

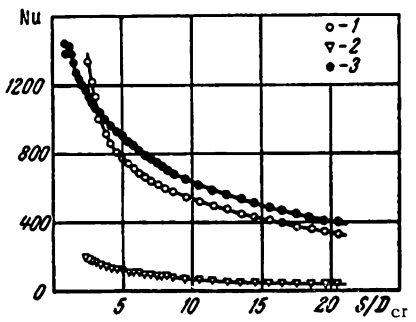


FIGURE 3. Comparison of calculated results for the heat transfer in the supersonic section of the nozzle with experimental data.

1 — set of conditions I (according to /5/); 2 — calculated according to /7/; 3 — calculated according to /8/.

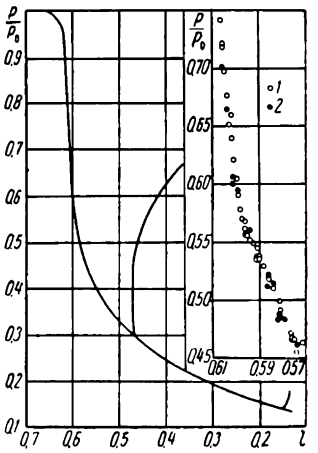


FIGURE 4. Distribution of the values of $\frac{p}{p_0}$ over the nozzle length in adiabatic experiments.

1 — $Re_{T_0} = 1.8 \cdot 10^5$; 2 — $Re_{T_0}$ ranging from $2.25 \cdot 10^5$ to $16 \cdot 10^6$.

In view of the particular effect of pressure gradients on the formation of the boundary layer, let us discuss in more detail the $\frac{p}{p_0}$ distribution curve for the trans-sonic flow velocity range (Figure 4). On the section (of the curve) corresponding to the nozzle throat, the maximum pressure gradients are not in the critical cross section but in the contraction, immediately before the cylindrical belt, and their values remain large (greater than anywhere else) over a relatively great length. The pressure gradient decreases afterward. In our case, the pressure gradient decreases by a factor of 9 over a short cylindrical section of the channel lying above the throat. In the diffuser section, directly beyond the throat, the pressure gradient again increases by a factor of about 2.5, i. e., the pressure gradient there remains lower (by a factor of about 3.5) than its maximum value in the contraction. The numerical values of the dimensionless gradients are 0.607, 0.069 and 0.157.

Symbols

$T_{00}$ — impact temperature at the entry to the experimental nozzle; $p$ — static pressure; $p_0$ — pressure at the inlet to the experimental nozzle; $q_w$ — heat flux density; $Re_{T_0}$ — Reynolds number; St — Stanton number; $\zeta$ — hydrodynamic resistance coefficient.

Bibliography


1. Gandel'sman, A.F., A.A. Gukhman, N.V. Ilyukhin, and L.N. Naurits. — ZhTF, No. 12. 1954.
2. Gukhman, A.A , A.F. Gandel'sman, and L.N. Naurits. — Energomashinostroenie, No. 7. 1957.
3. Gukhman, A.A. International Journal of Heat and Mass Transfer, — Vol. V. 1962.
4. Sergienko, A.A. and V.K. Gretsov. — DAN SSSR, Vol. 125, No. 4. 1959.
5. Gukhman, A.A., A.F. Gandel'sman, L.N. Naurits, and V.V. Usanov. — IFZh, No. 6. 1963.
6. Deich, M.E. and L.Ya. Lazarev.- IFZh, No. 4. 1964.
7. Avduevskii, V.S. and R.M. Kopyatkevich. — Izv. AN SSSR, OTN: Mekhanika i Mashinostroenie, No. 1. 1960.
8. Kalikhman, L.E. Turbulentnyi pogranichnyi sloi na krivolineinoi poverkhnosti, obtekaemoi gazom (The Turbulent Boundary Layer on a Curved Surface in a Gas Flow). — Oborongiz. 1956.
9. Leont'ev, A.A. and V.K. Fedorov. — IFZh, No. 8. 1961.



The Institute of Chemical Equipment Design, Moscow

V. L. Lel'chuk, G. I. Elfimov, and
Yu. P. Fedotov

# EXPERIMENTAL STUDY OF THE HEAT TRANSFER FROM PIPE WALLS TO MONO-, DI-, AND TRIATOMIC GASES AT LARGE TEMPERATURE GRADIENTS

The calculation of heat transfer from the wall to the gas in boosted-performance heat exchange equipment (in which the material temperature is close to the maximum permissible temperature) requires the use of reliable and fairly accurate equations. It is a known fact that the calculations are complicated by large temperature gradients existing in the equipment, and hence the effect of the changes in the physical properties of the heat transfer medium on the heat exchange must be taken into account.

Experimental studies of the heat transfer from the walls to a turbulent gas flow inside a tubular pipe with wall temperatures of up to 1400°K have been carried out during recent years at the All Union Institute of Thermal Technology.

One of the studies /1/ was concerned with heat transfer to the air in a heated pipe 18 mm in diameter, having an $L/D$ ratio of 140, when the gas at the inlet was at room temperature and the maximum value of $M$ at the exit was 0.6.

Subsequent studies were carried out with air in three pipes 12.25 mm in diameter, having $L/D$ ratios of 206, 150, and 77 at various air temperatures at the inlet (from room temperature to 870°K) and at values (of the flow) up to 1; in this study certain improvements were introduced into the experimental and computation procedures.

Since the effect of temperature on the thermal properties of different gases is not the same, analogous experiments were carried out with carbon dioxide and argon, which are used in technology as heat carriers.

The experiments with air were carried out in open systems and the medium was discharged into the atmosphere, while the experiments with the other gases were carried out in a closed system. After leaving the compressor, the gas passed successively through large-volume receivers, an apparatus for the removal of oil and moisture from the gas, a flow-rate measuring diaphragm, an electric furnace (preheater), the experimental section, and was then either discarded or passed through a condenser and returned to the compressor. In all cases, the experimental section was made of stainless steel (1Kh18N9T) while the pipes were connected to a DC motor (AND-30 or PSM-1000) in series with a standard resistance which served to measure the current.

Fundamentally, the experimental sections resembled in their construction the section described in /1/. However, the following improvements were

made: heat flow from the pipe to the inlet chamber was prevented by shielding the furnace; a short section of a pipe of about the same diameter, heated by an electric current, was welded between the experimental pipe and the inlet chamber in order to reduce the temperature "fall" at the end of the experimental pipe; all measurements were made to the end of the pipe, where a conical widening was made to mark the critical section.

The distribution of electrical potentials, wall temperature, and the pressures of the gases was measured over the length of the pipe. The gas temperature in the mixing chambers was also measured at the inlet and outlet.

In contrast to /1/, in our subsequent studies the thermocouples fitted to the pipe walls were calibrated in situ, and in calculating the temperature on the basis of the thermocouple readings, we took into account the temperature drop in the mica spacer between the junction and the wall.

In order to reduce the heat losses to a minimum, the experimental section was insulated thoroughly. The losses (which for a constant insulation thickness and a constant temperature of the surroundings depend solely on the wall temperature) were taken into account on the basis of special calibration experiments in which an electrical current was passed through the pipe without a gas flow inside it. In most experiments the overall heat losses through the insulation amounted to 1-3% of the heat supplied by the electric current, and only in 1/8 of the experiments were the losses substantial, reaching up to 10%.

All measurements (with a reliable correction for the heat losses, which were rather small) were used to calculate (for the various sections over the pipe length) the local values of the specific heat flux to the gas, the thermodynamic and impact temperatures of the gas, the velocity of the gas, the heat transfer coefficients, and the similarity criteria. The gas flow parameters were calculated on the basis of the one-dimensional theory, taking into account the variable heat capacity. The local heat transfer coefficients were calculated as the ratio of the specific heat flux to the difference between the actual and equilibrium wall temperatures. In the inlet sections of the pipes, where the change in the wall temperature over the length was nonlinear, we took into account the flow of heat along the walls.

The specific heat fluxes increased over the length of the pipe, because of the changes in its electrical resistivity. Depending on the temperature drop over the length of the pipe, the specific heat flux increased by 3-35%.

A comparison of the amount of heat taken up by the gas in the whole experimental section with the total amount of electrical energy supplied to the system (minus the heat losses) showed that the discrepancies in the thermal balance rarely exceeded 2%.

A brief description of our experiments is given in the table.

The experimental data were generalized on the basis of the dimensionless equation

$$\mathrm{Nu} = f\left(\mathrm{Re};\ \mathrm{Pr};\ \frac{T}{T_w};\ M;\ \frac{x}{d}\right),$$

where $M$ is the ratio of the stream velocity to the local speed of sound.

The calculations were carried out for various sections over the length, most often for the inlet sections and more rarely for the sections with a stabilized heat transfer.

Summary of the experiments

| Serial No. | Inlet temperature, °K | Reynolds number at the inlet, $Re_i \cdot 10^{-3}$ | Number of experiments | Gas | Pipe diameter, $d \cdot 10^3$, m | Relative pipe length, $L/D$ | Maximum wall temperature, °K | Temperature factor, $\frac{T_s}{w}$ | Calculated sections at $x/d > 50$ |
|---|---|---|---|---|---|---|---|---|---|
| 1 | 300 | 75.0 — 481.0 | 37 | air | 12.25 | 206 | 1270 | 0.48 — 0.860 | from $x/d$ = 53 to $x/d$ = 195, 11 sections in all |
| 2 | 470 | 53.8 — 298.0 | 26 | " | | | | | |
| 3 | 670 | 42.6 — 204.0 | 16 | " | | | | | |
| 4 | 870 | 37.2 — 150.0 | 10 | " | | | | | |
| 5 | 300 | 98.1 — 626.0 | 28 | " | | 151 | 1270 | 0.44 — 0.970 | from $x/d$ = 53 to |
| 6 | 470 | 76.5 — 278.0 | 11 | " | 12.25 | | | | $x/d$ = 139, 7 sections |
| 7 | 670 | 57.4 — 206.5 | 8 | " | | | | | in all |
| 8 | 870 | 49.4 — 150.4 | 13 | " | | | | | |
| 9 | 300 | 107.6 — 684.0 | 22 | " | | 77 | 1270 | 0.39 — 0.950 | from $x/d$ = 53 to |
| 10 | 470 | 78.4 — 332.4 | 10 | " | 12.25 | | | | $x/d$ = 69.4, 3 sections |
| 11 | 670 | 63.2 — 230.6 | 9 | " | | | | | in all |
| 12 | 870 | 55.7 — 152.6 | 6 | " | | | | | |
| 13 | 300 | 39.2 — 403.0 | 8 | " | 11.39 | 105 | 670 | 0.55 — 0.804 | $x/d$ = 59.3 and 85.6 |
| 14 | 300 | 21.0 — 607.5 | 26 | $CO_2$ | 11.39 | 105 | 1070 | 0.47 — 0.922 | " |
| 15 | 470 | 14.0 — 311.0 | 20 | $CO_2$ | 11.39 | 105 | 1070 | 0.47 — 0.922 | " |
| 16 | 300 | 39.0 — 418.2 | 36 | argon | 11.39 | 105 | 1270 | 0.37 — 0.890 | " |

In our experiments the variations in the Prandtl number (Pr) were insignificant, and we assumed that Nu is proportional to $Pr^{0.4}$. At constant $\frac{x}{d}$ values, the Reynolds number had the most pronounced effect on the heat transfer.

A plot of log $\frac{Nu}{Pr^{0.4}}$ against log Re (plotted for each section used for the calculations) makes it possible to determine the above function with a fair degree of accuracy, in spite of a certain dispersion due to the effect of other dimensionless numbers. It was found that for all sections used in the calculations (at least for those where $\frac{x}{d} > 10$) a value of $Nu/Pr^{0.4} \sim Re^{0.8}$ may be taken for all gases in the calculation of the physical properties, including the density in terms of those dimensionless numbers both on the basis of the stream temperature ($Nu_s$, $Pr_s$, $Re_s$) and on the basis of the wall temperature ($Nu_w$, $Pr_w$, $Re_w$).*

* The physical properties of air and carbon dioxide were calculated according to /4/, and those of argon according to /5/.

The effect of the temperature factor $T_s/T$ and of $M$ were determined for the above two variants for the calculation of similarity criteria.

A plot of $Nu_w/Pr_w^{0.4}Re_w^{0.8}$ against $\frac{x}{d}$ showed that in the inlet section the experimental data are clearly stratified depending on maximum wall temperature or, in other words, on the magnitude of the temperature factor $T_s/T_w$, and that $\frac{Nu_w}{Pr_w^{0.4}Re_w^{0.8}}$ decreases when the temperature factor is increased. The extent of the above stratification, as well as the overall dispersion of the experimental points, decreased with increasing $\frac{x}{d}$. At $\frac{x}{d} > 50$ the influence of the temperature factor on the stratification was negligible and the overall dispersion of experimental points for each gas was ±(4-6)%.

When the similarity criteria are calculated on the basis of the gas temperature the changes in $\frac{Nu_s}{Pr_s^{0.4}Re_s^{0.8}}$ as a function of $\frac{x}{d}$ are, in general, qualitatively the same as in the calculations based on $T_w$. However, in contrast to the previous calculation, the stratification as a function of the temperature factor increases with increasing $\frac{x}{d}$ and is the greatest at the section of stabilized heat transfer. At $1 < \frac{x}{d} < 10$ the deviation of all experimental points from a mean value does not exceed 6-7% (regardless of the temperature factor), while at $\frac{x}{d} > 30$ the deviations are as high as ±(20-30)%.

When the data were processed on the basis of the stream temperature, we found that the best agreement between the experiments is obtained when, in addition to the temperature factor, the compressibility of the stream is also taken into account. It is known from experiments on the heat transfer from the gas to the pipe at supersonic flow velocities /3/, that when the similarity criteria are calculated on the basis of the stream temperature we have $\frac{Nu_s}{Pr_s^{0.4}Re_s^{0.8}} \sim \left(1 + \frac{\varkappa - 1}{2} M^2\right)^{-0.5}$. No experimental data are available on the effect of the compressibility during the heat transfer from the wall to the gas. Hence, in order to take into account the effect of the compressibility we used (as in /3/) a correction factor

$$\left(1 + \frac{\varkappa - 1}{2} M^2\right)^{-0.5} = \left(\frac{T_0}{T_s}\right)^{-0.5},$$

where $T_0$ is the impact temperature.

Channels of a large relative length, for which the effect of the inlet section is small, are commonly used in heat exchangers for power application. At the same time, the highest wall temperatures exist at a distance from the inlet at the section of stabilized heat transfer. Hence, in this paper we deal only with the experimental results obtained at $\frac{x}{d} > 50$.

All our experimental data on the calculated sections, shown in the table, for all gases studied at various inlet temperatures, are shown in Figure 1

as a plot of $\lg \frac{Nu_w}{Pr_w^{0.4}}$ versus lg Re. In the last calculated sections in which heat losses occurred and there was a sharp change in the wall temperature, the dispersion of experimental data was 3-5% greater than in other sections in the stabilized heat transfer region; those sections are not shown in the figure. The dot-and-dash line represents the equation

$$\frac{Nu_w}{Pr_w^{0.4}} = 0.021\ Re_w^{0.8},$$

while the boundary dashed lines indicate a 10% deviation from the values plotted on the dot-and-dash line. It is evident that most of the experimental points lie within the limits of the above deviation range.

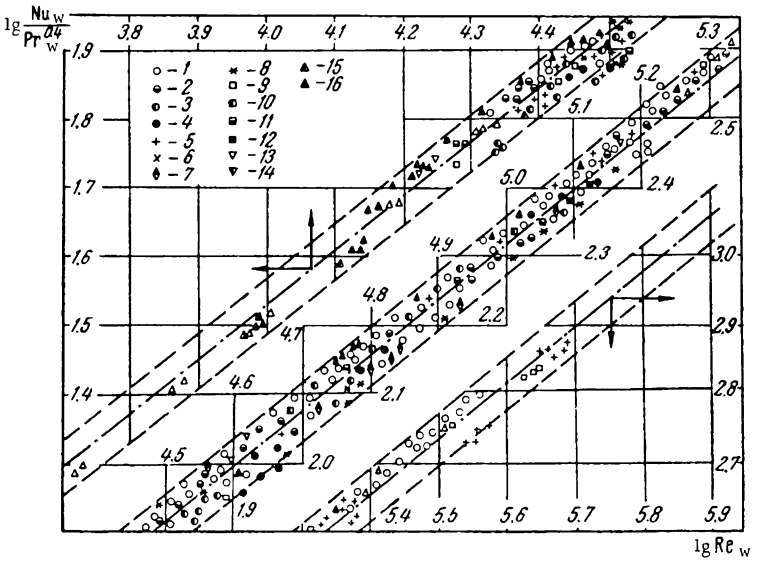


FIGURE 1. Experimental data on the heat transfer from the pipe walls to argon, air, and carbon dioxide at the section of stabilized heat transfer. The notation is the same as in the table.

An excellent agreement was obtained when the experimental data were compared with the experimental data of /1/ processed by our method.

Thus, in the investigated range of $Re_i$ values (calculated on the basis of the gas temperature at the inlet) between $14 \cdot 10^3$ and $684 \cdot 10^3$, of $T_s$ $T_w$ (temperature factor) values between 0.37 and 0.97, of $M$ values up to 0.95, and inlet temperatures from 300 to 870°K, the use of the following general equation may be recommended for all investigated gases:

$$Nu_w = 0.021\ Re_w^{0.8} Pr_w^{0.4} \pm 10\% \qquad (1)$$

Here,

$$Nu_w = \frac{\alpha d}{\lambda_w}.$$

$$Re_w = \frac{\rho_w W d}{\mu_w} = \frac{Gd}{F\mu_w}\ \frac{T_s}{T_w}$$

(the parameters with the subscript "w" are calculated on the basis of the wall temperature while those with the subscript "s" are calculated on the basis of the stream temperature).

However, Figure 1 shows that a certain stratification of the experimental points is observed, depending on the nature of the gas and its temperature at the inlet $T_i$. By plotting similar graphs for each of the gases, for a constant inlet temperature, we found the following equations:

for argon at

$$T_i \simeq 300^\circ K,\ Nu_w = 0.0224 Re_w^{0.8} Pr_w^{0.4} \pm 3\%;$$

for air at

$$T_i = 300^\circ K,\ Nu_w = 0.0214 Re_w^{0.8} Pr_w^{0.4} \pm 6\%;$$
$$T_i = 470^\circ K,\ Nu_w = 0.0209 Re_w^{0.8} Pr_w^{0.4} \pm 6\%;$$
$$T_i = 670^\circ K,\ Nu_w = 0.0199 Re_w^{0.8} Pr_w^{0.4} \pm 6\%;$$
$$T_i = 870^\circ K,\ Nu_w = 0.0188 Re_w^{0.8} Pr_w^{0.4} \pm 10\%;$$

for carbon dioxide at

$$T_i = 300^\circ K,\ Nu_w = 0.0211 Re_w^{0.8} Pr_w^{0.4} \pm 6\%;$$
$$T_i = 470^\circ K,\ Nu_w = 0.0206 Re_w^{0.8} Pr_w^{0.4} \pm 3\%.$$

The above equations show the maximum deviations expressed as percentages. At a gas temperature inlet of 870°K, the temperature gradients were small and the dispersion of the points was naturally greater.

Kutateladze /6/ derived a theoretical equation for the calculation of the heat transfer at large temperature gradients, approximately represented by the equation

$$\frac{Nu_s}{Nu_0} = \left(\frac{2}{\sqrt{T_w/T_s} + 1}\right), \qquad (2)$$

where $Nu_0$ and $Nu_s$ are the Nusselt numbers calculated on the basis of the stream temperature, for constant and variable physical properties respectively.

Petukhov and Popov /7/ derived a theoretical equation for the calculation of the heat transfer from the pipe walls to the gas in the region of stabilized heat transfer at small flow velocities and large temperature

gradients. The equation recommended by them is

$$\frac{Nu_s}{Nu_0} = \left(\frac{T_w}{T_s}\right)^{-0,5}, \tag{3}$$

in which $Nu_0$ is calculated from the equation

$$Nu_0 = \frac{\xi/8\, Re\, Pr}{k_1 + k_2 \sqrt{\xi/8}\,(Pr^{2/3} - 1)}, \tag{4}$$

where $k_1 = 1 + 3.4\,\xi$; $k_2 = 11.7 + \frac{1.8}{Pr^{1/3}}$; $\xi$ is the hydraulic resistance coefficient.

In order to compare the recommendations of /6/ and /7/ with the paper of Deissler /8/*, we calculated the values of

$$\frac{Nu_0}{Nu_s\left(1 + \frac{\varkappa - 1}{2} M^2\right)^{-0.5}}$$

from the experimental data for argon and air at $T_i \simeq 300°K$, for 3 sections at $\frac{x}{d} > 50$ (the compressibility must be taken into account in calculations based on the stream temperature).

As is evident from Figure 2,a, when $Nu_0$ is calculated by means of equation (4), the experimental data lie beneath the lines representing the equations from /6/ and /7/; the deviation from the calculated values is about 7% on the average, and in addition, when $\frac{T_w}{T_s} = 1$ we have $\frac{Nu_0}{Nu_s} < 1$.

Figure 2,b contains the same experimental results, but $Nu_0$ has been calculated by means of an equation derived by Mikheev

$$Nu_0 = 0.021\ Re^{0.8} Pr^{0.4}. \tag{5}$$

A comparison of Figures 2,a and 2,b leads to the conclusion that the theories of /6/ and /7/ represent with a fair degree of accuracy the dependence of $\frac{Nu_0}{Nu_s}$ on the temperature factor, while equation (4) should not be used to calculate $Nu_0$ in the investigated range.

Thus, the following equation is suitable for calculations of the similarity criteria on the basis of the stream temperature:

$$Nu_s = 0.021\ Re_s^{0.8} Pr_s^{0.4}\left(1 + \frac{\varkappa - 1}{2} M^2\right)^{-0.5}\left(\frac{T_w}{T_s}\right)^{-0.5} \tag{6}$$

* The Deissler graph was taken from /7/.

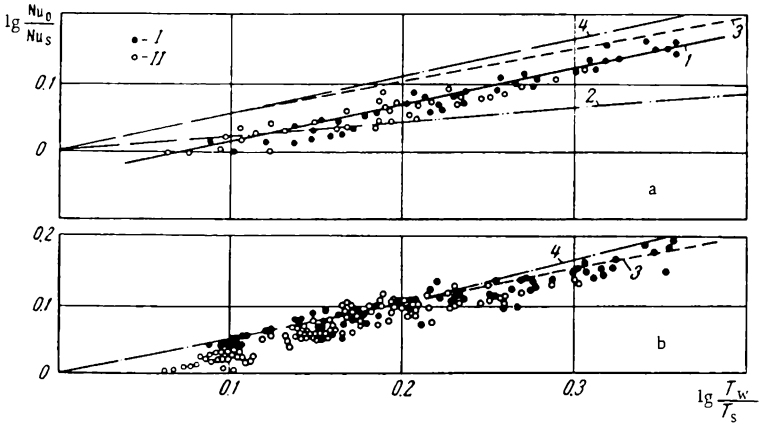


FIGURE 2. Comparison of our experimental data on the heat transfer to argon and air with theoretical equations /6-8/ for the calculation of $Nu_0$:

a — by equation (4); b — by equation (5); I — experiments with argon; II — with air ($x/d$ = 53.0; 118; 183); 1 — experimental data; 2 — /8/; 3 — /7/; 4 — /6/.

or, since

$$\left(1 + \frac{\varkappa - 1}{2} M^2\right) = \frac{T_0}{T_s},$$

we have

$$Nu_s = 0.021\ Re_s^{0.8}\ Pr_s^{0.4}\ \frac{T_s}{\sqrt{T_0 T_w}}. \qquad (7)$$

Bibliography

1. Lel'chuk, V.L. and B.V. Dyadyakin. — In sbornik: Voprosy teploobmena, Izd. AN SSSR. 1959; Teploenergetika, No. 9. 1958.
2. Lel'chuk, V.L. and G.I. Elfimov. — IFZh, No. 12. 1963.
3. Voronin, F.S. and V.L. Lel'chuk. — Teploenergetika, No. 4. 1963.
4. Vargaftik, N.B. prof., editor. Spravochnik Teplofizicheskie svoistva veshchestv (Handbook of the Thermal-Physical Properties of Substances). — Gosenergoizdat. 1956.
5. Tables of Thermal Properties of Gases. — U.S. Department of Commerce National Bureau of Standards, Circular 564.
6. Kutateladze, S.S. Osnovy teorii teploobmena (Principles of the Theory of Heat Transfer). — Mashgiz. 1962.
7. Petukhov, B.S. and V.N. Popov. — Teplofizika vysokikh temperatur, No. 1. 1963.
8. Deissler, R. — International Developments in Heat Transfer, Part III; International Heat Transfer Conference, Colorado, U.S.A. 1961.

The All-Union Institute of Thermodynamics im. F.E. Dzerzhinskii

L. S. Sterman and V. V. Petukhov

# INVESTIGATION OF THE HEAT TRANSFER TO ORGANIC LIQUIDS

When no changes in the state of aggregation occur, the heat transfer coefficients to organic liquids usually have relatively small values, and consequently large temperature gradients between the walls and the liquid are created at heat fluxes of any substantial magnitude. The physical properties of the liquid in the layer adjacent to the wall change markedly, and the heat transfer coefficients cannot be determined without taking these changes into account.

Investigations of the heat transfer to organic liquids with properties varying over the stream cross section have been carried out /2-7/. When the temperature is changed, the most pronounced change occurs in the viscosity of the liquids, and for this reason, several investigators have determined the effect of these changes. For instance, Sider and Teit /6/ have proposed the following equation for the calculation of the heat transfer to a liquid of variable properties:

$$Nu = 0.027\ Re^{0.8}\ Pr^{1/3} \left(\frac{\mu_f}{\mu_w}\right)^n, \qquad (1)$$

where the power index $n$ has a value of 0.14 for a liquid during its heating.

Studies on heat transfer to diphenyl, Santowax *R* and Santowax *OM* carried out by Silberberg and Huber /7/ revealed that at Reynolds numbers from 20,000 to 300,000 the use of equation (1) leads to substantial discrepancies between the experimental and calculated data. At low Re's the experimental values are lower than the calculated (by as much as $\sim 15\%$) while at high Re's the experimental values are somewhat higher (by $\sim 7\%$) than the calculated, i. e., the dependence of Nu on Re differs from that shown in equation (1). In order to eliminate this discrepancy, the following equation has been proposed /7/:

$$Nu = 0.015\ Re^{0.85}\ Pr^{0.27}. \qquad (2)$$

Equation (2) generalizes the existing experimental data with an accuracy of $\pm 7.9\%$.

An attempt to take into account not only the variable viscosity but also the changes in other physical constants has been made /4/, and the equation proposed is

$$Nu = 0.021\ Re^{0.8}\ Pr^{0.43} \left(\frac{Pr_f}{Pr_w}\right)^{0.25}. \qquad (3)$$

Investigations of the heat transfer to ditolylmethane (an organic liquid with properties resembling those of Dowtherm and diphenyl), which were carried out by Chechetkin and Kosterev /5/, and to glycerol by Kosterin and Magomedov /2/ revealed that in the Re range from $10^4$ to $10^5$, the experimental data fit fairly well into equation (3). However, as mentioned in /4/, equation (3) is more suitable for the case of cooling. In the opinion of the authors, the exponent of $Pr_f/Pr_w$ in the case of heating should be lower than in equation (3). The following equation for the calculation of the heat transfer in the case of a liquid of variable properties has been proposed in /4/:

$$Nu = \frac{0.125\,\xi\,Re\,Pr}{4.5\sqrt{\xi}\,(Pr^{2/3}-1.0)+1.01}\left(\frac{\mu_f}{\mu_w}\right)^n, \qquad (4)$$

where the values of the exponent $n$ are 0.11 for heating and 0.25 for cooling.

In /4/ the value of $\xi$ was calculated from the equation

$$\frac{1}{\sqrt{\xi}} = 1.82\lg Re - 1.64. \qquad (5)$$

Calculations based on the above equations often lead to markedly different values of Nu. In recent years diphenyl, monoisopropyldiphenyl (MIPD) and some other organic liquids with high boiling points have been used as heat exchange agents on an increasing scale. We have found that substantial differences exist between the values of the heat transfer coefficients to those liquids, calculated by means of equations (1) to (5), at large temperature gradients.

For this reason, the heat transfer coefficients to MIPD were determined experimentally, and the experimental results were compared with results calculated with the aid of the various equations; this made it possible to establish which of the equations proposed above is the most reliable.

In our investigations, the circulation velocity ranged from 4 to 15 m/sec, and the temperature gradient ranged from 13 to 150°K. Under these conditions the Reynolds number ranged from 25,000 to 420,000 while the Prandtl number ranged from 5 to 36.

The test apparatus (Figure 1,a) consists of a closed circuit with forced circulation of the liquid. The apparatus comprises the experimental section (1), heaters (2), and circulation pump (3), connected by means of steel (1Kh18N9T) pipes with a diameter of 0.057×0.003 m. A volume compensator (4), made of a pipe with an inner diameter of 0.195 m, was connected to the system by means of a pipe with a diameter of 8×1 mm. The pressure in the apparatus was produced by means of nitrogen which was supplied from the cylinder (9) to the vessel (4).

The liquid level in the vessel (4) was usually above the half-way mark, and as a result, the nitrogen could not enter the system directly or be dissolved in the liquid.

The heat exchange was studied in an experimental brass (L-62) pipe 0.012×0.001 m in diameter. In the experiments with MIPD, the pipe length was 0.640; 0.880; or 0.920 m. The pipe was heated by an alternating current which was passed through its walls.

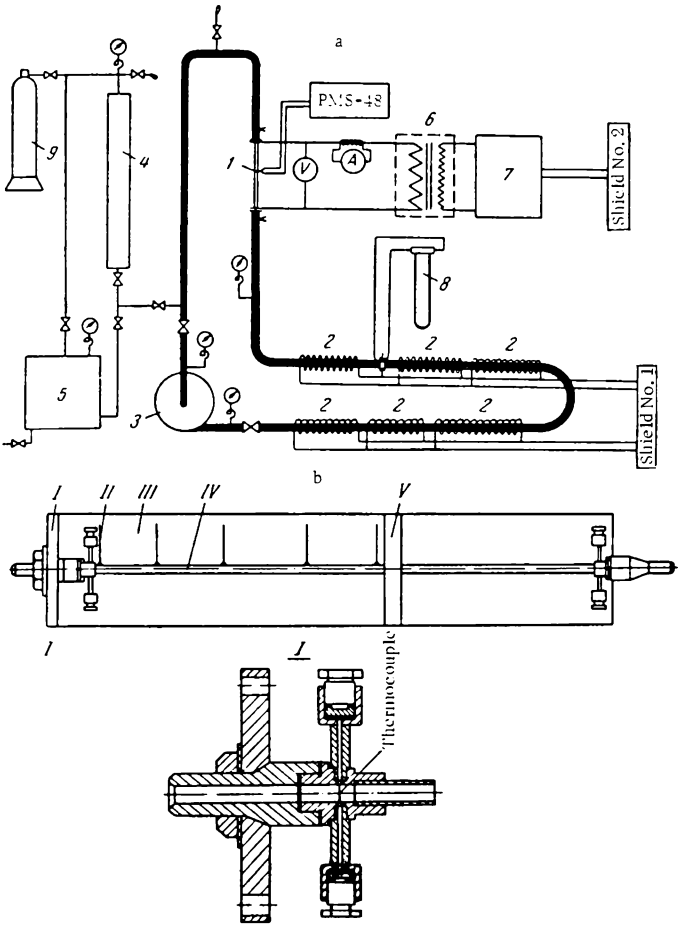


FIGURE 1. Schematic view of the test apparatus (a) and the experimental section (b).

1 — experimental section (b) (I — current-conducting flange; II — terminals for the measurement of the voltage; III — insulation; IV — experimental pipe; V — movable current-conducting flange); 2 — electric heaters; 3 — circulation pump; 4 — volume compensator; 5 — tank for closing the circuit; 6 — transformer type TPO-253; 7 — transformer type ROT-25/0.5; 8 — measuring orifice plate with the DT-50 differential manometer; 9 — nitrogen cylinder.

In the experimental section (Figure 1,b) a series of chromel-kopel'* thermocouples made of 0.00002 m wire were fitted along the pipe (IV) and served to measure the temperature of the external walls of the pipe. In the experiments with MIPD, 11 thermocouples were fitted along the pipe in one case, and 17 thermocouples in each of the other two cases. When 17 thermocouples were used, two thermocouples (at opposite sides of the pipe) were fitted at each of six marked spots along the pipe.

* [Kopel' — an alloy similar to constantan containing 56-57% copper and 44-43% nickel.]

When using the brass pipes, the errors in the determination of the temperature gradient over the wall could not have a substantial effect on the experimental results: the gradient over the walls ranged from 0.3 to 3°C, while the gradient between the wall and the liquid was 13-150°C.

The liquid temperature at the inlet and exit from the experimental section was also measured by chromel-kopel' thermocouples made of 0.00002 m wire. The hot junctions of these thermocouples were immersed directly in the liquid stream at the center of the pipe.

The liquid temperature in a given section was determined from the temperature at the inlet or exit of the experimental section and the amount of heat transmitted in the section up to or beyond that spot where the thermocouple was affixed.

The thermoelectromotive force was measured with a low-resistance potentiometer (PMS-48) having an accuracy of 1 microvolt. The heat flux was calculated from the power supplied. The voltage drop over a given section was measured by means of a milliammeter (of the D-528 type, (precision class 0.5) and a resistance box (KMS-6) connected in series with the ammeter. Such a circuit converted the ammeter into a multirange voltmeter, with a lower measurement limit of 0.5 v. The measuring device was calibrated in advance. The current flowing through the pipe was measured with an ELA ammeter (precision class 0.2)

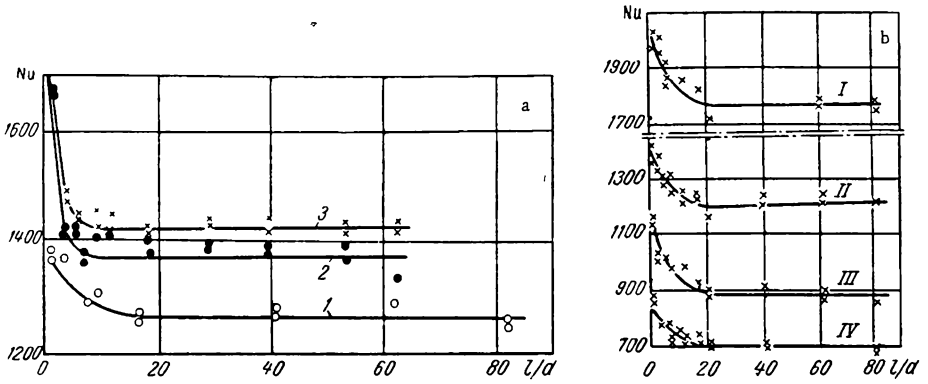


FIGURE 2. Local values of the Nusselt number at various heat fluxes (a), at a liquid circulation velocity of 10.3 m/sec and a liquid temperature of 413°K (1 — $q$ = 172,000; 2 — $q$ = 431,000; 3 — $q$ = 740,000 w/m$^2$) and at various liquid circulation velocities at a constant heat flux of 431,000 w/m$^2$ (b) (I — $w$ = 15.5; II — 10.3; III — 6.3; IV — 4.1 m/sec).

The experimental determinations of the coefficient of heat transfer to MIPD were carried out at circulation velocities of 4, 6, 10, and 15 m/sec. For each velocity, the values of the heat transfer coefficient were determined at specific heat fluxes of 172,000, 431,000, and 740,000 w/m$^2$. In the experiments with MIPD, the liquid temperature at the inlet to the experimental section varied between 343 and 553°K. The pressure was selected in such a way that surface boiling of the liquid did not occur. Usually, the wall temperature was below the saturation temperature by at least 20°.

In the experiments with MIPD, which were carried out with three experimental pipes (differing only in their lengths), the specific heat fluxes were 172,000 and 431,000w/m$^2$ in the pipe 0.880 m (or 88 $d$) long and 431,000 and 740,000w/m$^2$ in the pipe 0.640 m (or 64 $d$) long. The experiments with the pipe 0.920 m (92 $d$) long were carried out at a heat flux of 431,000w/m$^2$. Good agreement between the data of this heat flux was obtained for all pipes.

In the experiments we determined the local heat transfer coefficient at various distances from the inlet section.

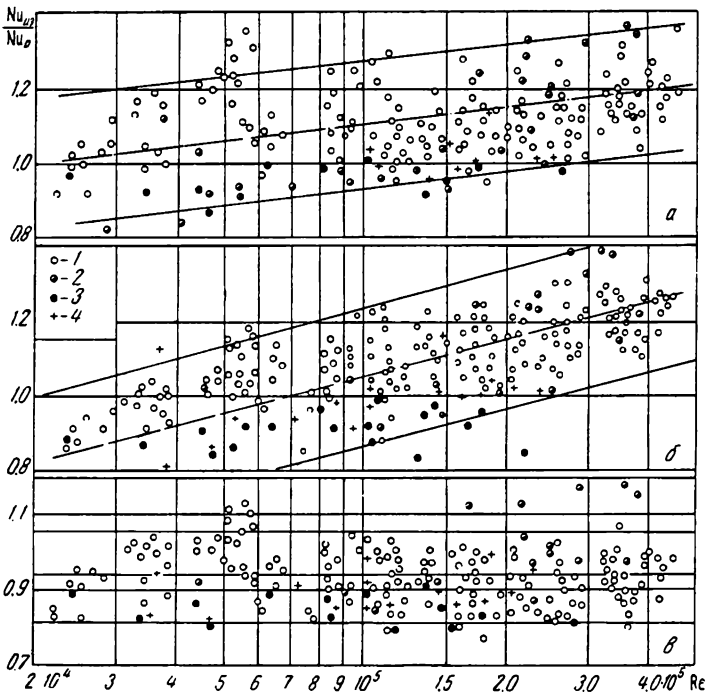


FIGURE 3. Comparison of the experimental and the calculated data:

a — according to the equation $Nu=0.027\ Re^{0.8} Pr^{1/3} \left(\frac{\mu_f}{\mu_w}\right)$ [6];

$$b - Nu = 0.021\ Re^{0.8}\ Pr^{0.43}\left(\frac{Pr_f}{Pr_w}\right)^{0.25} \quad [3];$$

$$c - Nu = \frac{0.125\,\xi\ Re\ Pr}{4.5\sqrt{\xi}\,(Pr^{2/3}-1.0)+1.07}\left(\frac{\mu_f}{\mu_w}\right)^n \quad [4].$$

1 — monoisopropyldiphenyl (MIPD); 2 — diphenyl according to /7/; 3 — Santowax OM according to /7/; 4 — Santowax $R$ according to /7/.

As is evident from Figure 2,a and b, the Nusselt number and hence, the heat transfer coefficient decreases sharply over the length of the pipe as the distance from the entrance is increased, and reaches constant values at a length $l > 15$-$20\,d$. An increase in the heat flux causes an increase in the heat transfer rate (at constant $t_f$).

In comparing our experimental data with results calculated on the basis of the equations proposed by various authors (Figure 3), we used the experimental data obtained at $l > 50\,d$, i. e., in the pipe sections in which the effect of the inlet conditions is completely eliminated.

In all calculations, the thermal properties of MIPD were taken from /1/.

The data in Figure 3 show that equations (1) give lower values of the heat transfer coefficient at $Re > 10^5$ (in comparison with the experimental values), while at $Re < 10^5$, the values are higher. The heat transfer coefficients calculated with the aid of equation (3) were lower than the experimental for all Re values. Similar calculations based on equation (2) showed that at $Re > 10^5$ and Pr between 4 and 8 the calculated values were higher than the experimental (by about 12%); at $Re < 10^5$ and $Pr > 15$ the discrepancy increased to 60%. The best agreement between the experimental and calculated data was obtained by using equation (4). However, even in that case the dispersion of results ranged from + 5 to -15%.

In our experiments the experimental data were obtained at Pr numbers between 6 and 36 and Re numbers ranging from 25,000 to 420,000.

The experimental data of /7/ are also shown in Figure 3. They were obtained at Re numbers between 20,000 and 300,000 and Pr numbers between 4.8 and 10.6. It is evident that most of the experimental values of heat transfer coefficients to Santowax *R* and Santowax *OM* are lower than the values calculated by means of equations (1), (3), and (4), within the whole range of Reynolds numbers (between 20,000 and 300,000).

The experimental data for diphenyl obtained in /7/ were higher than the values calculated by means of all the above equations.

Bibliography


1. Vargaftik, N.B. et al. — Izv. vysshikh uchebnykh zavedenii. Neft i Gaz, No. 3. 1963.
2. Kosterin, S.I. and A.D. Magomedov. — Izv. AN SSSR, OTN, No. 10. 1958.
3. Mikheev, M.A. — Izv. AN SSSR, No. 10. 1952.
4. Petukhov, B.S. and V.V. Kirillov. — Teploenergetika, No. 4. 1958.
5. Chechetkin, A.V. and F.M. Kosterov. — Khimicheskoe Mashinostroenie, No. 1. 1961.
6. Sider and Teit. — Ind. Eng. Chemistry, Vol. 28, No. 12. 1936.
7. Silberberg and Huber. Heat Transfer to Polyphenyls. — American Institute of Chemical Engineering. 1957.



The Moscow Power Institute

E. A. Krasnoshchekov, V. S. Protopopov,
Wang Feng, and I. V. Kuraeva

# EXPERIMENTAL STUDY OF THE HEAT TRANSFER IN THE SUPERCRITICAL REGION OF CARBON DIOXIDE

Experimental data obtained at small temperature gradients /1, 2/, i.e., under conditions such that the changes in the physical properties over the stream cross section are small, are described by equations valid for heat exchange during turbulent flow of a liquid of constant physical properties. As shown in /1/, the best agreement with the experimental data is obtained by using the equation

$$\mathrm{Nu}_0 = \frac{\xi}{8}\,\mathrm{Re}\,\mathrm{Pr}\frac{1}{12.7\sqrt{\frac{\xi}{8}}\,(\mathrm{Pr}^{2/3}-1)+1.07}, \qquad (1)$$

where

$$\xi = \frac{1}{(1.82\lg \mathrm{Re} - 1.64)^2}.$$

When the temperature gradients are such that the physical properties of the liquid change substantially across the stream, the heat transfer is no longer described by (1). Nevertheless, if the temperature gradients are relatively small and $T_w \lesssim 1.1\,T_m$ (range of the heat capacity peak) while the throughput is large enough (of the order of $\mathrm{Re} > 10^5$), the theoretical results calculated by assuming that the heat transfer obeys the rules of convective heat transfer in a single-phase medium of variable properties are in good agreement with the experimental data /4/. The empirical equations obtained for the above conditions /1, 5/ describe with a satisfactory degree of accuracy the available experimental data. However, at relatively large heat flux densities, when $T_f \leqslant T_m$ and $T_w \gg T_m$, the calculated results differ markedly from the experimental data, and the empirical equations yield values of the heat transfer coefficients which are too high.

Phenomena, resembling those characteristic of liquid boiling in pipes, have also been observed. These comprise the conditions under which there are sharp drops in the local heat transfer coefficients /6/ (a phenomenon resembling the crisis in boiling), and conditions that lead (according to /4, 7/) to strong pressure pulsations, noise, and an increase in the heat transfer rate (resembling the start of boiling of an underheated liquid at subcritical values of the parameters). Such heat transfer

conditions are created only when $T_f < T_m$ and $T_w > T_m$. Phenomena resembling the crisis in boiling occur at relatively small throughputs (of the order of $Re < 8 \cdot 10^4$) and moderately large heat loads, while pulsations and an increase in the heat transfer rate are observed at high throughputs and high heat flux densities.

However, in spite of the large number of experimental and theoretical studies, the rules governing the heat transfer in the supercritical region have not been adequately studied, and no recommendations for calculations have been published. We studied the heat exchange during turbulent flow of carbon dioxide of supercritical parameters in pipes during heating and with large temperature gradients.

The experimental section consisted of a steel pipe (steel 1Kh18N9T) with an inner diameter of $4.08 \cdot 10^{-3}$ m and an external diameter of $5 \cdot 10^{-3}$ m. The working section of the pipe (length $l = 51\ d$) was heated directly by the passage through it of an alternating current. A section where hydrodynamic stabilization took place (length $l = 49\ d$) was placed before the heated section. Measurements of the static pressure were made in the vicinity of the inlet and the exit of the heated section.

The temperature of the carbon dioxide at the inlet and exit of the experimental section was determined by means of copper-constantan thermocouples, the hot junctions of which were placed in stainless steel capillaries. The hot junction of the thermocouple near the exit was placed into the stream axis, behind a mixing device consisting of an assembly of special diaphragms.

The wall temperature was measured by means of nichrome-constantan thermocouples, the hot junctions of which were welded to the external surface of the pipe at twelve points over its length (at the side of the pipe). At three points ($l/d$ = 20, 30, and 40) additional thermocouples were fitted to the top and bottom generatrices of the pipe.

The experimental section was connected to a closed circulation system. The carbon dioxide was pumped into the system by means of a gear pump (without stuffing-box) with an electromagnetic drive. The throughput of the carbon dioxide was determined by measuring the pressure drop at the measuring diaphragm with a differential tensometric manometer /8/. The pressure at the inlet to the experimental section and in front of the measuring diaphragm was measured with a standard pressure gage.

The local values of the heat flux density at the inner pipe walls were determined by measuring the electrical current and the local values of the electrical resistance of the experimental pipe. Prior to measuring the calibration was carried out by plotting the temperature of the pipe wall against the resistance.

Experiments showed that the pipe is hydraulically smooth in the Re range between $1 \cdot 10^4$ and $8 \cdot 10^4$. In the Re range from $1 \cdot 10^5$ to $6 \cdot 10^5$ the friction coefficient was approximately constant ($\xi \approx 0.020$). In the Re range from $1 \cdot 10^5$ to $5 \cdot 10^5$ and at small temperature gradients ($t_w - t_f$ = 3.5-8.0°C) the heat transfer to carbon dioxide satisfied equation (1). We also carried out experiments under conditions of substantial changes in the physical properties of the liquid across the stream and in the temperatures and throughputs ($T_w < 1.1\ T_m$ and $Re > 1 \cdot 10^5$), for which the equations hold /1, 5/. The results of these experiments agree well with the above equations.

The main experiments were carried out at pressures of 785 and 981 n/cm$^2$*, at a mean calorimetric temperature of the liquid $t_f$ between 20 and 110°C, at temperature gradients up to 500°C, and at heat flux densities $q$ up to $2.6 \cdot 10^6$ w/m$^2$. The characteristic curves showing the changes in $t_f$, $t_w$, $q$, and the heat transfer coefficient $\alpha$ over the pipe length, at large temperature gradients, are shown in Figure 1.

As is evident from Figure 1, I the increase in the wall temperature over the pipe length is much more pronounced than the increase in the liquid temperature, and a corresponding sharp decrease in the heat transfer coefficient is observed. In the $x/d$ ratio range between 10 and 50 the decrease in $\alpha$ is by a factor of about 2. Under the above conditions ($t_f < t_m$ and $t_w \gg t_m$), the numerical values of the heat transfer coefficient were much lower than the values calculated by means of equation (1). Thus, at $x/d$ = 40, $t_m$ = 40°C and $t_w$ = 483°C, the heat transfer coefficient calculated by means of equation (1) was about 5.6 times the experimental value. Similar results were obtained in the experiments at a pressure $p$ = 785 n/cm$^2$ (Figure 1,IV).

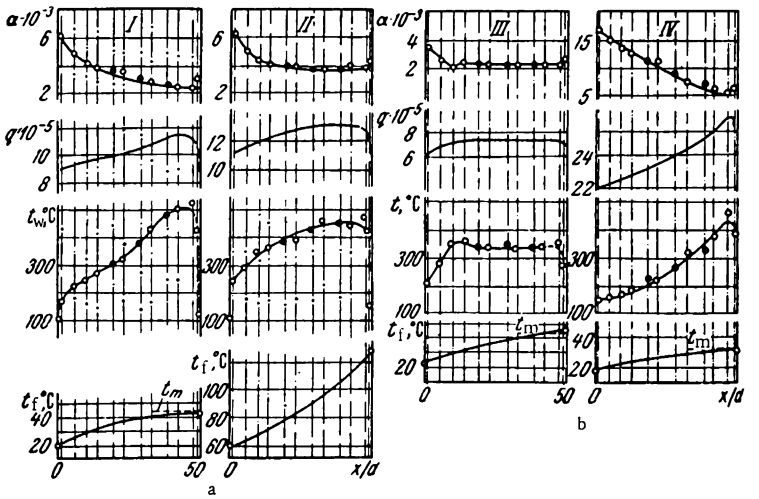


FIGURE 1. Distribution of $t_f$ (°C), $t_w$ (°C), $q$ (w/m$^2$) and $\alpha$ (w/m$^2$·°C) over the length of the experimental pipe.

I — $p$ = 971 n/cm$^2$, $G$ = 100 kg/hr, and $t_f < t_m$; II — $p$ = 971 n/cm$^2$; $G$ = 100 kg/hr, and $t_f > t_m$; III — $p$ = 971 n/cm$^2$, $G$ = 53.5 kg/hr; IV — $p$ = 785 n/cm$^2$, $G$ = 354 kg/hr.

The data in Figure 1,III show that at lower throughputs, when the liquid temperature is in the same range as in the experiments shown in Figure 1,I, IV, the wall temperature remains approximately constant over the pipe length (except for the section at $x/d < 10$) and the heat transfer coefficient has an approximately constant value over the length of the pipe at $x/d > 10$.

* At $p$ = 785 n/cm$^2$ $t_m$ = 33.4°C while at $p$ = 981 n/cm$^2$ $t_m$ = 44°C.

Thus the changes of the heat transfer coefficient over the pipe length at $t_f \leqslant t_m$ and $t_w \gg t_m$ may be of a different nature, depending on the heat load and the throughputs of the fluid. At the same time, the numerical values of the heat transfer coefficient are always lower than the values calculated using equation (1), and the heat transfer rate decreases as the temperature gradient is increased. However, the dependence of the heat transfer coefficient on the flow rate (and the dependence of Nu on Re) under the above conditions remains the same as the usual dependence in the case of heat transfer during turbulent flow in pipes ( $\alpha$ is approximately proportional to $G^{0.8}$ ).

When $t_f > t_m$ (Figure 1, II), the heat transfer on the pipe section with $x/d > 10$ remains practically constant, and its numerical value is only slightly lower than the values calculated with the aid of (1). Thus, if $t_f > t_m$, as the temperature of the liquid is increased, the heat transfer characteristics gradually become more similar to those of heat transfer in gases.

In order to continue our analysis, we used experimental data for three sections of the experimental pipe, with three thermocouples fitted to each of the sections.

When $T_f < 1.1\ T_m$ and $T_w \gg T_m$ (Figure 2,a, 1 and 3) the difference between the experimental values and values calculated by means of equation (1) increased with increasing temperature gradient. The largest deviation was observed at $T_f \approx T_m$ and at high values of $T_w$. In several cases the experimental values of $Nu_f$ were approximately one fourteenth of $Nu_0$. No reliable recommendations for the calculation of heat transfer under the above conditions have been published as yet. At $T_f > 1.1\ T_m$ (Figure 2,a, 2 and 4) the temperature-induced changes in the physical properties of the liquid are much smaller, and the effect of $T_w\ T_m$ on the heat transfer rate is relatively small.

A general dimensionless equation describing the heat transfer within the whole investigated temperature range was derived by assuming that the dependence of Nu on Re and Pr remains the same as under conditions far removed from the critical, while the effect of the variable physical properties may be accounted for by the introduction of correction factors that take into consideration the changes in the physical properties across the stream. An analysis showed that the experimental data are generalized satisfactorily by introducing into equation (1) two corrections, in terms of the density ratio $(\rho_w/\rho_f)^{0.3}$ and the heat capacity ratio $(\bar{c}_p/c_{p.\,f})^n$ where $\bar{c}_p = (i_w - i_f)/(t_w - t_f)$ is the mean integral heat capacity in the temperature range between $t_f$ and $t_w$. In that case, the value of the exponent $n$ increases from $n = 0.4$ at $T_w\ T_m \leqslant 1$ to $n \approx 0.7$ at $T_f \leqslant T_m$ and $T_w/T_m = 2.5$. When $T_f$ is increased from $T_m$ to $1.2\ T_m$ the above values of $n$ (corresponding to $T_w/T_m$) decrease to $n = 0.4$. In both cases $n$ changed linearly. As a result we obtained the following expressions:

$$Nu_f = Nu_0 \left(\frac{\rho_w}{\rho_f}\right)^{0.3} \left(\frac{\bar{c}_p}{c_{p\ f}}\right)^n, \qquad (2)$$

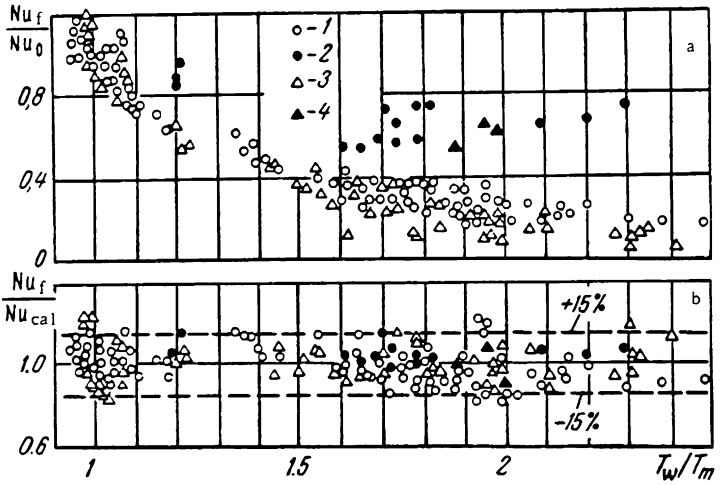


FIGURE 2. Comparison of experimental values of $Nu_f$ with values calculated using equation (1) at various relative wall temperatures $T_w/T_m$ (a) and with values calculated using equation (2) (b).

1 — 971 n/cm², $T_f < 1.1\,T_m$; 2 — 971 n/cm², $T_f > 1.1\,T_m$; 3 — 775 n/cm², $T_f \leqslant 1.1\,T_m$; 4 — 775 n/cm², $T_f > 1.1\,T_m$

where

$$n = 0.4 \text{ at } T_w T_m \leqslant 1 \text{ or } T_f T_m \geqslant 1.2;$$
$$n = n_1 = 0.22 + 0.18\,(T_w T_m) \text{ at } 1 \leqslant T_w T_m \leqslant 2.5;$$
$$n = n_1 + (5n_1 - 2)(1 - T_f T_m \text{ at } 1 \leqslant T_f T_m \leqslant 1.2.$$

Equation (2) gives correct values within the following ranges: $8 \cdot 10^4 < Re_f < 5 \cdot 10^5$; $0.85 < Pr_f < 65$; $0.09 < \rho_w \omega_f < 1.0$; $0.02 < \bar{c}_p c_{p,f} < 4.0$; $0.9 < T_w T_m < 2.5$; $4.6 \cdot 10^4 < q < 2.6 \cdot 10^6$ w/m²; $x/d \geqslant 15$.

The experimental data (Figure 2,b) are described by equation (2), the maximum deviation being ±20%.

However, it should be mentioned that at $T_f \leqslant T_m$ and $T_w \gg T_m$ the wall temperature depends on the heat flux density to a power much higher than unity; thus, the error in the calculation of $T_w$ (at given $q$, $T_f$ and Re) will be much greater than in the calculation of $\alpha$ (at given $T_w$, $T_f$, and Re).

In the temperature range $T_w \leqslant 1.1\,T_m$ or $T_f \geqslant 1.2\,T_m$ our experimental data, as well as the data of /1, 2, 5, 9/ agree well both with equation (2) and with the equations in /1, 5/.

For practical calculations (when the heat flux density is given and it is required to determine the wall temperature) it would be convenient to have $t_w$ as a function of $q$ and $t_f$ in an explicit form. To this end, we used equation (2) to calculate and plot $qd^{0.2}/(\rho w)^{0.8}$ as a function of $t_w$ and $t_f$ (Figure 3). The calculated curves were corrected on the basis of the experimental data.

The curves in Figure 3 show the same qualitative relationships as in /4/. However, the wall temperature range studied in /4/ was from $T_f \approx T_m$ to $T_w T_m = 1.4$. The results in Figure 3 are for the region up to $T_w/T_m = 2.5$. This made it possible to reveal a number of interesting

features of heat transfer at large temperature gradients in the case of great changes in the physical properties of the liquid across the stream.

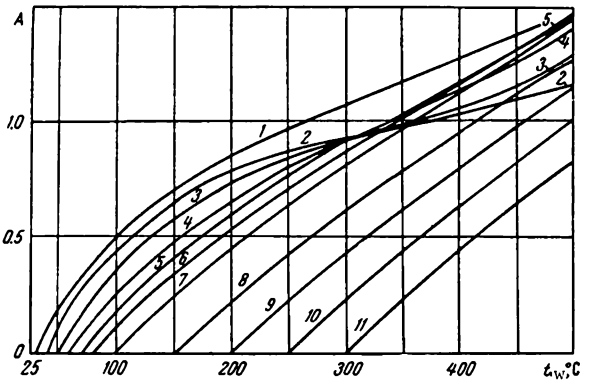


FIGURE 3. A plot of $A = \frac{qd^{0.2}}{(\rho w)^{0.8}} \frac{(w/m^2) \cdot m^{0.2}}{(kg/m^2 \cdot hr)^{0.8}}$ as a function of the wall temperature $t_w$ °C and the fluid temperature $t_f$°C, for the case of carbon dioxide at $p = 981$ n/cm$^2$.

1 — $t_f$ = 30; 2 — 40; 3 — 50; 4 — 60; 5 — 70; 6 — 80; 7 — 100; 8 — 150; 9 — 200; 10 — 250; 11 — 300°C.

The slope of the curves for $t_f$ = const. at $t_w \to t_f$ characterizes the heat transfer in the case of a fluid of constant physical properties. The change in the slope of the curves with increasing $t_w$ is explained by the effect of the variable physical properties of the liquid; the change in the properties is most pronounced at temperatures close to $t_m$ (at $p = 981$ n/cm$^2$ and $t_f$ between 20 and 60°C), while at higher temperatures the change is much smaller. Hence, the curves for $t_f$ = const. intersect at relatively high wall temperatures.

The curves in Figure 3 show the peculiar character of the changes in the wall temperature over the pipe length at a given heat flux density. At relatively small values of $q$ and relatively large values of $\rho w$ (e.g., at $p = 981$ n/cm$^2$ and $qd^{0.2}/(\rho w)^{0.8} \leqslant 0.9$), the wall temperature increases monotonously with increasing $t_f$, i.e., over the pipe length. At relatively large values of $q$ and relatively small values of $\rho w$, the changes in $t_w$ are no longer monotonous. The wall temperature increases over the pipe length and at $t_f \approx t_m$ it reaches a maximum value, then decreases, and increases monotonously again at higher $t_f$ values. Thus, a local decrease in the heat transfer rate is observed under the above conditions at $t_f \approx t_m$. If at the above pressure $qd^{0.2}/(\rho w)^{0.8} \approx 0.93$, the wall temperature remains practically constant when $t_f$ is increased from 40 to 70°C (the region in which the curves for $t_f$ = const. intersect). The same behavior was also observed in the experiment described earlier (see Figure 1, III).

Symbols

$l$ — length, m; $x$ — distance from the starting point of the heated section, m; $d$ — diameter of the experimental pipe, m; $T_w$ and $t_w$ — temperatures of the inner pipe surface, °K and °C respectively; $T_f$ and $t_f$ — mean calorimetric temperatures of the liquid at the given pipe section, °K and °C respectively; $T_m$ and $t_m$ — temperatures corresponding to the maximum heat capacity at the given pressure, °K and °C respectively; $G$ — throughput of fluid, kg/hr; $\rho w$ — mass velocity, kg/m$^2$·hr; $Nu_0$ — Nusselt number, as determined by means of equation (1) at a temperature $t_f$; $Nu_f$ — Nusselt number at a temperature $t_f$; $\xi$ — friction coefficient; $\rho_c$, $\rho_f$ — densities at $t_w$ and $t_f$; $c_{p.f}$ — heat capacity at a constant pressure and at $t_f$, kj/kg, °C; $\bar{c}_p = (i_w - i_f)/(t_w - t_f)$ — mean integral heat capacity in the temperature range between $t_f$ and $t_w$; $i_w$ and $i_f$ — enthalpy at $t_w$ and $t_f$ respectively, kj/kg.

Bibliography


1. Petukhov, B.S., E.A. Krasnoschekov, and V.S. Protopopov. — International Developments in Heat Transfer, Part III, Colorado, U.S.A. 1961.
2. Armand, A.A., N.V. Tarasova, and A.S. Kon'kov. — In sbornik: "Teploobmen pri vysokikh teplovykh nagruzkakh i drugikh spetsial'nykk usloviyakh," Edited by A.A. Armand. — Moskva, Gosenergoizdat. 1959.
3. Petukhov, B.S. and V.V. Kirillov. — Teploenergetika, No. 4. 1958.
4. Goldmann, K. — International Developments in Heat Transfer, Part III, Colorado, U.S.A. 1961.
5. Miropol'skii, Z.L. and M.E. Shitsman. — ZhTF, Vol. 27, No. 10. 1957.
6. Shitsman, M.E. — Teplofizika Vysokikh Temperatur, Vol. 1, No. 2. 1963.
7. Hines and Wolff. — Raketnaya Tekhnika, No. 3. 1962.
8. Protopopov, V.S. — Teploenergetika, No. 1. 1963.
9. Bringer, R.P. and J.M. Smith. — JAIChE, Vol. 3, No. 1. 1957.



The Moscow Power Institute

E. N. Dubrovina and V. P. Skripov

# CONVECTIVE HEAT TRANSFER IN THE SUPERCRITICAL REGION OF CARBON DIOXIDE

The existence of noticeable maxima in the heat transfer coefficient on isotherms and isobars in the supercritical region at small temperature gradients is attributed to a relationship between the heat transfer and the thermal properties of the substance. The thermal expansion coefficient $\beta$, the compressibility coefficient, the heat capacity $c_p$, and the thermal conductivity $\lambda$ have maxima near the critical point.

The Nusselt number Nu is a dimensionless number characterizing the heat transfer:

$$\mathrm{Nu} = \frac{\alpha l}{\lambda}, \tag{1}$$

where $\alpha$ is the heat transfer coefficient;
$l$ is the characteristic dimension, and
$\lambda$ is the thermal conductivity coefficient.

According to the theory of similarity, the relationship between the heat transfer coefficient and the thermal properties of a substance is expressed as follows:

$$\mathrm{Nu} = f(\mathrm{Gr} \cdot \mathrm{Pr}), \tag{2}$$

where the dimensionless Grashoff and Prandtl numbers are, respectively:

$$\left.\begin{aligned} \mathrm{Gr} &= \frac{gl^3 \beta \Delta t}{\nu^2} \\ \mathrm{Pr} &= \frac{\mu c_p}{\lambda} \end{aligned}\right\}. \tag{3}$$

The exact nature of function $f$ is usually determined by experiment.

The first experiments on the heat transfer near the critical point were carried out in 1939 by Schmidt, Eckert, and Grigull /7/. In 1960 Schmidt /8/ carried out a series of experiments with carbon dioxide and ammonia, and found that near the critical point (of the gas) the heat transfer by natural convection becomes extremely rapid. A great increase in the heat transfer coefficient during free convection in the supercritical region was also observed by Doughty and Drake /1/.

We continued with the experimental studies started by Skripov and Potashev /9/. In heat transfer studies, the system must be taken out of the thermodynamic equilibrium state and a temperature gradient must be created. The smaller the disturbance [of the equilibrium], the more pronounced is the extremal character of the heat transfer coefficient near the critical point. The above statement is doubtlessly correct since it is well known how sharp the maxima of the heat capacity and thermal expansion become when the critical point is reached from supercritical temperatures. Thus, in our experiments the temperature gradient was, as a rule, about 0.5°C.

The heat transfer by natural convection was studied for vertical and horizontal orientations of a thin platinum filament with respect to the direction of the gravity force. The dimensionless heat transfer equation comprises a term for the characteristic length of the heating surface. The smallness of the difference between the results obtained with the vertical and horizontal filaments shows that both cases must be characterized by the same linear dimension. The channel diameter, equal to 40 mm, was taken as the characteristic length.

Since the relationship between the heat transfer coefficient and the thermal parameters is reduced to the effect of these parameters on the nature of the natural convection, it would be of interest to examine the changes in the nature of the convection in the vicinity of the heated filament in the supercritical region, as induced by changes in temperature, pressure, and temperature gradient.

The heat transfer in the supercritical region was studied with carbon dioxide (according to Michels /10/, the critical temperature and pressure of carbon dioxide are 31.04°C and $7.38 \cdot 10^6$ n/m$^2$, respectively). Analysis of the gas obtained by the alkali absorption method showed that the carbon dioxide used was 99.7% pure.

The experimental apparatus consisted of a chamber with a thermostat and pressure regulation system (Figure 1), a measuring device, and an optical device.

The experiments were carried out in a stainless steel chamber immersed in a water thermostat (15 liter). The required temperature of the water in the thermostat was maintained manually, using a heater and a cooler, and was controlled by means of a mercury thermometer with 0.1°C graduations (a magnifying glass was used to take the readings). The temperature fluctuations in the thermostat were ±0.01°C. Before the measurements, the chamber was heated for 2 to 2.5 hours at the experimental temperature.

The chamber contained two cylindrical channels: a vertical channel (1) and a horizontal channel (8); each channel had a diameter of 40 mm and a length of 120 mm. The two channels were connected by an inclined bore (6). To permit visual observations of the convective streams in the vicinity of the heated filaments, the chamber was fitted with two thick glass windows (30 mm in diameter and 11 mm thick with teflon seals (3), and a central glass window (9). During the assembly the end windows were fitted into flanges (4) and (7), and fastened with internal nuts by means of a special wrench. A sufficiently high pressure inside the chamber caused self-sealing of the windows.

In our experiments a thin platinum filament (with a diameter of 29 $\mu$) served as a heater and as a resistance thermometer. One end of the

filament was fastened and soldered to a copper wire passing through the teflon cylinder (10), while the second end was soldered to rod (13). Two supports (12), made of stainless steel with a diameter of 2 mm, were set in the flange (2). The support ends were pressed into the ring (5). A rod (13) with a spring and two nuts (to regulate the tension of the filament) passed through the center of the ring. The current conductor was sealed and insulated with the aid of the cylinder (10) fitted to the flange (2); the cylinder was pressed into place by means of a nut (11).

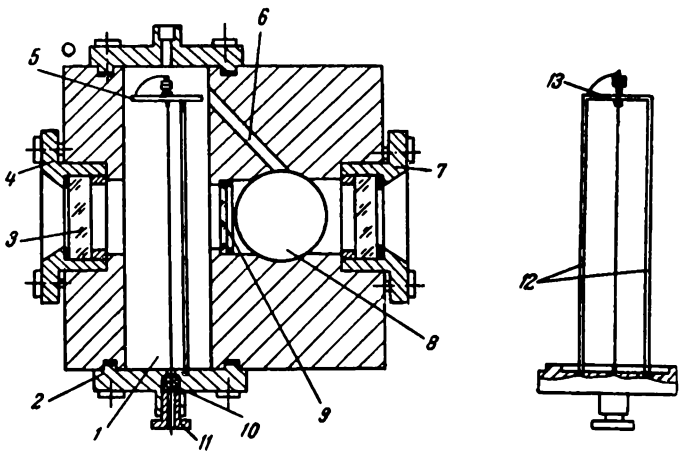


FIGURE 1. Vertical cross section of the chamber and the part with the platinum filament.

One of the parts with the platinum filament was fitted into the vertical channel and the other into the horizontal channel.

A direct current from a series of storage batteries was supplied to the platinum filament. A standard resistor (10 ohm), a resistance box, and a control milliammeter were connected in series with the filament. The current was measured by means of the PPTV-1 potentiometer. The resistance of the filament was calculated using the equation

$$R_x = \frac{R_s V_x}{V_s},$$

where $V_x$ is the voltage drop over the working section; and
$V_s$ is the voltage drop on the standard resistor.

The pressure required in the chamber was produced by changing the temperature of a steel cylinder filled with liquid carbon dioxide.

The whole pressurized system was separated by four needle valves into three sections: the chamber, the cylinder containing the liquid carbon dioxide (in the TS-15M thermostat), and a pressure gage with a blowdown valve. The working chamber and the pressure gage could be disconnected from the rest of the system, since the pressure established in them

remained constant over a long period. The pressure was measured with a standard spring pressure gage (0.35 precision class) with a scale of up to 250 kg/cm$^2$.

Before the measurements were taken the platinum filament was heated in air by passing a ~ 300 mamp current through it for 7 hours. The filament diameter was determined at several points by means of a vertical displacement measuring device (IZV-1), and by turning through 90°. The effective diameter was calculated using the equation

$$d_{\text{eff}} = \frac{d_{1\text{av}} + d_{2\text{av}}}{2},$$

where $d_{1\text{av}}$ and $d_{2\text{av}}$ are the average diameters at two positions of the filament differing by 90° (when turned around the axis); ($d_{1\text{av}}$=28.8 μ, $d_{2\text{av}}$=29.5 μ, $d_{\text{eff}}$ =29.2 μ). Assuming that the cross section of the filament is a circle with a diameter equal to the effective diameter let us determine the lateral surface of the filament (the heating surface)

$$F = \pi d_{\text{eff}} L$$
$$(L_{\text{hor}}=8.1\cdot 10^{-2}\ \text{m},\ L_{\text{vert}}=7.8\cdot 10^{-2}\ \text{m}, \qquad (4)$$
$$F_{\text{lat hor}}=7.4\cdot 10^{-6}\ \text{m}^2,\ F_{\text{lat vert}}=7.2\cdot 10^{-6}\ \text{m}^2).$$

In the first series of experiments we determined the dependence of the heat transfer coefficient on the pressure and on the 31.5, 32.0, 34.0, and 37°C isotherms, at a temperature gradient of 0.40-0.60°C and in the pressure range of (6-10)· 10$^6$ n/m$^2$ (Figure 2).

The specific heat flux and the heat transfer coefficient were calculated using the equation

$$q = \frac{V_s V_x}{R_s F}, \qquad (5)$$

where $V_s$ and $V_x$ are the voltage drops on the standard and the measured resistors, $R_s$ is the standard resistor (10 ohm), $F$ is the heating surface, and

$$\alpha = \frac{q}{\Delta t}. \qquad (6)$$

The voltage drop on the platinum filament and the standard resistor were measured with the PPTV-1 potentiometer. A mirror galvanometer with a sensitivity of 1.8· 10$^{-9}$ amp was used as the zero indicator.

The temperature gradient was determined as follows. For each isotherm at a pressure of 6· 10$^6$ n/m$^2$, we recorded the dependence of the filament resistance $R_x$ on the current $i$. At low heat loads $R_x$ was a linear function of $i^2$. Graphical extrapolation of the straight line for $R_x = ai^2$ to $i = 0$ yielded $R_0$ which corresponded to the ambient temperature in the chamber.

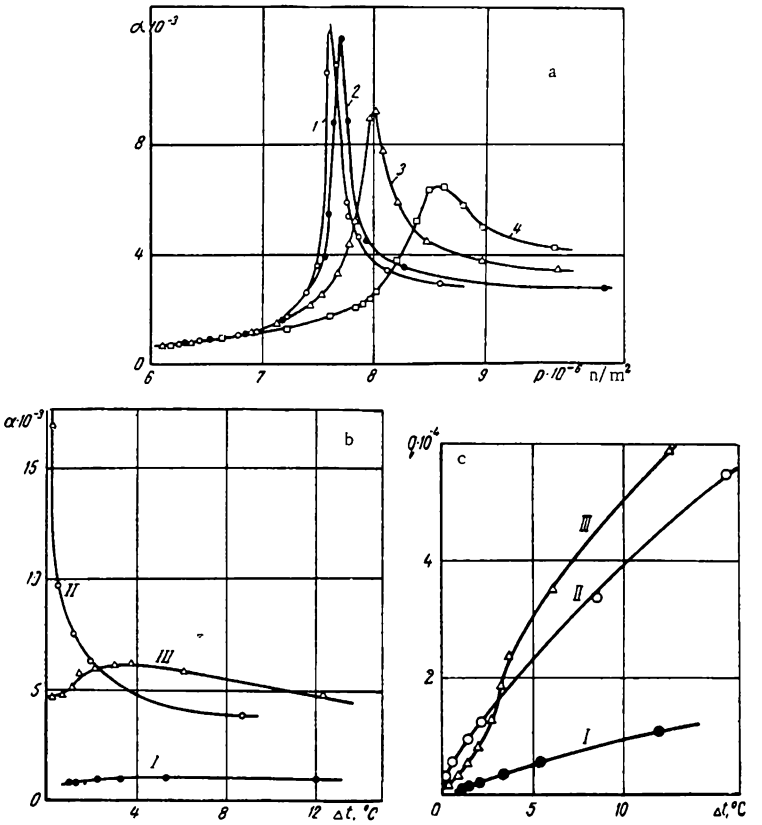


FIGURE 2. Dependence of the heat transfer coefficient α (w/m²·deg.) (for the horizontal filament).

a — on the pressure (n/m²) for isotherms in the supercritical range: 1 — 31.5; 2 — 32.0; 3 — 34.0; 4 — 37.0°C; b — on the temperature gradient $\Delta t$ for three isobars: I — $6 \cdot 10^6$; II — $8 \cdot 10^6$; III — $9.3 \cdot 10^6$ n/m²; c — dependence of the specific heat flux q(w/m²) on the temperature gradient $\Delta t$ for the above isobars.

Thus the temperature gradient is given by

$$\Delta t = \frac{R_x - R_0}{B}, \text{ where } B = \frac{\Delta R}{\Delta t}.$$

At temperatures between 30 and 50°, the value of $B$ (the temperature coefficient of the platinum resistance) was equal to 0.38 ohm/degree.

The curves in Figure 2 have clearly defined maxima. The nearer the temperature of the isotherm to the critical, the higher the maximum. When the temperature is increased, the pressure corresponding to the maximum at a temperature gradient of 0.5°C shifts to the side of higher values. Even at a temperature differing from the critical temperature by 6°C (i.e., the 37.0°C isotherm), the heat transfer coefficient is higher (by a factor of

more than 2) than in the case of a monotonous transition through the region of the maximum.

The data in Table 1 show that the values of $\alpha$ and $q$ for the vertical filament are lower than for the horizontal. Values of the heat transfer coefficient $\alpha$ and the specific heat flux $q$ at the point of maximum $\alpha$ are presented in Table 2 (for 4 isotherms). The values of $\alpha$ and $q$ decrease as the temperature recedes from the critical temperature.

TABLE 1. Dependence of the specific heat flux $q$ and the heat transfer coefficient $\alpha$ on the pressure (on the 31.5°C isotherm)

| Horizontal filament | | | | Vertical filament | | |
|---|---|---|---|---|---|---|
| $p \cdot 10^{-6}$ n/m$^2$ | $\Delta t$, °C | $q \cdot 10^{-3}$ w/m$^2$ | $\alpha \cdot 10^{-3}$ w/m$^2$·°C | $\Delta t$, °C | $q \cdot 10^{-3}$ w/m$^2$ | $\alpha \cdot 10^{-3}$ w/m$^2$·°C |
| 6.28 | 0.51 | 0.44 | 0.79 | 0.54 | 0.27 | 0.50 |
| 6.54 | 0.51 | 0.46 | 0.91 | 0.50 | 0.30 | 0.60 |
| 6.82 | 0.48 | 0.56 | 1.17 | 0.50 | 0.39 | 0.77 |
| 6.97 | 0.60 | 0.78 | 1.26 | 0.53 | 0.54 | 1.03 |
| 7.22 | 0.50 | 0.82 | 1.65 | 0.50 | 0.67 | 1.34 |
| 7.58 | 0.51 | 5.36 | 10.50 | 0.47 | 2.78 | 5.90 |
| 7.60 | 0.51 | 6.28 | 12.31 | 0.52 | 4.96 | 9.63 |
| 7.64 | 0.54 | 5.86 | 10.58 | 0.49 | 3.97 | 8.11 |
| 7.70 | 0.47 | 2.75 | 5.86 | 0.50 | 1.88 | 3.79 |
| 7.84 | 0.50 | 1.99 | 3.97 | 0.50 | 1.52 | 3.04 |
| 8.09 | 0.50 | 1.73 | 3.47 | — | — | — |
| 9.07 | 0.48 | 1.48 | 3.18 | 0.49 | 1.49 | 2.99 |
| 9.61 | 0.48 | 1.39 | 2.98 | 0.49 | 1.33 | 2.64 |

TABLE 2. Maximum values of $q$ and $\alpha$ on the various isotherms at a temperature gradient of 0.5°C

| Process parameters | | Horizontal filament | | Vertical filament | |
|---|---|---|---|---|---|
| $t$chamber °C | $p_{max} \cdot 10^{-6}$ n/m$^2$ | $q_{max} \cdot 10^{-3}$ w/m$^2$ | $\alpha_{max} \cdot 10^{-3}$ w/m$^2$·°C | $q_{max} \cdot 10^{-3}$ w/m$^2$ | $\alpha_{max} \cdot 10^{-3}$ w/m$^2$·°C |
| 31.5 | 7.60 | 6.2 | 12.4 | 4.95 | 9.9 |
| 32.0 | 7.68 | 5.9 | 11.8 | 4.4 | 8.8 |
| 34.0 | 8.00 | 4.5 | 9.0 | 3.2 | 6.4 |
| 37.0 | 8.61 | 3.2 | 6.4 | 3.0 | 6.0 |

The heat transfer coefficient for the vertical filament in the region of the maximum was lower than that reported in /9/. The difference could probably be attributed to the fact that the thermostat conditions in /9/ were not sufficiently good, and as a result an additional overall convection was created in the chamber at the transition pressure.

The curves in Figure 2,b are for a temperature of 34°C. Curve I shows that a change in the temperature gradient up to $\Delta t$ = 10°C causes no noticeable change in $\alpha$; curve II corresponds to the maximum heat transfer coefficient at a temperature gradient $\Delta t$ = 0.5°C. In these cases an increase in $\Delta t$ causes a rapid decrease in $\alpha$. Changes in the temperature and pressure have a particularly strong effect on the heat transfer coefficient in the region in which the coefficient has the maximum value. Curve III shows

the dependence of $\alpha$ on $\Delta t$ along a higher isobar. The pressure $p_{III} = 8.3 \cdot 10^6$ n/m$^2$ is higher than $p_{max}$ but is still sufficiently close to it. Curve III has a maximum which shows that maximum heat transfer may be achieved by changing the state, not only along the isotherm, but also along the isobar.

The temperature criterion in the experiment increases with increasing $\Delta t$, in spite of the fact that the chamber temperature remains constant. In the case of small temperature gradients, the temperature criterion may be taken as

$$t' = t_0 + \frac{\Delta t}{2} .$$

All the curves in Figure 2, c show the increase in the heat flux with increasing $\Delta t$, again for the 34°C isotherms. Close to the origin of coordinates, the most rapid increase in the heat flux occurs along the isobar $p_2 = p(\alpha_{max})$. On isobar III, an inflection point exists at a certain $\Delta t$; it corresponds to the maximum $\alpha$ on the $\alpha(\Delta t)$ curve, and the specific heat flux on the above isobar after the inflection point is higher than on the isobar II, corresponding to a pressure $p_{max}$.

A comparison of the values of the heat transfer coefficients for the horizontal and vertical filaments at a temperature gradient of 0.5°C shows that the $\alpha_{hor}/\alpha_{vert}$ ratio is about 1.5 at pressures of $6\text{-}7 \cdot 10^6$ n/m$^2$ and about 1.1 at pressures of $9\text{-}10 \cdot 10^6$ n/m$^2$. No sharp deviation of the $\alpha_{hor}/\alpha_{vert}$ ratio (from the above ranges) is observed in the region of the extreme values.

During the experiments we observed the state of the carbon dioxide in the middle part of the chamber. The convective streams were observed on a screen using a condenser and a system of lenses. A 25 w lamp served as the light source. By moving the lens, it was possible to bring into focus either the vertical or the horizontal filament. The field of observation within the chamber was a circle $15 \cdot 10^{-3}$ m in diameter. A "Start" reflex camera, without lens and loaded with A-2 highly-sensitive photographic film, was fitted in place of the screen when photographic pictures of the convection pattern were to be taken.

No convection in the vicinity of the filaments was observed at a pressure of $6 \cdot 10^6$ n/m$^2$. Slightly curved streams, running along the vertical filament with a period of 10-15 sec, appeared when the pressure was increased to $6.8 \cdot 10^6$ n/m$^2$. The closer the pressure to $p_{max}$, the more frequently do these streams appear, and they become curl-shaped. Finally, at the maximum point, the convection becomes turbulent with fine twists (the temperature gradient is maintained at 0.5°C). Continuous motion takes place near the vertical filament, with eddying and curling of the convective streams. At small $\Delta t$, the motion is confined to the vicinity of the filament.

As $\Delta t$ is increased, the shape of the convective streams changes and the region affected by the convection is extended. At large $\Delta t$ (of the order of 20-40°C), the convective streams become very fine and they cover the whole field of observation.

At a temperature gradient of 0.5°C, the heat transfer coefficient drops when the pressure is increased beyond $p_{max}$. The convection along the vertical filament slows down and becomes confined to the immediate vicinity of the filament; the convective streams again become curl-shaped.

At a temperature gradient of 0.5°C, the convective streams round the horizontal filament can only be observed under conditions corresponding

to the maximum heat transfer coefficient. The convection apparently has the form of a film which loses its stability and is divided into separate streams outside the field of observation. In the case of the 31.5°C isotherm, there were occasionally strong convective streams of a turbulent nature around the horizontal filament. At large $\Delta t$ (10-20°C), we observed two types of convective streams which replaced each other: the usual turbulent, and a more ordered jet-like stream. At a chamber temperature of 31.1°C (which is very close to the critical temperature), we observed opalescence (a dark band in the middle that covered the filament). Straight streams, almost perpendicular to the filament, suddenly rose over the whole field of observation. Reversion to a typically turbulent convection, with fine curls over the filament, took place subsequently. At a $\Delta t$ of 30-40°C, the two types of streams are found simultaneously in adjacent sections.

An interesting occurrence at the horizontal filament is observed when the current is switched on. A "string" divided into small cells separates from the filament. This cellular structure appears because of the hydrodynamic instability of the moving heated "string."

The conventional method of presenting heat transfer data as a function of the thermal properties of the substance and the system parameters involves the use of dimensionless equations. In an attempt to use equation (2), we found that no sufficient data are available for the near-critical state of carbon dioxide. The tabulated data are presented for temperature and pressure points spaced far apart from each other. Hence, only a few points were taken into account. The data obtained are shown in Table 3. The values of the viscosities and thermal conductivity coefficients, as well as that of the heat capacity $c_p$ (through the Prandtl number) were taken from the work of Michels /11, 12/. The compressibility coefficient $\beta$ and the density $\rho$ were found by using the equations of state of $CO_2$ proposed by Kazavchinskii and Katkhe /13/. The equation was calculated on the electronic digital computer "Ural-1" for a series of supercritical isotherms. For the last two isotherms, a correlation was made (with respect to the pressure) of the maximum heat exchange coefficient $\alpha$ with the maximum $\lambda$ and $\left(-\frac{\partial p}{\partial v}\right)_T$.

TABLE 3. The Nusselt number (Nu), the product Gr·Pr and their logarithms for helium and for the various states of carbon dioxide

| Substance | $t$, °C | $p \cdot 10^{-5}$ n/m$^2$ | Nu | lg Nu | Gr·Pr | lg Gr·Pr |
|---|---|---|---|---|---|---|
| He | 34.0 | 1.0 | $3.7 \cdot 10^2$ | 2.57 | $3.1 \cdot 10^2$ | 2.5 |
| $CO_2$ | 20.0 | 1.0 | $5.2 \cdot 10^2$ | 2.72 | $3.6 \cdot 10^4$ | 4.55 |
| $CO_2$ | 32.0 | 61.0 | $1.1 \cdot 10^3$ | 3.04 | $1.4 \cdot 10^9$ | 9.15 |
| $CO_2$ | 34.2 | 91.0 | $2.0 \cdot 10^3$ | 3.30 | $5.5 \cdot 10^9$ | 9.74 |
| $CO_2$ | 32.2 | 76.8 | $3.6 \cdot 10^3$ | 3.56 | $7.0 \cdot 10^{11}$ | 11.85 |
| $CO_2$ | 34.2 | 80.0 | $3.9 \cdot 10^3$ | 3.59 | $1.4 \cdot 10^{11}$ | 11.15 |

In our experiments, the product Gr·Pr for carbon dioxide varied over a wide range — from $3.6 \cdot 10^4$ to $10^{11}$. Turbulent convection was observed within the above range. This is in good agreement with the commonly accepted value of Gr·Pr > 1000 for convection in a confined space /14/. In contrast to the usual conditions, the convection appeared at low $\Delta t$ in our

experiments. At lower values of the product Gr·Pr, the heat exchange took place by molecular thermal conductivity. This was the case in the experiments with helium.

Bibliography


1. Doughty, D. L. and R.M. Drake. — Trans. ASME, No. 78, p. 1843. 1956.
2. Bringer, R.P. and J. M. Smith. — JAIChE, No. 3, p. 148. 1957.
3. Dickinson, N.J. and C.P. Welch. — Trans. ASME, No. 80, p. 746. 1958.
4. Shitsman, M.E. — Teploenergetika, No. 1, p. 68. 1959.
5. Goldman, K. — JAIChE, Chem. Eng. Progress Symposium Series, No. 11. 1954.
6. Griffith, J.D. and R.H. Sabersky. — ARS J. March, 1960.
7. Schmidt, E., Eckert, und V. Grigull. Jahrbuch der Deutschen Luftfahrtforschung, Bd. 11. 1939. AAF. — Translation, No. 527, Air Material Command, Wright Field, Dayton, Ohio.
8. Schmidt, E. — Int. J. Heat Mass Transfer, Vol. 1, p. 91. 1960.
9. Skripov, V.P. and P.I. Potashev. — IFZh, 5(2):30. 1962.
10. Michels, A., B. Blaisse, and C. Michels. — Proc. Roy. Soc., 160A(900):358. 1937.
11. Michels, A., A. Botzen, and W. Schuurman. — Physica, Vol. 23, No. 95. 1957.
12. Michels, A., J.V. Sengers, and P.S. Van der Gulik. — Physica, Vol. 28:1201. 1962.
13. Katkhe, O.I. — IFZh, Vol. 3, No. 10. 1960.
14. Mikheev, M.A. Osnovy teploperedachi (The Fundamentals of Heat Transfer). — Gosenergoizdat, Moskva-Leningrad. 1956.

V.N. Popov

# THEORETICAL CALCULATION OF THE HEAT TRANSFER AND FRICTION RESISTANCE FOR CARBON DIOXIDE IN THE SUPER-CRITICAL REGION

The method of calculation of heat transfer and friction resistance used in the present paper has been developed and described in detail in /1/. The heat transfer calculations are based on an analytical expression for the Nusselt number which was derived in /1/ for the case of steady, axi-symmetrical, turbulent flow of a noncompressible fluid of variable physical properties in pipes.

$$\frac{1}{\mathrm{Nu}_w} = 2\,\frac{\overline{c_{p_w}}}{\overline{c_p}} \int_0^1 \frac{\left(\int_0^R \frac{\rho w_x}{\overline{\rho w}}\, R\,dR\right)^2}{\frac{\lambda}{\lambda_w}\,\frac{\overline{c_{p_w}}}{\overline{c_p}}\left(1+\beta\,\mathrm{Pr}\,\frac{\varepsilon_\tau}{\nu}\right) R}\, dR, \qquad (1)$$

where

$$\mathrm{Nu}_w = \frac{q_w d}{\lambda_w (T_w - T_f)}; \quad \overline{c_p} = \frac{\int_{T_f}^{T_w} c_p dT}{T_w - T_f} = \frac{h_w - h_f}{T_w - T_f}; \quad R = \frac{r}{r_0}.$$

Equation (1) is valid for a pipe section at some distance from its inlet, i.e., for a section in which the hydrodynamic and thermal boundary layers are superimposed.

Equation (1) is based on the following assumptions:

1) the changes in the axial component of the mass velocity $\rho w_x$ along the pipe axis $x$ are small, i.e., $\frac{\partial(\rho w_x)}{\partial x} \approx 0$;

2) the pressure $p$ is constant across the pipe;

3) the longitudinal enthalpy gradient $\frac{\partial h}{\partial x}$ is constant across the pipe cross section, i.e., $\frac{\partial h}{\partial x} = f(x)$;

4) the density of the axial heat flux, which is a function of the thermal conductivity, is small compared with the density of the radial heat flux;

5) the effect of mass forces and of kinetic energy dissipation is negligible.

The term $\frac{\varepsilon_\tau}{\nu}$, in (1) was calculated by the Goldman method, by which the coefficient of turbulent transfer of momentum in the case of variable physical properties may be calculated by using the same expressions for constant physical properties, but the expressions must be written in terms of certain new variables. We used the equations derived by Reichardt /2/ as the expressions describing constant physical properties:

$$\frac{\varepsilon_\tau}{\nu} = k(\eta - \eta_n \operatorname{th} \eta/\eta_n) \quad \text{for } 0 \leqslant \eta \leqslant 50, \tag{2}$$

$$\frac{\varepsilon_\tau}{\nu} = \frac{k}{3}\eta(R^2 + 0{,}5)(R+1) \quad \text{for } \eta > 50,$$

where $k = 0{,}4$; $\eta_n = 11$; $\eta = \frac{v^* y}{\nu}$; $v^* = \sqrt{\frac{\tau_w}{\rho}}$.

In calculating $\frac{\varepsilon_\tau}{\nu}$ for variable physical properties, we used equation (2) in which the variable $\eta^+$, (proposed by Goldman) was substituted for $\eta$,

$$\eta^+ = \int_0^y \sqrt{\frac{\tau_w}{\rho}} \frac{dy}{\nu} = \int_0^{\eta_w} \frac{\mu_w}{\mu} \sqrt{\rho/\rho_w}\, d\eta_w \tag{3}$$

where

$$\eta_w = \frac{v_w^* y}{\nu_w}; \quad v_w^* = \sqrt{\frac{\tau_w}{\rho_w}}.$$

In this paper we assumed that $\varepsilon_q = \varepsilon_\tau$, i.e., that $\beta = 1$.

In calculating the value of $Nu_w$, we set as the starting parameters the $p$, $T_w$, $q_w d$ and the dimensionless pipe radius $\eta_{ow} = \frac{v_w^* r_0}{\nu_w}$. By using the method of successive approximation, we then found the profiles of temperature, velocity, $\frac{\varepsilon_\tau}{\nu}$, and Reynolds number $Re_w = \frac{\overline{\rho w} d}{\mu_w}$. These values being known, we were then able to calculate $Nu_w$ as well as the resistance coefficient $\xi_w$, since

$$\xi_w = \frac{8\tau_w \rho_w}{(\overline{\rho w})^2} = 32\left(\frac{\eta_{ow}}{Re_w}\right)^2. \tag{4}$$

It should be noted that on the basis of (4) and the equation for the axial component of the velocity /1/, it is possible to derive an analytical expression for the friction resistance coefficient $\xi_w$ during turbulent flow of a noncompressible fluid of variable physical properties in a pipe at some distance from the inlet (the expression is presented below without its derivation):

* The appropriate equations for temperature, velocity, $\frac{\varepsilon_\tau}{\nu}$, and Reynolds number, which were used in the calculations, have been presented in /1/.

$$\xi_w = \frac{8}{Re_w} \frac{1}{\int_0^1 \rho/\rho_w R \left( \int_R^1 \frac{R}{\mu/\mu_w \left(1 + \frac{\varepsilon_\tau}{\nu}\right)} dR \right) dR} \quad (5)$$

Results of the calculation of $Nu_w$ and $\xi_w$ for carbon dioxide in the supercritical region

The heat transfer and friction resistance for the case of carbon dioxide were calculated for $p = 98.1 \cdot 10^5$ n/m²*, for three values of $\eta_{ow}$ and five values of $T_w$ (Figure 1). Only the case of heating ($q_w > 0$) was dealt with. For each pair of $\eta_{ow}$ and $T_w$ values we set several values of $q_w d$, in such a way that the mean calorimetric temperature $T_f$ had several successive values in the range from $T_w$ to ~ 30°C. The physical properties of carbon dioxide used in the calculations were taken from those same sources used in /3, 4/. In Figure 1, $Nu_{ow}$ is the Nusselt number calculated from the relation $Nu = Nu_o$ (Re, Pr) derived for the case of constant physical properties**, in which $Re_w^* = Re_w \frac{\rho_w}{\rho_f}$ was used as the Reynolds number, and $Pr_w$ as the Prandtl number.

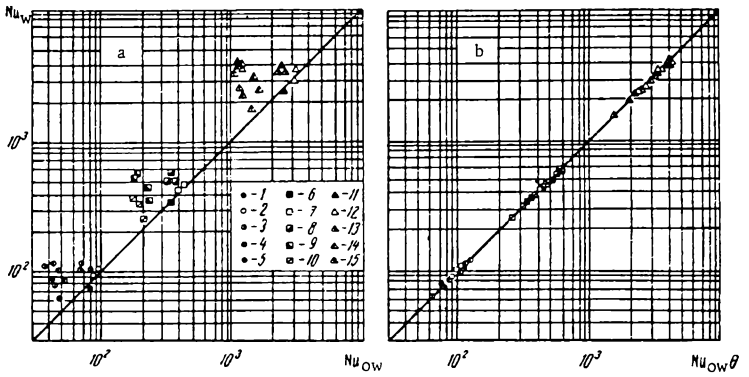


FIGURE 1. Calculated values of the heat transfer for carbon dioxide at $p = 98.1 \cdot 10^5$ n/m². 1, 2, 3, 4, 5 — at $T_w$ = 35, 45, 50, 70, 100°C, respectively; $\eta_{ow}$ = 445; 6, 7, 8, 9, 10 — the same, $\eta_{ow}$ = 2370; 11, 12, 13, 14, 15 — the same, $\eta_{ow}$ = 19,050.

Figure 1,a shows that as a result of the effect of temperature on the physical properties, the heat transfer under the conditions set for the calculations may change by a factor of more than three.

The calculated heat transfer data were generalized on the basis of the following considerations. The changes in the numerator of integrand (1), which describes the temperature dependence of the physical properties, are negligible, since during turbulent flow, the mass velocity profile is

* At $p = 98.1 \cdot 10^5$ n/m² the heat capacity of carbon dioxide reaches its maximum at about 44°C.

** The results obtained in the calculation of Nu for constant physical properties over a wide range of Pr and Re, and the interpolation equation describing those results, are presented in /1/.

fully developed. Assuming $\beta = 1$, the denominator of the integrand in (1) may be written as follows:

$$\frac{\mu}{\mu_w}\left(\frac{Pr_w}{Pr} + Pr_w \frac{\varepsilon_\tau}{\nu}\right). \tag{6}$$

The effect of the variable nature of the physical properties on the $\frac{\varepsilon_\tau}{\nu}$ ratio in (6) is characterized by the ratio $\eta^+/\eta_w$, which may be expressed directly by the variable physical properties in the following way. Let us deal with the integral in (3) by parts:

$$\eta^+ = z\eta_w - \int_1^z \eta_w(z)\, dz$$

or

$$\eta^+/\eta_w = z - \int_1^z \frac{\eta_w(z)}{\eta_w}\, dz, \tag{7}$$

where

$$z = \frac{\mu_w}{\mu}\sqrt{\rho/\rho_w}.$$

When $z$ changes from 1 to $z$, the $\frac{\eta_w(z)}{\eta_w}$ ratio in (7) changes from 0 to 1. Let us assume that the above ratio is approximately constant and equal to $\varkappa_1$. Then

$$\eta^+/\eta_w = (1-\varkappa_1)\frac{\mu_w}{\mu}\sqrt{\rho/\rho_w} + \varkappa_1. \tag{8}$$

Thus, the change in $Nu_w$, associated with the effect of the variable physical properties on $\frac{\varepsilon_\tau}{\nu}$, may be accounted for (in an approximate way) by means of the parameter $\psi$,

$$\psi = (1-\varkappa_1)\frac{\mu_w}{\mu_f}\sqrt{\frac{\rho_f}{\rho_w}} + \varkappa_1.$$

The dependence of $Nu_w$ on the variable ratio $\frac{Pr_w}{Pr}$, which is a term in (6), may be accounted for approximately by means of the parameter $Pr_w/\overline{Pr}$ in which $\overline{Pr}$ is the mean integral value of the Prandtl number in the temperature range between $T_f$ and $T_w$. However, since in the supercritical region

the temperature dependence of $\lambda$ and $\mu$ is similar, the parameter $c_{pw}/\bar{c_p}$, which is more convenient for calculations, may be substituted for the parameter $\frac{Pr_w}{\overline{Pr}}$.

The dependence of $Nu_w$ on the variable ratio $\mu/\mu_w$, which is a term in (6), may be accounted for by dealing with the integral in (1) by parts and applying the same assumptions used in deriving (8). In this case, by replacing the viscosity at the pipe center by the viscosity at $T_f$ (they are approximately equal) and taking into account the considerations expressed above, we may present the expression for $Nu_w$ as:

$$\frac{Nu_w \frac{c_{pw}}{\bar{c}_p}}{Nu_{ow}(Pr_w\ Re_o)} = \frac{f_1(\psi) f_2\left(\frac{c_{pw}}{\bar{c}_p}\right)}{(1-x_2) + x_2 \frac{\mu_w}{\mu_f}}. \tag{9}$$

The Reynolds number $Re_0$, which corresponds to the parameter $\tau_{low}$ for constant physical properties is determined from equation (4). The dependence of $\xi$ on Re for constant physical properties has been shown in /1/. In our calculations, the values of $\tau_{ow} = 445$, 2370, and 19,050 corresponded to $Re_0 = 14.5 \cdot 10^3$, $10^5$, and $999 \cdot 10^3$. From these data we found that $Re_0$ may be calculated (with an accuracy of $\pm 10\%$) from the value of $Re_w^*$ using equation

$$Re_0 = Re_w^* \left(\frac{\rho_f}{\rho_w}\right)^{1/3}. \tag{10}$$

It should be noted that for generalization of the calculated data, the value of $Nu_{ow}$ was calculated by using $Re_w^*$ instead of $Re_0$ in order to obtain a more convenient interpolation equation for calculations. The form of the functions $f_1$ and $f_2$, and the values of the constants $x_1$ and $x_2$ were determined on the basis of calculated data:

$$f_1(\psi) = \psi = (1-x_1) \frac{\mu_w}{\mu_f} \sqrt{\frac{\rho_f}{\rho_w}} + x_1 \tag{11}$$
$$(x_1 = 0.12; \quad x_2 = 1.0).$$

As is evident from Figure 2, the form of the function $f_2$ depends on $Re_0$:

$$f_2\left(\frac{c_{pw}}{\bar{c}_p}\right) = \frac{c_{pw}/\bar{c_p}}{x + (1-x) c_{pw}/\bar{c_p}}, \tag{12}$$

where

$$x = \frac{3}{Re_0^{0.21}}. \tag{13}$$

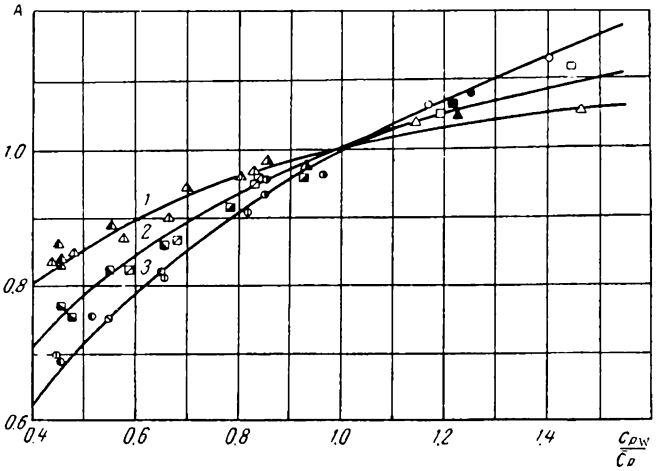


FIGURE 2. $\frac{Nu_w \frac{c_{pw}}{\bar{c}_p}}{Nu_{ow}\left(0.12 \frac{\mu_f}{\mu_w} + 0.88 \sqrt{\frac{\rho_f}{\rho_w}}\right)} = A$ as a function of $c_{pw}/c_p$ at $Re_0 = 999 \cdot 10^3$, $10^5$, and $14.5 \cdot 10^3$ (1, 2, 3). The symbols used for the calculated points are the same as in Figure 1. The solid line represents equation (14).

As a result, we obtained an equation which generalizes the calculated heat transfer data with a maximum dispersion of ± 3% and has the form:

$$\frac{Nu_w}{Nu_{ow}(Pr_w, Re_w)} = \frac{0.12 \frac{\mu_f}{\mu_w} + 0.88 \sqrt{\frac{\rho_f}{\rho_w}}}{\varkappa + (1-\varkappa)\frac{c_{pw}}{\bar{c}_p}}. \qquad (14)$$

In (14) $\varkappa$ was calculated with the aid of (13) using (10). If we assume that $\varkappa$ is independent of $Re_0$ and has a value of 0.25, dispersion is increased to ± 10%. The generalization of the experimental data by means of (14) is shown in Figure 1,b. In this figure, $\theta$ denotes the right-hand side of (14).

The experimental heat transfer data obtained in /3, 4/ and their comparison with equation (14) are shown in Figure 3 where $Nu_w^{ex}$ is the value of $Nu_w$ obtained from the experimental data; $Nu_{ow}^T$ is the Nusselt number calculated on the basis of $Re_w^*$, $Pr_w$, and the expression obtained in /1/ for the case of constant physical properties; $Nu_w^T$ is the value of $Nu_w$ calculated by means of equation (14), using (13) and (10) for those values of $T_w$, $T_f$, and $\rho w d$ used in the experiments /3, 4/. In /3/ $T_w$ changed in the range from ~ 30 to ~ 90°C, while $T_w - T_f$ ranged from a few degrees to ~ 60°C. In the experiments of other authors, $T_w$ ranged from ~ 30 to ~ 500°C while $T_w - T_f$ was between a few degrees to ~ 450°C. Figure 3,a shows that as a result of the effect of the variable physical properties, the heat transfer in /3/ changed by a factor of more than 5. As is evident from Figure 3,b, the values $Nu_w^{ex}$ and $Nu_w^T$ agreed with an accuracy of ± 20%. Such an agreement may be regarded as completely satisfactory, since the accuracy of the experimental data was within 10-15%.

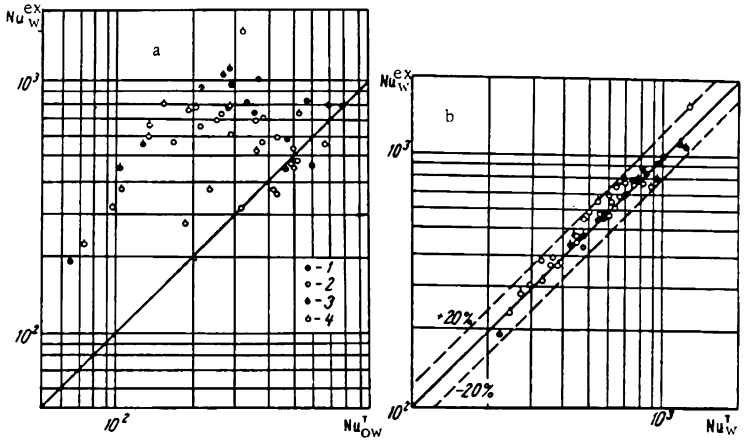


FIGURE 3. Comparison of heat transfer data for carbon dioxide calculated using equation (14) with experimental data /3, 4/.

1 – $p = 88.3 \cdot 10^5$ n/m$^2$ /3/; 2 – $98.1 \cdot 10^5$ /3/; 3 – $77.5 \cdot 10^5$ /4/; 4 – $97.1 \cdot 10^5$ n/m$^2$ /4/.

In Figure 4 $\xi_f = \xi_w \frac{\rho_f}{\rho_w}$, and $\xi_{of}$ is the friction resistance coefficient calculated from the function $\xi = \xi_0(\mathrm{Re})$ for constant physical properties /1/, using the same Reynolds number $\mathrm{Re}_f = \frac{\bar{\rho} w d}{\mu_f}$ which was used to obtain $\xi_f$.

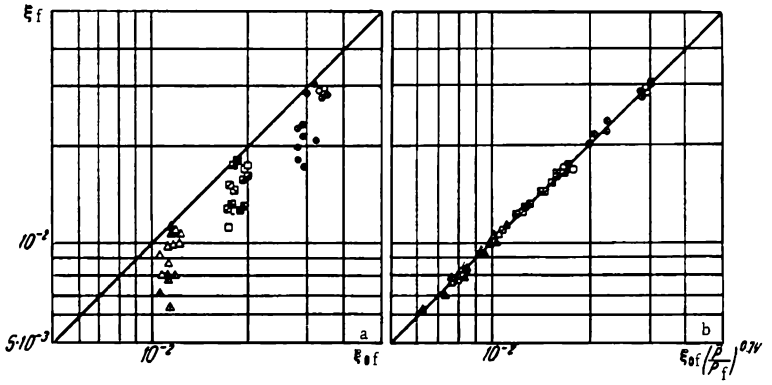


FIGURE 4. Calculated friction resistance for carbon dioxide at $p = 98.1 \cdot 10^5$ n/m$^2$. The symbols are the same as in Figure 1.

The calculated results are described (with an accuracy of ± 5%) by the equation

$$\frac{\xi_f}{\xi_{of}} = \left(\frac{\bar{\rho}}{\rho_f}\right)^{0.74}, \qquad (15)$$

where

$$\bar{\rho} = \frac{\int_{T_f}^{T_w} \rho \, dT}{T_w - T_f}.$$

The more simple equation

$$\frac{\xi_f}{\xi_{of}} = \left(\frac{\rho_w}{\rho_f}\right)^{0.4}$$

generalizes the calculated results with a lower accuracy (± 10 %).

## Symbols

$x$ — coordinate along the pipe axis; $r$ — flow radius; $r_0$ — pipe radius; $R$ — dimensionless flow radius; $d$ — pipe diameter; $y$ — distance from the wall; $\eta$ and $\eta_w$ — dimensionless distances from the wall; $\eta_{ow}$ — dimensionless pipe radius; $\eta+$ — variable proposed by Goldman; $q_w$ — heat flux density on the wall; $T_w$ — wall temperature; $T_f$ — mean calorimetric temperature of the liquid; $\tau_w$ — tangential stress on the wall; $w_x$ — axial velocity component; $\overline{\rho w}$ — mean (across the tube) mass velocity; $v^*$ and $v_w^*$ — dynamic velocities; $p$ — static pressure; $\varepsilon_\tau$ — coefficient of the turbulent momentum transfer; $\varepsilon_q$ — coefficient of the turbulent heat transfer; $\beta$ — ratio of the coefficient of turbulent heat transfer to the coefficient of turbulent momentum transfer; $Re_w$, $Re_w^*$, $Re_f$, and $Re_0$ — Reynolds numbers; Pr, $Pr_w$ — Prandtl numbers; $\lambda$ — thermal conductivity coefficient; $\mu$ — dynamic viscosity coefficient; $\nu$ — kinematic viscosity coefficient; $h$ — enthalpy; $c_p$ — heat capacity; $\bar{c}_p$ — mean integral value of the heat capacity in the temperature range from $T_f$ to $T_w$; $\rho$ — density; $\bar{\rho}$ — mean integral value of the density in the temperature range from $T_f$ to $T_w$.

Subscripts: $w$ — physical properties at $T_w$; $f$ — physical properties at $T_f$; o — constant physical properties.

## Bibliography


1. Petukhov, B.S. and V.N. Popov. — Teplofizika Vysokikh Temperatur, Vol. 1, No. 1. 1963.
2. Reichardt, H. Recent Advances in Heat and Mass Transfer. Editor Hartnett. — McGraw-Hill Book Company. 1961.
3. Petukhov, B.S., E.A. Krasnoshchekov, and V. S. Protopopov. — International Developments in Heat Transfer, Part III, Rep. 67. International Heat Transfer Conference, Colorado, U.S.A. 1961.



The Moscow Power Institute

I. T. Alad'ev, P. I. Povarnin, L. I. Malkina,
and E. Yu. Merkel'

# INVESTIGATION OF THE COOLING PROPERTIES OF ETHANOL AT PRESSURES UP TO $800 \cdot 9.8 \cdot 10^4$ n/m$^2$

The cooling properties of ethanol were studied in a loop under pressures of (300 and 800)$\cdot 9.8 \cdot 10^4$ n/m$^2$, during its flow within seamless stainless steel (1Kh18N9T) pipes of internal diameter 0.0006-0.0021 m and $l/d$ ratio 20-175.

In these experiments, the temperature of the wall in contact with the ethanol reached 973°K, the liquid temperature ranged from 288 to 623°K, and the flow velocity of the alcohol was 5-60 m/sec. The maximum specific heat fluxes reached $35 \cdot 10^6 \cdot 1.163$ w/m$^2$.

The following observations were made from these experiments.

1) The heat transfer at a pressure of $300 \cdot 9.8 \cdot 10^4$ n/m$^2$ was accompanied by thermal decomposition of the ethanol which formed a coke-like deposit on the contact surface.

At flow velocities lower than 30 m/sec decomposition of the ethanol started at wall temperatures of 623-673°K, and was practically independent of the temperature of the liquid. At velocities higher than 30 m/sec, no decomposition of the alcohol was observed, even when the wall temperature was as high as 973°K.

2) No thermal decomposition of the ethanol was observed at a pressure of $800 \cdot 9.8 \cdot 10^4$ n/m$^2$.

3) In a number of the experiments at a pressure of $300 \cdot 9.8 \cdot 10^4$ n/m$^2$, we observed the occurrence of pseudoboiling, which caused an increase in the heat transfer rate. No pseudoboiling was observed at a pressure of $800 \cdot 9.8 \cdot 10^4$ n/m$^2$.

4) In the case of a well-developed turbulent flow of ethanol, and in the absence of coke formation and pseudoboiling at $p \geqslant 300 \cdot 9.8 \cdot 10^4$ n/m$^2$, the heat transfer to the ethanol may be computed on the basis of the rules governing convective heat transfer. The data obtained satisfy the equation

$$\mathrm{Nu}_{l_x} = 0.021\, \mathrm{Re}_{l_x}^{0.8}\, \mathrm{Pr}_f^{0.43} \left(\frac{\mathrm{Pr}_f}{\mathrm{Pr}_w}\right)^{0.25} \left(\frac{l_x}{d}\right)^{0.2},$$

where $l_x$ is the pipe length from the point where the heating is started to the calculated section.

In their studies on heat transfer to fluids in the supercritical state, several authors /1-3/ observed a certain improvement of the heat transfer at $p > p_{cr}$, $t_w > t_{cr}$ and $t_f \ll t_{cr}$. This phenomenon was termed "pseudoboiling." In such a case, the curve representing the function $t_w = f(q)$ has the

characteristic plateau for boiling, in which an increase in the heat flux $q$ is accompanied by a negligible increase in the wall temperature $t_w$. The occurrence of pseudoboiling is often accompanied by a shrill whistling sound, as reported by Goldman /1/ and Khaines and Vol'f /3/.

Studies of the heat transfer to ethanol in the supercritical region ($p = 300 - 800 \cdot 9.8 \cdot 10^4$ n/m$^2$), as well as to methanol /4, 5/ and several other fluids, revealed an increase in the heat transfer rate that was accompanied by a whistling sound and attributed to pseudoboiling.

Two schemes representing the mechanism of pseudoboiling have been proposed. Goldman /1/ proposes the following scheme: large groups of liquid molecules split up upon contact with the heat transfer surface and cause the formation in the bulk of the liquid of cavities filled with gases consisting of single molecules. The growth and subsequent destruction of these low-density cavities in the liquid may be so vigorous that the boundary layer is destroyed and pulsation of the liquid occurs, this phenomenon being similar to nucleate boiling. As in the case of boiling, the observed increase in the heat transfer rate is caused by the additional agitation of the boundary layer due to the motion of these cavities.

Griffith and Sabersky /2/ photographed the formation and motion of pseudobubbles under supercritical conditions.

Khaines and Vol'f suggested a somewhat different theory concerning the mechanism of pseudoboiling. They assumed the change of the viscosity with temperature to be an important factor in the above mechanism. Thus, according to /3/, small changes in the temperature near the critical point may cause considerable changes in the viscosity. An incidental small increase in $t_w$ may, possibly, cause a noticeable decrease in the thickness of the laminary boundary layer, which should lead to a decrease in $t_w$ and a corresponding increase in viscosity. This should be accompanied by an increase in the thickness of the laminary boundary layer and in $t_w$, i.e., an unstable boundary layer may be the source of vibrations at supercritical pressures and the cause of the increase in the heat transfer rate in forced convection systems.

In our opinion, the phenomenon of pseudoboiling should be discussed more extensively. It is assumed that the turbulization of the boundary layer and the increase in the heat transfer rate associated with it always occur as a result of the formation of a new fluid phase of reduced density. Under subcritical conditions, this phase consists of vapor bubbles, and the process is termed boiling.

Under supercritical conditions, an analogous phenomenon may occur during various processes — dissociation, thermal decomposition, separation of lighter components from a mixture (e.g., a mixture of the kerosene type), etc. The following examples of such processes are cited:

a) Dissociation of molecules of a substance during heating, with the formation of pseudobubbles which behave like true bubbles and cause noticeable turbulization of the boundary layer. An example of this phenomenon is heat transfer to nitrogen tetroxide $N_2O_4$.

b) The initial phase of decomposition of a liquid, preceding the formation of a coke-like precipitate. In the case of alcohols, the initial products are aldehydes formed as a result of decomposition of the substance. Their density is lower than that of the alcohol, and together with the gases formed as a result of the decomposition ($CO_2$, $CH_4$, and others), they cause turbulization of the boundary layer. When they are detached from the layer

adjacent to the wall and enter the mainstream, the new compounds often recombine into the starting substance. Thus, decomposition of the substance is only partial. In such a case, the temperature plateau (analogous to subcritical boiling) on the $t_w = f(q)$ diagram extends to the values of $q$ (and, correspondingly, to higher values of $t_w$) at which a spontaneous increase in $t_w$ begins as a result of the deposition of a coke deposit, formed during the more vigorous decomposition, on the pipe walls.

c) Separation of lower-boiling fractions during heating of a liquid; these fractions consist of mixtures of various substances, e.g., in the case of heat transfer to kerosene. Data on the heat transfer to the $Jp$-4 fuel have been published in /6/.

It may be assumed that, depending on the process leading to the formation of a new phase and turbulization of the boundary layer, it is possible to calculate the amount of gaseous products formed by analogy with the calculations for subcritical boiling (from the ratio $\frac{\alpha_{boi}}{\alpha_{con}} > 1$). The optimum conditions for pseudoboiling could probably be computed.

An analysis of the experimental data on heat transfer to alcohols (ethyl and methyl) as well as to other organic coolants (with respect to the pseudoboiling process) leads to the following general comments:

1) There exists a certain optimum value of the reduced pressure $\pi = \frac{p}{p_{cr}}$, at which pseudoboiling is of maximum intensity. As is evident, a further increase in $\pi$ leads to a deterioration in the conditions needed for the formation of a new phase, and interferes with the pseudoboiling. Thus, although pseudoboiling of ethanol occurs at $p = 300 \cdot 9.8 \cdot 10^4$ n/m$^2$ ($\pi = 4.6$), it is completely absent at $p = 800 \cdot 9.8 \cdot 10^4$ n/m$^2$ ($\pi = 12.3$).

2) The wall temperature $t_w$ at which pseudoboiling occurs decreases with increasing flow velocity, and the plateau becomes less distinct.

3) Preliminary heating of the liquid leads to pseudoboiling at lower heat fluxes.

Contradictory results have been obtained for water, which is not a mixture of components, does not dissociate, and does not decompose at the wall temperatures reached in the experiments.*

Our experimental study of the pseudoboiling during heat transfer to water at $p = (250\text{-}350) \cdot 9.8 \cdot 10^4$ n/m$^2$ ($\pi = 1.1\text{-}1.55$) at flow velocities $w =$ $= 5\text{-}40$ m/sec in stainless steel (1Kh18N9T) pipes at liquid temperatures $t_f = 293\text{-}373$°K did not confirm the observations of Goldman.

In our experiments no pseudoboiling took place at any of the flow velocities at pressures of (250 and 300)$\cdot 9.8 \cdot 10^4$ n/m$^2$; in some experiments (at $w = 30$ m/sec), we did observe a certain increase in the heat transfer rate but the characteristic whistling sound (reported by Goldman /1/ also for the experiments with water) was not heard.

Bibliography

1. Goldman, K. — Trans. ASME, Vol. 76, No. 84. 1954.
2. Griffith, J.D. and R.H. Sabersky. — ARS Journal, No. 3: p. 289. 1960.

* The authors' considerations concerning the so-called pseudoboiling have not been adequately substantiated. Editor's note.

3. Khaines and Vol'f. — Raketnaya Technika, No. 3. 1962.
4. Alad'ev, I.T., P.I. Povarnin, L.I. Malkina, and E.Yu. Merkel'. — Teploenergetika, No. 8. 1963.
5. Alad'ev, I.T., L.I. Malkina, and P.I. Povarnin. — IFZh, No. 10. 1963.
6. Beili and Din. — Voprosy Raketnoi Tekhniki, No. 4. 1955.

The Power Institute im. G. M. Krzhizhanovskii

D. M. Kalachev, I. S. Kudryavtsev,
B. L. Paskar', and I. I. Yakubovich

# APPLICATION OF THE METHOD OF HIGH-FREQUENCY HEATING TO LIQUID-METAL HEAT TRANSFER MEDIA

In experimental equipment, liquid-metal heat transfer media are usually heated by the hot combustion products of various fuels, or electrically (d.c. or a.c.). The current is passed through a special conductor with subsequent transfer of the heat to the liquid metal, or is supplied directly to the heat transfer medium through the channel walls /1, 2/.

The use of the above two methods poses serious problems when the liquid metal is to be heated to a high temperature (1273°K or more). In such cases it is advantageous to use high-frequency induction heating /3, 4/, where the heat is released directly in the heated object, while it is in a high-frequency magnetic field. The specific heat flux transferred to the object is practically independent of the temperature of that object, and may reach thousands of kilowatts per square meter of its surface (up to $\sim 10^7$ w/m$^2$).

Induction heating eliminates direct contact between the current-conducting parts (which require forced cooling) and the walls of the channel for the heat exchange medium, which is very hot and often extremely corrosive. Thus, the upper temperature limit for the liquid to be heated is virtually eliminated.

Furthermore, the use of induction heating makes it possible to reduce the dimensions of the heating apparatus with a corresponding reduction in the volume filled by the liquid metal.

The method of high-frequency heating of liquid metals was tested on a laboratory-type loop, using a heavy metal alloy and a light alkali metal. The high-frequency current was supplied to the induction heater of the alloy from the PVV-80/8000 high-frequency converter and a capacitor bank.

The inductor (Figure 1) was built in the form of a solenoid with an inner diameter of 0.065 and a length of 0.450 m, from a shaped copper tube with a cross section of 10×10 and a wall thickness of 0.0015 m. There were 32 turns. The heat released in the inductor was removed by water (in the heavy-alloy loop) or by transformer oil (in the alkali-metal loop). The coolant was supplied to and removed from the inductor through rubber hoses, which ensured reliable electrical insulation.

In the heavy-metal loop, the inductor coil was surrounded by a section of the alloy loop consisting of a pipe (0.05 m in diameter, with a wall thickness of 0.0025 m) made of Kh18N10T stainless steel and having an $\sim$ 30° slope with respect to a vertical line.

The spacing and insulation of the inductor and the pipes was effected by filling the gaps between them with porcelain tubes and asbestos cord.

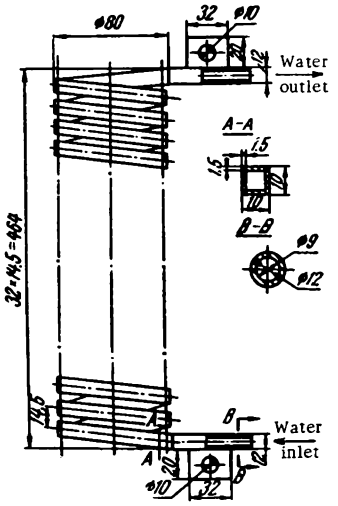


FIGURE 1. Schematic view of the inductor.

The light metal was heated by the inductor in a vertical Field tube (~ 0.5 m long and 0.044 m in diameter) made of Kh18N10T stainless steel. The Field tube was insulated from the inductor with mica and quartz cloth.

The high-frequency setup corresponded to the conventional circuits described in /3, 4/. The voltage at the leads of the high-frequency generator could be varied between 0 and 750 v. This voltage was supplied to an oscillatory circuit consisting of the inductor and a capacitor bank with a capacity of ~ 50 $\mu$f. The power released within the tube walls was directly proportional to the square of the voltage applied to the inductor.

When the experiments were completed, measurements were taken of the power at the generator busbars, the generator voltage and current, the metal and coolant temperatures at the inlet and exit of the generator, and the throughput of the metal and coolant.

During induction heating tests in the heavy-metal loop, the generator load ranged from 25 to 80 kw. We carried out five series of experiments in all, with a total duration of 110 hours. The experiments were carried out at a constant throughput of the alloy (~ 20,000 kg/hour). Depending on the experimental conditions, the alloy temperature ranged from 473 to 773°K.

The experiments in the light-metal loop were carried out at a load of 80 kw, the mean temperature of the metal in the heater was equal to ~ 1123°K, and the throughput of the metal was ~ 2000 kg/hour. The inductor performed under these conditions for ~ 150 hours.

On the basis of the experimentally measured electrical parameters, temperatures, and throughputs, we calculated the amount of heat taken up by the metal in the heater $Q_{us}$, the electrical power of the high-frequency generator $Q_{gen}$ and the heat losses in the inductor $Q_{ind}$.

The relationship between the useful amount of heat removed with the liquid metal and the high-frequency generator power (in the heavy-alloy loop) is shown in Figure 2. The efficiency of the heater (i.e., the ratio of

the above values $Q_{us}/Q_{gen}$ was ~ 75%. The efficiency in the light-metal loop was about 55-60%.

As the generator power was increased, there was an increase in the heat losses both in the inductor and in the current-conducting bars, corresponding to the slight inflection of the curve in Figure 2.

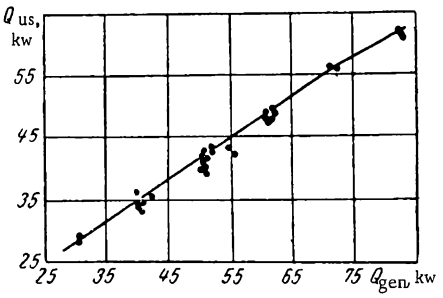


FIGURE 2. Useful amount of heat as a function of the power on the generator terminals.

Our experiments showed that the induction heating method has the advantages of a simple heater (loop tube and inductor) construction, smoothly regulated power and stability of the rate of heat generation, and the absence of any effect of the temperature (of the object to be heated) on the heat generation.

The induction method of heating flowing liquid metals tested by us may be recommended for use in liquid-metal setups.

Bibliography

1. Handbook of Liquid-Metal Coolants. [Russian translation. 1959.]
2. Andreev, P.A., A.A. Kanaev, and E.D. Fedorovich. Zhidkometallicheskie teplonositeli yadernikh reaktorov (Liquid-Metal Coolants for Nuclear Reactors). — Sudpromgiz. 1959.
3. Babat, G.I. Induktsionnyi nagrev metallov i ego promyshlennoe primenenie (Induction Heating of Metals and Its Industrial Uses). 1946.
4. Lozinskii, M.G. Promyshlennoe primenenie induktsionnogo nagreva (Industrial Uses of Induction Heating). 1958.

The Central Boiler-Turbine Institute im. I.I. Polzunov

## *II. HEAT EXCHANGE AND FRICTION RESISTANCE IN PIPES AND CHANNELS OF VARIOUS GEOMETRICAL SHAPES*

B. S. Petukhov and L. I. Roizen

### HEAT EXCHANGE DURING GAS FLOW IN PIPES WITH AN ANNULAR CROSS SECTION

Despite the considerable number of papers on heat transfer in pipes with an annular cross section /1-7/, the problem of the effect of shape (i. e., the internal-to-external pipe diameter ratio) on the heat transfer is still to be solved. For instance, it has been suggested /1, 2/ that the heat transfer in annular pipes be calculated by means of the equations for circular pipes, using the equivalent diameter. In another paper /3/ it is recommended that the effect of geometry be taken into account by the introduction of the parameter $(d_2/d_1)^{0.25}$.

A review /8/ lists 20 equations for the calculation of the heat transfer in annular pipes. Most of these equations are contradictory, and may be used only in special cases. This is caused, to a large extent, by the lack of experimental data obtained under identical conditions over a fairly extensive range of the geometrical parameter, with simultaneous measurement of the heat exchange on both the internal and external walls. Such data are essential for a reliable description of the effect of channel geometry on the heat transfer.*

The following expressions have been derived /9/ for the Nusselt numbers on the inner and outer walls for any heat load ratio:

$$\left.\begin{aligned} \mathrm{Nu}_1 &= \frac{\mathrm{Nu}_{1n}}{1+\frac{q_{w2}}{q_{w1}}\vartheta_1\mathrm{Nu}_{1n}} \\ \mathrm{Nu}_2 &= \frac{\mathrm{Nu}_{2n}}{1+\frac{q_{w1}}{q_{w2}}\vartheta_2\mathrm{Nu}_{2n}} \end{aligned}\right\}, \qquad (1)$$

where $\mathrm{Nu}_{1n}$, $\mathrm{Nu}_{2n}$, $\vartheta_1$, and $\vartheta_2$ are the Nusselt numbers and the dimensionless adiabatic temperatures on the inner and outer walls during unidirectional (asymmetric) heat flux,

$$\mathrm{Nu}_{1n}=\frac{q_{w1}d_e}{(t_{w1}-\bar{t})\lambda}; \qquad \vartheta_2=\frac{(t_{w2}^{ad}-\bar{t})\lambda}{q_{w1}d_e} \quad (q_{w2}=0); \qquad (2)$$

$$\mathrm{Nu}_{2n}=\frac{q_{w2}d_e}{(t_{w2}-\bar{t})\lambda}; \qquad \vartheta_1=\frac{(t_{w1}^{ad}-\bar{t})\lambda}{q_{w2}d_e} \quad (q_{w1}=0) \qquad (3)$$

* This gap has been filled to some extent by the recent paper of Kays and Leung /10/.

($t_{w1}, t_{w2}$ are the local values of the inner and outer (heated) wall temperatures; $t_{w1}^{ad}$, $t_{w2}^{ad}$ are the local temperatures of the adiabatic walls; $\bar{t}$ is the mean calorimetric temperature of the liquid).

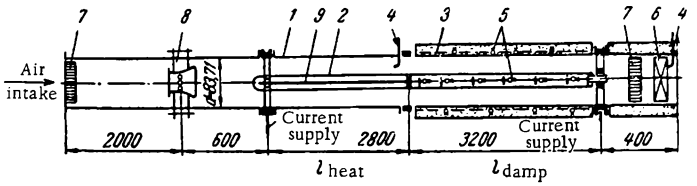


FIGURE 1. Schematic view of the experimental section.

1 — outer tube; 2 — inner tube; 3 — strip heater; 4, 5 — thermocouples; 6 — mixer; 7 — rectifier grid; 8 — Venturi tube; 9 — current-conducting bar.

Equation (1) is valid for both laminary and turbulent flow at any distance from the inlet. Using this equation it becomes possible to reduce the experimental study of heat transfer in annular pipes to the measurement of $Nu_{1n}$ and $\vartheta_2$ at $q_{w2} = 0$, and of $Nu_{2n}$ and $\vartheta_1$ at $q_{w1} = 1$.

We conducted an experimental study of the heat transfer during turbulent flow of air in annular pipes in the geometrical parameter ($d_1/d_2$) range between 0.07 and 0.84. The main measurements were made with unidirectional flow of the heat, i.e., at a constant heat flux density on one of the walls (the inner or outer) while the other wall was insulated. The heat transfer coefficient was measured on the heated walls, while the adiabatic wall temperature was determined on the thermally-insulated wall. Using equation (1) and the above data, it is possible to calculate the heat transfer coefficients on each of the walls during their simultaneous heating for any heat flux density ratio on the walls. In order to check the above ratios, some of the experiments were carried out with simultaneous heating of both walls.

The experimental section (Figure 1), formed from two concentric tubes, consisted of damping and heating sections. The geometry of the annular channel was changed by changing the inner tube. The study was carried out on six annular channels and one circular pipe, the geometrical parameters of which are tabulated below:

Geometrical characteristics of the channels

| $d_1 \cdot 10^3$, mm | $d_2 \cdot 10^3$, mm | $d_1/d_2$ | $d_e = (d_2 - d_1) \cdot 10^3$, mm | $l_{heat}/d_e$ | $l_{damp}/d_e$ |
|---|---|---|---|---|---|
| 0 | 83.71 | 0 | 83.71 | 38 | 34 |
| 6.01 | 83.71 | 0.0718 | 77.70 | 40 | 36 |
| 12.00 | 83.71 | 0.143 | 71.71 | 44 | 39 |
| 20.47 | 83.71 | 0.244 | 63.24 | 50 | 45 |
| 45.70 | 83.71 | 0.546 | 38.01 | 83 | 74 |
| 57.90 | 83.71 | 0.692 | 25.81 | 122 | 108 |
| 70.40 | 83.71 | 0.841 | 13.31 | 83 | 30 |

Symbols: $d_1$ — external diameter of the inner tube; $d_2$ — internal diameter of the outer tube; $d_e$ — equivalent diameter of the annular pipe; $l_{heat}/d_e$, $l_{damp}/d_e$ — the lengths of the heated and damping sections respectively.

The external brass tube (with a wall thickness of 0.003 m) was heated by an electrical heater of nichrome strip (with a cross section of $(10 \times 0.8) \cdot 10^{-3}$ m) uniformly wound on the tube surface over micanite cloth. The external surface of the heater was coated with refractory clay and thermally insulated with glass wool.

The inner stainless steel (1Kh18N9T) tubes, with a wall thickness of $(0.2\text{-}0.5) \cdot 10^{-3}$ m were fitted into special sprockets at the ends and suspended at one point (at the end of the damping section) by means of 0.001 m wire. In addition, the larger-diameter tube was centered more accurately by supporting it with two pins in the middle of the heated section, while the smaller-diameter tube was stretched with a spring. The inner tubes were heated directly by current passing through their walls. The current was conducted to the walls by means of the sprockets, and from the left sprocket to the heated section by means of a copper rod. The method used to connect the sprockets with the inner tubes allowed for free expansion of the latter.

A rectifier grid was fitted at the exit from the heated section, and a helical mixer was fixed behind it.

The wall temperatures of the external and internal tubes were measured with copper-constantan thermocouples. On the outer tube walls, the thermocouples were inserted into copper capillaries (soldered into the wall) at twelve points over the length. The thermocouples used to measure the wall temperature of the inner tube were mounted on the inside wall of the tube at thirteen points over its length and were separated from each other by cork partitions. The air temperature was also measured with thermocouples fitted at the inlet to the heated section and behind the mixing device. The thermoelectromotive force of the thermocouples was measured with a potentiometer of the R-375 type.

Alternating current from a voltage stabilizer was supplied to the electrical heater of the external tube. The heater power was measured with an astatic wattmeter of the 0.2 precision class. Direct current from a motor-generator set was supplied to the inner tube. The current strength was measured with the aid of a calibrated shunt, while the voltage drop on the shunt and the tube was measured with a potentiometer.

The air was driven into the experimental section by a high-pressure fan, first passing through the rectifier grid and the shortened Venturi tube which served to measure the throughput.

The Venturi tubes (we used two tubes for the various throughput ranges) were calibrated with water in advance. Special experiments were also carried out to determine the heat losses from the external tube to the surroundings. The heat losses usually did not exceed 10%.

Two series of experiments were carried out with each annular tube: 1) heating of the inner wall while the outer wall was thermally insulated; 2) heating the outer wall while the inner wall was insulated. Some of the experimental data were collected during simultaneous heating of both walls, when the heat flux densities on them were the same.

In order to check the experimental setup, we also measured the heat transfer during air flow in a circular pipe (the outer tube was used for that purpose) without an inner tube.

All measurements were taken at an equilibrium thermal state of the system. In all experiments the wall temperatures and the temperature gradients between the walls and the air were maintained approximately

the same, and were respectively equal to $t_w$ = 333-353°K and $t_w - \bar{t}$ = = 30-50°K. The difference between the amount of heat calculated from the electrical power supplied and from the changes in the enthalpy of the air at the inlet and outlet usually did not exceed 3%.

In the processing of the experimental data, the heat flux density associated with convection on the outer and inner tube walls was determined from the equations:

$$q_{w1} = \frac{Q_1 - Q_{rad}}{\pi d_1 l_{heat}}; \quad (4)$$

$$q_{w2} = \frac{Q_2 - Q_{rad} - Q_n}{\pi d_2 l_{heat}}, \quad (5)$$

where $Q_1$ and $Q_2$ are the electrical power released on the inner and outer tubes, respectively; $Q_n$ is the heat loss from the outer tube to the surroundings; $Q_{rad}$ is the heat flux due to radiation. In calculating $Q_{rad}$, it was assumed that the blackness of the inner (1Kh18N9T steel) and outer (brass) tube surfaces was $\varepsilon_1$ = 0.3 and $\varepsilon$ = 0.06, respectively. The magnitude of $Q_{rad}$ usually did not exceed 5% of the power released.

Equations (4) and (5) are valid at some distance from the inlet of the heated pipe section. When calculating $q_{w_2}$ near the inlet, we took into account the changes in the heat flux along the wall caused by the thermal conductivity. At $x/d_e \geqslant 2$, the magnitude of that scattering did not exceed 8% (the section of length $2d_e$ from the inlet was not taken into account). In calculating $q_{w_1}$, the changes in the heat flux were not taken into account since their magnitudes did not exceed 0.5%.

The temperatures of the outer surface of the inner tube and of the inner surface of the outer tube, $t_{w_1}$ and $t_{w_2}$, were obtained from measurements corrected for the temperature drop on the wall (for the inner tube), and for the insertion depth of the thermocouples (for the outer tube). These corrections did not exceed 0.15°C.

The mean calorimetric temperature of the air at a given distance from the beginning of the heated section was calculated using the equation

$$\bar{t} = t_0 + \frac{Q}{Gc_p} \frac{x}{l_{heat}}, \quad (6)$$

where $Q = Q_1$ when only the inner tube was heated ($q_{w_2} = 0$), $Q = Q_2 - Q_n$ when only the outer tube was heated ($q_{w_1} = 0$), and $Q = Q_1 + Q_2 - Q_n$ when both tubes were heated at the same time; $t_0$ is the air temperature at the inlet; $G$ and $c_p$ are the throughput and the heat capacity of air.

The values of $Nu_{1n}$, $Nu_{2n}$, $\vartheta_1$, and $\vartheta_2$ were calculated using equations (2) and (3), while Re was calculated using the equation

$$Re = \frac{Gd_e}{f\mu} \quad (7)$$

where $f$ is the cross-sectional area of the annular pipe.

The physical properties of air were taken as corresponding to the mean calorimetric temperature at the given section.

An evaluation of the accuracy of the experimental data showed that the maximum relative error in the determination of the Nusselt numbers was about 4%, and in the determination of $\vartheta$, about 8%.

As $x/d_e$ was increased, the local values of $Nu_{1n}$, $Nu_{2n}$, $\vartheta_1$, and $\vartheta_2$ approached (asymptotically) a fixed value known as the limiting value. The limiting values are denoted below as $Nu_{1n\infty}$, $Nu_{2n\infty}$, $\vartheta_{1\infty}$, and $\vartheta_{2\infty}$.

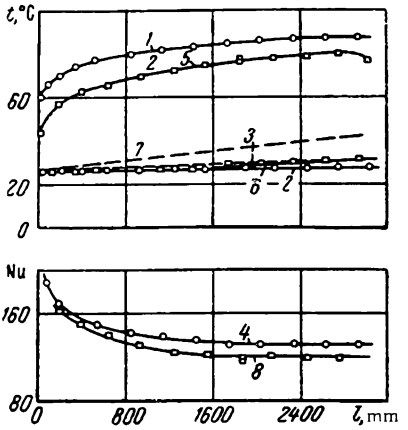


FIGURE 2. Changes in the temperature of the heated and adiabatic walls, the air temperature, and the Nu numbers over the length of an annular pipe with $d_1/d_2 = 0.244$.

1, 2, 3, 4 — respectively $t_{w_1}$, $t_{w_2}^{ad}$, $\bar{t}$, and $Nu_1$ at $q_{w_2} = 0$, $Re = 63 \cdot 10^3$; 5, 6, 7, 8 — $t_{w_2}$, $t_{w_1}^{ad}$, $\bar{t}$, and $Nu_2$ at $q_{w_1} = 0$, $Re = 67.5 \cdot 10^3$.

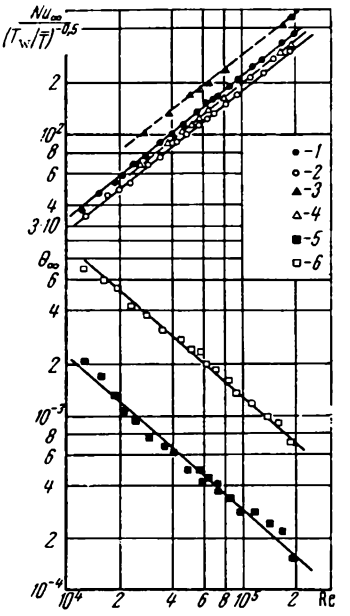


FIGURE 3. Limiting values ($Nu_\infty$ and $\vartheta_\infty$) as a function of Re for an annular pipe with $d_1/d_2 = 0.244$.

1 — $Nu_{1n\infty}$; 2 — $Nu_{2n\infty}$; 3, 4, — $Nu_{1\infty}$ and $Nu_2$ at $q_{w1}=q_{w2}$ from the results of direct measurements; 5 — $\vartheta_{2\infty}$; 6 — $\vartheta_{1\infty}$. The broken line represents values calculated from (1) for $q_{w1} = q_{w2}$.

Since the tubes were of a finite length and the experimental data somewhat dispersed, the limiting values of $Nu_{1n\infty}$ and $Nu_{2n\infty}$ were determined from the mean temperatures on a certain section at some distance from the inlet, within which the local values of the Nusselt number Nu changes by not more than 3%. This section was 1.2 m from the point where heating began, and measured about 1.6 m in length. The limiting values of $\vartheta_{1\infty}$ and $\vartheta_{2\infty}$ were determined in exactly the same manner. In this case, the section for which the mean values were taken was 1.8 m from the point where heating began and measured 1 m in length. Within that section, the deviations from the local values did not exceed 12% for channels 2 and 3, and 6% for the remaining channels (see Table).

In order to exclude the effect of variable physical properties, the experimental values of the Nusselt numbers were corrected by introducing the correction factor $(T_w/\bar{T})^{0.5}$ and were thus converted to values corresponding to a temperature factor equal to unity.

The processing of the experimental data on heat transfer in a circular pipe (without an inner tube) yielded the equation

$$Nu_{cp\infty} = 0.0186\ Re^{0.8}, \qquad (8)$$

which describes the experimental data with an accuracy of ±5% and is in agreement (with the same accuracy as above) with the empirical equations of Mikheev and MacAdams as well as with theoretically calculated results /11/.

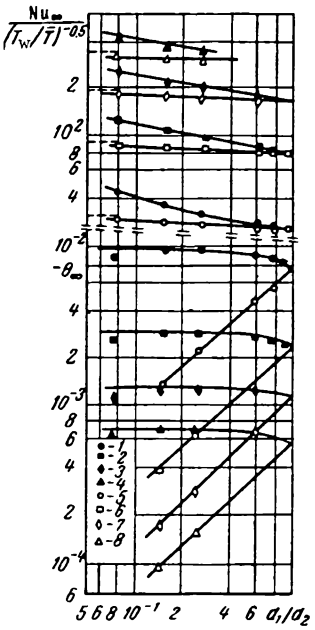


FIGURE 4. Limiting values $Nu_\infty$ and $\vartheta_\infty$ in annular pipes as a function of $d_1/d_2$.

1, 5 — Re = $10^4$; 2, 6 — Re = $= 4\cdot10^4$; 3, 7 — Re = $10^5$; 4, 8 — Re = $2\cdot10^5$ (1-4 — $Nu_{1n\infty}$, $\vartheta_{1\infty}$; 5-8 — $Nu_{2n\infty}$, $\vartheta_{2\infty}$). The broken lines represent the values of $Nu_\infty$ for a circular pipe.

In our experimental studies of the changes in the temperatures of the heated and adiabatic walls, the mean calorimetric temperature of the air, and the local Nu numbers over the length of an annular pipe with $d_1/d_2 = 0.244$ during the heating of one wall only (outer or inner, see Figure 2) we found that at $x/d_e \geqslant 20$ the $Nu_{1n\infty}$ and $Nu_{2n\infty}$ numbers and the temperature differences $t_{w1}^{ad} - \bar{t}$ and $t_{w2}^{ad} - \bar{t}$ assumed constant values.

The values of $Nu_{1n\infty}$ and $Nu_{2n\infty}$ were proportional to $Re^{0.8}$. A similar dependence was observed for the remaining annular pipes except for the cases of the inner walls of the pipes with $d_1/d_2 = 0.0718$ and 0.143. For the first of these, the value of $Nu_{1n\infty}$ was approximately proportional to $Re^{0.76}$, and for the second, to $Re^{0.78}$. For this reason, the difference between the limiting values $Nu_{1n\infty}$ and $Nu_{2n\infty}$ for the pipes with $d_1/d_2 = 0.0718$ and 0.143 increases with increasing Re. The limiting values $\vartheta_{1\infty}$ and $\vartheta_{2\infty}$ were proportional to $Re^{-0.88}$.

The calculated $Nu_{1\infty}$ and $Nu_{2\infty}$ for equal values of $q_{w1}$ and $q_{w2}$ (Figure 3) are in good agreement with directly measured values (as should be expected).

The changes in the limiting values $Nu_{1n\infty}$, $Nu_{2n\infty}$, $\vartheta_{1\infty}$, and $\vartheta_{2\infty}$ as a function of $R_1 = d_1/d_2$ are shown in Figure 4. As is evident from the figure, the values of $Nu_{n\infty}$ and $-\vartheta_\infty$ on the inner wall were higher than on the outer wall. As $R_1$ was increased, the difference between the above values decreased, reaching zero at $R_1 = 1$, i.e., in the case of a flat tube with one-side heating. At $R_1 \to 0$, the value of $Nu_{2n\infty}$ approaches the value of the same number for a circular pipe (the broken lines).

This result can readily be explained on the basis of the available data on the velocity profile during turbulent flow in annular pipes /12, 13/. The velocity profile in annular pipes is asymmetric with respect to the walls —

the point of maximum velocity is shifted in the direction of the inner wall, and thus the velocity gradient on the inner wall is always larger than on the outer wall, and the difference between them increases as $d_1 d_2$ is reduced. Hence, $Nu_{1n\infty} \geqslant Nu_{2n\infty}$ and the difference between them also increases with decreasing $d_1/d_2$.

In order to derive generalized equations for the heat transfer during turbulent gas flows in pipes with annular cross sections, we used our own data in conjunction with those of Doroshchuk and Frid /3/, and of Kays and Leung /10/.

Doroshchuk and Frid measured the heat transfer to air in annular pipes with $d_1/d_2$ = 0.38-0.83 and $l_{heat}\, d_e$ = 35-125 in experiments in which only the inner wall was heated, and in which the value of Re ranged from $2 \cdot 10^4$ to $5.5 \cdot 10^4$.

Kays and Leung /10/ investigated the heat transfer to air in pipes with $d_1/d_2$ = 0.193-0.50 and $l_{heat}/d_e$ = 23-70 in experiments in which both the inner and outer walls were heated, and the values of Re ranged from $10^4$ to $1.6 \cdot 10^5$.

In /3/, measurements were made only of the local heat transfer at a constant heat flux density on the walls; in /10/ the local adiabatic wall temperatures were also measured. The results of these measurements are apparently the most reliable (among the investigations carried out with gases), as indicated, in particular, by the fairly good agreement between the results. Hence, we used only those data in our generalization. We took into account only those data for the range of established thermal and hydrodynamic stabilization, i.e., the limiting values of the Nusselt numbers and the adiabatic wall temperatures.*

The dependence of $Nu_{1n\infty}/Nu_{cp\infty}$ and $Nu_{2n\infty}/Nu_{cp\infty}$ (where $Nu_{cp\infty}$ was calculated from equation (8) using the equivalent diameter**) on $d_1 d_2$ is shown in Figure 5. Equation (8) describes with satisfactory accuracy both our experimental data, and the data of /10/ on the heat transfer in a circular pipe.

Our experimental data and the results of /10/ are in very good agreement, while the results of /3/ are 10-12% lower.

For all investigated pipes, our results and the results of /10/ are described with an accuracy of ±5% by the equations

$$\frac{Nu_{1n\infty}}{Nu_{cp\infty}} = 0.86 \times (d_1/d_2)^{-0.16}\zeta, \qquad (9)$$

$$\frac{Nu_{2n\infty}}{Nu_{cp\infty}} = 1 - 0.14 \times (d_1/d_2)^{0.6}, \qquad (10)$$

where $\zeta = 1 + 7.5\left(\frac{d_2/d_1 - 5}{Re}\right)^{0.6}$ at $d_1/d_2 < 0.2$, and $\zeta = 1$ at $d_1/d_2 \geqslant 0.2$ ($\xi$ is a correction

* In /10/, because of the short length of the working section, the limiting values of the Nusselt number were found by extrapolation of the experimental data over the length, while the limiting adiabatic wall temperatures are not reported at all.

** Each point on Figure 5 corresponds to a series of experiments at various Re and at $d_1/d_2$ = const.

factor accounting for the fact that according to our data, the exponent of the Re number was smaller than 0.8 at $d_1/d_2 \leqslant 0.143$).

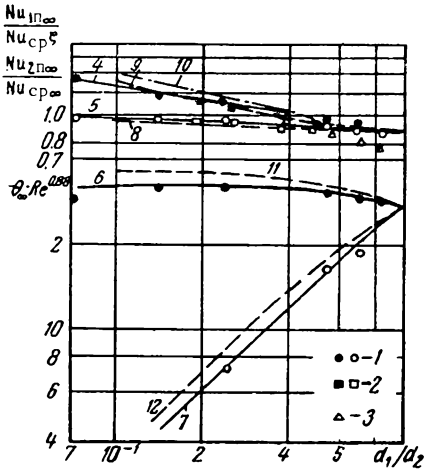


FIGURE 5. Generalization of the experimental data on heat transfer in pipes with an annular cross section.

1 — the results of our experiments; 2, 3 — experimental data of /10/ and /3/, respectively (the dark points represent $Nu_{1n\infty}$, $\vartheta_{1\infty}$; the light points represent $Nu_{2n\infty}$, $\vartheta_{2\infty}$); 4, 5, 6, 7 — equations (9), (10), (11), (12), respectively. Results of theoretical calculations (10): 8 — $Nu_{2n\infty}$; 9, 10 — $Nu_{1n\infty}$ at $Re > 3\cdot10^4$ and $Re = 10^4$; 11 — $\vartheta_{1\infty}$; 12 — $\vartheta_{2\infty}$.

Equation (9) may be used in the range $0.07 \leqslant d_1/d_2 \leqslant 1$, while (10) may be used in the range $0 \leqslant d_1/d_2 \leqslant 1$. Both equations are valid in the range $10^4 \leqslant Re \leqslant 3\cdot10^5$ at Pr equal to $\sim 0.7$.

In the case of a tube with $d_1/d_2 = 1$ (flat tube with heating from one side) equations (9) and (10) yield $Nu_{1n\infty} = Nu_{2n\infty} = 0.86\,Nu_{cp\infty}$. Thus, equations (9) and (10) satisfy the conditions of finite transitions.

The results of a theoretical calculation of heat transfer in annular pipes (based on the data of /10/) are also shown in Figure 5. They are in good agreement with the experimental data, except for the values of $Nu_{1n\infty}$ at $Re < 3\cdot10^4$, which are higher than the experimental values (at $Re = 10^4$ the discrepancy is as high as 20%). The dependence of $\vartheta_{1\infty}\,Re^{0.88}$ and $\vartheta_{2\infty}\,Re^{0.88}$ on $d_1/d_2$ (derived from our experimental data*) is also shown in Figure 5. The experimental results are satisfactorily described by the equations

$$\vartheta_{1\infty} = 32\,[0.16\,(d_1/d_2)^2 - 1]\,Re^{-0.88}\,, \qquad (11)$$

$$\vartheta_{2\infty} = \vartheta_{1\infty}\,d_1/d_2.^{**} \qquad (12)$$

* No other experimental data are available.

** Equation (12) is derived from the integral equations obtained in /9/.

These equations are valid for the same ranges as equations (9) and (10). In the case of $d_1/d_2 = 1$ (i.e., for a flat tube with heating from one side) $\vartheta_{1\infty}=\vartheta_{2\infty} = -26.9\,\mathrm{Re}^{-0.58}$.

The results of a theoretical calculation of the adiabatic wall temperatures, based on the data of /10/ (Figure 5), show that discrepancy between theory and experiment does not exceed 10%.

Equations (9) to (12) make it possible to calculate the heat transfer and adiabatic wall temperatures in the case of one-directional heating (external or internal). In the case of heat transfer through both walls (at any ratio of heat flux density), the heat transfer coefficients on the inner and external walls are calculated using equation (1).

Bibliography


1. Averin, E.K., A.Ya. Inayatov, N.S. Kondrat'ev, V.A. Kusikov, M.A. Mikheev, and O.S. Fedynskii. — In sbornik: "Teploperedacha i teplovoe modelirovanie," Izd. AN SSSR. 1959.
2. Mikheev, M.A. — In sbornik: "Teploperedacha i teplovoe modelirovanie," Izd. AN SSSR. 1959.
3. Doroshchuk, V.E. and F.P. Frid. — In sbornik: "Teploobmen pri vysokikh teplovykh nagruzkakh i drugikh spetsial'nykh usloviyakh," Gosenergoizdat. 1959.
4. Davis, E.S. Trans. of ASME, Vol. 65. 1943.
5. Monrad, C.C. and J.F. Pelton. Trans. Amer. Inst. Chem. Engrs., Vol. 38. 1942.
6. Walger, O. Chem. Ing.-Techn., Vol. 25, Nos. 8, 9. 1953.
7. Stephan, K. Chem. Ing.-Techn., Vol. 34, No. 3. 1962.
8. Quirrenbach, F.J. Allgemeine Wärmetechnik, Vol. 9, No. 13. 1960.
9. Petukhov, B.S. and L.I. Roizen. — IFZh, No. 3. 1963.
10. Kays, W.M. and E.Y. Leung. Int. J. Heat Mass Transfer, Vol. 6, No. 7. 1963.
11. Petukhov, B.S. and V.N. Popov. — Teplofizika Vysokikh Temperatur. No. 1. 1963.
12. Knudsen, J.G. and D.L. Katz. Fluid Dynamics and Heat Transfer. New York. 1958.
13. Rothfus, R.R., C.C. Monrad, and V.E. Senecal. — Ind. Engrng. Chem., Vol. 48, No. 12. 1950.



The Moscow Power Institute
The All-Union Institute of
Electrical Engineering im.
V.I. Lenin

P. I. Puchkov and O. S. Vinogradov

# HEAT TRANSFER AND HYDRAULIC RESISTANCE IN ANNULAR CHANNELS WITH SMOOTH AND ROUGH HEAT TRANSFER SURFACES

The use of annular channels with inner heat transfer surfaces in heat exchangers and other thermal equipment makes it necessary to define the recommendations for heat transfer calculations more accurately. Dimensionless equations of the type

$$\mathrm{Nu} = C\,\mathrm{Re}^m \mathrm{Pr}^n, \tag{1}$$

which are commonly used for circular pipes, cannot be used for the unambiguous determination of heat transfer in any smooth annular apertures. One of the conditions for the application of dimensionless equations is the geometrical similarity of the constructions for which the equation is valid. Thus, while smooth circular tubes (of sufficient length) are geometrically similar at any diameter, annular apertures with various external-to-internal diameter ratios are generally not similar. Hence, the equation must comprise an additional factor to take into account the relative dimensions of the annular aperture $f(d_2/d_1)$.

Thus, the equation of heat transfer in an annular aperture has the general form

$$\mathrm{Nu} = f(\mathrm{Re},\ \mathrm{Pr},\ d_2/d_1) \tag{2}$$

or

$$\mathrm{Nu} = C\,\mathrm{Re}^m \mathrm{Pr}^n f(d_2/d_1). \tag{3}$$

The results of many investigations on heat transfer in annular apertures differ noticeably both in their absolute values (i. e., the values of the coefficient C) and the nature of the function $f(d_2/d_1)$.

In spite of the difference between the experimental data (which may be attributed to differences in experimental conditions), two contradictory general principles exist: the first confirms the fact that the heat transfer in annular channels with internal heating is independent of the aperture dimensions, while the second indicates that the heat transfer decreases with decreasing relative aperture dimensions.

In order to obtain additional experimental data, we carried out special experiments on the heat transfer and resistance in smooth annular channels at $d_2/d_1 = 1.185 - 8.24$.

The geometrical parameters of the channels are given in Table 1.

TABLE 1. Geometrical parameters of the working sections

| Calorimeter diameter, $d_1$, m | Channel diameter, $d_2$, m | $d_2/d_1$ | Working section length $L$, m | Equivalent diameter $d$, m | Heat transfer surface, $F$, $m^2$ | Cross section of the aperture $s$, $m^2$ | $L/d$ | $L/d_1$ |
|---|---|---|---|---|---|---|---|---|
| 0.054 | 0.115 | 2.13 | 1.0 | 0.061 | 0.1695 | $8.09 \cdot 10^{-3}$ | 16.4 | 18.5 |
| 0.054 | 0.107 | 1.98 | 1.0 | 0.053 | 0.1695 | $6.7 \cdot 10^{-3}$ | 18.9 | 18.5 |
| 0.054 | 0.098 | 1.82 | 1.0 | 0.044 | 0.1695 | $5.24 \cdot 10^{-3}$ | 22.7 | 18.5 |
| 0.054 | 0.092 | 1.70 | 1.0 | 0.038 | 0.1695 | $4.34 \cdot 10^{-3}$ | 26.4 | 18.5 |
| 0.054 | 0.076 | 1.41 | 1.0 | 0.022 | 0.1695 | $2.24 \cdot 10^{-3}$ | 45.5 | 18.5 |
| 0.054 | 0.064 | 1.185 | 1.0 | 0.010 | 0.1695 | $0.925 \cdot 10^{-3}$ | 100.0 | 18.5 |
| 0.013 | 0.040 | 3.80 | 1.5 | 0.027 | 0.0530 | $1.12 \cdot 10^{-3}$ | 55.6 | 115.0 |
| 0.013 | 0.064 | 4.92 | 1.5 | 0.051 | 0.0530 | $3.09 \cdot 10^{-3}$ | 29.4 | 115.0 |
| 0.013 | 0.107 | 8.24 | 1.5 | 0.094 | 0.0530 | $8.85 \cdot 10^{-3}$ | 16.0 | 115.0 |

Despite their simple construction and the possibility they present of obtaining true countercurrent flows, annular channels have a marked drawback, namely, the heat transfer coefficient obtained with them is noticeably lower than in the case of crosswise flow. Hence, use of annular channels requires an increase in the heat transfer rate.

One way to obtain such an increase in the heat transfer rate is to use roughened surfaces.

The effect of surface roughness on the heat transfer and hydraulic resistance has been the subject of many investigations. Seleznev /2/, Teverovskii /3/, Nunner /4/, Grass /5/, and Dipprey and Sabersky /6/ have published the results of their studies on surface roughness of various types and degrees: hemispherical protrusions, pointed or truncated pyramids /2/, pointed triangular teeth /3/, rings of various shapes, dimensions, and intervals /4/, diaphragms of various diameters, intervals and edge shapes /5/. The authors of /6/ made an attempt to produce the so-called "sandy" roughness of Nikuradze, by electroplating nickel on a cylinder with sand of various particle size glued to its surface.

Several investigators /7-12/ measured heat transfer and hydraulic resistance in annular apertures with roughened internal surfaces.

Walker /7/ studied roughness of various types (rectangular, triangular) and dimensions. However, since he neither gives tabulated data nor plots experimental points in his diagrams, it is not possible to analyze the experimental results.

Bauer /8/ studied the effect of roughness (rectangular transverse fins and triangular grooves) spaced at various intervals along the pipe axis.

Kattchec and Mackevicz /11/ used a naphthalene model (based on the analogy between heat and mass transfer) to determine the local heat transfer over the perimeter of a single roughness element in the form of a transverse rectangular fin. Their results agree qualitatively with our concepts of the nature of heat transfer in the case of nonstreamlined bodies.

Sheriff, Gumley, and France /12/ also studied the effect of rectangular-fin roughness (of various fin dimensions and intervals). Their results were plotted as a function of the heat transfer and the ratio of the height of the roughness to the thickness of the laminary sublayer (the latter having been calculated for a circular pipe).

TABLE 2. Geometrical dimensions of roughened surfaces

| Type of roughness | Height of roughness, $h \cdot 10^3$, m | Interval between roughness elements, $s \cdot 10^3$, m | Mean volume diameter of calorimeter, $d_m \cdot 10^3$, m | Channel diameter, $d_c \cdot 10^3$, m |
|---|---|---|---|---|
| Triangular | 0.50 | 2 | 53.10 | 106 |
| " | 1.00 | 2 | 52.40 | 106 |
| " | 1.00 | 3 | 52.25 | 106 |
| " | 1.50 | 2 | 51.60 | 106 |
| " | 2.50 | 2 | 50.50 | 106 |
| " | 0.50 | 5 | 53.00 | 106 |
| " | 1.00 | 5 | 52.20 | 106 |
| " | 2.50 | 5 | 50.30 | 106 |
| " | 2.50 | 5 | 50.30 | 81 |
| " | 2.50 | 5 | 50.30 | 76 |
| " | 2.50 | 5 | 50.30 | 64 |
| " | 1.00 | 10 | 52.15 | 106 |
| "Transverse" roughness | 1.00 | 5 | 52.60 | 106 |
| Forward flow | 1.00 | 5 | 52.60 | 76 |
| " " | 1.00 | 5 | 52.60 | 64 |
| Reverse flow | 1.00 | 5 | 52.60 | 106 |
| Coiled wire, $d = 1.2 \times 10^{-3}$ m | 1.20 | 50 | 54.10 | 106 |
| " " " " | 1.20 | 10 | 54.30 | 106 |
| " " " " | 1.20 | 5 | 54.50 | 106 |
| Coiled wire, $d = 3.5 \times 10^{-3}$ m | 3.50 | 100 | 54.15 | 106 |
| " " " " | 3.50 | 50 | 54.50 | 106 |
| " " " " | 3.50 | 10 | 56.00 | 106 |
| Knurled surface | 0.82 | 2.25 | 50.00 | 106 |
| Multiple-thread spiral, $h = 1 \cdot 10^{-3}$ m | 1.00 | 11.5 | 52.20 | 106 |

However, the above studies are clearly insufficient for a complete understanding of the effect of roughness on heat transfer and hydraulic resistance.

In order to obtain additional data and to establish the empirical relationships, we carried out experiments on heat transfer and hydraulic resistance in annular apertures with roughened internal surfaces of various types and dimensions (there were 24 such surfaces). The geometrical characteristics are shown in Table 2.

## Experimental setup and working section

The heat transfer studies in smooth annular apertures were carried out in a setup having a closed circulation loop, at an air pressure $P = (1\text{-}3) \cdot 1.02 \cdot 10^{-4}$ n/m$^2$.

The air temperature was measured on the diaphragms at the inlet and outlet of the working section with chromel-alumel thermocouples (0.0003 m in diameter). The air-flow rate through the diaphragm was determined from the pressure difference measured using a differential manometer filled with distilled water or mercury (depending on the magnitude of the

gradients). The diaphragm was calibrated in advance with the aid of a Prandtl tube. The pressure drop in the working section was determined by measuring the static pressures at the inlet and outlet cross sections. On each section, four static openings (0.6-1 mm in diameter) were connected to each other and to the differential manometer.

The centrifugal blower was driven by a d. c. motor, and thus the rotational speed could be smoothly varied over a fairly wide range.

The working section consisted of a steel pipe of diameter $d_2$, into which was inserted a smooth or roughened calorimeter made of smooth cylindrical steel or duralumin tubes 0.054 m in diameter, with heating elements (nichrome wire coils) inserted in them. The calorimeters were heated by current from a d. c. generator*, using copper buses and flexible conducting wire. The current strength and the voltage drop on the calorimeter were measured with portable laboratory instruments of the M-16 type (precision class 0.2).

The temperature of the calorimeter surface was determined from the readings of 7 to 28 thermocouples. Two types of thermocouples were used: chromel-alumel, with a diameter of 0.0003 m (spot-welded to the steel pipe with the aid of the discharge of a special capacitor) and copper-constantan, with a diameter of 0.00015 m (inserted into the shell of the calorimeter to a depth of 0.0005 m). The difference between the thermocouple readings in the above two cases did not exceed 1 %. The dispersion of results obtained for one section did not exceed 1.5%. The connecting wires running to the thermocouples passed through grooves cut in the calorimeter shell. The grooves with the thermocouples were cemented with dental cement. The cold junctions were immersed in thawing ice. Thermometer readings were taken by a potentiometric method. The calorimeter ends were insulated with textolite sleeves, and the calorimeter was centered (with respect to the channel axis) at the upper and lower grids with the aid of adapters. The whole working channel was insulated with asbestos cord.

In the cases of $d_2/d_1 = 3.08$, 4.92, and 8.24, the inner heat-transfer surface consisted of a stainless-steel tube $13/2 \cdot 10^{-3}$ m in diameter, which was inserted in channels 0.04, 0.064, and 0.107 m in diameter and heated by a. c. from the line, using an AOMK-type autotransformer. Copper-constantan thermocouples 0.00015 m in diameter were fastened to the surface and led out to the ends through grooves.

A conventional tube (produced commercially) having a slightly roughened surface was used in the experiments. After additional treatment, the cleanness of the surface was checked by means of an MIS-11 microscope (used to determine the absolute magnitude of surface roughness).

The maximum heights of the surface protrusions determined by the above method were much lower than the allowed heights (according to /8/); hence, the tube surface could be regarded as being hydraulically smooth.

## Smooth annular apertures

The experiments** were carried out with a calorimeter surface heated to $t_w = 373 \pm 10°K$. The air temperature was varied within the range

* The d. c. generator regulated the electric power supplied to the calorimeter smoothly and accurately.

** The technicians N. M. Burgvits, I. N. Kovaleva, S. N. Shuraeva, S. N. Yakovleva, and V. N. Andronova took part in the experimental work and in the processing of the experimental data.

$t_a$ = 298 — 318°K. The values of the temperature factor, $\frac{T_w}{T_a}$, ranged from 1.14 to 1.25. The experimental data were processed in terms of similarity numbers:

a) Nusselt's

$$\mathrm{Nu} = \frac{\alpha d}{\lambda} = \frac{Qd}{F \Delta t \lambda} ;$$

b) Reynolds'

$$\mathrm{Re} = \frac{wd}{\nu} = \frac{Gd}{\rho g \Omega \nu} ,$$

where $Q = UI$ is the heat generated by the heating element, w; $F = \pi d_1 L$ is the heat transfer surface of the calorimeter, $m^2$; $t_w$ is the arithmetic mean temperature of the calorimeter surface, °K; $t_s = \frac{t_{in} + t_{out}}{2}$ is the stream temperature, taken as the arithmetic mean of the temperatures at the inlet and outlet, °K; $G \frac{9.81}{3600}$ is the mass flow rate of air, measured by the diaphragm, n/sec; $w$ is the mean velocity in the channel, m/sec; $\lambda \cdot 1.163 \frac{w}{M°K}$ ; $\nu \frac{1}{3600} \frac{M^2}{sec}$ ; $\rho \cdot 9.81 \frac{n \cdot sec^2}{M^4}$ ; $C_p \left[ \frac{kcal}{kg°K} \right]$ are the thermal conductivity and kinematic viscosity coefficients, the density, and the heat capacity of air, respectively, referred to the mean temperature and pressure in the working channel.

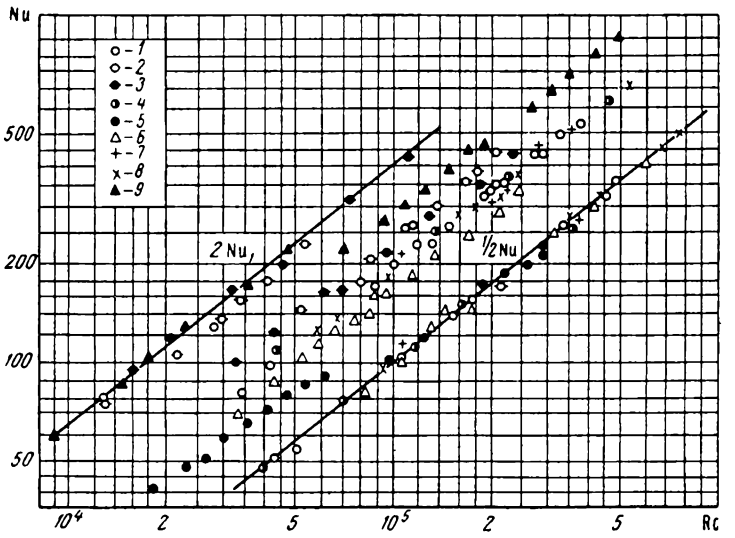


FIGURE 1. Heat transfer in smooth annular channels. The experimental data were processed according to the equation $Nu_1 = 0.02, Re_1^{0.8}$ at $d = d_2 - d_1$.
1 — $d_2/d_1$ = 1.82; 2 — 1.92; 3 — 3.08; 4 — 2.13; 5 — 1.185; 6 — 1.41; 7 — 1.98; 8 — 1.7; 9 — 8.24.

Since some of the experiments were carried out on relatively short heated sections $\left(\frac{L}{d}=16-115\right)$, we introduced a correction factor $\varepsilon = f(\mathrm{Re}, L/d)$ (in accordance with /14/) in the case of apertures with $\frac{L}{d}<50$.

Figure 1 shows marked stratification of the experimental points for the various channels; the stratification becomes more pronounced as $\frac{d_2}{d_1}$ is reduced. A geometric factor $\left(\frac{d}{d_1}\right)^{0.2}$ is introduced in order to obtain an single-valued relationship. The points recalculated by taking into account the above parameter in the form $\frac{\mathrm{Nu}}{(d/d_1)^{0.2}} = f(\mathrm{Re})$ lie (with a dispersion of only 6%) on a straight line obeying the equation

$$\mathrm{Nu} = 0.023\,\mathrm{Re}^{0.8}\,\mathrm{Pr}\,(d/d_1)^{0.2} \tag{4}$$

or

$$\mathrm{Nu} = 0.020\cdot\mathrm{Re}^{0.8}\,(d/d_1)^{0.2}. \tag{5}$$

By multiplying both sides in equation (5) by $\frac{d_1}{d}$, we obtain

$$\frac{\alpha d_1}{\lambda} = 0.02\left(\frac{wd_1}{\nu}\right)^{0.8},$$

i. e.,

$$\mathrm{Nu}_1 = 0.02\,\mathrm{Re}_1. \tag{6}$$

Thus, a single-valued relationship may be obtained by taking the inner tube diameter as the geometrical criterion.

Figure 1 shows the experimental results calculated using the diameter of the heat transfer tube as the criterion (in the form $^1/_2\mathrm{Nu}_1 = f(\mathrm{Re}_1)$) for annular apertures with $d_2/d_1 = 1.185 - 2.13$ and $2\,\mathrm{Nu}_1 = f(\mathrm{Re}_1)$ for $d_2\,d_1 = 3.08 - 8.24$. The results processed in the above manner are in good agreement with equation (6).

The experimental results on the hydraulic resistance in the case $d_2/d_1 = 1.185 - 2.13$ are in good agreement with the well-known Blasius-Nikuradze equation.

## Roughened apertures

The following types of roughness were investigated:

1) triangular teeth of various heights and various distances between the teeth (Figure 2);

2) spirals made of 1.2 and 3.5 mm wire wound on a smooth tube (Figure 3);

3) inclined protrusions ("slanting" roughness)* (Figure 4,a,b). Since the shape of this roughness was nonsymmetrical with respect to the stream, the experiments were carried out with streams flowing in both directions,

* The so-called "slanting" roughness was used for the first time in 1949 by V. M. Antuf'ev.

thus, for the sake of convenience, the flow in Figure 4,a would be referred to as "forward" and in Figure 4,b as "reverse" flow;

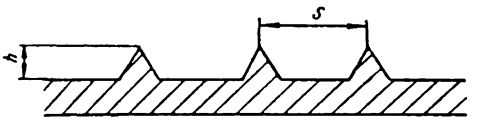


FIGURE 2. Roughness in the form of triangular teeth.

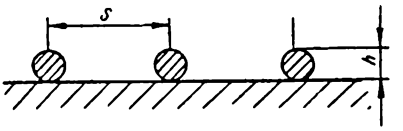


FIGURE 3. Roughness in the form of a spiral.

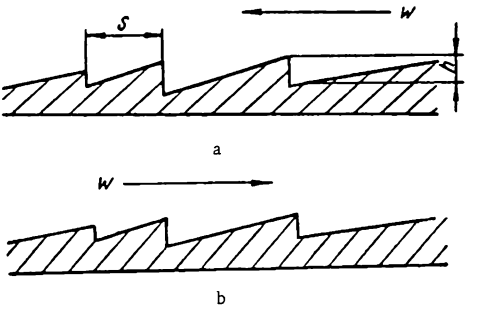


FIGURE 4. "Slanting" roughness.

4) rectangular pyramids, produced by knurling;

5) multiple-start thread of rectangular profile.

The triangular and "slanting" roughness, as well as the knurls and the multiple-start thread, were lathe-turned on thin-walled tubes. In this way, the roughness threads and the tube formed one unit.

The second type of roughness was produced using 1.2 mm nichrome wire and insulated electrical wire with an external insulation diameter of 3.5 mm. In both cases, the wire was tightly wound on the smooth calorimeter and fastened at the ends.

The equivalent diameter (the difference between the internal diameter of the external channel and the mean-volume diameter of the internal tube) was taken as the criterion. The heat transfer was referred to the surface of a smooth cylinder of diameter equal to the mean-volume diameter of the calorimeter. The same approach was used in determining the cross section and velocity of flow.

The heat transfer in roughened annular apertures depends, apparently, on the following parameters (at Pr = 0.71 = const):

1) Re — the Reynolds number. The experiments showed that in the given range of Reynolds numbers, all heat-transfer curves for the

roughened annular apertures could be regarded as equidistant curves for smooth apertures, their slope, corresponding to an exponent of the Reynolds number, equal to 0.8.

2) $\frac{d}{d_m}$ — the relative dimension of the annular aperture. According to our experimental data, the heat transfer in smooth annular apertures (in the case of internal heating) obeys the equation (for air)

$$\mathrm{Nu} = 0.02 \cdot \mathrm{Re}^{0.8} (d/d_1)^{0.2},$$

where $d_1 = d_m$ is the diameter of the inner smooth tube, equal to the mean-volume diameter of the roughened tube. We shall assume that the value 0.2 is true also for roughened apertures.

3) $\frac{h}{d}$ — the relative height of the roughness.

4) $\frac{s}{d}$ — the relative distance between the roughness elements.

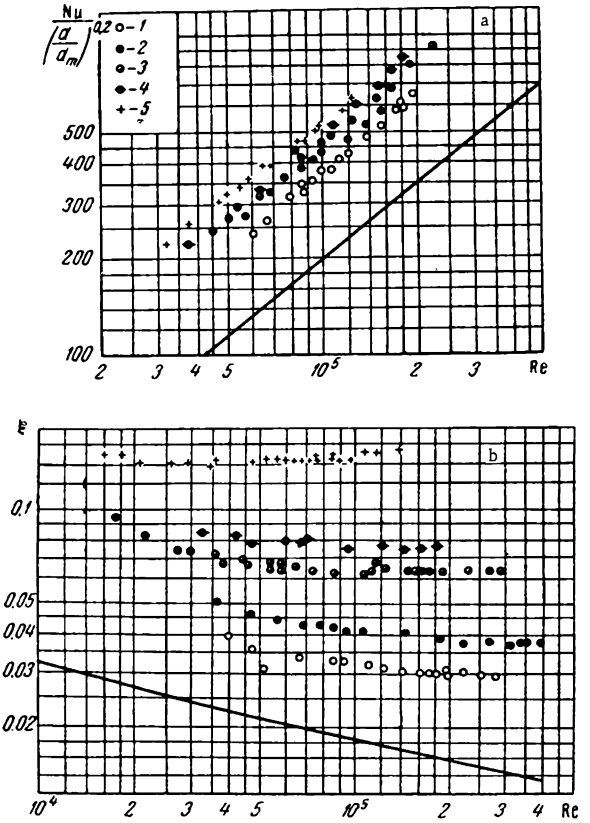


FIGURE 5. Heat transfer and hydraulic resistance in an aperture with triangular roughness at $h/s = 0.5$.

1 — $h/d = 0.0187$; 2 — 0.045; 3 — 0.0815; 4 — 0.0973; 5 — 0.183.

Hence, the equation for air is

$$\mathrm{Nu} = f(\mathrm{Re};\ d/d_m;\ h/d;\ s/d)$$

or, in an exponential form

$$\mathrm{Nu} = C\,\mathrm{Re}^{0.8}(d/d_m)^{0.2}(h/d)^p(s/d)^q\,, \tag{7}$$

where $p$ and $q$ have generally variable values.

Figures 5 and 6 show the experimental results corrected for the diameter ratio $(d/d_m)^{0.2}$ for heat transfer in tubes with triangular and "slanting" roughness, when $h/s$ = const.

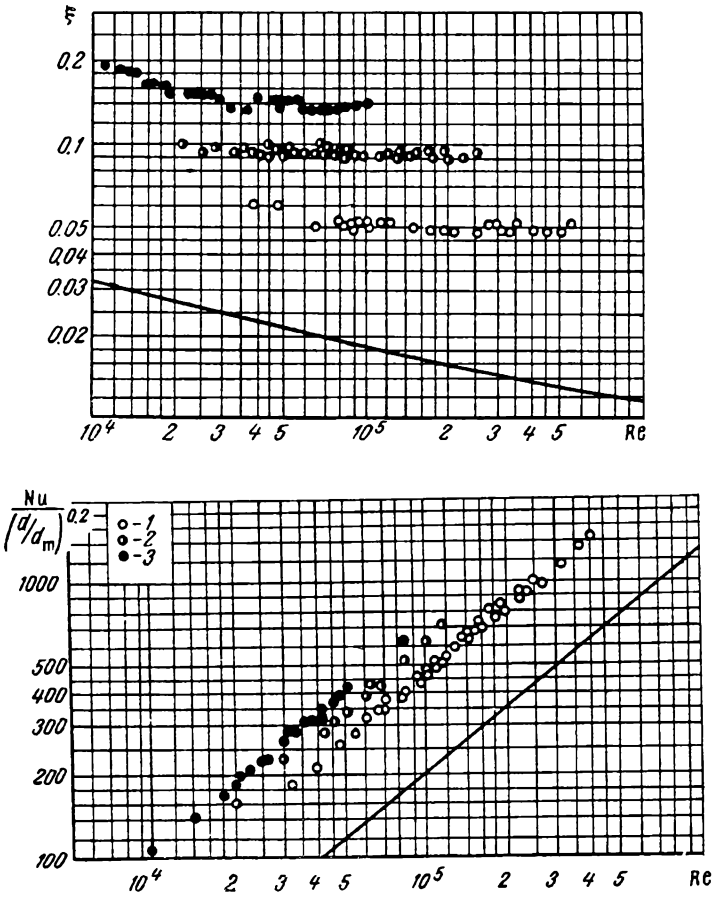


FIGURE 6. Heat transfer and hydraulic resistance in an aperture with "slanting" roughness at $h/s$ = 0.2.

1 — $h/d$ = 0.0187; 2 — 0.0427; 3 — 0.0877.

The results obtained in comparing roughened and smooth apertures are shown in Figure 7 as functions:

$$\mathrm{Nu}/\mathrm{Nu}_0 = f(h/d) \text{ and } \xi/\xi_0 = f(h/d),$$

where Nu and $\xi$ refer to roughened tubes and $\mathrm{Nu}_0$ and $\xi_0$ to smooth tubes.

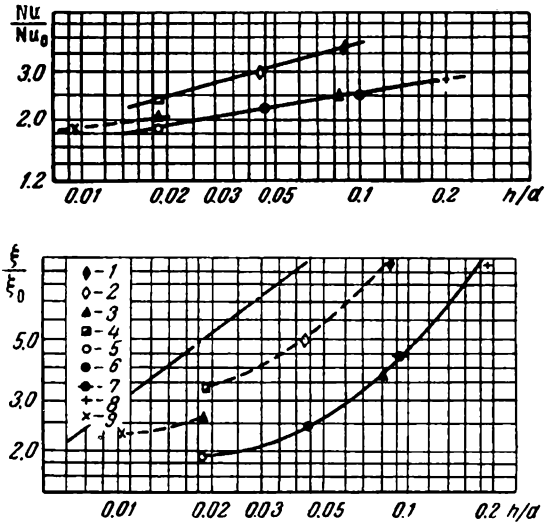


FIGURE 7. Effect of the relative roughness dimension on the heat transfer and hydraulic resistance at $R = 10^5$. The curves denoted by — . — . — . — . taken from /8/.

In the case of triangular roughness at $h = \frac{1}{2}s$ the above function should have the form (from equation (7)):

$$\mathrm{Nu}/\mathrm{Nu}_0 = c\,(h/d)^{p+q}\,2^q\,. \tag{8}$$

Since a straight line may be drawn through the experimental points in Figure 7 (in the given range of $\frac{h}{d}$), it is evident that $p$ and $q$ are constant and equation (8) may take the following form

$$\frac{\mathrm{Nu}}{\mathrm{Nu}_0} = 3.5\left(\frac{h}{d}\right)^{0.16}$$

or, taking (5) into account

$$\mathrm{Nu} = 0.07\,\mathrm{Re}^{0.8}\,(d/d_m)^{0.2}\,(h/d)^{0.16} \tag{9}$$

In the case of "slanting" roughness at $h = \frac{1}{5}s$ we have the following equation

$$\mathrm{Nu} = 0{,}13\,\mathrm{Re}^{0.8}\,(d/d_m)^{0.2}\,(h/d)^{0.26}. \tag{10}$$

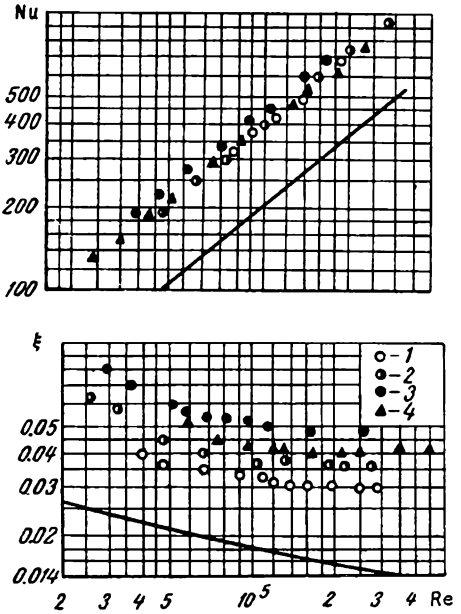


FIGURE 8. Effect of the distance between roughness elements at $h$ = const ($h/d \approx 0.0186$) for triangular roughness.
1 — $s/d$ = 0.00373; 2 — 0.056; 3 — 0.093; 4 — 0.186.

The above equations can, apparently, be used only for identical changes in the two roughness parameters $\left(\frac{h}{d} \text{ and } \frac{s}{d}\right)$, i. e., at $\frac{h}{s}$ = const. As is evident from Figures 8, 9, and 10, a simple exponential relationship cannot be obtained with changing $\frac{s}{d}$ and constant $\frac{h}{d}$.

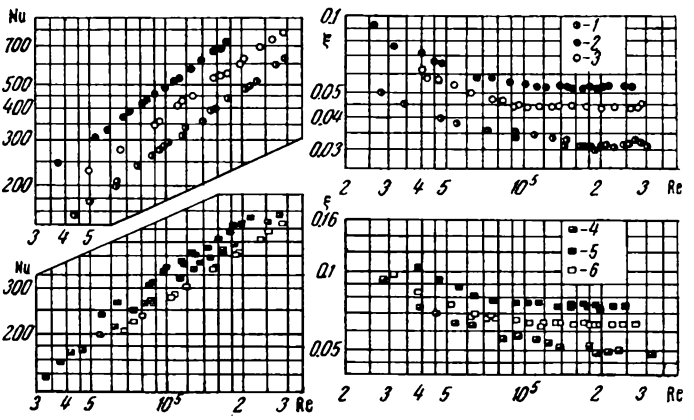


FIGURE 9. Heat transfer and hydraulic resistance in annular apertures with roughness in the form of coiled wire.
1 — $s/d$ = 0.972; 2 — 0.194; 3 — 0.097 ($h/d$ = 0.023); 4 — 2.00; 5 — 0.97; 6 — 0.193 ($h/d \approx 0.0685$).

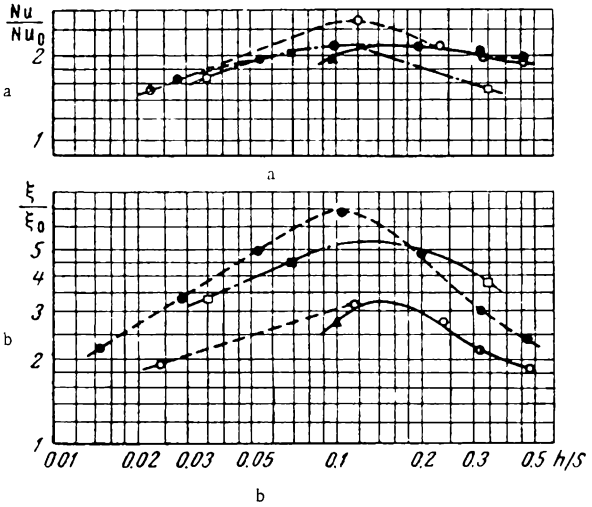


FIGURE 10. Effect of $h/s$ on the heat transfer and hydraulic resistance at $Re = 4 \cdot 10^4$. The curve denoted by — — — — — shows the results for rectangular roughness taken from /9/.

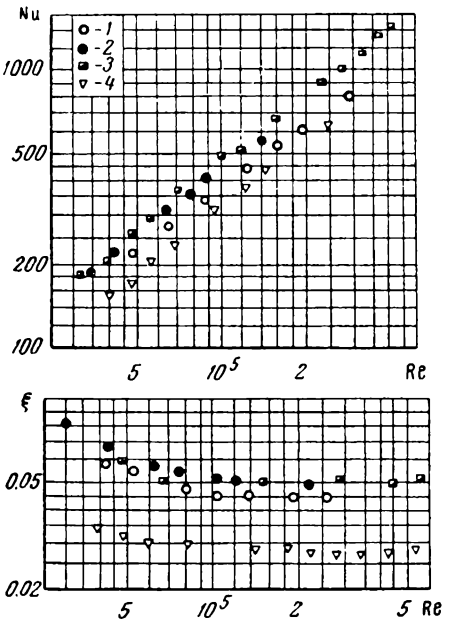


FIGURE 11. Effect of the shape of roughness on the heat transfer and hydraulic resistance.

1 — coiled wire; 2 — triangular; 3 — "slanting," forward flow; 4 — "slanting," reversed flow.

The functions for hydraulic resistance are more complicated (Figure 4) and are described by equations:

for roughness of the triangular type at $h/s = 0.5$

$$\frac{1}{\sqrt{\xi}} = 3.6 \lg \frac{d}{h}, \tag{11}$$

and for "slanting" roughness at $h/s = 0.2$

$$\frac{1}{\sqrt{\xi}} = 2.55 \lg d/h. \tag{12}$$

The above equations may be used within the ranges of parameter variations investigated in this work.

Thus, the effect of roughness of a given shape may be accounted for by introducing empirical functions for the relative roughness dimensions. In general, the roughness may be of many various shapes, however, and thus the effect of the roughness shape at equal geometric ratios remains to be solved.

A comparison of roughness with $h = 0.001$ m and $s = 0.005$ m in the cases of triangular, "slanting" (forward and reversed flows), and coiled wire roughness shows that in some cases, the shape has a marked effect on the heat transfer and hydraulic resistance (Figure 11).

A comparison of the results obtained for "slanting" roughness with forward and reversed flows shows the following. If the flow adjacent to the roughened wall is considered as a flow adjacent to the complex of elements constituting the given rough surface, the rate of heat transfer (and the increase in the resistance) depend on the angle of incidence. When the flow is normal to the surface, the heat transfer rate is about six times the rate for longitudinal flow.

## Conclusions

1) Empirical equations have been obtained for the heat transfer during air flow in smooth annular apertures with an inner heat-transfer surface for a wide range of values of the relative dimensions of the annular apertures.

2) An investigation was made into heat transfer and hydraulic resistance in annular apertures with roughened inner heat-transfer surfaces, having roughness of various shapes and dimensions.

3) Empirical equations are presented for the calculation of the heat transfer and hydraulic resistance for two types of roughened surfaces as functions of their relative dimensions.

4) The effect of the roughness shape on heat transfer and hydraulic resistance for identical geometrical dimensions was demonstrated.

5) It was shown that it is impossible to determine the effect of the distance between (or the concentration of) roughness elements on the surface unambigiously, since at a constant roughness height, the effect of this distance has a maximum at $h/s \approx 0.1$—$0.2$ and depends on the shape of the roughness.

Bibliography


1. Puchkov, P.I. and O.S. Vinogradov. — Energomashinostroenie, No. 11. 1963.
2. Seleznev, A.A. — Teploenergetika, No. 7. 1955.
3. Teverovskii, B.M. O vliyanii sherokhovatosti poverkhnosti na gidravlicheskoe soprotivlenie i konvektivnyi teploobmen (On the Effect of Surface Roughness on the Hydraulic Resistance and Convective Heat Transfer). — Candidate's Thesis, Kuibyshev KAI. 1956.
4. Nunner, V. — VDI-Forschungsheft, 455, B22, 1956.
5. Grass, G. — Allg. Wärmetechnik, Vol. 7, No. 4. 1956.
6. Dipprey, D.F. and R.H. Sabersky. — Int. J. Heat Mass Transfer, Vol. 6, No. 5. 1963.
7. Walker, V. — Nuclear Engineering, Vol. 6, No. 59. 1961.
8. Bauer, H. — Kerntechnik, Vol. 9. 1961.
9. Kemeny, G.A. and J.A. Cyphers. — Trans. ASME, J. Heat Transfer, Ser. C, Vol. 83, No. 2. 1961.
10. Hall, W.B. — J. Mech. Engng. Sci., Vol. 4, No. 3. 1962.
11. Kattchec, N. and W.V. Mackevicz. — Nuclear Science and Engineering, Vol. 16, No. 1. May 1963.
12. Sheriff, N., P. Gumley, and J. France. — Reactor Group U.K. Atomic Energy Authority No. 447 (R). 1963.
13. Murin, G.A. — Izvestiya VTI, No. 10. 1948.
14. Alad'ev, I.T. — Izvestiya AN SSSR, OTN, No. 11. 1951.



The Central Boiler and Turbines Institute im. I.I. Polzunov

L. M. Zysina-Molozhen and I. B. Uskov

# EXPERIMENTAL INVESTIGATION OF THE HEAT TRANSFER ON THE END WALL OF A BLADE CHANNEL [IN TURBINES]

It is well known that the effectiveness of gas turbine plants is markedly affected by the initial temperature of the working fluid. Thus, when the gas temperature is increased above 750°C, the efficiency of gas turbine plants becomes the same as that of steam turbines. In view of the metals available to the turbine industry, a great increase in the temperature of their working fluid necessitates cooling of the various elements of the turbine coming into contact with it.

In general the total heat removed from the gas consists of two compounds: of the heat removed from the gas through the blades (due to the thermal conductivity of the blade material and the temperature gradient between the blade tip and root) and of the heat removed from the gas through the interblade land of the rotor body. In modern gas turbines, the cross-sectional area of the blade fin at the root is smaller (by a factor of 1.5 to 2) than the surface area of the blade channel, while the heat transfer coefficients on these surfaces have rather similar values. Thus, a considerable fraction of the heat reaches the rotor through the end wall of the blade channel. However, only a limited number of papers deal with heat transfer on the end wall of the blade channel. The only experimental work in this field was carried out at the IEN of the Ukrainian Academy of Sciences /1/, and according to it, the heat transfer rate (in the Re range between $1.4 \cdot 10^5$ and $6 \cdot 10^5$) should be calculated using the empirical equation

$$\mathrm{Nu} = \left(0.032 + 0.014\,\frac{\beta}{100}\right)\mathrm{Re}^{0.8}\left(\frac{t}{b}\right)^{-0.175}, \qquad (1)$$

where $\beta$ is the deflection angle of the fluid; $t$ is the cascade pitch; $b$ is the chord line; Nu and Re are the Nusselt and Reynolds numbers referred to the chord line and the velocity at the cascade inlet (in terms of physical constants calculated on the basis of the mean (over the channel) gas temperature).

There are a number of theoretical papers in which an attempt was made to derive a method for the calculation of the three-dimensional dynamic boundary layer created on the end wall of the blade channel during flow adjacent to a blade cascade. Markov /2/ proposes a method for the calculation of the secondary losses, based on a solution of the spatial boundary layer equation. Moreover, the paper of Stepanov and Naumova

makes recommendations for the determination of the velocity profile constituents and of the flow lines in the three-dimensional boundary layer created in the vane channel.

The most general solution of the dynamic part of the three-dimensional boundary layer problem was derived by Bogdanova /3/. However, the numerical solution of specific problems using this method requires a knowledge of the parameters determining the longitudinal and transverse components of the pressure gradients in the external flow.

The experimental study on the structure and nature of secondary currents on the end wall in the blade channel (for the determination of secondary losses) has been the subject of many papers reviewed fairly comprehensively in /4/. The special features of flow in the boundary layer on the end wall are determined, on one hand, by the influence of transverse pressure gradients of the blade channel on the flow, and on the other hand, by the interaction of the boundary layers formed on the end wall and the lateral surface of the blade fin in the angular region.

Loitsyanskii /5/ and Bol'shakov /6/ have studied the interference of dynamic boundary layers during fluid flow on the inner angle between two flat plates. Zysina /7/ evaluated the effect of boundary layer interference on heat transfer. The data of /7/ show that for certain values of the temperature factor and the ratio of the cascade pitch to the characteristic thickness of the interfering boundary layers, the effect of the interaction becomes considerable, and the results for the angular region differ markedly from the heat transfer rate calculated for the case of a stream (without a gradient) adjacent to a flat plate.

Theoretical solutions for the evaluation of the effect of transverse pressure gradients on the heat transfer rate have not been published.

Thus, it is evident that experimental studies aimed at providing equations for computing the heat transfer rate on the end wall of blade channels are necessary. In this paper we present the results of an experimental determination of the average heat transfer coefficients for the above problem.

The setup used for the studies is schematically as follows. Air at required parameters is supplied from external air blowers through a receiver into a plate air heater consisting of two sections, where it is heated to the required temperature by heat from the combustion of kerosene products in a combustion chamber. Because of the high resistance of the air heater, the air flow at its outlet is leveled. Further leveling of the flow occurs in the honeycomb smoothener fitted immediately behind the air heater in the direction of flow. The concurrent flow system employed in the heat exchange circuit of the air heater provides practical stability (with time) of the heated air temperature at the inlet of the nozzle. After passing the nozzle section, the hot-air stream reaches (at a given incidence angle) a blade cascade consisting of nine cylindrical turbine blades of the investigated section (the blade height is 0.09 m). Flow along the cascade axis (at its inlet and outlet in the described setup) may be leveled by any known method. Immediately in front of the cascade, at a minimum distance from its elements, the boundary layer was separated (by suction) from the surface of the supply channel, passing subsequently (in the flow direction) into the end wall between the sections.

All necessary thermal and dynamic measurements of the flow characteristics were carried out on the three central blades and the channels formed by them. The end walls of these three channels served as the heat-extracting surfaces of the water-cooled flow calorimeter. A schematic view of the working section is shown in Figure 1. The main part is the shell of the flow calorimeter (3), with pressure (2) and overflow (9) sleeves. The side, end, and bottom walls of the calorimeter were coated with an insulating layer which (as shown by control experiments) virtually eliminated the heat transfer between the air surrounding the calorimeter and the water used to cool it. The upper supporting wall was made of brass. For each section and each cascade element there were separate walls of appropriate shape. Only the end wall of the middle blade channel, formed between two teflon ($\lambda$ = 0.0232 w/m·deg) blades was in direct contact with water on the calorimeter side and with air on the reverse side. The two other end walls (positioned at the calorimeter lid) were either insulated against contact with the air stream by means of shaped asbestos-cement pieces (5) of thickness $\delta$ = 0.01 m, or else they were covered with Schmidt-type thermometers whose total thickness was also 0.01 m. The teflon blades (4) could be replaced by any other similarly shaped blades. For instance, the pressure distribution measurements were made with brass blades positioned along the section enclosure, and which were bled at two sections over their height (the middle and root).

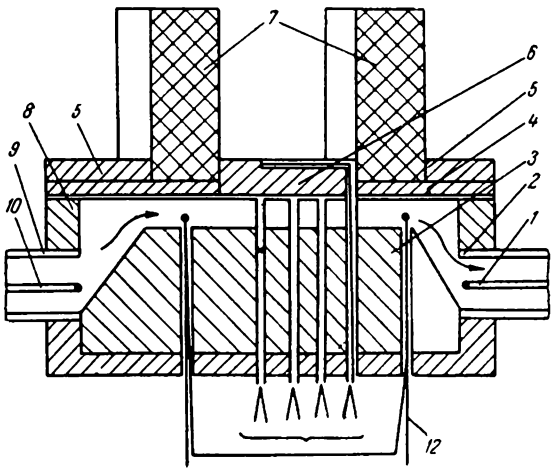


FIGURE 1. Schematic view of the working section.

The main parameter determined experimentally was the heat transfer coefficient, calculated by the equation:

$$\alpha = \frac{Q}{F(t_0 - t_w)}, \qquad (2)$$

where $Q$ is the heat flux through the end wall; $F$ is the surface area of the end wall; $t_0$ is the mean gas temperature in the channel; $t_w$ is the end wall temperature averaged over the surface.

The value of the heat transfer coefficient was calculated from experimental results obtained for three types of turbine sections at various gas velocities and temperatures (at the cascade inlet), various flow angles, various pitch-chord ratios, and various values of the temperature factor.

The use of three different blade sections, having markedly different velocity profiles, made it possible to prepare recommendations for a fairly wide selection of gas turbine cascades; it should be borne in mind that we deal here only with the root section responsible for the direct shaping of the stream over the end wall of the blade channel.

The heat flux through the end wall of the blade channel was measured during the experiments by a calorimetric method; the water flow through the calorimeter was determined by weighing and continuously recorded by an electronic recorder of the 0.5 precision class. The calorimetric temperature gradient with respect to the cooling water was measured using a differential chromel-kopel' hyperthermocouple (diameter 0.0005 m) with amplification of the e. m. f. by a factor of five; continuous recording was made by an electronic potentiometer of the 0.5 class. The heat flux through the thermally-insulated calorimeter walls was measured with separately calibrated thermometers. The end wall temperature was measured with copper-constantan thermocouples (diameter 0.15 mm) positioned on the four channel sections; the thermocouple embedding scheme has been described in /8/; the thermal e. m. f. was recorded continuously by an electronic potentiometer of the 0.5 precision class. The air temperature in the channel was assumed to be equal to the temperature measured at the inlet of the nozzle.

Adjustment experiments showed that measurement at such points in the flow direction (with fairly good external insulation of the input channel) introduces practically no error; the thermal e. m. f. was recorded continuously by an electronic potentiometer of the 0.5 precision class.

The static pressure distribution along the section enclosure and on the end wall of the blade channel, as well as at one pitch distance from the inlet section of the cascade, was measured through the respective drain holes (0.0005 m in diameter) with U-tube pressure gages filled with water.

The total head at the inlet of the acceleration contraction was measured by a conventional Prandtl tube; in subsequent calculations we neglected the total head losses in the nozzle and the supply channel, since the adjustment experiments showed that these losses are negligible in comparison with the absolute magnitude of the total head. The outlet angle was measured with a conventional angle gage. In addition, measurements of the temperature and velocity fields in the boundary layer were made directly on the end wall of the blade channel; appropriate microthermocouples and microtubes were used for these measurements. The purpose of these experiments was to check the validity of an approximate theoretical solution (proposed in /10/) of the problem of heat transfer in the spatial boundary layer discussed here. When the above method was used, the error in the experimental determination of the heat transfer rate did not exceed $\Delta\alpha = 10\%$.

In the experiments, we studied the heat transfer to the end wall of the cascade channel made of the T-Z and 494 profiles and of the upper section profile of the moving blade of the first stage of a gas turbine (700-5) with a chord $b$ = 0.06 m, relative pitch $\bar{t}$ = 0.533 and $\bar{t}$ = 0.9 at inflow angles $\beta_1$ = 27°30' and 86°. The calculated velocity distribution along the profile enclosure of some of the investigated cascades is shown in Figure 2. The velocity profiles show that the experiment comprised virtually the entire possible range of velocity changes in the blade channels of modern gas turbines.

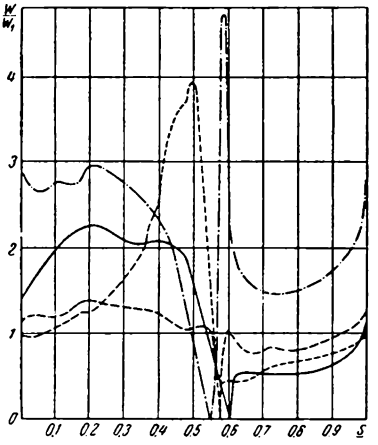


FIGURE 2. Velocity distribution along the enclosures of some of the studied profiles.

Aerodynamic blowdown of a cascade of blades (T-Z profile, with a pitch $\bar{t}$ = 0.9) at the optimum inflow angle $\beta_1$ = 27°30' confirmed that the experimental and calculated velocity distributions along the profile enclosure are in satisfactory agreement. In subsequent experiments, it was thus possible to eliminate the need to measure pressure distribution over the blade, and to use as a basis the distributions calculated by the method of Zhukovskii /11/.

The experiments extended over flow conditions corresponding to Reynolds numbers between $3 \cdot 10^4$ and $4.5 \cdot 10^5$. The Reynolds numbers were calculated on the basis of the velocity at the cascade inlet and the length of the profile enclosure divided by $\pi$ was taken as the criterion; the value of the kinematic viscosity coefficient was selected on the basis of the air temperature at the inlet.

In such a case, the temperature factor $\psi = T_w/T_0$ (where $T_w$ is the end wall temperature and $T_0$ is the temperature of the air stream) ranged from 0.54 to 0.90. It should be mentioned that in modern gas turbines operating at gas inlet temperatures $T_0$ = 700 $\simeq$ 850°C, designed for temperatures of the order of $T_0 \simeq$ 1100 — 1200°C, and characterized by Reynolds numbers Re $\neq 5 \cdot 10^4 - 2 \cdot 10^5$, the value of $\psi$ is 0.7 — 0.8 (if the wall temperature is taken as $T_w$ = 450 — 750°C).

Thus, the experiments encompassed virtually the entire range of variations in the criteria for the heat transfer process in modern and future gas turbines.

The results obtained in the processing of the experimental data are shown in Figure 3, as a plot of Nu vs. Re. The figure shows that the experimental points for each of the cascades studied differ in the profile geometries, the flow angles, and the pitch, and may be described by equations of the Nu = $= C \cdot \mathrm{Re}^n$ type which may be classified into three groups.

At Re $< 6 \cdot 10^4$, all points are grouped round a family of parallel lines, the exponent of Re being $n$ = 0.5; at Re $> 10^5$, the points are grouped round a line with $n$ = 0.8; at Re between $6 \cdot 10^4$ and $10^5$, there exists a transition region in which Nu increases sharply with increasing Re. For the sake of comparison, a dashed line in Figure 3 represents the curves corresponding to values of Nu which were calculated using equations valid for the case of a gradient-free flow around a flat plate.

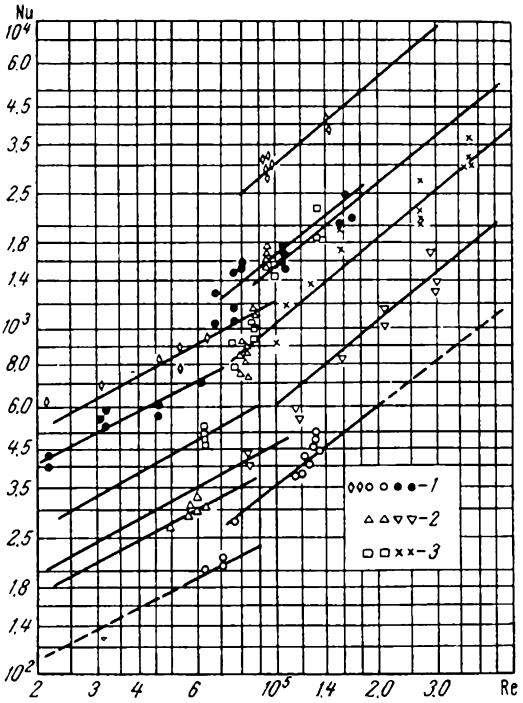


FIGURE 3. Heat transfer rate on the end wall of a blade channel.

1 — profile T-z; 2 — profile T; 3 — profile 494.

It is evident that the experimental points for the end walls lie on a curve which is qualitatively similar to the curves representing function Nu = Nu(Re) for the case of gradient-free flow round a plate; in some cases the experimental points fall on the broken lines, while in other cases, the lines remain parallel for the given sections but the experimental curves are displaced markedly with respect to the broken lines since the values corresponding to Nu differ considerably.

This displacement may be represented quantitatively as the change in the coefficient $C$ in function $Nu = C\,Re^n$. As we mentioned above, the following equations are valid:

$$\begin{aligned} Nu &= C_{lam} Re^{0.5} \quad \text{at} \quad Re < 6 \cdot 10^4 \\ Nu &= C_{turb} Re^{0.8} \quad \text{at} \quad Re > 10^5, \end{aligned} \tag{3}$$

where $C_{lam}$ and $C_{turb}$ are variables characteristic of the end wall of each of the cascades studied.

It may be noted that the peculiar parallel displacement of the lines for the various cascades is associated with the effect of transverse and longitudinal pressure gradients in the external flow over the end wall. The magnitude of the transverse pressure gradients depends on the velocity distribution along the profile enclosure in the cascade and is a function of

the profile geometry, the cascade pitch, and the flow angles. It is evident that more marked displacement of the experimental heat transfer rates from the values characteristic of gradient-free flow round a plate should be expected as the pressure gradient is increased.

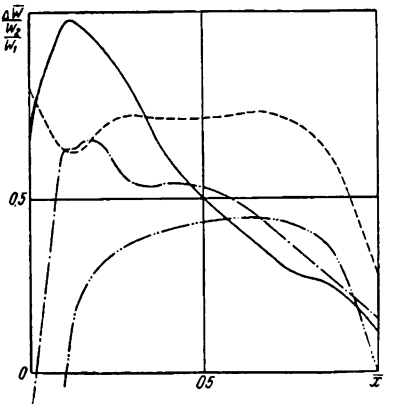


FIGURE 4. The function $\Delta\bar{W}=\Delta W(\bar{X})$.
— profile $T$; $\bar{t}=0.583$, $\beta_1=27°30'$;
— — $\bar{t}=0.900$, $\beta_1=27°30'$;
— — $\bar{t}=0.900$, $\beta_1=86°$;
— — $\bar{t}=0.583$, $\beta_1=86°$.

Figure 4 presents curves showing the variations in a dimensionless parameter selected to characterize the transverse pressure gradient

$$\Delta\bar{W}=\frac{W_{1\text{convex}}-W_{1\text{concave}}}{W_2},$$

along the curved axis of the blade channel for some of the cascades studied. An examination of the curves in Figures 3 and 4 leads to the observation that for pressure variations of a more or less similar nature, the heat transfer rate on the end wall is lower if the cascade pitch is smaller; this can probably be attributed to the effect of interference from boundary layers on the end wall butt with the generating surfaces of the profile. This is qualitative proof of the validity of the conclusion arrived at in theoretical paper /7/, that it is necessary to make a correction for interference from boundary layers in the calculation of heat transfer in such cases where the thickness of the boundary layer on intersecting surfaces is of the same order as the cascade pitch.

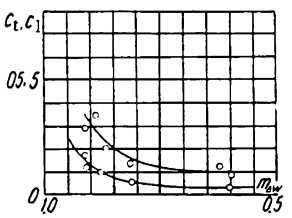


FIGURE 5. The function $C_t = C_t(m)$.

In our experiments, we were unable to eliminate the effect of the temperature factor on the magnitude of the correction introduced into the heat transfer rate calculated by the above-mentioned equations; this is in

agreement with the data of /9/, according to which the temperature factor should cause a change of about 10% (which is the accuracy of our experimental study) in the heat transfer rate within the parameter ranges $M = 0.2 - 0.4$ and $\psi > 0.5$.

An examination of the curves in Figure 4 shows clearly that the most pronounced change in $\Delta W$ (a parameter associated with the transverse and longitudinal pressure gradients) occurs at the inlet and outlet of the blade channel. It is evident that the most pronounced effect of the above parameter on the nature of the flow on the end wall is observed at the outlet, where the boundary layer is relatively thick.

Since the difference between the heat transfer rates on the end wall and on a flat plate (in gradient-free flow) is expressed only by the coefficient $C$, it would be natural to correlate the experimentally determined changes in $C_{lam}$ and $C_{turb}$ with the changes in $\Delta \overline{W}$.

Curves showing the changes in $C_{lam}$ and $C_{turb}$ with the changes in the slope of the curve representing function $\Delta W = \Delta(\bar{x})$ in the outlet section of the blade channel ($m = \frac{\Delta(\Delta \overline{W})}{\Delta \bar{x}}$) are shown in Figure 5.

It is evident that the value of $m$ is within a fair degree of accuracy a single-valued function of the coefficients $C$.

The accumulation of experimental data on heat transfer on the end wall of the blade channel would probably make it possible to correct the obtained relationships to a certain extent. However, it is possible even now to indicate with a fair degree of reliability the limits of the region in which the effect of a transverse pressure gradient causes a noticeable deviation in the heat transfer rate (on the end wall of a curved channel) from gradient-free flow round a plate.

On the basis of the above analysis, it seems to us that the importance should be stressed of the conclusion that there is no aerodynamic basis to the tendency of deriving equations of the type (1), in which the effect of the three-dimensional nature of the flow on the end wall is expressed by means of the geometrical parameters of the cascade ($\overline{l}_1$, $\beta_1$, etc.). From the aspect of the physics of the process, it would be justified to link the heat transfer rate on the end wall with the pressure (velocity) distribution in the channel. This is an unambiguous measure of the nature of the flow around the end wall, and is a result of the overall effect of the channel geometry and the stream parameters on the flow. On the other hand, no such unambiguous effect could be expected in the derivation of equations of the type (1) since it is possible to obtain identical distributions of the transverse velocity gradients (and, hence, identical values of Nu) for different cascades, e.g., at different $\beta_1$ and $\overline{t}$. For instance, this can be deduced from a careful examination of the distribution of experimental points in Figures 3 and 4.

The relationships derived in this paper (equation (3) and Figure 5) are recommended for the approximate calculation of heat transfer on the end walls of blade channels.

In the calculations, determination of $m$ is not difficult since in the calculation of the fluid flow, it is customary to calculate the velocity distribution in the blade profile enclosure (in a cascade); such a calculation method has been programmed for electronic computers and is extensively used in gas-turbine plants.

Bibliography

1. Sidun, V.M. — Trudy Instituta teploenergetiki AN UkrSSR, No. 24 1963.
2. Markov, N.M. Raschet aerodinamicheskikh kharakteristik lopatochnogo apparata turbomashin (Computation of the Aerodynamic Characteristics of the Blade Apparatus of Turbine Plants). — Mashgiz. 1955.
3. Bogdanova, V.V. — Izvestiya AN SSSR, OTN, No. 1. 1960.
4. Sears, W.R. — Appl. Mech. Rev., No. 7:7. 1954.
5. Loitsyanskii, L.G. — Trudy TsAGI, No. 249. 1936.
6. Loitsyanskii, L.G. and V.P. Bol'shakov. — Trudy TsAGI, No. 279. 1936.
7. Zysina-Molozhen, L.M. — IFZh, Vol. VI, No. 5. 1936.
8. Uskov, I.B. — Tekhn. arkh. TsKTI, No. 630430-3014. 1960.
9. Zysina-Molozhen, L.M., I.N. Soskova, and I.G. Shapiro. — Tekhn. arkh. TsKTI, No. 11212330-3944. 1963.
10. Uskov, I.B. — Trudy TsKTI, No. 48. 1964.
11. Zhukovskii, M.I. Raschet obtekaniya reshetok profilei (Cascade Flow Computations). — Mashgiz. 1960.

The Central Boiler and Turbines Institute
im. I.I. Polzunov

Yu. P. Finat'ev

# CALCULATION OF THE HYDRAULIC RESISTANCE OF ANNULAR CHANNELS

Channels with annular cross sections (of the tube-in-tube type) have found extensive application in various branches of technology. The hydraulic resistance of such channels is usually calculated by using the equations for circular tubes, and the so-called hydraulic diameter ($d_h$) of the annular channel is taken as the criterion

$$d_h = \frac{4f}{P},$$

where $f$ is the cross-section area and $P$ is the whole perimeter.

However, the experimental data /3, 5, 9, 11/ processed by the above method are not always in agreement with one another and with the corresponding functions for circular tubes. The principal reasons for this disagreement have not been established.

The sole theoretical paper dealing with the analytical calculation of the hydraulic resistance of annular channels is that of Ginevskii and Solodkin /2/.

Some qualitative evaluations of the range of possible use of the hydraulic diameter for the calculation of friction losses in annular apertures were presented in a monograph /1/.

## Determination of the position of maximum velocity in an annular channel

Experimental measurements of the axial velocity profiles in annular apertures show that the maximum velocity is on a cylindrical surface whose radius $v_m$ is smaller than $\delta/2$. Thus, the velocity profile is asymmetric with respect to the middle of the channel (Figure 1).

Such a curving of the profile is associated in the first place with the difference in the washed areas of the inner and outer cylinders, which leads to differences in the frictional stress on those surfaces. In general, it may be written that

$$r_m = f\left(\frac{r_1}{r_2}, \mathrm{Re}_{z_a}\right).$$

In order to establish the above function, let us assume that the laws governing the turbulence taking place adjacent to the wall, and hence the velocity profiles on the inner and outer cylinder surfaces, are analogous and are described by the same equations. The effect of surface curvature need not be taken into account because of the small thickness of the laminar sublayer as compared with the radii of the cylinder.

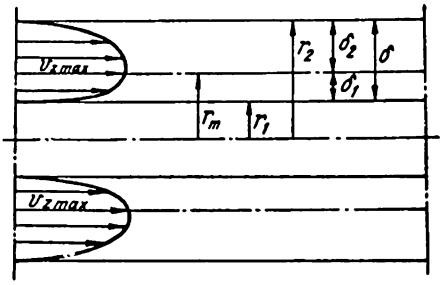


FIGURE 1. Schematic view of the annular channel, with conventional notation.

In order to solve the above problem we shall examine the turbulent flow in an annular space, consisting of two streams, one on the inner and the other on the outer cylinders, the boundary between them being a cylindrical surface for which $\tau_z = 0$ and on which the velocity $v_z$ has a maximum.

Thus, in the annular layer next to the inner cylinder, the friction varies from $\tau_{z1}$ on the cylinder wall to $\tau_z = 0$, while next to the outer cylinder, the range is from $\tau_{z2}$ to $\tau_z = 0$. In the case of flow in an annular channel, the Navier-Stokes equations may be replaced by the equilibrium equations for an annular layer, since the only factor determining the motion is the pressure gradient between the ends of the annular channel and the flow is regarded as equilibrium flow.

Let us write the equilibrium condition in cylindrical coordinates in the form of the momentum conservation equation

$$\frac{dp}{dz} = \frac{1}{r} \frac{d(\tau_z r)}{dr}.$$

In such a case we obtain the following expression, valid for equilibrium flow near the inner cylinder (we assume that the direction from the inner to the outer cylinder is the positive direction)

$$\frac{dp}{dz} = -\frac{1}{r} \frac{d(\tau_z r)}{dr}.$$

Separation of variables is followed by integration. After the integration we assume $\frac{dp}{dz}$ = const. and obtain

$$\tau_z r = -\frac{r^2}{2} \frac{dp}{dz} + C_1.$$

The integration constant is obtained from the condition $\tau_z = 0$ at $r = r_m$. Thus we can write

$$\tau_{z_1} = \frac{1}{2} \frac{dp}{dz} \frac{r_m^2 - r_1^2}{r_1}. \tag{1}$$

By an analogous method, we obtain the following expression for the frictional stress on the outer cylinder

$$\tau_{z_2} = \frac{1}{2} \frac{dp}{dz} \frac{r_2^2 - r_m^2}{r_2}. \tag{2}$$

Division of (1) by (2) yields

$$\frac{\tau_{z_1}}{\tau_{z_2}} = \frac{r_m^2 - r_1^2}{r_2^2 - r_m^2} \frac{r^2}{r_1} = \frac{(r_m - r_1)(r_m + r_1)}{(r_2 - r_m)(r_2 + r_m)} \frac{r_2}{r_1}. \tag{3}$$

Since $r_m - r_1 = \delta_1$ and $r_2 - r_m = \delta_2$ we have

$$r_2 + r_1 = 2r_1 + \delta_1 \quad \text{and} \quad r_m + r_2 = 2r_2 - \delta_2.$$

Substitution of the above values in (3) yields

$$\frac{\tau_{z_1}}{\tau_{z_2}} = \frac{(2r_1 + \delta_1)\delta_1}{(2r_2 - \delta_2)\delta_2} \frac{r_2}{r_1}. \tag{4}$$

By dividing and multiplying the right-hand term in (4) by $\delta$, we obtain

$$\frac{\tau_{z_1}}{\tau_{z_2}} = \frac{\dfrac{2r_1 + \delta_1}{\delta}}{\dfrac{2r_2 - \delta_2}{\delta}} \frac{\delta_1}{\delta_2} \frac{r_2}{r_1}. \tag{5}$$

We use the following notation

$$\frac{\delta_2}{\delta_1} = \alpha, \quad \frac{r_1}{r_2} = \beta.$$

Let us make the transformations

$$\frac{2r_1 + \delta_1}{\delta} = 2 \frac{1}{\dfrac{r_2}{r_1} - 1} + \frac{1}{1 + \dfrac{\delta_2}{\delta_1}} \tag{6}$$

and

$$\frac{2r_2 - \delta_2}{\delta} = 2 \frac{1}{1 - \dfrac{r_1}{r_2}} - \frac{1}{1 + \dfrac{\delta_1}{\delta_2}}. \tag{7}$$

By substituting (6) and (7) in (5) and using the above notation, we obtain

$$\frac{\tau_{z_1}}{\tau_{z_2}} = \frac{1}{\beta\alpha} \frac{2\beta(1+\alpha)+(1-\beta)}{2(1+\alpha)-\alpha(1-\beta)}. \tag{8}$$

By using equation (8), it is fairly simple to find the position of the maximum velocity.

By accepting the above assumption, and using the Blasius equation for the tangential stress on the channel wall

$$\tau_z = 0.0225\rho v^2 z_{max} \left( \frac{1}{\frac{v_{zmax}\delta}{\nu}} \right)^{0.25},$$

which is equivalent to the condition for the validity of an exponential (with an exponent of 1/7) function for the velocity profiles in the inner and outer cylinders:

$$\frac{v_z}{v_{zmax}} = \left( \frac{y}{\delta_{1,2}} \right)^{1/7}.$$

The profiles calculated using the above equation are compared with the experimental profiles obtained by us /4/ and other authors /9, 11/ in Figure 2. The profiles are in good agreement, which confirms the validity of our assumptions. A similar agreement is observed also for large values of $Re_z$, when the value of the exponent is 1/9 or 1/10. Let us write now:

for the inner cylinder

$$\tau_{z_1} = 0.0225\rho v_{zmax}^2 \left( \frac{1}{\frac{v_{zmax}\delta_1}{\nu}} \right)^{0.25}, \tag{9}$$

for the outer cylinder

$$\tau_{z_2} = 0.0225\rho v_{zmax}^2 \left( \frac{1}{\frac{v_{zmax}\delta_2}{\nu}} \right)^{0.25}. \tag{10}$$

Division of (9) by (10), taking into account the fact that in both cases the values of $v_{zmax}$ are equal, yields

$$\frac{\tau_{z_1}}{\tau_{z_2}} = \left( \frac{\delta_2}{\delta_1} \right)^{1/4} = \alpha^{1/4}. \tag{11}$$

By equating (8) to (11), we obtain an equation for the calculation of the position of the maximum velocity in the channel:

$$\alpha^{1/4} = \frac{1}{\beta\alpha} \frac{2\beta(1+\alpha)+(1-\beta)}{2(1+\alpha)-\alpha(1-\beta)}. \tag{12}$$

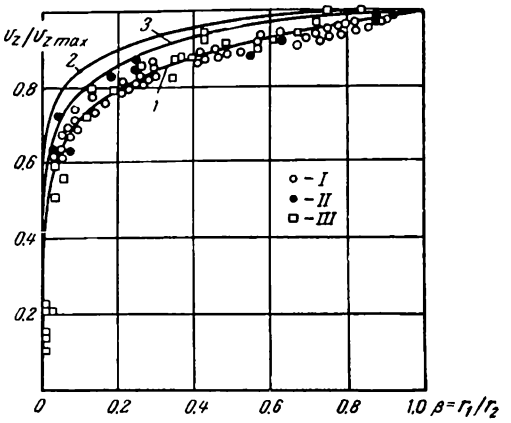


FIGURE 2. Comparison of calculated and experimental velocity profiles at $Re_{za} = 10^4 - 3 \cdot 10^4$.

1 — exponential velocity profile (exponent $\frac{1}{7}$);

2, 3 — calculated (according to /2/) velocity profiles for the inner and outer cylinders respectively; I— experimental data from /4/; II — from /11/; III — from /10/.

As is evident from equation (12), $r_m$ is independent of $Re_{za}$ and depends only on the flow conditions and channel geometry, which is in agreement with the conclusions of /2/ and shows the inaccuracy of the conclusion according to which the radii corresponding to the maximum velocity in turbulent and laminary flows are equal /10/.

The $v_m$ calculated using equation (12), the calculated curves for turbulent flow (from /2/) and for laminary flow (from /8/), and our own experimental data as well as experimental data from /9-11/ are compared in Figure 3.

## Calculation of the hydraulic resistance of an annular channel

Substitution of the values of $\delta_1 = \frac{\delta}{\alpha + 1}$ and $\delta_2 = \frac{\alpha\delta}{\alpha + 1}$ in (9) and (10), respectively, yields

$$\tau_{z_1} = 0.0225\,\rho v_{z\max}^2 \left[\frac{1}{\frac{v_{z\max}\,\delta}{\nu(\alpha+1)}}\right]^{0.25},$$

$$\tau_{z_2} = 0.0225\,\rho v_{z\max}^2 \left[\frac{1}{\frac{v_{z\max}\,\delta}{\nu}\,\frac{\alpha}{(\alpha+1)}}\right]^{0.25} \qquad (13)$$

We introduce the notation

$$\mathrm{Re}_{z\max} = \frac{v_{z\max}\,\delta}{\nu},$$

$$C_{f_1} = \frac{\tau_{z_1}}{\rho v_{z\max}^2} = 0.0225\left(\frac{\alpha+1}{\mathrm{Re}_{z\max}}\right)^{0.25}, \qquad (14)$$

$$C_{f_2} = \frac{\tau_{z_2}}{\rho v_{z\max}^2} = 0.0225\left(\frac{\alpha+1}{\alpha\,\mathrm{Re}_{z\max}}\right)^{0.25}.$$

Using (1) and (2) and some simple transformations /2/, we can derive an equation for the overall coefficient of friction

$$C_f = \frac{C_{f_2} + C_{f_1}\beta}{1+\beta} \qquad (15)$$

and after substituting the values of $C_{f_1}$ and $C_{f_2}$:

$$C_f = \frac{0.0225\left(\frac{\alpha+1}{\mathrm{Re}_{z\max}}\right)^{0.25}\left(\frac{1}{\alpha^{0.25}}+\beta\right)}{1+\beta}. \qquad (16)$$

It is convenient to use the conventional notation for the coefficient of friction and the Reynolds number.

Let us write $v_{za} = Av_{z\max}$, where $v_{za}$ is the mean value of the flow velocity in the channel; $A$ is a coefficient characterizing the degree of filling of the profile.

By using the relation $\lambda = \frac{8\tau_z}{\rho v_{za}^2}$, we obtain $C_f = \frac{\lambda A^2}{8}$ and we can rewrite (16) as

$$\lambda = \frac{0{,}214\,(\alpha+1)^{0.25}\left(\frac{1}{\alpha^{0.25}}+\beta\right)}{A^{1.75}(1+\beta)\,\mathrm{Re}_{za}^{0.25}}, \qquad (17)$$

where $\mathrm{Re}_{za} = \frac{v_{za}\,2\delta}{\nu}$.

Since we have established that in the case of an annular aperture the velocity profile is exponential, we shall look for a relationship between $v_{za}$ and $v_{z\max}$ on the basis of the above condition.

Let us write an equation for the mean velocity of the stream between $r_1$ and $r_m$

$$v_{z_1} = \frac{2}{(r_m^2 - r_1^2)}\int_{r_1}^{r_m} v_z\,r\,dr. \qquad (18)$$

is substituted by

$$\frac{v_z}{v_{z\max}} = \left(\frac{r-r_1}{r_m-r_1}\right)^{1/n}$$

and integration is carried out

$$\bar{v}_{z_1} = \frac{2v_{z\max}}{r_m^2 - r_1^2} \times \int_{r_1}^{r_m} \frac{(r - r_1)^{1/n}}{(r_m - r_1)^{1/n}} r dr = \frac{2}{(r_m^2 - r_1^2)(r_m - r_1)^{1/n}} \times$$

$$\times \left[ \frac{(r_m - r_1)^{1/n+2}}{1/n + 2} + \frac{r_1}{1/n + 1} (r_m - r_1)^{1/n+1} \right].$$

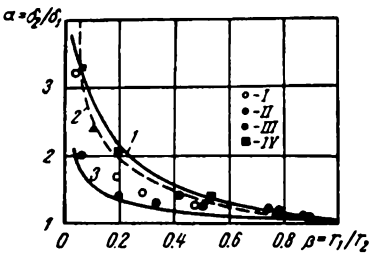


FIGURE 3. Dependence of the position of the maximum velocity in an annular channel on the $r_1/r_2$ ratio.

1 — calculated using equation (12) for $n = 7$; 2 — theoretical, from /2/; 3 — theoretical, for a laminar flow /8/; I — experimental from /10/ for $n = 7$; II — experimental from /9/ for $n = 7$; III — experimental from /11/ for $n = 10$ IV — experimental from /11/ for $n = 10$.

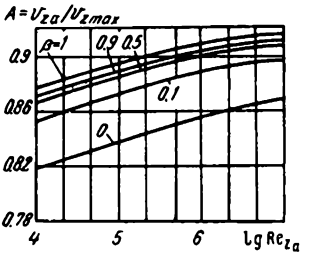


FIGURE 4. $A = \frac{v_{za}}{v_{z\max}}$ as a function of $\lg \mathrm{Re}_{za}$ for various values of $\beta$.

The result is

$$\bar{v}_{z_1} = \frac{v_{z\max}\, 2n \left( n - \frac{r_m}{r_m + r_1} \right)}{(n+1)(2n+1)}. \qquad (19)$$

For the stream in the outer cylinder, analogous steps yield (on the basis of an exponential profile):

$$\frac{v_z}{v_{z\max}} = \left( \frac{r_2 - r}{r_2 - r_m} \right)^{1/n},$$

and after integration between $r_m$ and $r_2$,

$$\bar{v}_{z_2} = \frac{2v_{z\max}}{(r_2^2 - r_m^2)(r_2 - r_m)^{1/n}} \times \int_{r_m}^{r_2} (r_2 - r)^{1/n} r dr$$

or

$$\bar{v}_{z_1} = \frac{v_{z\max} 2n\left(n + \frac{r_m}{r_2 + r_m}\right)}{(n+1)(2n+1)}. \qquad (20)$$

Since the total throughput in the annular channel is expressed by the sum of the throughputs through the annular layers on the inner and outer cylinders, equations (19) and (20) yield

$$\frac{v_{za}}{v_{z\max}} = \frac{2n\left[\left(n + \frac{r_m}{r_m + r_1}\right)(r_m^2 - r_1^2) + \left(n + \frac{r_m}{r_m + r_2}\right)(r_2^2 - r_m^2)\right]}{(r_2^2 - r_1^2)(n+1)(2n+1)}$$

After transformation

$$\frac{v_{za}}{v_{z\max}} = \frac{2n\left(n + \frac{r_m}{r_2 + r_1}\right)}{(n+1)(2n+1)}, \qquad (21)$$

or, by expressing $\frac{r_m}{r_2 + r_1}$ by means of $\beta$ and $\alpha$,

$$A = \frac{v_{za}}{v_{z\max}} = \frac{2n\left[n + \frac{\alpha\beta + 1}{(1+\alpha)(1+\beta)}\right]}{(n+1)(2n+1)}. \qquad (22)$$

In the case of a circular tube where $\beta = 0$ and $\alpha \to \infty$, we obtain $A = \frac{2n^2}{(n+1)(2n+1)}$; for a plane channel where $\beta \approx 1$ and $\alpha = 1$, we have $A = \frac{n}{n+1}$.

The calculations made using equation (22) are shown in Figure 4, as $v_{za}/v_{z\max}$ plotted as a function of $\mathrm{Re}_{za}$, which corresponds to different values of $n$ in the above equation (at given values of $\beta$).

When we substitute in equation (17) the value of $A$ from (22) with an exponent of 1/7, we obtain an expression for the resistance of a smooth channel at $\mathrm{Re}_{za} < 10^5$. The error in the determination of the resistance of annular channels by using the Blasius resistance law (using the hydraulic diameter) may be evaluated by taking the ratio of the resistance coefficient from (22) to the coefficient calculated using the equation derived by Blasius. As is evident from Figure 5, the error may be as high as 6%.

On the basis of the above account, it is possible to understand the deviations (in the direction of higher values) in the experimental data for hydraulic resistance of annular channels as compared with values calculated by the Blasius equation, especially at small clearances. The function

$$\tau_{z_1}/\tau_{z_2} = f(\beta),$$

which is of great importance in the study of heat transfer processes in annular channels, is shown graphically in Figures 5 and 6.

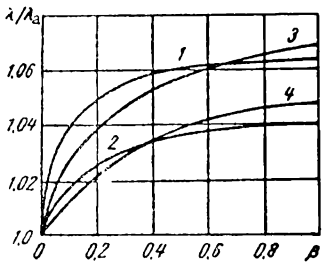


FIGURE 5. The relative hydraulic resistance coefficient of an annular channel as a function of β.

1, 2 — calculated using equation (28) at $n = 7$ and $n = 10$, respectively; 3, 4 — calculated values (from /2/) at $Re_{za} = 10^4$ and $Re_{za} = 10^7$, respectively; ($\lambda_a$ is the hydraulic resistance coefficient of an annular channel calculated by the corresponding equations for circular channels by using the hydraulic diameter).

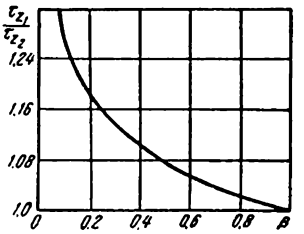


FIGURE 6. The ratio of the frictional stress on the inner cylinder wall to the stress on the outer cylinder wall as a function of β at $Re_{za} = 10^4 - 10^5$.

A somewhat different relationship between $\tau_{z1}/\tau_{z2}$ and α would naturally exist at higher $Re_{za}$ (above $10^5$), but its nature can be established by solving the problem in a general form.

It is well known that in the case of an exponential velocity distribution

$$\varphi = B(n)\eta^{1/n}, \qquad (23)$$

the value of the exponent decreases with increasing $Re_{za}$, while in the limiting case of very large values of $Re_{za}$, the relationship is asymptotic and is described by an equation comprising a logarithm as the limit of the very small exponent.

However, it was difficult to establish the function $\tau_{z1}/\tau_{z2} = f(\alpha)$ from the exponential velocity distribution law, and it was necessary to use an approximation of the logarithmic profile of the exponential relationship.

Such an approach is perfectly valid (and is used quite often) since the logarithms describe the envelope of a family of exponential curves, and the accuracy of the approach increases with increasing Reynolds number.

Equation (23) is written in the form

$$\frac{v_z}{v_*} = B(n)\left(\frac{yv_*}{\nu}\right)^{1/n};$$

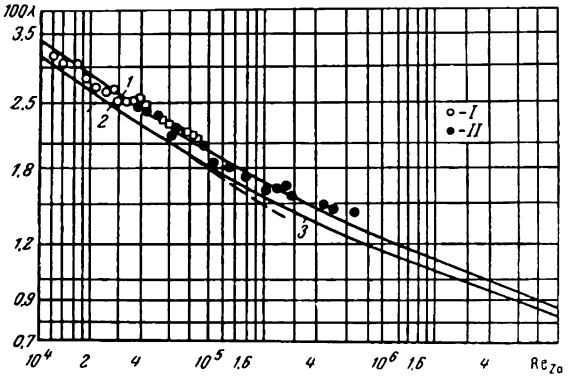


FIGURE 7. The resistance law for a smooth annular channel as compared with the resistance law for circular cross-section tubes.

1 — calculated by means of equation (28) for $\beta = 0.5$; 2, 3 — calculated by means of the Blasius and Prandtl equations, respectively; I — our experimental data at $\beta = 0.95$; II — experimental data from /11/ at $\beta = 0.525$.

solution of the above equation with respect to $v_*$ yields

$$v_* = \frac{v_z}{B^{n/n+1}\left(\frac{v_z y}{\nu}\right)^{1/n+1}}. \tag{24}$$

By taking the case of the maximum velocity $v_{z\max}$ and bearing in mind that $v_* = \sqrt{\frac{\tau_z}{\rho}}$, we obtain the following expressions for the frictional stresses:

on the inner cylinder

$$\tau_{z_1} = \frac{\rho v_{z\max}^2}{B^{2n/n+1}\left(\frac{v_{z\max}\,\delta_1}{\nu}\right)^{2/n+1}}, \tag{25}$$

on the outer cylinder

$$\tau_{z_2} = \frac{\rho v_{z\max}^2}{B^{2n/n+1}\left(\frac{v_{z\max}\,\delta_2}{\nu}\right)^{2/n+1}}. \tag{26}$$

Division of (25) by (26) yields

$$\frac{\tau_{z_1}}{\tau_{z_2}} = \left(\frac{\delta_2}{\delta_1}\right)^{2/n+1} = \alpha^{2/n+1}. \tag{27}$$

At $n = 7$, which corresponds to a velocity profile with an exponent of 1/7, we do in fact obtain equation (11) for the Blasius range.

The position of the maximum velocity is shown in Figure 3 as a function of the exponent.

After some simple transformations, the resistance law for an annular channel may be written in the following form

$$\lambda = \frac{8 \cdot 2^{2/n+1} (\alpha + 1)^{2/n+1} (1/\alpha^{2/n+1} + \beta)}{(AB)^{2n/n+1} (1 + \beta) \mathrm{Re}_{za}^{2/n+1}}. \qquad (28)$$

Values calculated using the above equation are shown in Figure 7. The same figure contains the experimental data of /11/ as well as our own experimental data obtained with very large $\beta$ values ($r_1/r_2 = 0.95$); the experimental values agree well with the calculated curve.

Assuming in equation (28) that $\beta = 0$ and $\alpha = \infty$, we obtain the exponential resistance law for a smooth circular tube

$$\lambda_{sc} = \frac{8 \cdot 2^{2/n+1}}{(AB)^{2n/n+1} \mathrm{Re}_{za}^{2/n+1}}.$$

Bibliography


1. Novikov, I.I. and K.D. Voskresenskii. Prikladnaya termodinamika i teploperedacha (Applied Thermodynamics and Heat Transfer). — Gosatomizdat, Moskva. 1961.
2. Ginevskii, A.S. and E.E. Solodkin. — Prom. Aerodinamika, No. 20, Oborongiz. 1961.
3. Kosterin, S.I., Yu.A. Koshmarov, and Yu.P. Finat'ev. — IFZh, No. 5. 1962.
4. Finat'ev, Yu.P. — Candidate's Thesis, Power Inst. im. Krzhizhanovskii. 1962.
5. Mikryukov, V.E. — IFZh, VII, No. 22. 1937.
6. Mal'tsev, V.V. — VEP, No. 6. 1959.
7. Nikuradze, I. — In sbornik: "Problemy turbulentnosti". ONTI, Moskva-Leningrad. 1936.
8. Lamb, G. Gidrodinamika (Hydrodynamics). — GTI, Moskva-Leningrad. 1947.
9. Croop, E.I. and R.R. Rothfus. — A. J. Ch. E., Vol. 8, No. 2. 1962.
10. Rothfus, R.R., C.C. Monrad, and V.E. Senecal. — Industrial and Engineering Chemistry, Vol. 42, No. 12. 1950.
11. Lorens, F.R. — Institut für Strömungsmaschinen der Techn. Hochschule Karlsruhe, No. 2, Berlin. 1932.
12. Barlybaev, Kh.A., S.V. Bukhman, K.A. Zhurgembaev, and B.P. Ustimenko. Teplo i massoperenos (Heat and Mass Transfer), III — Gosenergoizdat, Moskva-Leningrad. 1963.
13. Koshmarov, Yu.A. — IFZh, No. 5. 1962.
14. Shiller, L. Dvizhenie zhidkosti v trubakh (Flow of Fluids in Tubes). — ONTI. 1936.



The Institute of Mechanics of the
Academy of Sciences of the USSR

B. P. Ustimenko, K. A. Zhurgembaev,
and D. A. Nusupbekova

# CALCULATION OF THE CONVECTIVE HEAT TRANSFER FOR AN INCOMPRESSIBLE LIQUID IN CHANNELS WITH COMPLICATED SHAPES

The study of convective heat transfer during flow in channels is of great importance for many technological devices (high-output heat exchangers, reactors, etc.). The theoretical analysis of turbulent convective heat transfer problems (which is almost always applied in practice) makes extensive use of the Reynolds hydrodynamic theory of heat transfer.

The analysis of laminar flow conditions, based on rigid mathematical treatment, is also of considerable importance and makes it possible to establish the physical nature of the various phenomena and to derive quantitative relationships which are also valid for turbulent flow.

In this paper, we present calculated results for the [hydraulic] resistance and heat transfer during laminar flow of a viscous incompressible liquid in straight or curved plane channels at different heat flux ratios on the channel walls, as well as approximate calculations of the turbulent convective heat transfer in channels with the aid of a hydrodynamic integrator.

## Calculation of the velocity profile and the resistance in a plane curved channel

The literature /1/ reports a general solution of the dynamic problem for the movement of an incompressible liquid in a channel whose cross section is bounded by two circular arcs (with radii $r_1$ and $r_2$) having a common center.

The stream is assumed to be flat, and the particle displacement occurs strictly along the concentric arcs, at a velocity $v_\varphi$ described by equation

$$v_\varphi = \frac{C}{2\mu} r\left(\ln r - \frac{1}{2}\right) + C_1 r + \frac{C_2}{r}, \qquad (1)$$

where $\mu$ is the viscosity coefficient; $C_1$ and $C_2$ are the integration constants; and $C$ is a constant.

This solution will now be examined in more detail. Determination of the integration constants $C_1$ and $C_2$ from the boundary conditions

$$v_\varphi = 0 \text{ at } r = r_1 \text{ and } r = r_2$$

and substitution of their values in equation (1) yields

$$v_\varphi = \frac{1}{2\mu}\frac{dP}{d\varphi} r_1 \left\{ \bar{r}\ln\bar{r} - \frac{r_2^2 \ln\frac{r_2}{r_1}}{r_2^2 - r_1^2}\left(\bar{r} - \frac{1}{\bar{r}}\right)\right\}. \qquad (2)$$

where $\bar{r} = \frac{r}{r_1}$.

By introducing the curvature parameter $m = \frac{h}{r_1}$ (where $h$ is the channel half-width) we may rewrite (2) as:

$$v_\varphi = \frac{1}{2\mu} r_1 \frac{dP}{d\varphi}\left\{(1+m+\bar{y})\ln(1+m+\bar{y}) - \frac{R^2 \ln R}{R^2-1}\left(1+m+\bar{y} - \frac{1}{1+m+\bar{y}}\right)\right\}. \quad (3)$$

Here $\bar{y} = \frac{y}{r}$ and $y$ is the distance measured from the channel center,

$$R = \frac{r_2}{r_1} = 2m + 1.$$

Let us find the mean velocity $\bar{v}_\varphi$ by using the equation

$$\bar{v}_\varphi = \frac{1}{r_2 - r_1}\int_{r_1}^{r_2} v_\varphi \, dr. \qquad (4)$$

Substituting (in the above equation) the value of $v_\varphi$ from (2) and integrating, we obtain

$$\bar{v}_\varphi = -\frac{dP}{d\varphi}\frac{1}{8\mu}\frac{r_1}{R-1}\left\{R^2 - 1 - \frac{4R^2\ln^2 R}{R^2-1}\right\} \qquad (5)$$

or

$$\bar{v}_\varphi = -\frac{dP}{d\varphi}\frac{1}{16\mu}\frac{h}{m^2}\left\{4m(m+1) - \frac{(1+2m)^2\ln^2(1+2m)}{m(m+1)}\right\}.$$

The dimensionless velocity $\frac{v_\varphi}{\bar{v}_\varphi}$ distribution over the channel cross section is shown in Figure 1, for different values of the curvature parameter

It is evident that as $m$ is increased, the maximum in the velocity profile shifts in the direction of the inner channel wall. The resistance coefficient $\xi$ is determined from the equation

$$-\frac{dP}{r_c d\varphi} = \frac{\xi}{2(r_2 - r_1)}\frac{\rho\bar{v}_\varphi^2}{2}, \qquad (6)$$

where $r_c = \frac{r_1 + r_2}{2}$.

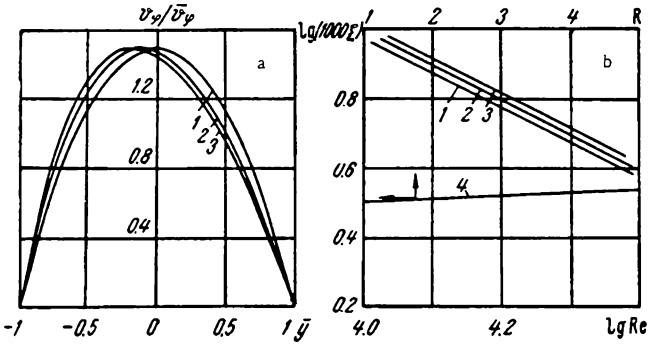


FIGURE 1. Dimensionless velocity $\frac{v_\varphi}{\bar{v}_\varphi}$ profile and resistance coefficient $\xi$ in a plane curved channel.

a — 1 — straight channel; 2 — $R=2$; 3 — $R=3$; b — 1 — straight channel; 2 — $R=4$; 3 — $R=10$; 4 — the function $\xi=f(R)$ for Re = $3\cdot10^4$.

By substituting the value of the mean velocity from (5) in the above equation, we obtain

$$\xi = \frac{96}{\mathrm{Re}}\left\{\frac{\frac{4}{3}(R-1)^4}{(R^2-1)^2-4R^2\ln^2 R}\right\} \tag{7}$$

or, in terms of the curvature parameter $m$

$$\xi = \frac{96}{\mathrm{Re}}\left\{\frac{\frac{64}{3}m^4}{[(1+2m)^2-1]^2-4(1+2m)^2\ln^2(1+2m)}\right\}.$$

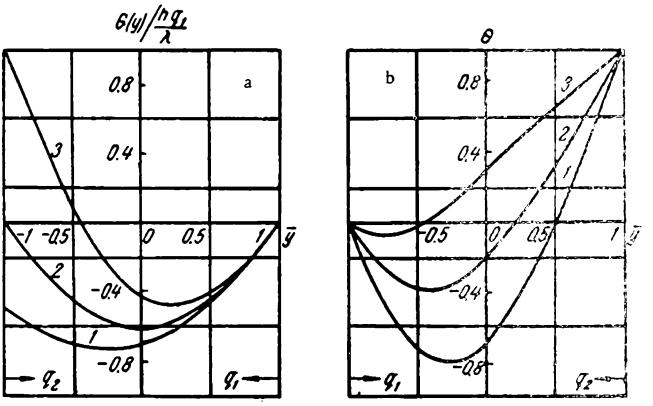


FIGURE 2. Distribution of the dimensionless excess temperature in a straight (a) and a curved (b) plane channel.

a — 1—$q_{21}$=0.5; 2 — $q_{21}$=1; 3 — $q_{21}$=2; b — 1—$R$=1; 2 — $R$=3; 3 — $R$=21 ($q_{21}$=1).

It is evident that when (7) is transformed to the boundary condition at $R \to 1$ we obtain a value $\xi_1$, which coincides with the conventional value of the resistance coefficient for a plane straight channel

$$\xi = \frac{96}{\mathrm{Re}}.$$

Values of the resistance coefficient are plotted in Figure 2 as functions of the Reynolds number and the curvature parameter. In curved channels, the resistance coefficient increases as the curvature parameter is increased.

Heat transfer in a plane straight channel

Let us assume an incompressible liquid flowing with a mean velocity $\bar{v}$ in a flat straight channel whose half-width is $h$. The flow is laminar, and the velocity field satisfies the equation

$$v = \frac{3}{2}\bar{v}\left[1 - \left(\frac{y}{h}\right)^2\right]. \tag{8}$$

The same velocity distribution should be maintained also when heat transfer takes place. It is assumed that the viscosity is independent of the temperature. Let us assume that starting from a certain cross section, the heat flux densities $q_1$ and $q_2$ on each channel wall are constant.

We shall analyze a general case in which the heat fluxes on the walls $q_1$ and $q_2$ are not equal.*

For such a flux, the heat transfer equation is

$$v\frac{\partial T}{\partial x} = a\frac{\partial^2 T}{\partial y^2}. \tag{9}$$

A solution for (9) at boundary conditions

$$\begin{aligned} y &= +h, \quad q = q_1, \\ y &= -h, \quad q = q_2 \end{aligned} \tag{10}$$

should be in the form

$$T(x, y) = Ax + G(y). \tag{11}$$

Substitution in equation (9) of equations (8) and (11) yields a differential equation

$$\frac{3}{2}\bar{v}A\left[1 - \left(\frac{y}{h}\right)^2\right] = a\frac{d^2G(y)}{dy^2},$$

* A particular solution for the case of $q_1 = q_2 = \text{const.}$ was derived in /2/; a case in which one wall is adiabatic while a heat flux $q = \text{const.}$ passes through the other was also analyzed in /2/.

whose solution is

$$G(y) = -\frac{q_1}{\lambda}(y-h) - \frac{3}{2}\frac{\bar{v}A}{a}\left[\frac{2}{3}hy - \frac{y^2}{2} + \right.$$
$$\left. + \frac{1}{12h^2}y^4 - \frac{1}{4}h^2\right], \qquad (12)$$

where $\lambda$ is the thermal conductivity coefficient, and $a$ is the thermal diffusivity coefficient. The stream temperature on the channel wall at $y = -h$ is

$$T_2 = T_1(x, -h) = Ax + G(-h) =$$
$$= T_1 + G(-h) = T_1 - 2h\frac{q_1}{\lambda} + 2\frac{v}{a}Ah^2$$

hence

$$\bar{T}_2 - T_1 = -2h\frac{q_1}{\lambda} + 2h^2\frac{\bar{v}A}{a}. \qquad (13)$$

The constant $A$ in the above equations is found from the energy balance equation

$$A = \frac{q_1 + q_2}{\rho C_p v \cdot 2h}. \qquad (14)$$

By substituting the expression for $A$ in (13) and using the notation $q_{21} = \frac{q_2}{q_1}$ we obtain

$$T_2 - T_1 = \frac{h}{\lambda}q_1(q_{21} - 1). \qquad (15)$$

The average (with respect to the streaming flow) excess temperature over the cross section is determined by equation

$$\bar{G}(y) = \frac{\int_{-h}^{h}\rho C_p v G(y)\,dy}{\int_{-h}^{h}\rho C_p v\,dy}, \qquad (16)$$

and, after substituting the values from (8) and (12) in equation (16),

$$\bar{G}(y) = T_1 - \frac{q_1 h}{\lambda} \times \left[1 - \frac{9}{35}(q_{21} + 1)\right] \qquad (17)$$

is obtained.

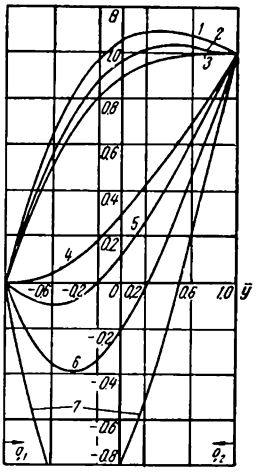


FIGURE 3. Dimensionless excess temperature profiles for different values of the heat flux ratios $q_{21}$ at $R = 3$.

1—$q_{21}$=0.1; 2—$q_{21}$=0.05; 3—$q_{21}$=0; 4—$q_{21}$=∞; 5—$q_{21}$=2, 6—$q_{21}$=1; 7—$q_{21}$=0.7

Let us now derive an expression for the Nusselt number on the basis of the heat transfer coefficient $\alpha_1$, with respect to the wall channel at $y = h$:

$$\mathrm{Nu}_1 = \frac{\alpha_1 d_{\mathrm{equ}}}{\lambda} = \frac{q_1 d_{\mathrm{equ}}}{\lambda [G(h) - \bar{G}]} \tag{18}$$

By substituting in (18) the value of $\bar{G}$ from (17), we obtain

$$\mathrm{Nu}_1 = \frac{140}{26 - 9q_{21}}. \tag{19}$$

The Nusselt number $\mathrm{Nu}_2$ with respect to the other channel wall at $y = -h$ is determined in a similar way:

$$\mathrm{Nu}_2 = \frac{\alpha_2 d_{\mathrm{equ}}}{\lambda} = \frac{q_2 d_{\mathrm{equ}}}{\lambda [G(-h) - \bar{G}]}, \tag{20}$$

or, after substitution of equations (15) and (17),

$$\mathrm{Nu}_2 = \frac{140 q_{21}}{9 - 26 q_{21}}. \tag{21}$$

The expression for the overall Nusselt number, calculated on the basis of the total heat flux $q_0$ and the total heated surface, is thus

$$\mathrm{Nu}_0 = \frac{\alpha_0 d_{\mathrm{equ}}}{\lambda} = \frac{q_0 d_{\mathrm{equ}}}{\lambda (T_2 - T_1)}. \tag{22}$$

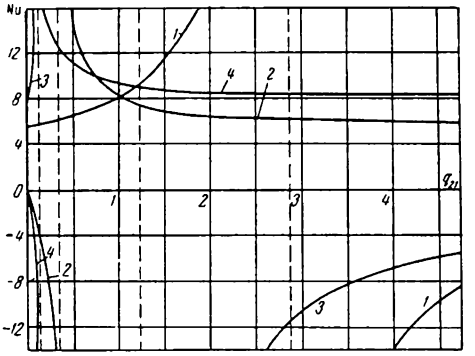


FIGURE 4. Effect of the heat flux ratio $q_{21}$ on the Nusselt numbers ($Nu_1$ and $Nu_2$) for straight (curves 1, 2) and plane curved (curves 3, 4) channels at $R=3$.

1 and 2 — $Nu_1$, $Nu_2$ (straight channel); 3 and 4 — $Nu_1$, $Nu_2$ (curved channel).

In the above equation

$$q_0 = \frac{q_1F_1 + q_2F_2}{F_1 + F_2},$$

where $F_1$ and $F_2$ are the heated surfaces.

By substituting the value from equation (13) in (22), we obtain

$$Nu_0 = 2\frac{q_{21} + 1}{q_{21} - 1}.$$

The distribution of the dimensionless excess temperature over the cross section of a plane straight channel is shown in Figure 2a, for different values of the heat flux ratio $q_{21}$. It is evident that as the heat flux ratio $q_{21}$ is increased the extremum in the temperature profile shifts in the direction of the wall where smaller heat flux takes place. The effect of the heat flux ratio $q_{21}$ on the Nusselt numbers $Nu_1$ and $Nu_2$ is shown in Figure 4.

## Heat transfer during circular laminar flow

Let us examine the equation for heat transfer during laminar flow of a viscous incompressible liquid in a plane curved channel

$$v_r\frac{\partial T}{\partial r} + \frac{v_\varphi}{r}\frac{\partial T}{\partial \varphi} + v_x\frac{\partial T}{\partial x} =$$
$$= a\left(\frac{\partial^2 T}{\partial r^2} + \frac{1}{r}\frac{\partial T}{\partial r} + \frac{1}{r^2}\frac{\partial^2 T}{\partial \varphi^2} + \frac{\partial^2 T}{\partial x^2}\right).$$

The following equations should be satisfied for plane flow:

$$v_r = 0, \quad v_x = 0, \quad \frac{\partial^2 T}{\partial \varphi^2} = 0, \quad \frac{\partial^2 T}{\partial x^2} = 0.$$

In such a case the equation would be

$$v_\varphi \frac{\partial T}{\partial \varphi} = \frac{a}{r_1} \frac{\partial}{\partial \bar{r}} \left( \bar{r} \frac{\partial T}{\partial \bar{r}} \right), \tag{23}$$

where $\bar{r} = \frac{r}{r_1}$ subject to the boundary conditions:

$$\begin{aligned} \bar{r} &= 1, \quad q = q_1 = \text{const}, \\ \bar{r} &= R = \frac{r_2}{r_1}, \quad q = q_2 = \text{const}. \end{aligned} \tag{24}$$

The solution of equation (23) with the boundary conditions (24) should have the form

$$T = A r_1 \varphi + G(r). \tag{25}$$

Substituting (25) in (23) and integrating (bearing in mind the boundary conditions (24)), we obtain

$$\begin{aligned} G(r) = &- \frac{r_1 q_1}{\lambda} \ln \bar{r} + \left[ (Rq_2 + q_1) r_1 \left\{ \ln \bar{r} (\bar{r}^2 + 1) + \right. \right. \\ &+ 1 - \bar{r}^2 - \frac{R^2 \ln R}{R^2 - 1} \left. \left. [\bar{r}^2 - 2 \ln \bar{r} (\ln \bar{r} + 1) - 1] \right\} \right] \times \\ &\times \left[ \lambda \left( 1 - R^2 + \frac{4R^2 \ln^2 R}{R^2 - 1} \right) \right]^{-1}. \end{aligned} \tag{26}$$

The constant $A$ is determined from the energy balance equation

$$A = \frac{Rq_2 + q_1}{r_1 \bar{v}_\varphi (R - 1) \rho C_p}.$$

We shall now derive an expression for the function $G(r)$ on the channel wall at $r = r_2$:

$$\begin{aligned} G(r_2) = T_2 - T_1 = &- \frac{r_1}{\lambda} q_1 \ln R + \left[ (Rq_2 + q_1) r_1 \left\{ \ln R (R^2 + 1) + 1 - R^2 - \frac{R^2 \ln R}{R^2 - 1} \times \right. \right. \\ &\times [R^2 - 2 \ln R (\ln R + 1) - 1] \left. \left. \right\} \right] \left[ \lambda \left( 1 - R^2 + \frac{4R^2 \ln^2 R}{R^2 - 1} \right) \right]^{-1}. \end{aligned} \tag{27}$$

Let us write an expression for the Nusselt number for a curved channel. For this purpose, the flow region is divided into two parts from the line passing through the temperature extremum (adiabatic wall) to the channel walls. All values related to the region between that line and the inner wall

are marked by the subscript 1, while the other region is marked by the subscript 2.

The expression for the Nusselt number $Nu_1$ is then

$$Nu_1 = \frac{\alpha_1 d_{equ}}{\lambda} = \frac{q_1 2(R-1) r_1}{\lambda [G(r_1) - \bar{G}]}. \tag{28}$$

By substituting an expression for the average (with respect to flow rate) temperature in (28), we obtain

$$\bar{G} = \frac{\int_{r_1}^{r_2} \rho C_p V_\varphi \Delta T dy}{\int_{r_1}^{r_2} \rho C_p V_\varphi dy} = \frac{q_1 r_1}{\lambda [4R^2 \ln^2 R - (R^2-1)^2]} \times$$

$$\times \left\{ (R^4 \ln R - R^4 + 2R^2 \ln^2 R - R^2 \ln R + \right.$$

$$+ 2R^2 - 2R^2 \ln^3 R - 1) + \frac{Rq_{21} + 1}{4R^2 \ln^2 R - (R^2-1)^2} \times$$

$$\times \left[ -\frac{9}{2} R^6 \ln R - \frac{3}{4} R^6 + 2R^6 \ln^2 R + 9R^4 \ln R + \right.$$

$$+ \frac{3}{4} R^2 - 2R^2 \ln^2 R - 2R^6 \ln^3 R + 8R^4 \ln^3 R -$$

$$- 2R^2 \ln^3 R - \frac{9}{2} R^2 \ln R + \frac{8}{3} R^4 \ln^5 R +$$

$$\left. \left. + \frac{3}{8} R^8 - \frac{3}{8} \right] \right\}, \tag{29}$$

and ultimately

$$Nu_1 = \{2(R-1)[(R^2-1)^2 - 4R^2 \ln^2 R]\} \times$$

$$\times \left\| (R^4 \ln R - R^4 + 2R^2 \ln^2 R - R^2 \ln R + 2R^2 - 2R^2 \ln^3 R - 1) + \right.$$

$$+ \frac{Rq_{21} + 1}{4R^2 \ln^2 R - (R^2-1)^2} \left[ -\frac{9}{2} R^6 \ln R - \frac{3}{4} R^6 + 2R^6 \ln^2 R + \right.$$

$$+ 9R^4 \ln R + \frac{3}{4} R^2 - 2R^2 \ln^2 R - 2R^6 \ln^3 R +$$

$$+ 8R^4 \ln^3 R - 2R^2 \ln^3 R - \frac{9}{2} R^2 \ln R +$$

$$\left. \left. + \frac{8}{3} R^4 \ln^5 R + \frac{3}{8} R^8 - \frac{3}{8} \right] \right\|^{-1}. \tag{30}$$

By analogy, we obtain the following expression for $Nu_2$:

$$Nu_2 = \frac{\alpha_2 d_{equ}}{\lambda} = \frac{q_2 2(R-1) r_1}{\lambda [G(r_2) - \bar{G}]} =$$

$$= \{2q_{21}(R-1)[(R^2-1)^2 - 4R^2 \ln^2 R]\} \times$$

$$\times \left\{ 2R^2 \ln^2 R - R^4 + R^2 \ln R + 2R^2 + 2R^2 \ln^3 R - 1 - \ln R + \right.$$

$$+ \frac{Rq_{21}}{4R^2 \ln^2 R - (R^2-1)^2} \left( -\frac{7}{2} R^6 \ln R - \frac{7}{4} R^6 + 4R^6 \ln^2 R + \right.$$

$$+ 6R^4 \ln R + \frac{7}{4} R^2 + 4R^2 \ln^2 R + 4R^2 \ln^3 R -$$

$$- \frac{3}{2} R^2 \ln R - \frac{16}{3} R^4 \ln^5 R - \frac{11}{8} + \frac{3}{8} R^8 - \ln R +$$

$$\left. \left. + 2R^5 + R^4 - 4R^3 + 2R - 8R^3 \ln^2 R - 8R^4 \ln^4 R \right) \right\}^{-1} \qquad (31)$$

As in the case of a straight plane channel, let us derive an expression for the overall Nusselt number on the basis of the total heat flux:

$$Nu_0 = \frac{\alpha_0 d_{equ}}{\lambda} = \frac{q_0 d_{equ}}{\lambda (T_2 - T_1)}, \qquad (32)$$

where

$$q_0 = \frac{q_1 F_1 + q_2 F_2}{F_1 + F_2} = q_1 \frac{1 + Rq_{21}}{1 + R}.$$

Substitution of the value of $T_2 - T_1$ (from (27)) in (32) ultimately gives

$$Nu_0 = \{2(R-1)(1+Rq_{21})\} \left\{ (R+1) \left[ -\ln R + \right. \right.$$

$$\left. + \frac{Rq_{21} + 1}{4R^2 \ln^2 R - (R^2-1)^2} \right] \{ -\ln R + 2R^2 - 1 - R^4 +$$

$$\left. + 2R^2 \ln^3 R + 2R^2 \ln^2 R + R^2 \ln R \} \right\}^{-1}. \qquad (33)$$

The dimensionless temperature $\vartheta = \frac{T - T_1}{T_2 - T_1}$ distribution over the cross section for $q_{21} = 1$ is shown in Figure 2,b for various values of the curvature parameter $m$. It is evident that as $m$ increases, the dimensionless temperature extremum shifts to the side of the inner wall. The effect of the heat flux density ratio $q_{21}$ on the dimensionless temperature ($\vartheta$) profile is shown in Figure 3.

The distribution of the Nusselt numbers $Nu_1$ and $Nu_2$ for the flow analyzed here is shown in Figure 4.

Solution of the turbulent convective heat transfer problem with the aid of the hydrodynamic integrator

The heat transfer equation for equilibrium turbulent flow of a liquid within a channel is:

$$\frac{\partial \vartheta}{\partial \bar{x}} = \frac{1}{\bar{W}(\bar{y})\,\bar{y}^k}\,\frac{\partial}{\partial \bar{y}}\left(\bar{y}^k\,\bar{a}_{\text{eff}}\frac{\partial \vartheta}{\partial \bar{y}}\right). \tag{34}$$

The values $k = 0$ and 1 correspond to plane and circular channels, respectively. In (35) $\bar{x} = \frac{xa}{W_{\text{av}}R^2}\,\frac{W_{\text{av}}}{W_m}$ and $\bar{y} = \frac{y}{R}$ denote generalized coordinates; $a_{\text{eff}} = 1 + \frac{a_{\text{turb}}}{a}$ is the effective thermal diffusivity coefficient; $\bar{W} = \frac{W}{W_m}$ is the dimensionless turbulent velocity profile; and $\vartheta = \frac{t - t_w}{t_0 - t_w}$ is the dimensionless excess temperature.

The terms $\bar{W}(\bar{y})$ and $\bar{a}_{\text{eff}}$ in (34) are usually regarded as known from the solution of the corresponding dynamic problem (or from experiment) and from the use of the assumptions of the hydrodynamic theory of heat transfer /2/.

In the case of a constant wall temperature, the boundary conditions for equation (34) are

$$\begin{aligned} &\text{at } \bar{x} = 0 \quad 0 < \bar{y} < 1, \quad \vartheta(0, \bar{y}) = 1; \\ &\text{at } \bar{x} > 0 \quad \bar{y} = 1, \quad \vartheta(\bar{x}, 1) = 0. \end{aligned} \tag{35}$$

In the case of a constant heat flux ($q$ = const.) on the channel walls $\vartheta = \frac{t}{t_0}$, and the boundary conditions are replaced by:

$$\text{at } \bar{x} > 0 \text{ and } \bar{y} = 1 \quad \vartheta = 1 + m_0 x, \tag{36}$$

where $m_0$ is constant.

The Nusselt number is determined from the equation

$$\text{Nu} = \frac{-2\left(\frac{\partial \vartheta}{\partial y}\right)\bar{y} = 1}{\vartheta_{\text{av}}} \tag{37}$$

or, in the case of $q_w$ = const.

$$\text{Nu} = \frac{-2\left(\frac{d\vartheta}{d\bar{y}}\right)_{\bar{y}=1}}{\vartheta_{\text{av}} - \vartheta_w}. \tag{38}$$

The fundamental equation for the apparatus is (in a generalized form) /4/

$$\frac{\partial H}{\partial \bar{\tau}} = \frac{L}{\frac{d\bar{f}}{d\bar{z}}}\,\frac{\partial}{\partial \bar{z}}\left(\frac{M}{\frac{d\bar{\rho}}{d\bar{z}}}\,\frac{\partial H}{\partial \bar{z}}\right), \tag{39}$$

where

$$\bar{\tau} = \frac{\tau}{\sum_{i=1}^{n} \rho \sum_{i=1}^{n} fLM}; \quad \bar{z} = \frac{z}{S}; \quad H = \frac{h - h_w}{h_0 - h_w};$$

$l$. and $M$ are normalizing factors.

By comparing (34) and (39), it is simple to find the modeling conditions under which they become similar equations and the process in the apparatus is a true model of the actual process:

$$\left.\begin{aligned} \bar{\tau} &= \bar{x} \\ \bar{z} &= \bar{y} \\ \bar{H}(\bar{\tau}, \bar{z}) &= \vartheta(\bar{x}, y) \end{aligned}\right\}, \qquad (40)$$

$$\frac{L}{\frac{d\bar{f}}{d\bar{z}}} = \frac{1}{\bar{W}(\bar{y})\,\bar{y}_k},$$

$$\frac{M}{\frac{d\bar{\rho}}{d\bar{z}}} = \frac{1}{\bar{y}_k \bar{a}_{\text{eff}}}.$$

The boundary conditions for equation (40) are also selected on the apparatus in such a way that they correspond to the boundary conditions of the thermal problem (35) and (36). Using the modeling condition (40), it is possible to determine the capacities of the integrator vessels, the resistance, the relationship between the working time of the apparatus $\tau$ and the $x$ coordinate, etc., which information is necessary for adjustment of the apparatus to the solution of the actual problem, and the recalculation of the experimental data to correspond to the actual thermal process. For instance, the capacity $\bar{f}_i$ of the integrator vessels and the resistance $\bar{\rho}_i$ of its capillaries are determined from the equations

$$\left.\begin{aligned} \bar{f}_i(\bar{z}) &= L \int_{i-1}^{i} \bar{y}_k \bar{W}(\bar{y})\, d\bar{y} \\ \bar{\rho}_i(\bar{z}) &= M \int_{i-1}^{i} \frac{d\bar{y}}{\bar{y}^k a_{\text{eff}}} \end{aligned}\right\}, \qquad (41)$$

where

$$L = \frac{1}{\int_0^1 \bar{y}^k W(\bar{y})\, d\bar{y}}; \quad M = \frac{1}{\int_0^1 \frac{d\bar{y}}{\bar{y}_k a_{\text{eff}}}}.$$

As in the earlier case, the Nusselt number is determined by means of equations that are analogous to (38) and (39):

$$\text{Nu} = \frac{-2\left(\frac{\partial H}{\partial \bar{z}}\right)_{\bar{z}=1}}{H_{\text{av}}}, \qquad (42)$$

$$\mathrm{Nu} = \frac{-2\left(\frac{\partial H}{\partial \bar{z}}\right)_{\bar{z}=1}}{H_{av} - H_w}. \qquad (43)$$

However, the calculation of the Nusselt number by the above method requires graphical differentiation of the profile $H$ obtained on the wall of the apparatus.

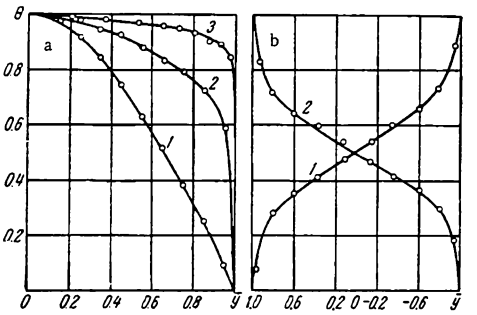


FIGURE 5. Relative temperature distribution in circular (a) and plane (b) channels.

a — $\mathrm{Re} = 3 \cdot 10^4$, $t_w = \mathrm{const}$; 1 — $\mathrm{Pr}^* = 0.01$; 2 — $\mathrm{Pr}^* = 1$; 3 — $\mathrm{Pr}^* = 10$; (the continuous lines are based on data from the values /2/, while the points are based on data from the integrator); b — 1 — $\mathrm{Re} = 9370$; 2 — $\mathrm{Re} = 17{,}100$ (the continuous lines are experimental /5-7/, while the points are based on data from the integrator).

The graphical differentiation over the transverse coordinate is not sufficiently accurate due to the very rapid change of $H$ on the channel wall during turbulent flow.

Hence, the Nusselt number was calculated using the following equation /4/:

$$\mathrm{Nu} = \frac{2vM\sum_{1}^{n}\rho}{h_{av} - h_w}, \qquad (44)$$

where $v$ is the flow rate (per second) of the liquid through the integrator.

A comparison of the integrator data for the heat transfer in circular and plane channels with the available experimental /5-7/ and calculated /2/ data is shown in Figure 5.

Figure 5,a shows the relative temperature $\vartheta$ profiles in the cross section of a circular channel, for the case of a constant wall temperature at $\mathrm{Re} = 3 \cdot 10^4$ and generalized Prandtl numbers ($\mathrm{Pr}^*$) of 0.01, 1, and 10:

$$\mathrm{Pr}^* = \frac{\mathrm{Pr}}{\mathrm{Pr}_{turb}}.$$

Figure 5,b shows the relative temperature $\vartheta$ profiles in the cross section of a plane channel, for two values of the Reynolds number (Re = 17,100 and 9370) and for a Prandtl number Pr = 0.72.

The solutions were found for the following boundary conditions:

$$\bar{x} = 0, \quad -1 \leqslant \bar{y} \leqslant 1, \quad \vartheta(0, \bar{y}) = 1,$$
$$\bar{x} > 0, \quad \bar{y} = 1, \quad \vartheta(0, 1) = \vartheta_{\omega_1},$$
$$\bar{x} > 0, \quad \bar{y} = -1, \quad \vartheta(0, -1) = \vartheta_{\omega_2}.$$

The figures show that the calculated and experimental results (continuous lines) agree well with the points obtained on the hydrodynamic integrator.

The calculated heat transfer coefficient was compared with the Mikheev equation and showed satisfactory agreement. This confirms that the hydrodynamic integrator has a future for the calculation of turbulent convective heat transfer under the inner problem conditions.

Bibliography


1. Slezkin, N.A. Dinamika vyazkoi neszhimaemoi zhidkosti (The Dynamics of Viscous Incompressible Liquids). — GIITA. 1955.
2. Groeber, H., S. Erk, and U. Grigull. Die Grundgesetze der Wärmeübertragung. Berlin, Springer. 1955. [Russian Translation. 1958.]
3. Jansen, L. Schweizerische Bauzeitung. 13 September, 1952.
4. Ustimenko, B.P. and K.A. Zhurgembaev. — Isvestiya AN KazSSR, Ser. energeticheskaya, No. 1:19. 1961.
5. Corcoran, W.H., B.H. Sage, F. Page, and W.G. Schlinger. — Industrial and Engineering Chemistry, Vol. 44, No. 2. 1952.
6. Page, F., B.H. Sage, W.H. Corcoran, and W.G. Schlinger. — Industrial and Engineering Chemistry, Vol. 44, No. 2. 1952.
7. Cavers, S.D., H.T. Hsu, B. Scheinger, and B.H. Sage. — Industrial and Engineering Chemistry, Vol. 45, No. 10. 1953.



The Power Institute of the Academy of Sciences of the KazSSR

I.S. Kochenov, L.I. Baranova, and
V.V. Vasil'ev

# FLOW IN CHANNELS WITH PERMEABLE WALLS

The pressure change in a channel with permeable walls is described by the motion equation, which can be written in the following averaged form (for a constant cross-section channel in which the velocity on the wall is perpendicular to the axis):

$$dp = -\beta\rho w^2\left(\frac{dw}{w} + \frac{d(\beta G)}{\beta G}\right) - \xi\frac{\rho w^2}{2}\frac{dx}{d}, \qquad (1)$$

where

$$\xi = \frac{8\tau_w}{\rho w^2}, \qquad \beta = \frac{1}{F}\int_F \left(\frac{u}{w}\right)^2 dF.$$

As is evident from the above equation, the pressure gradient depends not only on the influence of friction on the flow (which is described by the second term in the right-hand side of the equation) but also on a dynamic effect associated with pulse transfer between the main and outflow streams (which is described by the first term in the right-hand side and which becomes predominant in the case of large outflows).

The first term in the right-hand side of equation (1) contains a variable (over the length) averaging the velocity coefficient $\beta$. It can be calculated if the velocity profile is known. It has been shown /1/ that for quasi-stabilized sections, the coefficient $\beta$ may be presented as a function of any two local numbers from the three related dimensionless numbers: $\mathrm{Re} = \frac{wD}{\nu}$, $\mathrm{Re}_\perp = \frac{v_w D}{\nu}$, and $K_\perp = \frac{v_w}{w}$.

Such functions may be studied experimentally even without plotting the velocity profile, but in that case it becomes necessary to measure (in addition to the pressure gradient and the flow rate) the tangential stress on the porous wall, which involves experimental difficulties. Moreover, in engineering practice, it is rather inconvenient to make use of two variable coefficients, each of them a function of two local dimensionless numbers. For these reasons, we propose a new method for the calculation of pressure changes in channels with permeable walls.

Equation (1) is rewritten in a dimensionless form

$$-\mathrm{Eu} \equiv \frac{dP}{dX} = 16\beta K_\perp\left[1 + 0.5\frac{d\ln\beta}{d\ln G}\right] - \xi. \qquad (2)$$

The changes in $\beta$ are relatively small, especially in streams with outflow through the wall. In streams with small outflows and inflows, the coefficient of friction $\xi$ has a value close to that of the coefficient of friction in a channel with impermeable walls ($\xi_0$).

In flows with a large absolute value of $K_\perp$, the coefficient of friction contributes only slightly to the determination of the Eu number. Hence, the arbitrary Euler number $Eu_*$ calculated from the equation

$$Eu_* = 16K_\perp - \xi_0, \tag{3}$$

is equal at first approximation to the true Euler number described by equation (2).

The accurate equation has the form

$$-\frac{dP}{dX} \equiv Eu = \varepsilon Eu_*, \tag{4}$$

where $\varepsilon$ is a variable coefficient whose nature has to be analyzed.

By definition

$$\varepsilon = \frac{16\beta K_\perp \left(1 + 0.5\dfrac{d\ln\beta}{d\ln G}\right) - \xi}{16K_\perp - \xi_0}. \tag{5}$$

A term-by-term analysis of equation (5) shows that $\varepsilon$ is a function of two local dimensionless numbers, Re and $K_\perp$ (or $Re_\perp$ and $K_\perp$, or Re and $Re_\perp$). The value of $\varepsilon$ is close to unity.

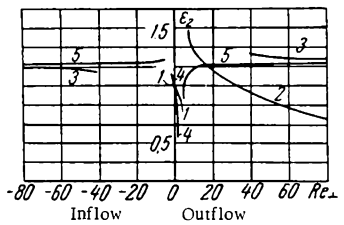


FIGURE 1. Plot of $\varepsilon_2$ as a function of $Re_\perp$.

1 — Berman's solution for a plane aperture with small outflow; 2 — White's solution for a plane aperture with large outflow; 3 — Juan's solution for a plane aperture with large outflow; 4 — Juan and Finkelstein's solution for a tube with small outflow; 5 — Juan and Finkelstein's solution for a tube with large outflow.

The above method was used to process the theoretical results of several authors who studied laminar /2-5/ and turbulent /6-7/ flows in a circular tube with permeable walls; it was found that $\varepsilon$ is a function of only one of the Reynolds numbers — the Reynolds number for the outflow ($Re_\perp$) (see Figure 1).

This conclusion must be accepted with some reservation, since all available solutions /2-7/ have been obtained by assuming that the current function may be presented as a product of two cofactors, one of which is a function of the longitudinal coordinate alone, while the other is a function solely of the transverse coordinate. The above assumption does not completely satisfy the given velocity distribution at the entry to the section with the outflow. Hence, some of the theoretical papers (e. g., /2/) assume a disruption of the velocity on the stream axis at $X = 0$, while other papers (e. g., /5-7/) assume an unbalanced flow rate.

In spite of the disagreement in the available theoretical data, the conclusion reached on processing them (namely, that the $Re_\perp$ number should

be one of the main factors determining the coefficient $\varepsilon$) is, in our opinion, quite convincing. Hence, the experimental data should be processed in the form

$$\varepsilon = f(\mathrm{Re}_\perp, K_\perp).$$

In order to study the above function, we built an experimental setup and carried out some preliminary experiments.

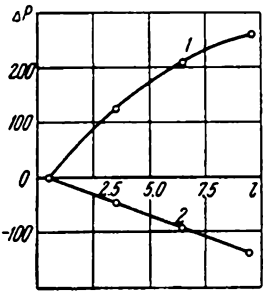


FIGURE 2. Nature of the pressure changes over the channel length.

1 — experiment with outflow;
2 — without outflow.

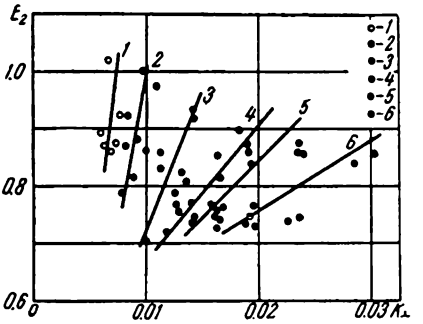


FIGURE 3. The dimensionless number $\varepsilon_2$ as a function of $K_\perp$ at:

1 — $\mathrm{Re}_\perp$ = 300; 2 — 400; 3 — 500; 4 — 600; 5 — 700; 6 — 700 [sic].

The working section consisted of a channel 0.013 m in diameter and 0.1 m long. The section was constructed from 270 disks (0.00025 m thick), maintained 0.0001 m apart by means of special spacers. The disks were grouped in sections (27 disks in each section).

The outflows from each section were isolated from one another, and the outflow rate was controlled by control valves. The total outflow rate through all sections was maintained constant ($v_w$ = const.). They were determined by measuring the pressure drops with special measuring tubes. In addition to the measurements of the outflow rates at 10 sections, we measured the main flow rate in front of and behind the working section.

The pressure drop between the sections was measured with the aid of a battery-actuated differential manometer; the pressure on the channel walls was measured with the aid of tubes 0.00125 × 0.0002 m in diameter.

The measured hydraulic curve in an experimental channel without outflow (with closed control valves) was positioned higher (by 8%) than the Blasius curve.

The experiments were carried out with flow rates corresponding to Reynolds numbers between 15,000 and 50,000, using water as the working fluid.

The range of outflow coefficients was $8 \cdot 10^{-4} \leqslant K_\perp \leqslant 8 \cdot 10^{-3}$. Such outflows should be regarded as large. The nature of the pressure changes along the channel is shown in Figure 2. As is evident from the figure, in the presence of outflow, the pressure increases along the channel, and the calculations show that despite the higher values of the coefficient of

friction in streams with outflow, there was in many cases (at high $K_\perp$) an increase not only in the static pressure but also in the total kinetic energy of the liquid over the length. To the best of our knowledge, this is an unprecedented experimental observation.

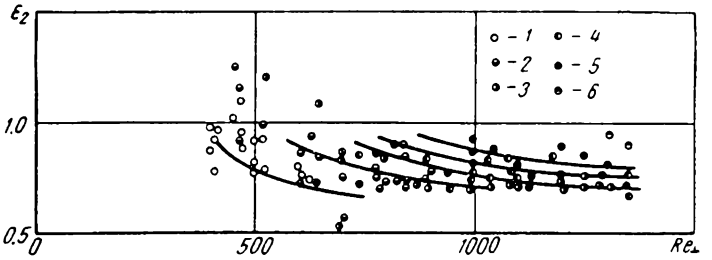


FIGURE 4. A plot of $\varepsilon_2$ as a function of $Re_\perp$ when $K_\perp$ was changed within the ranges:

1 — from 0.008 to 0.015; 2 — from 0.015 to 0.025; 3 — from 0.025 to 0.035; 4 — from 0.035 to 0.045; 5 — from 0.045 — 0.060; 6 — from 0.070 to 0.080.

There were about 300 experiments on flow with outflow in all. The results of their preliminary processing are shown in Figures 3 and 4.

The data in Figure 4 show that in the range studied, the value of $\varepsilon_2$ ranges from 0.7 to 1. It increases with increasing $K_\perp$ and decreases somewhat with increasing $Re_\perp$.

Bibliography

1. Kochenov, I.S. — Trudy MIIT, No. 139. 1961.
2. Berman, A.S. — J. Appl. Phys., Vol. 24, No. 9. 1953.
3. Juan, S.W. — J. Appl. Phys., Vol. 27, No. 3. 1956.
4. White, F.M., B.F. Barfield, and M.J. Goglia. — J. Appl. Mech., Vol. 25, No. 4. 1958.
5. Juan, S.W. and A.B. Finkelstein. — Trans. ASME, Vol. 78, No. 4. 1956.
6. Juan, S.W. — J. Math. and Phys., Vol. 38, No. 3. 1959.
7. Juan, S.W. and E.B. Brogren. — Phys. Fluids, Vol. 4, No. 3. 1961.

Moscow

M. E. Podol'skii

# THE ATTRACTIVE ACTION OF A NONISOTHERMAL LUBRICATING LAYER

As a result of the temperature dependence of the viscosity of lubricating oils, a close relationship exists between the heat transfer and the hydrodynamic processes in the lubrication layer of a sleeve bearing. These problems have been discussed in many papers, which may be divided into two groups. In the papers of the first group, it is assumed that no heat is exchanged between the layer and the surrounding part, and that most of the increase in temperature takes place along the layer. The papers in the second group are based on the assumption that the convective heat transfer with the moving lubricant is not important, and it is assumed that the temperature is constant along and variable across the layer. At the same time, the simultaneous change in the temperature (and, hence, in the viscosity) over both the length and the thickness of the layer is connected with some new qualitative phenomena, which were not observed when the longitudinal and transverse temperature gradients were treated separately. The first to report this phenomenon was apparently Zienkiewicz /1/, who made rather complicated calculations to prove that with adequately selected boundary conditions (for the temperature), hydrodynamic forces may be created even in the case of parallel frictional surfaces. Cameron /2/ reached similar conclusions by assuming that the viscosity is a known linear function of the longitudinal and transverse coordinates. According to Zienkiewicz and Cameron, the force created in a lubrication layer of constant thickness pushes away the friction surfaces.

In this paper, we shall present (mainly for the case of an axial sleeve bearing) an approximate solution of the hydrodynamic equation and the energy balance, taking into account the viscosity changes over the length and the thickness of the layer. The boundary conditions (for the temperature) were selected on the basis of an analysis of the heat distribution within a shaft. A more detailed study was made of the flow of a lubricant between parallel friction surfaces. The derived equations show that because of the temperature dependence of the viscosity, the friction surfaces are attracted to each other.

1) The plane-parallel flow of the lubricant is described by the following system of equations:

$$\frac{\partial p}{\partial x} = \frac{\partial}{\partial y}\left(\mu \frac{\partial u}{\partial y}\right), \quad \frac{\partial p}{\partial y} = 0, \quad \frac{\partial u}{\partial x} + \frac{\partial v}{\partial y} = 0. \tag{1}$$

Thermal balance equations must be added to the equations in one of two forms:

$$u\frac{\partial T}{\partial x}+v\frac{\partial T}{\partial y}=\frac{\lambda}{\rho c}\frac{\partial^2 T}{\partial y^2}+\frac{\mu}{I\rho c}\left(\frac{\partial u}{\partial y}\right)^2 \tag{2}$$

or

$$\begin{aligned}\frac{\partial}{\partial x}(uT)+\frac{\partial}{\partial y}(vT)=\frac{\lambda}{\rho c}\frac{\partial^2 T}{\partial y^2}+\\ +\frac{1}{I\rho c}\left\{\frac{\partial}{\partial y}\left(\mu u\frac{\partial u}{\partial y}\right)-u\frac{\partial}{\partial y}\left(\mu\frac{\partial u}{\partial y}\right)\right\}\end{aligned} \tag{2a}$$

and by an equation expressing the viscosity as a function of temperature

$$\mu=\mu(T). \tag{3}$$

The boundary conditions for the velocity and pressure may be taken in the following forms ($h$ being the thickness of the lubricant layer):

$$\left.\begin{array}{c}\text{at}\quad y=0\quad u=U,\quad v=0\\ \text{at}\quad y=h\quad u=0,\quad v=0\\ \text{at}\quad x=0\quad p=0,\ \text{at}\quad x=a\quad p=0\end{array}\right\}. \tag{4}$$

By introducing the variables

$$\xi=x,\quad \eta=\int_0^y\frac{dy}{\mu}, \tag{5}$$

the system of equations (1) and (2a) is transformed into

$$\mu\frac{\partial p}{\partial\xi}=\frac{\partial^2 u}{\partial\eta^2},\quad \frac{\partial p}{\partial\eta}=0,\quad \frac{\partial(u\mu)}{\partial\xi}+\frac{\partial v_1}{\partial\eta}=0, \tag{6}$$

$$\begin{aligned}\frac{\partial}{\partial\xi}(u\mu T)+\frac{\partial}{\partial\eta}(v_1T)=\frac{\lambda}{\rho c}\frac{\partial}{\partial\eta}\left(\frac{1}{\mu}\frac{\partial T}{\partial\eta}\right)+\\ +\frac{1}{I\rho c}\frac{\partial}{\partial\eta}\left(u\frac{\partial u}{\partial\eta}\right)-\frac{1}{I\rho c}u\frac{\partial^2 u}{\partial\eta^2}.\end{aligned} \tag{7}$$

where

$$v_1=v+u\mu\frac{\partial\eta}{\partial x}. \tag{8}$$

The boundary conditions (4) and the variables (5) are written as follows:

$$\left.\begin{array}{c}\text{at}\quad \eta=0\quad u=U,\quad v_1=0^*\\ \text{at}\quad \eta=\tilde{h}\quad u=0,\quad v_1=0,\quad \tilde{h}=\int_0^h\frac{\partial y}{\mu}\\ \text{at}\quad \xi=0\quad p=0,\quad \text{at}\quad \xi=a\quad p=0\end{array}\right\}. \tag{9}$$

* According to (8) $v_1(\xi,\ \eta=0)=\mu U\left.\frac{\partial\eta}{\partial x}\right|_{y=0}$. Since $\frac{\partial\eta}{\partial x}=\int_0^y\frac{\partial}{\partial x}\times\left[\frac{1}{\mu(x_1a)}\right]da+\frac{1}{\mu(x,\ y)}\frac{dy}{dx}$, we have on the line $y=0$ $\frac{\partial\eta}{\partial x}=0$.

Let us analyze the function (3). Many equations for this function have been proposed to date. Below we shall use the most convenient hyperbolic function for our subsequent analysis (the first two terms in the series of the Bachinskii equation /3/).

$$\mu\tau = b, \quad \tau = d + T, \tag{10}$$

where $b$ and $d$ are constants depending on the brand of oil.

Since, as follows from (2) the thermal balance equation does not change its form when a constant component is added, equation (7) may be written (taking into account (10)) as follows

$$\frac{\partial u}{\partial \xi} + \frac{1}{b}\frac{\partial}{\partial \eta}(v_1 \tau) = \frac{\lambda}{\rho c b^2}\frac{\partial}{\partial \eta}\left(\tau \frac{\partial \tau}{\partial \eta}\right) + \frac{1}{l \rho c b}\frac{\partial}{\partial \eta}\left(u \frac{\partial u}{\partial \eta}\right) - \frac{1}{l \rho c b} u \frac{\partial^2 u}{\partial \eta^2}. \tag{11}$$

We shall solve the derived equations by the method of integral relations. Under the conditions of the problem discussed here, the method of integral relations should be applied with greatest advantage to the system of equations (6) and (11), since the velocity profile, for instance, may be described more simply in terms of the variables $\xi$ and $\eta$ than in terms of the variables $x$ and $y$. By integrating equations (6) and (11) (taking into account the boundary conditions (9)) and by adding to them the integral condition for the relationship between $y$ and $\eta$, we obtain the system of integral relations in the following form:

$$h \frac{\partial p}{\partial \xi} = \frac{\partial u}{\partial \eta}\Big|_0^{\tilde{h}}, \quad \int_0^{\tilde{h}} \mu u d\eta = q_1,$$

$$\frac{\partial}{\partial \xi}\int_0^{\tilde{h}} u \, d\eta = \frac{\lambda}{\rho c b^2} \tau \frac{\partial \tau}{\partial \eta}\Big|_0^{\tilde{h}} + \frac{1}{l \rho c b} u \frac{\partial u}{\partial \eta}\Big|_0^{\tilde{h}} - \frac{1}{l \rho c b}\int_0^{\tilde{h}} u \frac{\partial^2 u}{\partial \eta^2} d\eta, \tag{12}$$

$$h = \int_0^{\tilde{h}} \mu \, d\eta.$$

2) We shall now examine the temperature conditions on the boundaries of the lubricant layer. On the pad surface, the nature of the temperature changes is determined by the heat transfer coefficient from the pad to the lubricant in contact with it, and it depends to a great extent on the design of the bearing. It is assumed below that the pads are thermally insulated, i.e.,

$$\text{at } y = h \quad \frac{\partial T}{\partial y} = 0 \tag{13}$$

or

$$\text{at } \eta_1 = \tilde{h} \quad \frac{\partial T}{\partial \eta} = 0 \quad \left(\frac{\partial \tau}{\partial \eta_1} = 0\right). \tag{13a}$$

The motion of the bearing surface with respect to the layer is, apparently, the most important feature of the boundary conditions on the side of the collar. Heat fluxes of various densities pass through a unit area of the

collar (depending on its position with respect to the layer) as a result of the above motion. Naturally, it may be assumed that as the speed of the motion increases, these heat flux densities approach an average value, and the collar temperature becomes constant in the direction of rotation, i. e., in the direction of motion of the bearing surface, according to the scheme of the two-dimensional problem. In order to determine the validity and the range of application of the above assumption, we shall analyze the propagation of heat in the collar by simulating the collar (in the case of a two-dimensional body) by a bearing plate subjected to forward motion (see figure).

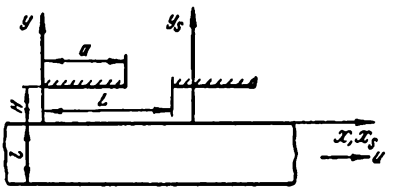


Propagation of heat in a moving collar.

The equation for the propagation of heat in the bearing plate is (in a system of coordinates rigidly bound to the plate)

$$\frac{\partial T}{\partial t} = a_s^2\left(\frac{\partial^2 T}{\partial x_s^2} + \frac{\partial^2 T}{\partial y_s^2}\right), \tag{14}$$

where $a_s$ is the heat diffusivity coefficient of the material of the collar.

In a fixed [non-moving] system of coordinates, $x$, $y$, (14) assumes the form

$$\frac{\partial T}{\partial t} + U\frac{\partial T}{\partial x} = a_s^2\left(\frac{\partial^2 T}{\partial x^2} + \frac{\partial^2 T}{\partial y^2}\right). \tag{14a}$$

In view of the stationary nature of the boundary condition in a fixed system of coordinates, it is only necessary to work out stationary solutions of equation (14a). Moreover, by using the method of dimensionless analysis, it is found that since $a_s^2/UL \ll 1$*, the term $a_s^2\partial^2 T/\partial x^2$ is small in comparison with $U\partial T/\partial x$. Thus, equation (14a) may be replaced by a simpler equation

$$\frac{\partial T}{\partial x} = \frac{a_s^2}{U}\frac{\partial^2 T}{\partial y^2}. \tag{14b}$$

Let us find a solution of equation (14b) for a case in which the heat flux density at one boundary of the plate changes in accordance with the sinusoidal law, while no heat transfer takes place between the second boundary and the surroundings. The boundary conditions corresponding to such a case would be

$$\text{at } y = 0 \quad \frac{\partial T}{\partial y} = \frac{q_m}{l}\sin\frac{\pi x}{L}, \quad \text{at } y = -l \quad \frac{\partial T}{\partial y} = 0 \tag{15}$$

* In the case of steel $a_s^2 = 1.4 \cdot 10^{-5}$ m$^2$/sec. Assuming $U = 50$ m/sec and $L = 6 \cdot 10^{-2}$ m, we obtain $a_s^2/UL = 4.66 \cdot 10^{-6}$.

where $l$ is the thickness of the plate.

By looking for a solution in the form

$$T = T_0 + lmf\left(\frac{y}{l}\right)\exp\left(\frac{\pi x}{L}i\right),$$

and satisfying the conditions set up in (15), we obtain

$$\left.\begin{aligned} f\left(\frac{y}{l}\right) &= \frac{\beta q_m}{1+i}\left[sh\frac{(1+i)y}{\beta l} + cth\frac{1+i}{\beta}ch\frac{(1+i)y}{\beta l}\right] \\ \beta^2 &= \frac{2}{\pi}\frac{L}{l}\frac{a_s^2}{Ul} \end{aligned}\right\}. \qquad (16)$$

From here, for the boundary $y = 0$, we obtain

$$T - T_0 = \frac{q_m}{\sqrt{2}}\frac{\beta}{ch\,2\beta^{-1} + \cos 2\beta^{-1}}\frac{sh^2\beta^{-1} + \cos^2\beta^{-1}}{sh^2\beta^{-1} + \sin^2\beta^{-1}} \times$$
$$\times\left\{sh\frac{2}{\beta}\sin\pi\left(\frac{x}{L} - \frac{1}{4}\right) - \sin\frac{2}{\beta}\cos\pi\left(\frac{x}{L} - \frac{1}{4}\right)\right\}.$$

The following approximation is valid at small $\beta$ *:

$$\max\frac{|T - T_0|}{T_0} \approx \frac{q_m\beta}{\sqrt{2}T_0}. \qquad (17)$$

Using (17), it is possible to evaluate the temperature fluctuations on the collar boundary from known values of $q_m$ and $T_0$. The values of the last two parameters depend on the heat evolution rate and the conditions of heat transfer from the layer to the collar.

Let us analyze the problem of the temperature field in a lubricant layer between two parallel friction surfaces ($h = H = \text{const.}$); the surface temperature of the bearing is assumed to be constant. For simplicity, and bearing in mind the approximate nature of the solutions to be reached, it is assumed also that the viscosity of the lubricant is independent of the temperature. Under such conditions, the solution** of the system of equations (1) and (2) with the boundary conditions (4) and (13) can be written in the following form:

$$T = T_0 + \frac{\mu U^2}{2l\lambda}\left[1 - C\exp\left(-\frac{8\lambda x}{\rho cUH^2}\right)\right] \times \left[1 - \left(1 - \frac{y}{H}\right)^2\right]. \qquad (18)$$

* For instance, at $U = 50$ m/sec, $L = 6\cdot10^{-2}$ m, $l = 3\cdot10^{-2}$ m, and $a_s^2 = 1.4\cdot10^{-5}$ m$^2$/sec, we obtain $\beta = 3.44\cdot10^{-3}$.

** The problem was solved by the method of integral relations, and the temperature profile selected was in the form of a quadratic parabola. If the law governing the temperature changes over the layer thickness is approximately described by a polynomial of the fourth degree, the change in the final results is negligible (e.g., in equation (19), the numerical value in the term for the exponent would be 15/2 instead of 8).

Correspondingly, the average temperature (over the layer thickness) is described by

$$T_m = T_0 + \frac{\mu U^2}{3l\lambda}\left[1 - C\exp\left(-\frac{8\lambda x}{\rho c U H^2}\right)\right]. \qquad (19)$$

The constants in (18) (the bearing surface temperature $T_0$ and the constant $C$) may be determined on the basis of the following considerations.

The first condition follows from the equality of the heat fluxes entering and leaving the collar. Assuming, for simplicity, that the total amount of heat withdrawn from the collar is zero, we obtain from (18)

$$C = \frac{k}{1 - e^{-k}}, \quad k = \frac{8\lambda x}{\rho c U H^2}. \qquad (20)$$

The second condition followed from the examination of the average lubricant temperature at the inlet to the clearance, and is determined by the conditions of mixing of the hot grease leaving the clearance with the cold grease flowing in the channel between the greasing pads. The amount of cold grease in the total stream at the entrance to the clearance must be equal to the amount of side leakage /4/ (which always occurs in actual bearings because of the finite dimensions of the greasing pads). Using $r$ to denote its fraction in the stream at the inlet, we obtain the following expression for the average temperature at the inlet

$$rT_i + (1-r)\left[T_0 + \frac{\mu U^2}{3l\lambda}\left(1 - \frac{ke^{-k}}{1-e^{-k}}\right)\right],$$

where $T_i$ is the temperature of the cold grease entering the channel between the pads. By determining the average temperature at the inlet using (19) and (20), and expanding $e^{-k}$ into a series*, we obtain the following approximate equation:

$$T_0 = T_i + \frac{1}{6}\frac{2-r}{r}\frac{\mu U^2}{l\lambda}k. \qquad (21)$$

The order of magnitude of $q_m$ may be evaluated by equating the differences between the maximum and minimum values of the heat flux densities through the bearing surface, obtained by using (15) and (18). From there, we obtain the following expression (subtracting (21) from (17)):

$$\max\frac{|T-T_0|}{T_0} \approx \frac{\frac{\beta}{2\sqrt{2}}\frac{\mu U^2}{l\lambda}k\frac{l}{H}\frac{\lambda}{\lambda_s}}{T_i + \frac{1}{6}\frac{2-r}{r}\frac{\mu U^2}{l\lambda}k} < \frac{3}{\sqrt{2}}\frac{r}{2-r}\frac{l}{H}\frac{\lambda}{\lambda_s}\beta.$$

* At $\lambda/\rho c = 0.705\cdot10^{-7}$ m$^2$/sec, $U = 50$ m/sec, $a = 4\cdot10^{-2}$ m, $H = 5\cdot10^{-3}$ m, and $k = 0.18$.

In addition to the above parameters, we shall assume that $\lambda = 12.6 \cdot 10^{-2}$ w/m·deg and $\lambda_s = 5.04 \cdot 10$ w/m·deg. According to Yanovskii /5/, the value of $r$ ranges from 0.2 to 0.26. Assuming $r = 0.26$, and substituting the numerical values, we obtain

$$\max \frac{|T - T_0|}{T_0} < \frac{3}{\sqrt{2}} \frac{0.26}{1.74} \frac{3 \cdot 10^{-2}}{5 \cdot 10^{-5}} \frac{12.6 \cdot 10^{-2}}{5.04 \cdot 10} \times$$
$$\times 3.44 \cdot 10^{-3} = 1.64 \cdot 10^{-3} < 0.2\%.$$

Thus, our calculations show that the temperature of the lubricant layer at the boundary with the bearing surface is, indeed, nearly constant. Therefore, the boundary condition on the side of the bearing collar assumes the form

$$\text{at } y = 0 \quad T = T_0 \quad (T_0 = \text{const}) \tag{22}$$

or

$$\text{at } \eta = 0 \quad T = T_0 \quad (\tau = \tau_0). \tag{22a}$$

3) In order to solve the system (12) with the boundary conditions (9), (13a), and (22a), we shall assume that

$$u = U\{1 - \eta_1 - \varphi(\eta_1 - \eta_1^2)\}, \tag{23}$$
$$\mu = \mu_0\{1 - \psi(2\eta_1 - \eta_1^2)\}, \tag{24}$$
$$\eta_1 = \frac{\eta}{\bar{h}}. \tag{25}$$

Taking (10) into account, and introducing the notation

$$\Theta = \frac{\mu_0 \bar{h}}{h}, \quad q = \frac{2q_1}{UH}, \quad \xi = a\zeta, \quad h = H\delta(\xi), \tag{26}$$

we obtain, after substituting (23) and (24) in (12),

$$\frac{H^2}{2Ua\mu_0} \frac{dp}{d\zeta} = \frac{\varphi}{\delta^2\Theta}, \tag{27}$$
$$1 - \frac{1}{3}\varphi - \frac{1}{2}\psi + \frac{7}{30}\varphi\psi = \frac{q}{\delta\Theta}, \tag{28}$$
$$\frac{d}{d\zeta}\delta\Theta\left(1 - \frac{\varphi}{3}\right) = -\frac{4\lambda a}{\rho cUH^2}\frac{\psi}{\delta\Theta} + \frac{2\mu_0^2 Ua}{I\rho cbH^2} \times$$
$$\times \frac{1}{\delta\Theta}\left(1 + \frac{\varphi^2}{3}\right), \tag{29}$$
$$1 - \frac{2}{3}\psi = \frac{1}{\Theta}. \tag{30}$$

A more detailed analysis of the flow of grease between the parallel friction surfaces ($\delta = 1$, $h = H$) yields the following.

The elimination of $\psi$ from (28) and (30) gives

$$\varphi = \frac{3}{4}\frac{1 - Q_1\Theta^{-1}}{-0.05 + 1.05\Theta^{-1}}, \quad Q_1 = 4q - 3. \tag{31}$$

As follows from (26), (9), and (10), the symbol $\Theta$ stands for the ratio of the average temperature (over the layer thickness) $\tau_m$ to the bearing surface temperature $\tau_0$. We shall assume below that the ratio is smaller than three:

$$\Theta < 3. \tag{32}$$

In this case, the following expression would be valid with an accuracy of 10%:

$$\varphi = \frac{3}{4}\Theta\left(1 - \frac{Q_1}{\Theta}\right). \tag{33}$$

It is now possible to arrive at some conclusions concerning the nature of the pressure changes within the layer. Since the average layer temperature, and hence $\Theta$, increase with increasing $\zeta$, the boundary condition (9) for the pressure may be satisfied only if $\varphi(\zeta=0)<0$ (see (27) and (33)). However, it follows from (27) that in such a case the pressure $p$ is negative. In other words, the nonisothermal flow of grease in a clearance of constant thickness causes, under the above conditions, the creation of forces that attract the friction surfaces.

In order to obtain quantitative results, it is necessary to integrate equations (27) to (30). The solution may be written as quadratures, but this is very cumbersome. Considerable simplification may be achieved by assuming that the value of $\varphi$ is small.

In practice, it is sufficient to assume that

$$|\varphi| < 0.3. \tag{34}$$

Then, by using (33), it is possible to transform equations (27) and (29) to:

$$\frac{d\bar{p}}{dz} = \frac{z-1}{z}(z - Q), \tag{35}$$

$$\frac{dz}{d\zeta} = k_1 \varkappa^3 \frac{z}{(z-1)^2}, \tag{36}$$

where

$$p = \frac{3}{2}\frac{\mu_0 U a}{H^2}\frac{1}{k_1 \varkappa^3}\bar{p}, \quad z = \varkappa\Theta + 1, \quad Q = 1 + \varkappa Q_1,$$
$$k_1 = \frac{6\lambda a}{\rho c U H^2}, \quad \varkappa = \frac{\mu_0^2 U^2}{3Ib\lambda} - 1. \tag{37}$$

When condition (9) is satisfied, we obtain

$$Q = \frac{F_1(z_2) - F_1(z_1)}{F_2(z_2) - F_2(z_1)}, \qquad (38)$$
$$F_1(z) = 0.5z^2 - z, \quad F_2(z) = z - \ln z.$$

A relationship between $z_2$ and $z_1$ is established by integration of (36),

$$\Psi(z_2) - \Psi(z_1) = k_1 x^3, \quad \Psi(z) = 0.5z^2 - 2z + \ln z. \qquad (39)$$

The overall hydrodynamic reaction of the layer is determined by the equation

$$\left.\begin{aligned} P = -\frac{\mu_0 U a^2}{H^2}\Phi, \quad \Phi = \frac{3I}{2(k_1 x^3)^2} \\ I = \int_{z_1}^{z_2} \frac{\Psi(z)}{z}(z-1)(z-Q)\,dz = \left\{\frac{1}{2}\Psi^2 + (Q-1)\times\right. \\ \left.\times\left[\frac{z^2}{4} - 2z + \frac{\ln^2 z}{2} - z\left(\frac{z^2}{6} - z + \ln z - 1\right)\right]\right\}\Bigg|_{z_1}^{z_2} \end{aligned}\right\}. \qquad (40)$$

When $x$ is small ($|x| < 0.05 - 0.10$), equations (39) and (40) become much simpler. The following equations are valid in such a case:

$$\left.\begin{aligned} \Theta^3 = \Theta_1^3 + 3k_1\zeta \\ \Phi = \frac{9}{20}\frac{k_1}{\Theta_1^3}\frac{(t+1)^2 + t}{(t+1)(t^2+t+1)^2}, \quad t = \frac{\sqrt[3]{\Theta_1^3 + 3k_1}}{\Theta_1} \end{aligned}\right\}. \qquad (41)$$

4) Let us work out an example. By taking the values of $U$, $\lambda$, $\rho$, $c$, $H$, and $a$ the same as above (see pages 120-123), assuming that $z_1 = 3.30$ and $z_2 = 4.42$, and using equations (37) and (39), we obtain

$$k_1 x^3 = 2.38, \quad x = 2.6 \quad (k_1 = 0.75k = 0.135), \quad \Theta_1 = 0.885, \quad \Theta_2 = 1.320.$$

It follows from here (see (10)) that in the case of brand-T turbine oil, for example ($b \approx 0.05$ kg-sec·deg/m$^2$, $d \approx 312$°K /6/), the accepted values of $z_1$ and $z_2$ correspond to the following bearing surface temperature and average temperatures of the grease at the inlet and outlet of the clearance:

$$T_0 = 342°\,\text{K}, \quad T_1 = 338.5°\,\text{K}, \quad T_2 = 351.6°\,\text{K}.$$

Once the values of $z_1$ and $z_2$ are known, we obtain, by using equation (38), $Q = 3.869$, and by using equation (40), $\Phi = 0.0474$. From (33) and (37), it follows also that conditions (32) and (34) are satisfied (max $\Theta = 1.32$, max $\varphi = 0.165$).

As is well known, the magnitude of the hydrodynamic reaction during isothermal plane-parallel flow of a lubricant in a wedge-shaped clearance may be determined using equation (40), where $H$ is the minimum thickness of the layer and the maximum value of $\Phi$ is 0.16. Thus, at least under the conditions of the present example, the attraction force created in the layer

between parallel friction surfaces is of the same order of magnitude as the supporting force in the Kingsbury thrust bearing. The following reservation must be made here. Since a liquid has no tensile strength, no attraction forces are created as a rule, since disruption of the layer by cavitation occurs when the pressures drop below a certain limiting value. At the same time, cavitation cannot take place if the grease pressure outside the layer is high enough, in which case an attractive force may exist. Similar behavior is observed in sleeve bearings that operate under high pressures in the lubricating layer.

In the above case, the appearance of attraction causes a drop in the loading capacity of the bearing. This is especially true in the case of axial sleeve bearings with self-adjusting pads. The rocking supports of such pads are shifted (to a certain optimum distance) from the middle to the side of the outlet edge. At the same time, the above solution shows that the resultant of the attractive forces is shifted from the middle to the side of the inlet edge, and in this way creates a momentum that turns the pad in a direction reducing sharpness of the grease wedge, thus reducing the hydrodynamic reaction.

Bibliography


1. Zienkiewicz, O. C. — IX Congrès International de Mécanique Appliquée, Actes, IV. 1957.
2. Cameron, A.— Trans. ASME, Vol. 1. 1959.
3. Korovchinskii, M.V. Teoreticheskie osnovy raboty podshipnikov skol'zheniya (Theoretical Foundations of the Operation of Sleeve Bearings). — Moskva, Mashgiz. 1959.
4. Khanovich, M.G. K voprosu o raschete upornykh podshipnikov skol'zheniya (On the Calculation of Axial Sleeve Bearings). — Trudy III Vsesoyuznoi konferentsii po treniyu i iznosu v mashinakh, Vol. III, Izd. AN SSSR. 1960.
5. Yanovskii, M.I. Konstruirovanie i raschet na prochnost' detalei parovykh turbin (Design and Strength Calculations for Parts of Steam Turbines). — Izd. AN SSSR. 1947.
6. Nechiporenko, V.A. Resul'taty eksperimental'nogo issledovaniya opornykh podshipnikov sudovykh turbozubchatykh agregatov (Results of an Experimental Investigation of Block Bearings for Ship Turbine Gear Sets). — Trudy NTO sudostroitel'noi promyshlennosti, Leningradskoe oblastnoe pravlenie, No. 2. 1960.



The Shipbuilding Institute, Leningrad

V. N. Zmeikov and B. P. Ustimenko

# HYDRODYNAMICS AND HEAT TRANSFER IN A CONVOLUTED STREAM BETWEEN TWO COAXIAL CYLINDERS

Studies of the heat transfer and hydrodynamics in the annular channel between two rotating cylinders have been the subject of many papers /1, 5-9, 11, 13/. In these papers, the main attention was devoted to the overall characteristics of the heat transfer and resistance, while insufficient attention was paid to the detailed structure of the flow: its velocity and temperature profiles, and especially the pulse characteristics. At the same time, an understanding of the latter is absolutely essential for the elucidation of the physical mechanism of the process and for the derivation of efficient heat transfer and resistance calculation methods.

In this paper, we present the results of an investigation of the hydrodynamics and heat transfer in an annular channel with a rotating inner cylinder, together with detailed experimental data on the velocity and temperature distribution and the pulse characteristics of the flow; we propose a method for the calculation of the heat transfer based on the use of the hydrodynamic theory of heat transfer and new equations describing the velocity profiles and the resistance coefficients.

The investigations were conducted on a setup consisting of two coaxial and well balanced metallic cylinders; the inner cylinder was rotated by a d-c motor. The angular velocity was continuously regulated by a rheostat up to 283 rad/sec and was controlled with the aid of a tachometer, having an accuracy of $\pm 1$ rad/sec. The polished cylinder surfaces formed an annular channel, whose length and height were 0.4 and 0.0049 m, respectively; the inner cylinder diameter was 0.212 m.

In order to study the thermal problem, an electric heater providing a constant heat flux on the cylinder surface was placed within the inner cylinder. The outer cylinder was enclosed by a water jacket, with water from a thermostat flowing through the jacket. This provided a constant wall temperature, which was maintained with the aid of four nichrome-constantan thermocouples embedded in the wall. Mixing chambers, with differential thermocouple junctions (used to measure the increase in the temperature of the cooling water) fitted to them, were mounted at the inlet and outlet of the cooling jacket. The water flow rate was measured at fixed time intervals with a volumetric flowmeter (the accuracy of measurement was 1.5%).

The packing used in the measurement was introduced into the channel through 5 special holes; microinstruments, by means of which the coordinates could be fixed with an accuracy of $0.01 \cdot 10^{-3}$ m, were fitted to the holes. Holes with a diameter of $0.45 \cdot 10^{-3}$ m were made in the channel walls in order to measure the static pressure.

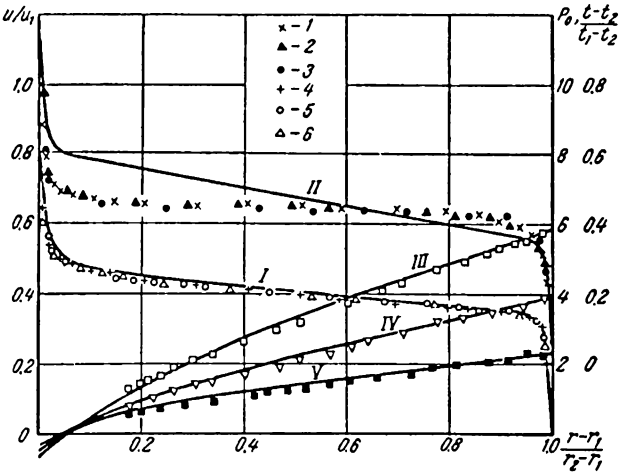


FIGURE 1. The distribution of $\frac{u}{u_1}$, $\frac{t-t_2}{t_1-t_2}$, and $p_0$ in an annular channel at $w$ = 283, 230, and 178 rad/sec. Calculated results (continuous lines: I — according to equations (3) — (6); II — according to equations (13) — (15); III, IV, V — by the method proposed in /1/ (the experimental points are based on measurements with a static packing). Experiments: 1, 4 — $w$ = 283; 2, 5 — $w$ = 230; 3, 6 — $w$ = 178.

The total pressure was measured with the aid of Pitot tubes. In the region of the boundary layer (adjacent to the walls), the tube readings were markedly affected by their diameters as a result of the differences between the flow conditions in their vicinity. In order to exclude the influence of the dimensions of the packing, the total pressure profile near the cylinder walls was determined by means of three geometrically similar tubes (with diameters of $0.23 \cdot 10^{-3}$, $0.36 \cdot 10^{-3}$, and $0.53 \cdot 10^{-3}$ m, and an inner-to-outer diameter ratio of 0.6), followed by extrapolation to a tube of zero diameter.

The static pressure in the channel cross section was measured with the aid of the static packing, having a shape corresponding to the current flow lines. On the other hand, it was also calculated by the method of /1/, for a known static pressure on the nonrotating cylinder wall. The data obtained by these two methods are compared in Figure 1 and show good agreement.

The tangential frictional stress on the channel walls was determined by the method of /2/, which was generalized to cover curved flow and was developed for the cases of straight flows in aerodynamic tubes, on smooth plate surfaces, etc. The tangential frictional stress was also measured with the aid of the ETAM-3A electrothermoanemometer. The data obtained by these methods were in satisfactory agreement, the deviations not exceeding 10% (see Figure 2).

The ETAM-3A thermoanemometer was used to determine the intensity of pulsations in the velocity vector component, the temperature, and the correlation during various flow conditions. The pulsations of the velocity vector component were isolated by the method developed for a heated turbulent stream. The temperature profiles in the channel cross sections were measured with special temperature probes (nichrome-constantan

thermocouples made of wires with a diameter of $0.1 \cdot 10^{-3}$ m) placed in a conventional injection needle with a diameter of $0.9 \cdot 10^{-3}$ m. All the thermocouples were connected to a PPTN-1 potentiometer with the M-25/7 mirror galvanometer serving as the zero instrument.

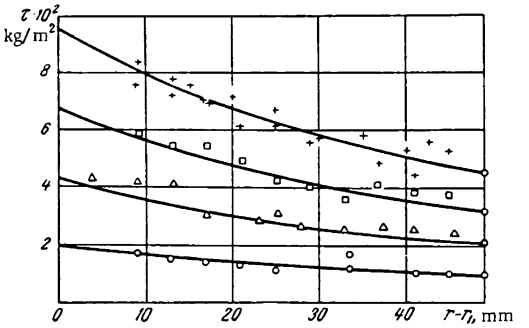


FIGURE 2. Distribution of the frictional stress $\tau$ in an annular channel at $n$ = 283, 230, 178, and 105 rad/sec. The continuous curves were obtained with Pitot tubes, while the experimental points were obtained by measurements with a thermoanemometer.

The total heat flux reaching the nonrotating cylinder (the heat was removed by the cooling water) consisted of a convection component from the rotating air stream, of radiation transfer from the heated inner cylinder (up to 3% of the total), of the heat transferred by conduction through the ends (up to 5%), and finally, of natural convection from the surrounding medium to the walls of the cooling jacket (up to 2%).

An evaluation of the errors made in the measurement of the velocity profile, the static pressure, and the temperature shows that they did not exceed 2% in the main flow region. The error in the determination of the velocity and temperature pulsations did not exceed 20%, and that in the Nusselt number did not exceed 10%.

## Hydrodynamics of a stream flowing within an annular channel with a rotating inner cylinder

Data on the experimental flow conditions are shown in Table 1.

In the table below, $w$ and $u_1$ are the angular and linear rotation velocities of the inner cylinder, $\mathrm{Re} = \frac{u_1(r_2 - r_1)}{\nu}$ is the Reynolds number, $Ta = \frac{w\left(\frac{r_2 + r_1}{2}\right)^{\frac{1}{2}}(r_2 - r_1)^{\frac{3}{2}}}{\nu}$ the Taylor number, $\tau_{w_2}$ is the tangential frictional stress on the stationary wall, and $r_1$ and $r_2$ are the cylinder radii.

TABLE 1. Data on the flow conditions

| $w$, rad/sec | $u_1$, m/sec | Re | Ta | $\tau_{w2}\cdot 10^2$, n/m$^2$ | $\bar{u}_{*1}$, m/sec | $p_0$, n/m$^2$ |
|---|---|---|---|---|---|---|
| 52.4 | 5.54 | 17,000 | 12,850 | — | — | 2.16 |
| 73.3 | 7.76 | 32,800 | 18,000 | 3.44 | 0.176 | 3.92 |
| 104.7 | 11.10 | 34,000 | 25,600 | 8.43 | 0.274 | 7.85 |
| 125.7 | 13.32 | 40,800 | 30,800 | 11.20 | 0.316 | 11.30 |
| 157.0 | 16.65 | 51,000 | 38,500 | 16.50 | 0.384 | 18.15 |
| 178.0 | 18.86 | 57,700 | 43,600 | 20.20 | 0.425 | 23.05 |
| 209.5 | 22.20 | 68,000 | 51,300 | 26.70 | 0.489 | 31.40 |
| 230.5 | 24.40 | 74,700 | 56,500 | 31.40 | 0.530 | 38.25 |
| 262.0 | 27.75 | 85,000 | 64,200 | 39.30 | 0.539 | 48.10 |
| 283.0 | 30.00 | 91,800 | 69,300 | 45.20 | 0.636 | 56.80 |

The dimensionless velocity profile is shown in Figure 1 (in the coordinates $\frac{u}{u_1} = f\left(\frac{r-r_1}{r_2-r_1}\right)$) referred to the rotation velocity of the inner cylinder in the channel cross section, as a function of the relative distance from the walls. As is evident from the figure, the experimental points for different flow conditions lie on the same curve (with a small dispersion) indicating the similarity of the flow in the studied range of $w$ ($w>180$ rad/sec).

For a large fraction of the stream (about 85%), the angular momentum $ur$ is constant, which corresponds to the law of potential rotation of the liquid. A sharp change in $u_r$ occurs only in the vicinity of the channel walls. The distribution of the dimensionless angular momentum is represented by a single general curve for different values of $w$ in the turbulent flow range (i.e., at $w>180$ rad/sec).

The flow conditions in the vicinity of the inner and outer cylinders are determined by the physical properties of the liquid (density and kinematic viscosity coefficient), the tangential frictional stress on the walls, the surface curvature radius $R$, and the distance from the wall $y$.

Dimensional analysis shows that the following equation should be fully satisfied in the above case

$$\varphi = f\left(\eta, \frac{y}{R}\right), \tag{1}$$

where

$$\varphi = \frac{u}{u_*}; \quad u_* = \sqrt{\frac{\tau_w}{\rho}}; \quad \eta = \frac{yu_*}{\nu}.$$

The effect of the dimensionless number $y/R$ in the thin layers immediately in contact with the cylinder walls may be neglected because of its small value, and the equation then assumes the conventional form for flow in channels and over plane plates:

$$\varphi = f(\eta). \tag{2}$$

The dimensionless velocity $\varphi$ for the flow studied here is shown in Figure 3 as a function of $\eta$. In the case of the boundary layer on the inner rotating cylinder, the value of $\varphi$ stands for the excess velocity $\frac{u_1-u}{u_{*1}}$ and,

correspondingly, $\eta_1 = \frac{yu_{*1}}{\nu}$; on the outer cylinder wall it stands for $\frac{u_2 - u}{u_{*2}}$ and, correspondingly, $\eta_2 = \frac{yu_{*2}}{\nu}$

As is evident from the figure, the whole flow range is described by a single general curve, which is independent of the rotation velocity of the inner cylinder (at least in the case of $\omega > 180$ rad/sec). The experimental points for the flows on the outer and inner cylinders and for different rotation velocities lie on the same curve (with small dispersion).

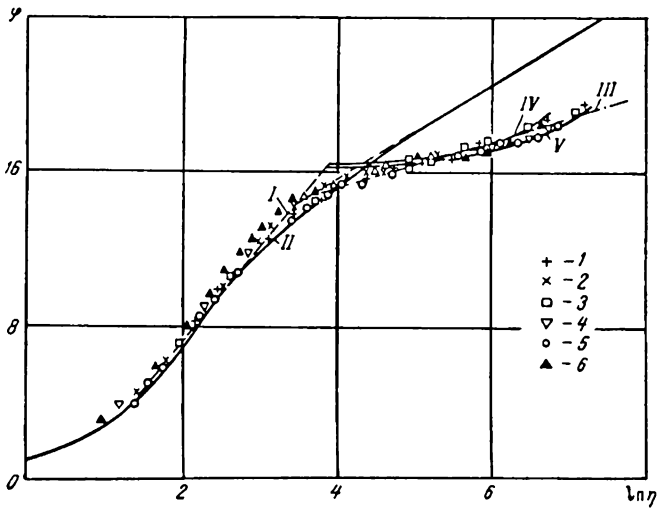


FIGURE 3. General dimensionless velocity profile, $\varphi$.

I — calculated on the basis of the three-layer concept of Karman /4/; II — by the Spalding equation /5/; III — by equation (7); IV and V — by equations (3) — (6); 1, 3, 5 — experimental points on the rotating cylinder; 2, 4, 6 — experimental points on the stationary cylinder.

For the sake of comparison we have shown in Figure 3 also the calculated velocity profiles corresponding to the well-known Karman concept /3/ (curve 1) and the Spalding equation /4/ (curve 2), which are valid for boundary-layer flow on the surfaces of flat plates and channels. Up to $\eta \approx 50$ the experimental points are in good agreement with our curves, confirming the validity of the concepts developed in this paper.

In this way, the turbulent boundary layer formed during flow adjacent to cylinder walls may be divided roughly into three regions (as in the case of flow adjacent to a smooth flat surface /3/).

1) The laminar sublayer region ( $0 \leqslant \eta \leqslant 5$ ), where the velocity profile is described by the linear equation valid for the flows on the inner and outer cylinders:

$$\varphi_1 = \frac{u_1 - u}{u_{*1}} = \eta_1 \quad \text{at} \quad 0 \leqslant \eta \leqslant 5,$$
$$\varphi_2 = \frac{u}{u_{*2}} = \eta_2 \quad \text{at} \quad 0 \leqslant \eta_2 \leqslant 5. \qquad (3)$$

2) The transition layer ($5 \leqslant \eta \leqslant 50$), where the velocity profile is described by a logarithmic equation:

$$\varphi_1 = \frac{1}{x}\ln\eta_1 + A \approx 5\left(1+\ln\frac{\eta_1}{5}\right) \quad \text{at} \quad 5 \leqslant \eta_1 \leqslant 50,$$
$$\varphi_2 = \frac{1}{x}\ln\eta_2 + A \approx 5\left(1+\ln\frac{\eta_2}{5}\right) \quad \text{at} \quad 5 \leqslant \eta_2 \leqslant 50. \tag{4}$$

As in the case of flow adjacent to a plane plate, we have here $A = -3.05$ and $x = 0.2$.

3) The turbulent region ($\eta > 50$), where the velocity profile satisfies the potential rotation law

$$ur = \text{const} \approx \frac{1}{2}u_1 r_1. \tag{5}$$

In the above case the velocity profiles for the regions on the inner and outer walls are described by

$$\varphi_1 = \varphi_0 - \frac{1}{2}\frac{\bar{\eta}_{01}}{1+\bar{\eta}_1} \quad \text{at} \quad 50 \leqslant \eta_1 \leqslant \eta_{c1},$$
$$\varphi_2 = \frac{1}{2}\frac{\bar{\eta}_{02}}{1-\bar{\eta}_2} \quad \text{at} \quad 50 \leqslant \eta_1 \leqslant \eta_{c2}. \tag{6}$$

Above, we have introduced some new symbols:

$$\bar{\eta}_{01} = \frac{\eta_{01}}{\eta_1^*}, \quad \bar{\eta}_{02} = \frac{\eta_{01}}{\eta_2^*}, \quad \eta_{01} = \frac{u_1 r_1}{\nu},$$
$$\bar{\eta}_1 = \frac{\eta_1}{\eta_1^*}, \quad \bar{\eta}_2 = \frac{\eta_2}{\eta_2^*},$$
$$\eta_1^* = \frac{r_1 u_{*1}}{\nu}, \quad \eta_2^* = \frac{r_2 u_{*2}}{\nu}, \quad \varphi_0 = \frac{u}{u_{*1}},$$
$$\eta_{c1} = \frac{(r_2 - r_1)u_{*1}}{2\nu}, \quad \eta_{c2} = \frac{(r_2 - r_1)u_{*2}}{2\nu}$$

It is not difficult to transform equation (5) (for the velocity profile in the central flow zone) to a limiting form (asymptotic velocity distribution law* for large values of the convolution Reynolds number $\mathrm{Re}_{\mathrm{con}} = \frac{u_{*1}r_1}{\nu}$) for narrow annular channels ($r_2/r_1 \to 1$). The experimental data collected by us, as well as the data of other investigators /5/, show that equation (5) agrees well with experimental results even at much greater channel heights.

* To this end, in the case of thin layers on the cylinder walls ($y \ll r_1$ and $r_2$), equation (4) is written in terms of the angular momentum ($ur$). By deriving an expression for $ur/u_1r_1$ and passing to limits at $\mathrm{Re}_{\mathrm{con}} \to \infty$, we obtain equation (5).

Thus, under developed turbulent-flow conditions (which are characterized by a similarity of the velocity profile, and, as shall be shown below, of the temperature profile and the relative quadratic pulsation of the velocity component), the velocity profile in the channel cross section is described by equations (3) to (6).

Curve I in Figure 1 and curves IV and V in Figure 3, which were plotted on the basis of equations (3) to (6), are in good agreement with the measured results. In the range of $n$ discussed here, equation (6) is approximated with adequate accuracy by the following logarithmic functions:

$$\varphi_1 = 1.2 \ln \eta_1 + 10.3, \quad \varphi_2 = 1.2 \ln \eta_2 + 10.3. \tag{7}$$

By equating the second equations from (4) and (7) at their common value of ($\eta = 50$), and determining the resistance coefficients on the inner and outer channel walls by the equations

$$f_1 = \frac{2}{\rho u_1^2} \tau_{w1} \text{ and } f_2 = \frac{2}{\rho u_2^2} \tau_{w2},$$

where

$$u_2 = \frac{r_2}{r_1} u_1 \text{ and } f_2 = f_1 \left( \frac{r_1}{r_2} \right)^4,$$

we derive an asymptotic equation for the resistance coefficient

$$\sqrt{f_1/2} = 0.0303 + 50/\eta_{01}. \tag{8}$$

A comparison of the experimental results with results calculated using (8) shows that the agreement between them is quite good, and it becomes better as $Re_{con}$ increases (see Table 2).

TABLE 2. Comparison of experimental and calculated results

| $\omega$, rad/sec | $Re_{con}$ | $\eta_{01}$ | $f_1 \cdot 10^4$ | | | $f_2 \cdot 10^4$ | | |
|---|---|---|---|---|---|---|---|---|
| | | | experimental | calculated by equation (8) | calculated by equation (9) | experimental | calculated by equation (8) | calculated by equation (9) |
| 52.4 | — | 36,700 | — | 20.48 | 24.75 | — | 4.49 | 5.42 |
| 73.3 | — | 51,400 | — | 19.56 | 23.65 | — | 4.28 | 5.18 |
| 104.7 | 2,650 | 73,500 | 26.0 | 19.20 | 22.65 | 5.7 | 4.21 | 4.96 |
| 125.7 | 3,060 | 88,000 | 24.1 | 19.06 | 21.95 | 5.3 | 4.17 | 4.80 |
| 157.0 | 3,720 | 110,000 | 22.7 | 18.92 | 21.40 | 5.0 | 4.14 | 4.68 |
| 178.0 | 4,120 | 125,000 | 21.6 | 18.85 | 21.05 | 4.7 | 4.12 | 4.60 |
| 209.5 | 4,740 | 147,000 | 20.7 | 18.78 | 20.70 | 4.5 | 4.11 | 4.53 |
| 230.5 | 5,130 | 162,000 | 20.1 | 18.74 | 20.35 | 4.4 | 4.10 | 4.46 |
| 262.0 | 5,740 | 184,000 | 19.6 | 18.69 | 20.00 | 4.2 | 4.09 | 4.34 |
| 283.0 | 6,160 | 199,000 | 19.2 | 18.67 | 19.85 | 4.2 | 4.09 | 4.34 |

For the range of $n$ discussed here, the best agreement with the experimental data is obtained by using the equation for the resistance coefficient derived by equating equations (6) and (7) at the value $(r_1+r_2)2$:

$$\frac{1}{\sqrt{f_2/2}}\left[\frac{r_1^2}{r_2(r_1+r_2)}\right]=1.2\ln\left[\frac{1}{2}\frac{u_2(r_2-r_1)}{\nu}\sqrt{f_2/2}\right]+10.3. \qquad (9)$$

Heat transfer in a stream flowing in an annular channel with rotating inner cylinder

The thermal measurements were made under the flow conditions described in Table 1. The specific convective heat flux from the outer to the inner cylinder, determined on the basis of the mean logarithmic surface of the cylinders, ranged from 678 to 982 w/m$^2$· hr, while the temperature gradient $(t_1-t_2)$ ranged from 40 to 80°C. The modified Taylor number

$$(\mathrm{Ta})_m=\left[\frac{\omega^2(r_1+r_2)(r_2-r_1)^3}{2\nu^2}\right]\frac{1}{F_g},$$

where $F_g$ is a geometric factor /7/, ranged from $1.67\cdot10^7$ to $1.59\cdot10^9$.

The dimensionless temperature profile $\frac{t-t_2}{t_1-t_2}=f\left(\frac{r-r_1}{r_2-r_1}\right)$ is shown in Figure 1 for different values of the parameter $n$. Starting at $\omega$ values of about 160-180 rad/sec, the experimental points obtained under different flow conditions are grouped around a single curve (the experimental points show a small dispersion), indicating in all cases the similarity of the flow (as in the case of the dynamic problem).

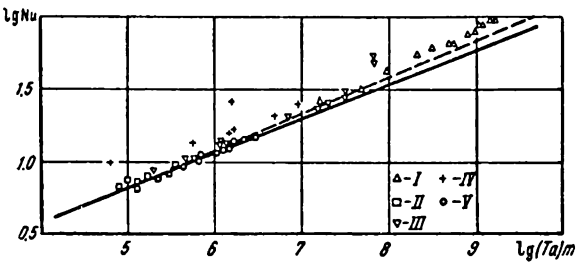


FIGURE 4. Dependence of the Nusselt number (Nu) on the modified Taylor number $(\mathrm{Ta})_m$.

– – – – calculated by equation (7); ——— calculated by equation (9); I — experimental data of the authors; II — experimental data from /10/; III — experimental data from /8/; IV — experimental data from /7/; V — experimental data from /9/.

The temperature of the rotating air stream decreases rapidly in the boundary layer on the inner and outer cylinders, but drops negligibly in

the central zone. The figure shows that at $\omega$ between 180 and 283 rad/sec, the temperature changes in the central turbulent flow zone (ccopying about 80% of the channel width) are only 4% of the total temperature gradient $t_1 - t_2$.

The Nusselt number $\mathrm{Nu} = \frac{2q(r_2 - r_1)}{\lambda(t_1 - t_2)}$ is shown in Figure 4 as a function of the experimental modified Taylor number $(\mathrm{Ta})_m$. For the sake of comparison, the same figure also contains experimental data from /6-9/. As is evident from the figure, there is good agreement with the data of /7/ for the range of $(\mathrm{Ta})_m$ values common for the two investigations. The continuous and the dashed lines were plotted on the basis of the empirical equations recommended in /7, 9/.

We now compute the temperature profile in an annular channel under developed turbulent flow conditions. Let us analyze the flow region on the outer wall. The expression for the tangential frictional stress

$$\tau = -\rho(\nu + \nu_T) r \frac{d}{dr}\left(\frac{u}{r}\right),$$

written in terms of universal variables (taking into account the condition for the conservation of the momentum of the friction, $\tau r^2 = \tau_{w2} r_2^2$) has the form

$$1 = \left(1 + \frac{\nu_T}{\nu}\right)(1 - \bar{\eta}_2) \frac{d}{d\bar{\eta}_2}\left(\frac{\varphi}{1 - \bar{\eta}_2}\right). \tag{10}$$

By transforming the expression for the heat flux density $q/\rho C_p = -(a + a_T)\frac{dT}{dr}$ (bearing in mind the condition for its conservation, $qr = q_2 r_2 = \text{const.}$) in terms of new generalized variables

$$\vartheta_2 = \frac{T - T_2}{T_{*2}} \quad \text{and} \quad \eta_2,$$

(where $T_{*2} = \frac{q}{\rho C_p u_{*2}}$), we obtain

$$1 = \frac{1}{\sigma}\left(1 + \frac{\sigma \nu_T}{\sigma_T \nu}\right)(1 - \bar{\eta}_2) \frac{d\vartheta_2}{d\eta_2}. \tag{11}$$

where $\sigma$ and $\sigma_T$ are the physical and the turbulent Prandtl numbers.

By equating the right-hand sides of equations (10) and (11), we obtain an equation for the determination of the temperature profile for a known velocity profile

$$\frac{d\vartheta_2}{d\bar{\eta}_2} = \frac{1 + \frac{\nu_T}{\nu}}{\frac{1}{\sigma}\left(1 + \frac{\sigma}{\sigma_T}\frac{\nu_T}{\nu}\right)}(1 - \bar{\eta}_2) \frac{d}{d\bar{\eta}_2}\left(\frac{\varphi_2}{1 - \bar{\eta}_2}\right). \tag{12}$$

In a similar way we can easily derive equations for the determination of the temperature profile on the rotating wall of the channel.

By substituting equations (which describe the velocity profiles) in the derived equations for the outer (12) and the inner channel zones (3) to (6), and integrating within the respective limits, we obtain the following expressions for the temperature profiles in annular channel cross sections:

$$\vartheta_1 = \sigma\eta_1, \qquad 0 \leqslant \eta_1 \leqslant 5,$$

$$\vartheta_2 = \sigma\eta_2, \qquad 0 \leqslant \eta_2 \leqslant 5,$$

$$\vartheta_1 = 5\sigma_T \ln\left[\frac{\sigma}{\sigma_T}\left(\frac{\eta_1}{5} - 1\right) + 1\right] + 5\sigma, \quad 5 \leqslant \eta_1 \leqslant 50, \tag{13}$$

$$\vartheta_2 = 5\sigma_T \ln\left[\frac{\sigma}{\sigma_T}\left(\frac{\eta_2}{5} - 1\right) + 1\right] + 5\sigma, \quad 5 \leqslant \eta_2 \leqslant 50, \tag{14}$$

$$\vartheta_1 = \sigma_T \bar{\eta}_{01} \ln \frac{\eta_1^* + \eta_1}{\eta_1^* + 50} + 5\sigma_T \ln\left[1 + 9\frac{\sigma}{\sigma_T}\right] + 5\sigma \text{ for } 50 \leqslant \eta_1 \leqslant \eta_{c_1},$$

$$\vartheta_2 = \sigma_T \bar{\eta}_{02} \ln \frac{\eta_2^* - 50}{\eta_2^* - \eta_2} + 5\sigma_T \ln\left[1 + 9\frac{\sigma}{\sigma_T}\right] + 5\sigma \text{ for } 50 \leqslant \eta_2 \leqslant \eta_{c_2}. \tag{15}$$

In the derivation of equations (13) to (15) we made the simplification that in the laminar sublayer $\frac{\nu_T}{\nu}$ and $\frac{a_T}{a} \ll 1$ while in the central turbulent flow region $\frac{\nu_T}{\nu}$ and $\frac{a_T}{a} \gg 1$. In Figure 1, the continuous line (II) plotted on the basis of equations (13) to (15) is in satisfactory agreement with the experimental data, the deviations not exceeding 10%. The sharper decrease in the calculated temperature in the central flow region is apparently caused by the fact that the calculations did not take into account the heat transfer by secondary eddy currents /5/, whose effect increases with decreasing rotation velocity of the inner cylinder.

We now determine the Nusselt numbers $Nu_1$, $Nu_2$, and Nu, calculated on the basis of the heat transfer coefficients from the inner ($\alpha_1$) and the outer ($\alpha_2$) channel walls, and also on the basis of the overall coefficient ($\alpha$) referred to the total temperature gradient between the walls.

On the outer wall, the Stanton number ($St_2$) is written in the following form

$$St_2 = \frac{Nu_2}{Pe_2} = \frac{\alpha_2}{C_p \rho_2 u_2}, \tag{16}$$

where

$$Nu_2 = \frac{2(r_2 - r_1)\alpha_2}{\lambda_2}; \quad Pe_2 = \frac{2(r_2 - r_1)u_2}{a_2} \text{ is the Peclet number.}$$

By substituting the value of $\alpha_2 = \frac{q_2}{t_c - t_2}$ in (16) and using the equation $u_{*2} = \sqrt{\frac{f_2 u_2}{2}}\, u_2$ (where $t_c$ is the temperature at the center of the channel and $f_2$ is the resistance coefficient), we ultimately obtain

$$St_2 = \sqrt{f_2/2}\,/\vartheta_{2c}, \quad Nu_2 = \sqrt{f_2/2}\, Pe_2/\vartheta_{2c}. \tag{17}$$

By analogy, for the flow region on the inner wall we have

$$St_2 = \sqrt{f_2/2}/\vartheta_{1c},\ Nu_1 = \sqrt{f_1/2}\,Pe_1/\vartheta_{1c}. \tag{18}$$

The values of $\vartheta_{1c}$ and $\vartheta_{2c}$ are calculated using equations (15) at the points $\eta_{c1}$ and $\eta_{c2}$. By transforming in the same way as above, we obtain the following expression for the St and Nu numbers:

$$St = \sqrt{f_1/2}\,\vartheta_{1-2},\ Nu = \sqrt{f_1/2}\,Pe_1/\vartheta_{1-2}, \tag{19}$$

where

$$Nu = \frac{2(r_2 - r_1)\alpha}{\lambda_c} = \frac{2(r_2 - r_1)}{\lambda_c}\,\frac{q_2 F_2}{Fu(t_1 - t_2)};$$

$Fu$ is the mean logarithmic surface area of the channel wall, while the use of the subscript $c$ with the thermal conductivity coefficient means that it refers to the temperature criterion

$$\frac{t_1 + t_2}{2},\ \vartheta_{1-2} = \frac{Fu}{F_1}\,\frac{\rho_c}{\rho_1}\left(\vartheta_{1c} + \sqrt{\frac{\rho_1}{\rho_2}}\,\vartheta_{2c}\right).$$

A comparison of experimental data with calculated data (equations (17) to (19)) in Table 3 shows that they are in good agreement, and that (as should be expected) the agreement improves as the parameter $n$ increases.

TABLE 3. Comparison of experimental and calculated data

| $\omega$, rad/sec | $(Ta)_m \cdot 10^{-7}$ | $Nu_2$ | | | $Nu_1$ | | | Nu | | |
|---|---|---|---|---|---|---|---|---|---|---|
| | | experimental | calculated | deviation, % | experimental | calculated | deviation, % | experimental | calculated | deviation, % |
| 178 | 65.8 | 149 | 115 | 23 | 163 | 124 | 24 | 80 | 58 | 27.0 |
| 210 | 92.0 | 161 | 130 | 19 | 168 | 143 | 15 | 84 | 66 | 20.0 |
| 230 | 110.0 | 167 | 144 | 14 | 175 | 155 | 11 | 87 | 73 | 16.0 |
| 262 | 146.0 | 173 | 162 | 6 | 194 | 180 | 7 | 93 | 84 | 10.0 |
| 283 | 158.6 | 180 | 175 | 3 | 214 | 195 | 10 | 100 | 94 | 6.4 |

## Turbulent structure of the stream in an annular channel with rotating inner cylinder

As we mentioned above, the turbulent structure of the stream in an annular channel with a rotating inner cylinder was studied with the aid of the ETAM-3A thermoanemometer, under the flow conditions described in Table 1.

Figure 5 shows the profiles of the mean square pulsations of the velocity vector components $\left(\varepsilon_\varphi = \sqrt{\overline{v_\varphi'^2}}/\bar{u},\ \varepsilon_z = \sqrt{\overline{v_z'^2}}/\bar{u},\ \text{and}\ \varepsilon_r = \sqrt{\overline{v_z'^2}}/\bar{u}\right)$

and the temperature $\varepsilon_t = \sqrt{\overline{t'^2}}/\bar{t}$ referred to the averaged local velocity and the temperature in the channel cross section. The experimental points obtained under different flow conditions ($w$ = 178, 230, 262, and 283 rad/sec) lie with little dispersion on the same curves, thus confirming the similar nature of the flow pulsation characteristics.

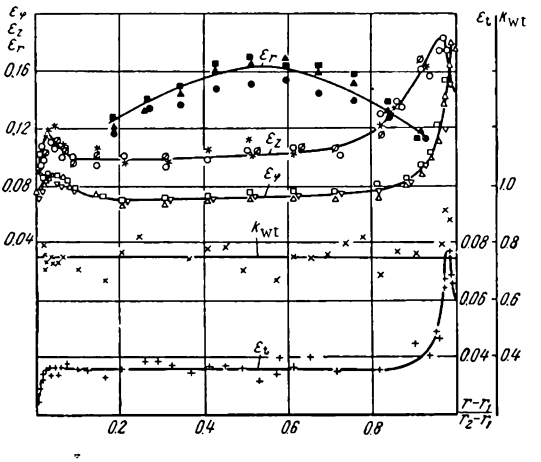


FIGURE 5. Distribution of the rates of pulsation of the velocity $\varepsilon_\varphi$, $\varepsilon_z$, and $\varepsilon_r$ (at $w$ = 283, 230, and 178 rad/sec), the temperature, and the correlation coefficient, $\varepsilon_t$, $K_{wt}$ (at $w$ = 283 rad/sec).

A comparison of our experimental data with results obtained in the measurement of the velocity pulsation rate in a straight-line flow in a flat channel /10/ leads to the following observations.

Within relatively thin layers in the vicinity of the annular channel (where the tangential frictional stress may be regarded as approximately constant), the distribution of the stream pulsation characteristics (as that of the averaged values) has the same nature in the cases of both curved and straight-line flows. In both cases a maximum in the distribution of the pulsation rate ($\varepsilon_\varphi$ and $\varepsilon_r$ in the case of curved flow, and $\varepsilon_x$, $\varepsilon_y$, and $\varepsilon_z$ in the case of straight-line flow) is observed near the wall, at a distance smaller than 0.1 $d$ (where $d$ is the half-width of the channel). As the point of the maximum pulsation rate is passed (in the direction of the wall) these components rapidly drop to zero.

The specific characteristics of convoluted flow are exhibited in the central zone of the channel, where the effect of the walls is negligible and the effect of the centrifugal force field is fully exhibited. In contrast to straight-line flows no isotropic turbulence is observed here: ($\varepsilon_\varphi \neq \varepsilon_z \neq \varepsilon_r$), i. e., the radial component of the mean square pulsation of the velocity vector $\varepsilon_r$ is noticeably larger (by a factor of nearly 2) than $\varepsilon_\varphi$ and $\varepsilon_z$ and reaches a maximum value.

The latter circumstance could apparently explain the high rates of the transfer processes in the central flow zone, leading to the leveling of the velocity profile, the angular momentum, and the temperature.

The correlation of $\overline{v'_\varphi v'_r}$ determining the tangential frictional stress ($\tau = -\rho\overline{v'_\varphi v'_r}$) is shown in Figure 2. The correlation coefficient $K_{\varphi z} = \overline{v'_\varphi v'_z}/\sqrt{\overline{v'^2_\varphi}}\sqrt{\overline{v'^2_z}}$ has a value of nearly zero over the entire channel cross section, while $K_{\varphi r} = \overline{v'_\varphi v'_r}/\sqrt{\overline{v'^2_\varphi}}\sqrt{\overline{v'^2_r}}$ is virtually constant, and has a value of about 0.4.

The results of our experimental measurements of the temperature pulsations, and the velocity-temperature correlation shown in Figure 5 indicate that the $\varepsilon_t$ profile is similar to those of $\varepsilon_\varphi$ and $\varepsilon_z$. The temperature pulsation rate $\varepsilon_t$ has a maximum in the vicinity of the channel walls, and remains nearly constant in the central zone of the channel.

The correlation coefficient $K_{W't} = \overline{W't'}/\sqrt{\overline{W'^2}} \times \sqrt{\overline{t'^2}}$ (where $W'$ is the effective velocity pulsation acting on the packing threads) remains virtually constant within the central zone of the channel in the case of developed turbulent-flow conditions.

Bibliography


1. Wattendorf, F. Proceedings of the Royal Society (A), 191. 1935.
2. Preston. Mekhanika (Mechanics). A Collection of Translations and Reviews, No. 6:34. 1955.
3. Karman, T. — Trans. ASME, Vol. 61:705-710. 1939.
4. Spalding, D. B. — Trans. ASME, series E, No. 3. 1961.
5. Taylor, G. — Proceedings of the Royal Society (A), 151. 1935.
6. Gazley, C. — Trans. ASME, Vol. 80, No. 1. 1958.
7. Fujio Tachibana, Suceo Fukui and Hisao Mitsumura. — Bulletin of ISME, Vol. 3, No. 9. 1960.
8. Bjerklund, I.S. and W. M. Kays. — Trans. ASME S.C., Vol. 81, No. 3. 1959.
9. Becker and Kay. Heat Transfer, 2. — Proceedings of the American Society of Mechanical Engineers [Russian translation. 1962.]
10. Pai Shih. Turbulent Flow of Liquids and Gases [Russian translation. 1962.]
11. Kosterin, S.I. and Yu. P. Finat'ev. — IFZh, No. 8. 1962.
12. Koshmarov, Yu. A. — IFZh, No. 5. 1962.
13. Dorfman, L. A. Gidrodinamicheskoe soprotivlenie i teplootdacha vrashchayushchikhsya tel (Hydrodynamic Resistance and Heat Transfer in the Case of Rotating Bodies). — Moskva, Fizmatgiz. 1960.
14. Eckert, E.R. and R. M. Drake. The Theory of Heat and Mass Transfer. [Russian translation. 1961.]



The Power Institute of the Academy of Sciences of the KazSSR

aid of pneumatic Piton tubes made of stainless steel. The stream temperature was measured using chromel-alumel thermocouples. The thermocouple heads were screened by protective ceramic jackets. The construction of the sensitive elements was such that the walls of the channel could be approached to a distance of 0.00075 m. The walls of the experimental section were cooled with water.

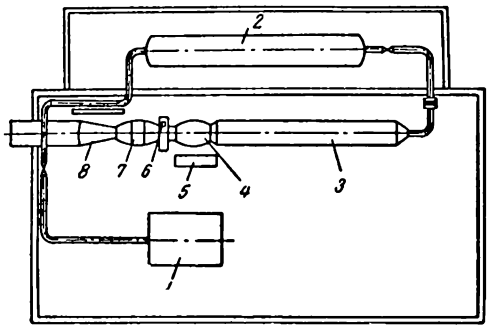


FIGURE 1. Schematic view of the experimental section.

1 — compressor; 2 — receiver; 3 — electric heater; 4 — VK-1F combustion chamber; 5 — heating apparatus; 6 — ejector; 7 — transient sections; 8 — experimental section.

The experiments involved 6 sets of conditions. Each set of conditions was characterized by certain given temperatures and gas velocities at the inlet of the experimental section.

The stagnation temperature of the potential gas flow ranged from 913 to 1303°K. The potential flow velocity at the inlet of the experimental section was maintained between 136 and 200 m/sec. The wall temperature ranged from 313 to 328°K, depending on the initial temperature of the mainstream.

The experiments extended over the Reynolds number range of (50 — 150)× $\times 10^3$ and the temperature factor range $\bar{T}_w = \frac{T_w}{T_{0i}} = 0.4—0.25$. In the course of the experiments we measured the temperature and velocity profiles in the cross section of the flow and the static pressure in each section. In a 0.75 m section, the measurements were made at five cross-section planes. In addition, we measured the consumption of the cooling water, the water temperature at the inlet and outlet of each of the five experimental sections, and the channel wall temperature. The composition of the combustion products passing through the experimental section was determined by analysis of the gas (the experimental section has been described in detail in /6/).

The experimental data obtained on the velocity and temperature profiles enabled us to determine the integral characteristics of the thermal and hydrodynamic boundary layers, i.e., the momentum thickness

$$\vartheta = \int_0^\infty \frac{\rho u}{\rho_1 u_1}\left(1 - \frac{u}{u_1}\right) dy;$$

the dynamic displacement thickness

$$\delta^* = \int_0^\infty \frac{\rho}{\rho_1}\left(1 - \frac{u}{u_1}\right) dy;$$

the energy loss thickness

$$\varphi = \int_0^\infty \frac{\rho u}{\rho_1 u_1}\left(\frac{T_{01} - T_0}{T_e - T_w}\right) dy;$$

and the thermal displacement thickness

$$\Delta^* = \int_0^\infty \frac{\rho}{\rho_1}\left(\frac{T_{01} - T_0}{T_e - T_w}\right) dy.$$

The frictional coefficients were determined by means of the integral pulse equation and Klauzer's method, described in detail in /7/. The heat flux on the wall was determined by a heat balance method based on the heating of the cooling water in each section of the experimental section.

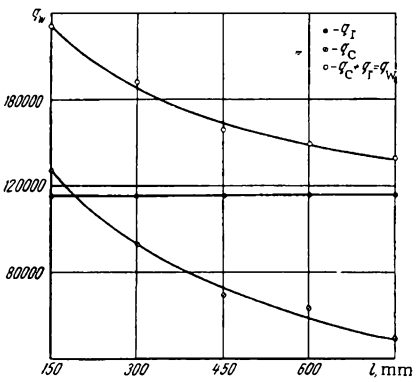


FIGURE 2. Changes (over the experimental section length) in the total $q_w$, the radiant $q_r$ and the convective $q_c$ heat fluxes, under one of the sets of experimental conditions (at Re = $131 \cdot 10^3$ and $\bar{T}_w = 0.284$).

The generalization of the experimental data obtained in terms of the integral characteristics of the turbulent boundary layer, the friction coefficients, and the heat flux on the walls enabled us to establish the empirical relationship between those terms and to analyze the effect of the temperature factor on friction and heat transfer under the conditions discussed here.

The experimentally measured heat flux comprises radiant and convective heats. The radiant heat flux consists of the heat radiated by carbon dioxide, water vapor, and the flame. The fraction of carbon dioxide in the combustion products did not exceed 0.062 by volume, and that of water vapor did not exceed 0.064 by volume.

It has been shown experimentally /9/ that when this fraction of $CO_2$ is below 0.071, the amount of heat radiated from the $CO_2$ is negligible. The same statement is valid also in the case of water vapor at low concentrations in the combustion gases. Hence, the entire amount of radiant heat (from the gas to the wall) came from the flame. The amount of radiant heat was large with respect to the heat transferred by convection, although the convective heat transfer in the case of the stream velocities used in our experiments cannot be neglected.

The radiant heat flux between the gas and the channel walls was determined by the equation proposed in /11/ and /12/:

$$q_r = \frac{\sigma_0 H_p [(aT_{01})^4 - T_w^4]}{\frac{1}{A_{as}} - \frac{1}{2}} \text{ w/m}^2. \quad (1)$$

It has been proposed /12/ that the following values should be used under the conditions discussed here: $A_{as} = 0.85$; $a\sqrt{\varepsilon_{corr}} = 0.96$.

It is evident that the heat flux measured on the basis of the cooling water balance includes the value of $q_w = q_l + q_c$.

The value of $q_c$ was determined from the known (equation (1)) value of the radiant heat flux $q_r$ and the known value of the total heat flux $q_w$.

The ratio of the convective to the radiant component of the heat flux (Figure 2) did not remain constant, but changed over the length of the experimental section. The rate of convective heat flux decreased more rapidly than that of the total heat flux, since the radiant heat flux remained constant over the channel length.

On the basis of the experimental data, we calculated the values of the Stanton number for convection, $St_c$, and for radiation, $St_r$ (Figure 3):

$$St_c = \frac{q_c}{\rho_1 u_1 c_{p_1} (T_{0_1} - T_w)};$$

$$St_r = \frac{q_r}{\rho_1 u_1 c_{p_1} (T_{0_1} - T_w)}.$$

The observed experimental relationship $\frac{St_r}{St_c} = f(Re)$, where $Re = \frac{u_1 d}{\nu_1}$, shows that the ratio of the radiant to convective components under the above conditions depends to a great extent on the Reynolds number. At $Re \simeq 5 \cdot 10^4$, the radiant heat transfer accounts for about 50% of the total heat flux on the wall. At $Re \simeq 15 \cdot 10^4$, the radiant heat transfer accounts for only about 20% of the total heat flux.

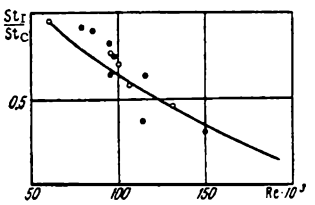


FIGURE 3. $St_r/St_c$ as a function of Re.

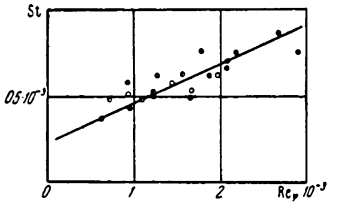


FIGURE 4. The function $St = f(Re_\varphi)$.

It is evident that as the Reynolds number increases there must be a decrease in the relative contribution of the radiant heat transfer because of the increased relative contribution of the convective heat transfer to the total heat flux on the wall.

Thus, we reach the conclusion that in the presence of developed turbulent flow with combustion, the nature of the heat transfer mainly

depends on the gas velocity. At gas velocities lower than 100 m/sec (i. e., in our case at Re $\cong 5 \cdot 10^4$), the radiant heat transfer between the gas stream and the cooled wall is considerable. At gas velocities higher than 100 m/sec, the relative contribution of the radiant heat flux decreases, and at even higher velocities (above 200 m/sec) its contribution is much smaller than that of the convective component of the heat flux.

The collected experimental data make it possible to analyze the effect of radiant heat transfer on the changes in the Stanton number over the length of the experimental section. The plot of St as a function of $Re_\varphi$ in Figure 4 (where $St = \frac{q_w}{\rho_1 u_1 c_{p_1}(T_{0_1} - T_w)}$, $Re_\varphi = \frac{u_1 \varphi}{\nu_1}$, and $q_w$ is the total heat flux in the wall, $w/m^2$) shows an increase in the Stanton number with increasing $Re_\varphi$.

By comparing the relationship obtained by us with the analogous functions from /6, 14/, we find both qualitative and quantitative differences. These differences may apparently be attributed to the effect of radiant heat transfer on the derived experimental function. The radiant heat transfer causes an increase in the absolute value of the Stanton number (Figures 2 and 3).

Comparison of experimental values of $St_C$ with values calculated by means of equations from /9/, for a tube ($\bar{T}_w = 0.274$, $T_w = 315.5$, $T_{01} = 1157°$ K)

| Experimental channel section | $St_C$ calculated in accordance with /9/ | Experimental $St_C$ in the diffuser channel | Re | Experimental value of $\zeta = \frac{C_f}{2} Re_\theta^{1/4}$ |
|---|---|---|---|---|
| 1 | 0.001720 | 0.00177 | 115,000 | 0.01340 |
| 2 | 0.001640 | 0.00150 | 97,000 | 0.01250 |
| 3 | 0.001100 | 0.00146 | 96,000 | 0.00840 |
| 4 | 0.000950 | 0.00106 | 93,000 | 0.00725 |
| 5 | 0.000319 | 0.00046 | 90,000 | 0.00242 |

Our data for $St_C$ are in good agreement with the experimental data of /9/ (see the table), which confirms the validity of the conclusions of /2, 6/, according to which the Stanton number has little effect on the positive longitudinal pressure gradient in convective heat transfer.

Thus, the heat transfer in a moving gas stream during combustion should be calculated using the function

$$St_n/St_C = f(Re).$$

The collected experimental data on the frictional coefficient make it possible to propose an equation for the calculation of friction as a function of the temperature factor $\bar{T}_w$ (Figure 5). The temperature range is from 0.8 to 0.25.

In addition to the experimental data on friction, obtained with gas flow under the conditions discussed here (i. e., at high temperatures and during combustion), Figure 5 contains also the experimental data of /6, 14/ for $\bar{T}_w = 0.7$.

The experimental function $\zeta = f(\Gamma)$ shows that the experimental data for the coefficient of friction obtained at different values of the temperature

factor (between 0.8 and 0.25), may be approximated by the following expression:

$$\zeta = 0.0128\left(\frac{2}{\sqrt{\bar{T}_w+1}}\right)^2 \frac{1}{(1-\Gamma)^{20}}. \qquad (2)$$

In (2), the effect of the temperature factor on the friction is accounted for by the introduction of a correction for nonisothermal conditions $\left(\frac{2}{\sqrt{\bar{T}_w+1}}\right)^2$.

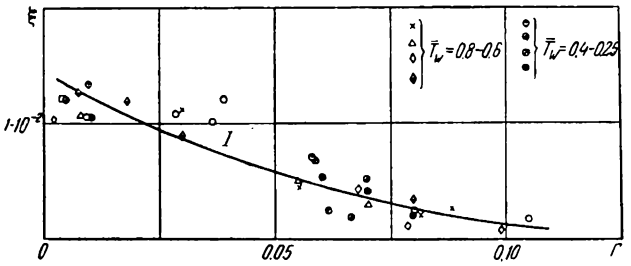


FIGURE 5. The function $\xi = f(\Gamma)$*.

I — $0.0128\left(\frac{2}{\sqrt{\bar{T}_w+1}}\right)\frac{1}{(1-\Gamma)^{20}}$.

Equation (2) is similar to equation (3-2) in /6/, which was derived by generalization of the experimental data on the friction during turbulent flow of hot air in diffusers with cooled walls, for a temperature factor $\bar{T}_m \geqslant 0.6$.

The experimental function $F(\Gamma) = f(\Gamma)$ presented in /6/ (equation (4 — 4)) remains unchanged. Hence, the method proposed in /6/ (for the calculation of the dynamic boundary layer) may be extended to the calculation of friction in subsonic gas streams during their flow in diffuser channels with cooled walls, at temperature factor values between 0.8 and 0.25.

The following sequence is suggested for the calculation of heat transfer under the above conditions.

1) The radiant heat flux in the wall is determined by the method of /11, 12/, from known expressions for the temperature changes in the potential flow, the wall temperature, and degree of blackness of the wall.

2) The value of $St_r$ is determined from the known expression for the changes in the potential flow velocity and the radiant heat flux in the wall.

3) The $St_r/St_c$ ratio (and from there the value of $St_c$) is determined from the calculated Re, with the aid of the curve in Figure 3.

4) The value of $q_c$ is determined from the expression for $St_c$.

5) Finally, the value of $q_w = q_r + q_c$ is determined for the existing conditions.

* The dispersion of experimental points (25 — 30%) on Figures 3, 4, and 5 is within the limits of experimental accuracy.

Symbols

$\rho$ — static density in the boundary layer; $u$ — velocity in the direction of the $x$ axis in the boundary layer; $\rho_1$ — static density of the potential flow; $u_1$ — velocity of the potential flow in the direction of the $x$ axis; $T_e$ — equilibrium temperature of the potential flow; $T_0$ — stagnation temperature in the boundary layer; $\sigma_0$ — radiation constant of an ideal black body; $H_p$ — surface area absorbing the radiant heat, $m^2$; $a$ — similarity coefficient of the temperature layer; $T_{01}$ — temperature of the hot medium; $T_w$ — wall temperature; $A_{as}$ — coefficient characterizing the properties of the surface absorbing the radiant heat; $\varepsilon_{corr}$ — the corrected degree of blackness; $q_c$ — convective component of the heat flux, kcal/$m^2$; $q_w$ — measured heat flux on the wall, kcal/$m^2$; $d$ — inner diameter of the corresponding sections of the experimental section, m; $\nu_1$ — kinematic viscosity of the potential flow; $\varphi$ — energy loss thickness, calculated on the basis of the thermal balance of the cooling water, m; $\xi = \frac{c_f}{2} \mathrm{Re}_\theta^{1/4}$ — shape parameter for friction; $c_f$ — coefficient of friction; $\Gamma = \left(\frac{\theta}{u_1} \frac{du_1}{dx}\right) \mathrm{Re}_\theta^{1/4}$ — shape parameter for the longitudinal pressure gradient.

Bibliography


1. Kalikhman, L.E. Turbulentnyi pogranichnyi sloi na krivolineinoi poverkhnosti, obtekaemoi gazom (The Turbulent Boundary Layer on a Curved Surface in Contact with a Gas Stream). — Moskva, Oborongiz. 1956.
2. Kutateladze, S.S. and A.I. Leont'ev. — IFZh, No. 6. 1961.
3. Zysina, L.M. — IFZh, No. 6. 1962.
4. Van Draist. — Mekhanika, No. 1. 1951.
5. Ievlev, V.M. — Doklady AN SSSR, Vol. 86, No. 6. 1952.
6. Leont'ev, A.I., A.N. Oblivin, and P.N. Romanenko. — PMTF, No. 5. 1961.
7. Oblivin, A.N. — IFZh, No. 3. 1962.
8. Vinkler, E. — Prikladnaya Mekhanika, Vol. 28. 1961.
9. Lel'chuk, V.L. and F.S. Voronin. — Teploenergetika, No. 4. 1963.
10. Kutateladze, S.S. and A.I. Leont'ev. Turbulentnyi pogranichnyi sloi szhimaemogo gaza (The Turbulent Boundary Layer in a Compressible Gas). — Moskva, Izd. SO AN SSSR. 1962.
11. Konakov, P.K. — Izv. AN SSSR, OTN, No. 6. 1950.
12. Konakov, P.K., S.S. Filimonov, and B.A. Khrustalev. — ZhTF, Vol. 27, No. 5. 1957.
13. Filimonov, S S., B.A. Khrustalev, and V.N. Adrianov. — ZhTF, Vol. 30, No. 6. 1960.
14. Filimonov, S.S., B.A. Khrustalev, and V.N. Adrianov. Konvektivnyi i luchistyi teploobmen (Convective and Radiant Heat Transfer). — Izd. AN SSSR. 1960.
15. Schlichting, H. Boundary Layer Theory. — New York, McGraw-Hill. 1955.
16. Oblivin, A.N. Candidate's thesis. — MEI. 1962.

17. Petukhov, B.S. Opytnoe izuchenie protsessov teploperedachi (Experimental Study of Heat Transfer Processes). — Gosenergoizdat. 1952.
18. Petukhov, B.S. and V.V. Kirillov. — Teploenergetika, No. 5. 1960.

Moscow

## *III. INVESTIGATION OF THE HEAT TRANSFER AND [HYDRODYNAMIC] RESISTANCE IN THE ENTRY SECTIONS OF TUBES AND CHANNELS*

B.S. Petukhov and Chang Chêng-Yung

### HEAT TRANSFER IN THE HYDRODYNAMIC ENTRY SECTION OF A ROUND TUBE DURING LAMINAR LIQUID FLOW

In many heat transfer systems, the entry to the heated (or cooled) section of the tubes coincides with the entry of the liquid into the tube. In such a case, the velocity and temperature profiles change simultaneously over the length, or in other words, the heat transfer takes place within the hydrodynamic entry section.

However, most published theoretical papers deal with the heat transfer during stabilized laminar flow, while very few are concerned with the heat transfer within the hydrodynamic entry section. For example, the latter problem has been discussed (for the case of constant wall temperature) by Sparrow /1/ for tubes with a flat cross section, and by Stephan /2/ for round and flat tubes. An approximate solution of the problem of heat transfer in a flat tube with a constant heat flux density on the wall ($q_w$ = const.) has been obtained by Siegel and Sparrow /3/. A numerical calculation of the heat transfer in a round tube at $q_w$ = const. was made by Kays /4/ for a single value of the Prandtl number (Pr = 0.7). This calculation gave too high values for the heat transfer. Thus, there is as yet no complete solution of the problem of heat transfer within the hydrodynamic entry section of a round tube at $q_w$ = const. We shall present below a solution of this problem, derived by using the approximate methods of the boundary layer theory.

The problem of heat transfer within the hydrodynamic entry section of a round tube at $q_w$ = const. is solved by making the following assumptions: 1) the flow and the heat transfer are steady; 2) the liquid is incompressible and its physical properties are constant; 3) the changes in the heat flux caused by thermal conductivity along the [tube] axis and the heat of friction are negligible; 4) the temperature and velocity of the liquid in the inlet cross section are uniformly distributed, and the velocity vector coincides with the tube axis; 5) the heat flux density on the inner surface of the tube wall is maintained constant.

Taking into account conditions 1), 2), and 3), the energy equation is

$$w_x \frac{dt}{\partial x} + w_r \frac{\partial t}{\partial r} = a \frac{1}{r} \frac{\partial}{\partial r}\left(r \frac{\partial t}{\partial r}\right). \qquad (1)$$

The boundary conditions for the temperature are

$$\text{at } x = 0 \text{ and } 0 \leqslant r \leqslant r_0, \quad t = t_0; \qquad (2)$$

$$\text{at } x \geqslant 0 \text{ and } r = r_0, \quad \frac{\partial t}{\partial r} = \frac{q_w}{\lambda}. \qquad (3)$$

We now apply equation (1) to the thermal boundary layer region. The equation is transformed using the continuity equation, multiplied by $rdr$, and integrated over the thickness of the thermal boundary layer. The following integral relations are obtained as a result:
if $\Delta \leqslant \delta$,

$$\int_{1-\bar{\Delta}}^{1} W_x \Theta R dR = 4 \frac{1}{\mathrm{Pe}} \frac{x}{d}; \tag{4}$$

if $\Delta > \delta$,

$$\int_{1-\bar{\delta}}^{1} W_x \Theta R dR + \int_{1-\bar{\Delta}}^{1-\bar{\delta}} W_1 \Theta R dR = 4 \frac{1}{\mathrm{Pe}} \frac{x}{d}. \tag{4a}$$

$$\bar{\Delta} = \frac{\Delta}{r_0}; \quad \bar{\delta} = \frac{\delta}{r_0}; \quad R = \frac{r}{r_0}; \quad W_x = \frac{w_x}{w_0}; \quad W_1 = \frac{w_1}{w_0};$$

$$\Theta = \frac{(t - t_0)\lambda}{q_w r_0}; \quad \mathrm{Pe} = \frac{w_0 2r_0}{a}.$$

In order to be able to use equations (4) and (4a), it is necessary to know the distributions of $W_x(R)$ and $\Theta(R)$ within the thickness of the boundary layer.

In accordance with Schiller /5/, we present the velocity profile over the hydrodynamic boundary layer cross section in the form of a quadratic parabola:

$$\frac{w_x}{w_1} = 2\frac{y}{\delta} - \left(\frac{y}{\delta}\right)^2$$

or

$$\frac{w_x}{w_1} = 2\frac{1-R}{\bar{\delta}} - \frac{(1-R)^2}{\bar{\delta}^2} \quad (1-\bar{\delta} \leqslant R \leqslant 1), \tag{5}$$

while the velocity changes in the flow core over the tube length are represented by the equation

$$\frac{w_1}{w_0} = \frac{6}{6 - 4\bar{\delta} + \bar{\delta}^2}, \tag{6}$$

where $y = (r_0 - r)$ is the distance from the wall to the discussed point in the boundary layer. The value of $W_x$ is evidently equal to the product of equations (5) and (6).

The dimensionless thickness $\bar{\delta}$ of the hydrodynamic boundary layer may be calculated on the basis of one of the known theories for the hydrodynamic entry section. In this connection, we made use of the work of Landhaar /6/, which contains tabulated numerical values of $\frac{w_1}{w_0} = f\left(\frac{1}{\mathrm{Re}}\frac{x}{d}\right)$. Using the above equation and equation (6), we can readily calculate for various values of $\frac{1}{\mathrm{Re}}\frac{x}{d}$ (see the table).

Dependence of $\bar{\delta}$ on $\frac{1}{\mathrm{Re}}\frac{x}{d}$

| $\frac{1}{\mathrm{Re}}\frac{x}{d}$ | $8.35\cdot10^{-5}$ | $3.95\cdot10^{-4}$ | $9.75\cdot10^{-4}$ | $2.00\cdot10^{-3}$ | $3.53\cdot10^{-3}$ |
|---|---|---|---|---|---|
| $\bar{\delta}$ | 0.1 | 0.2 | 0.3 | 0.4 | 0.5 |
| $\frac{1}{\mathrm{Re}}\frac{x}{d}$ | $5.8\cdot10^{-3}$ | $9.18\cdot10^{-3}$ | $1.46\cdot10^{-2}$ | $2.51\cdot10^{-2}$ | $6.43\cdot10^{-2}$ |
| $\bar{\delta}$ | 0.6 | 0.7 | 0.8 | 0.9 | 0.99 |

The velocity profile in the hydrodynamic entry section is fully determined by equations (5) and (6) and the relations are shown in the table. When $\frac{1}{\mathrm{Re}}\frac{x}{d}$ is increased, $\bar{\delta}\to1$, $W_1\to2$. and $\frac{w_x}{w_0}\to(1-R^2)$, i. e., the velocity profile for the entry sections assumes a parabolic shape, characteristic of steady flow.

Firstly, the function for $\Theta(R)$ should satisfy the conditions on the outer boundary of the thermal boundary layer, and on the wall

$$\Theta_{R=1-\bar{\Delta}}=0,\quad \left(\frac{\partial\Theta}{\partial R}\right)_{R=1-\bar{\Delta}}=0,$$
$$\left(\frac{\partial\Theta}{\partial R}\right)_{R=1}=1,\quad \left(\frac{\partial^2\Theta}{\partial R^2}\right)_{R=1}=-1 \tag{7}$$

(the last condition arises from the energy equation). Secondly, at $\bar{\Delta}=1$, it should be transformed into the well-known expression for the temperature field in steady heat transfer

$$t-t_0'=\frac{q_w r_0}{\lambda}\left[\left(\frac{r}{r_0}\right)^2-\frac{1}{4}\left(\frac{r}{r_0}\right)^4\right]. \tag{8}$$

At $\bar{\Delta}<1$ $t_0'=t_0$.

The last condition is satisfied if $\bar{\Delta}\leqslant\bar{\delta}$. If $\bar{\Delta}>\bar{\delta}$, it is not satisfied in the strictest sense of the term, since in such a case, the velocity profile differs from a parabolic curve. Assuming that the difference is small, we shall accept that equation (8) is approximately valid also at $\bar{\Delta}>\bar{\delta}$.

In order to select an adequate function, we first apply equation (8) in general terms to the thermal boundary layer region in the entry section of the tube. To this end, $\Delta(x)$ should be substituted for $r_0$ in (8). In that case, $\frac{r}{r_0}\equiv1-\frac{y}{r_0}$ should be replaced by $1-\frac{y}{\Delta}\equiv1-\frac{r_0}{\Delta}+\frac{r}{\Delta}$. As a result, we obtain the expression

$$\Theta=\bar{\Delta}\left[\left(1-\frac{1}{\bar{\Delta}}+\frac{R}{\bar{\Delta}}\right)^2-\frac{1}{4}\left(1-\frac{1}{\bar{\Delta}}+\frac{R}{\bar{\Delta}}\right)^4\right],$$

which satisfies all the above conditions.

However, calculations made using the above equation show that it does not satisfactorily describe the temperature distribution in the cross section of the boundary layer. Much better results may be obtained by introducing

a term containing a logarithm* into the equation. Thus, the function $\Theta(R)$ finally takes the following form:

$$\Theta = \tilde{\Delta}\left[\xi^2 - \frac{1}{4}\xi^4 + (1-\tilde{\Delta})(\xi \ln \xi)^2\right], \tag{9}$$

where $\xi = 1 - \frac{1}{\tilde{\Delta}} + \frac{R}{\tilde{\Delta}}$. Equation (9) also satisfies all the above conditions. It comprises an as yet unknown term, i.e., the thickness $\tilde{\Delta}$ of the thermal boundary layer.

In order to determine the value of $\tilde{\Delta}$, we substitute in the integral equation (4) the values of $W_x(R)$ (from (5) and (6)) and of $\Theta(R)$ (from (9)). After integration, we obtain

$$\frac{6\tilde{\Delta}^3}{(6-4\tilde{\delta}+\tilde{\delta}^2)\tilde{\delta}}\left[\frac{3}{20} - \frac{13}{420}(1+2\tilde{\delta})\frac{\tilde{\Delta}}{\tilde{\delta}} + \frac{53}{3360}\frac{\tilde{\Delta}^2}{\tilde{\delta}}\right] +$$

$$+\frac{6\tilde{\Delta}^2}{6-4\tilde{\delta}+\tilde{\delta}^2}\left\{(1-\tilde{\Delta})^2\left[\frac{2}{27}\left(2\frac{\tilde{\Delta}}{\tilde{\delta}} - \frac{\tilde{\Delta}^2}{\tilde{\delta}^2}\right) - \frac{2}{32}\frac{\tilde{\Delta}}{\tilde{\delta}}\left(1-\frac{\tilde{\Delta}}{\tilde{\delta}}\right) + \right.\right.$$

$$\left. + \frac{2}{125}\frac{\tilde{\Delta}^2}{\tilde{\delta}^2}\right] + (1-\tilde{\Delta})\tilde{\Delta}\left[\frac{1}{32}\frac{\tilde{\Delta}}{\tilde{\delta}}\left(2-\frac{\tilde{\Delta}}{\tilde{\delta}}\right) - \frac{4}{125}\frac{\tilde{\Delta}}{\tilde{\delta}} \times\right.$$

$$\left.\left. \times\left(1-\frac{\tilde{\Delta}}{\tilde{\delta}}\right) + \frac{1}{108}\frac{\tilde{\Delta}^2}{\tilde{\delta}^2}\right]\right\} = 4\frac{1}{\mathrm{Pe}}\frac{x}{d}. \tag{10}$$

The algebraic equation (10) is valid if $\tilde{\Delta} \leqslant \tilde{\delta}$. By using the integral equation (4a), we can readily obtain a similar equation for the case of $\tilde{\Delta} > \tilde{\delta}$.

Since the dependence of $\tilde{\delta}$ on $\frac{1}{\mathrm{Re}}\frac{x}{d}$ is known, equation (10) may be used to determine the thickness $\tilde{\Delta}$ of the thermal boundary layer as a function of $\frac{1}{\mathrm{Pe}}\frac{x}{d}$ and Pr.

By definition, the local heat transfer coefficient $\alpha \equiv \frac{q_w}{t_w - \bar{t}}$. If $\tilde{\Delta} < 1$ (when $t_0' = t_0$), the value of $t_w - \bar{t}$ may be represented as

$$t_w - \bar{t} = (t_w - t_0') - (\bar{t} - t_0). \tag{11}$$

From equation (9), we have (for $R = 1$)

$$t_w - t_0' = t_w - t_0 = \frac{3}{8}\frac{q_w d}{\lambda}\tilde{\Delta}.$$

From the heat balance, we have

$$\bar{t} - t_0 = \frac{2q_w x}{w_0 \rho c_p r_0} = 4\frac{q_w d}{\lambda}\frac{1}{\mathrm{Pe}}\frac{x}{d}.$$

Thus, in the case of $\tilde{\Delta} < 1$, the expression for the local Nu number is

$$\mathrm{Nu} \equiv \frac{\alpha d}{\lambda} = \frac{1}{\frac{3}{8}\tilde{\Delta} - 4\frac{1}{\mathrm{Pe}}\frac{x}{d}}. \tag{12}$$

* The necessity for a logarithmic term in the expression for $\Theta(R)$ can be demonstrated by analysis of the energy equation using the method of successive approximations.

The above expression is valid for both $\bar{\Delta} \leqslant \bar{\delta}$ and $\bar{\Delta} > \bar{\delta}$. Beginning with the value of the equivalent length (at which $\bar{\Delta}$ becomes equal to unity), we should distinguish between two cases:

$$\bar{\Delta} \leqslant \bar{\delta} \text{ and } \bar{\Delta} > \bar{\delta}.$$

In the first case, the stabilization of the velocity profile is completed either before or simultaneously with the stabilization of the temperature profile. Hence, when $\bar{\Delta}$ becomes equal to unity, the heat transfer is stabilized and the Nusselt number assumes a constant (limiting) value, denoted here by $\mathrm{Nu}_\infty$. According to (12),

$$\mathrm{Nu}_\infty = \frac{1}{\frac{3}{8} - 4\frac{1}{\mathrm{Pe}}\frac{l_{\mathrm{t.e.}}}{d}}.$$

The equivalent length of the thermal entry section is determined from (10) by assuming that $\bar{\delta} = 1$ and $\bar{\Delta} = 1$. Then

$$\frac{1}{\mathrm{Pe}}\frac{l_{\mathrm{t.e.}}}{d} = 0.0365.$$

Hence, $\mathrm{Nu}_\infty = 4.36$, which is in agreement with known data.

In the second case, the velocity profile changes over the length continue after $\bar{\Delta}$ becomes equal to unity. For this reason, the heat transfer is stabilized in that section of the tube in which the velocity profile has been stabilized. Equation (11) should not be used for the section for whose length $\bar{\Delta}=1$ and $\bar{\delta} \leqslant 1$, since in that case, $t_0' \neq t_0$. The value of $t_w - \bar{t}$ for that section may be determined by using the equation

$$t_w - \bar{t} = \frac{2}{w_0 r_0^2}\left[\int_0^{r_0-\delta}(t_w - t)\, w_1 r dr + \int_{r_0-\delta}^{r_0}(t_w - t)\, w_x r dr\right].$$

At $\bar{\Delta} = 1$, equation (9) is transformed into (8). By using (8), (5), and (6), we calculate $(t_w - \bar{t})$ and then the Nusselt number. As a result, we obtain

$$\mathrm{Nu} = \frac{6 - 4\bar{\delta} + \bar{\delta}^2}{1 - \frac{1}{2}\bar{\delta}^2 + \frac{1}{10}\bar{\delta}^3 + \frac{3}{20}\bar{\delta}^4 - \frac{1}{14}\bar{\delta}^5 + \frac{1}{112}\bar{\delta}^6}. \qquad (13)$$

At $\bar{\delta} = 1$,

$$\mathrm{Nu} = \mathrm{Nu}_\infty = 4.36.$$

In this case, the length of the thermal entry section corresponds to the length of the hydrodynamic entry section and may be determined from the table as the value of that argument for which $\bar{\delta} = 0.99$:

$$\frac{1}{\mathrm{Re}}\frac{l_{\mathrm{t.e.}}}{d} \simeq 0.064 \text{ or } \frac{1}{\mathrm{Pe}}\frac{l_{\mathrm{t.e.}}}{d} \simeq \frac{0.064}{\mathrm{Pr}}.$$

The Nusselt numbers were calculated in the range $10^{-7} \leqslant \frac{1}{Pe}\frac{x}{d} \leqslant 10^{-1}$ for Prandtl numbers equal to 0.7, 1, 10, 100, 1000, and $\infty$. The results are shown in Figures 1 and 2.

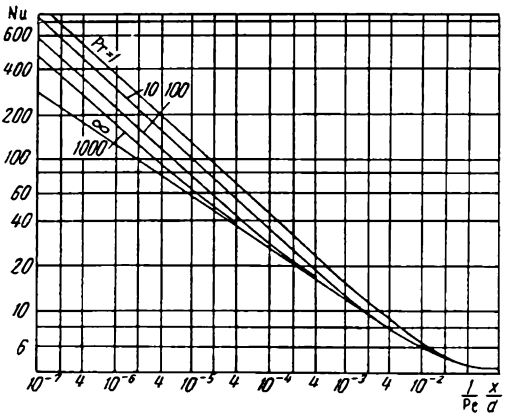


FIGURE 1. Changes in the Nusselt number in the entry section of a round tube during changes in the velocity profile over the length (according to our calculations).

The curve in Figure 1 for $Pr = \infty$ is the limiting curve and corresponds to a parabolic velocity profile over the whole tube length. This is a direct result of the fact that the ratio of the lengths of the thermal and hydrodynamic entry sections is proportional to the Prandtl number. For a certain given value of $\frac{1}{Pe}\frac{x}{d}$, the heat transfer in the hydrodynamic entry section becomes more intensive as the Pr number is decreased (as should be expected).

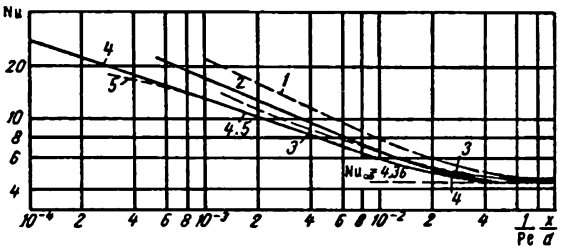


FIGURE 2. Comparison of values of the Nusselt number obtained as a result of our calculations and the calculation of other authors.

1 — calculated by Kays for the hydrodynamic entry section at Pr = 0.7; 2 — our calculations, for the same conditions; 3 — calculated by Kays for a parabolic velocity profile; 4 — our calculations for the same conditions; 5 — solution of Siegel, Sparrow, and Hollman for a parabolic velocity profile.

In Figure 2, the results of our calculations for Pr = 0.7 and Pr = ∞ (parabolic velocity profile) are compared with other calculated data. In the case of a parabolic velocity profile, the results of our calculations agree with the accurate solution of Siegel, Sparrow, and Hollman /7/, except for a narrow range of values of $\frac{1}{\mathrm{Pe}}\frac{x}{d}$ (from $2\cdot 10^{-2}$ to $7\cdot 10^{-2}$), where the discrepancy is 5%. The results of Kays' numerical calculations (for a parabolic velocity profile) /4/ are about 20% higher. The same discrepancy is observed between our calculations and those of Kays, when the velocity and temperature profiles develop simultaneously over the length at Pr = = 0.7. The above data show fairly conclusively that the Nusselt numbers obtained by the numerical calculations of Kays are higher than the actual values.

An asymptotic expression for the Nusselt number is readily derived when $\frac{1}{\mathrm{Pe}}\frac{x}{d}$ is small and the velocity profile is parabolic. In this case ($\bar{\Delta} \ll 1$ and $\bar{\delta} = 1$), equation (10) assumes the form

$$2\bar{\Delta}^3\frac{3}{20} + 2\left(\frac{4}{27} - \frac{2}{32}\right)\bar{\Delta}^3 = 4\frac{1}{\mathrm{Pe}}\frac{x}{d},$$

i. e.,

$$\bar{\Delta}^3 = 8.5\frac{1}{\mathrm{Pe}}\frac{x}{d}.$$

By determining $\bar{\Delta}$ from the above equation, substituting its value in (12), and eliminating the term $4\frac{1}{\mathrm{Pe}}\frac{x}{d}$ (which is negligibly small as compared with $\frac{3}{8}\bar{\Delta}$), we obtain

$$\mathrm{Nu} = 1.31\left(\frac{1}{\mathrm{Pe}}\frac{x}{d}\right)^{-1/3}, \qquad (14)$$

which is in excellent agreement with the equation derived in /8/.

For low values of $\frac{1}{\mathrm{Re}}\frac{x}{d}$ (i. e., near the inlet of the tube, where the thickness of the boundary layers is small), it is possible to derive another asymptotic expression for the Nusselt number. In the case of $\bar{\delta} \ll 1$ and $\bar{\Delta} \ll 1$, equation (10) assumes the form

$$\frac{\bar{\Delta}^3}{\bar{\delta}}\left(0.2355 - 0.0265\frac{\bar{\Delta}}{\bar{\delta}}\right) = 4\frac{1}{\mathrm{Pe}}\frac{x}{d}.$$

The calculation results show that the $\frac{\bar{\Delta}}{\bar{\delta}}$ ratio depends mainly on the Prandtl number, and in the case of $0.7 \leqslant \mathrm{Pr} \leqslant 1000$ and $\frac{1}{\mathrm{Re}}\frac{x}{d} \leqslant 4\cdot 10^{-4}$ (or $10 \leqslant \mathrm{Pr} \lesssim 1000$ and $\frac{1}{\mathrm{Re}}\frac{x}{d} \leqslant 2\cdot 10^{-3}$), the above ratio is expressed by the equation

$$\frac{\bar{\Delta}}{\bar{\delta}} \simeq 0.54\,\mathrm{Pr}^{-1/3}.$$

By substituting the above value in the preceding equation, we obtain

$$0.54\,\tilde{\Delta}^2 \mathrm{Pr}^{-1/3}\,(0.2355 - 0.0143\,\mathrm{Pr}^{-1/3}) = 4\,\frac{1}{\mathrm{Pe}}\,\frac{x}{d}.$$

Since the second term in the parentheses is small with respect to the first term, it is evaluated by approximation, assuming Pr = 1. We thus obtain

$$\tilde{\Delta} = 5.8\left(\frac{1}{\mathrm{Pe}}\,\frac{x}{d}\right)^{1/3}\mathrm{Pr}^{1/6}.$$

By substituting the above expression in (12) and neglecting the term $4\,\frac{1}{\mathrm{Pe}}\,\frac{x}{d}$ (because of its small value), we obtain

$$\mathrm{Nu} = 0.46\left(\frac{1}{\mathrm{Re}}\,\frac{x}{d}\right)^{-1/3}\mathrm{Pr}^{1/3}. \qquad (15)$$

Equation (15) coincides exactly with the equation for local heat transfer in the case of longitudinal flow around a plate at $q_w$ = const. /9/. Thus, the heat transfer near the tube inlet is approximately governed by the same laws as in the case of a plate.

The use of the following interpolation equation (16) is suggested for the whole range of $\frac{1}{\mathrm{Re}}\,\frac{x}{d}$ values corresponding to hydraulic entry section (except for very small values):

$$\frac{\mathrm{Nu}}{\mathrm{Nu_{st}}} = 0.35\left(\frac{1}{\mathrm{Re}}\,\frac{x}{d}\right)^{-1/6}\left[1 + 2.85\left(\frac{1}{\mathrm{Re}}\,\frac{x}{d}\right)^{0.42}\right], \qquad (16)$$

(where $\mathrm{Nu_{st}}$ is the Nusselt number for steady flow at $q_w$ = const.); equation (16) describes the calculated results in the range $10^{-4} \leqslant \frac{1}{\mathrm{Re}}\,\frac{x}{d} \leqslant 0.064$ and $0.7 \leqslant \mathrm{Pr} \leqslant 1000$ with an accuracy of about 6%. At $\frac{1}{\mathrm{Re}}\,\frac{x}{d}$ values higher than 0.064, the velocity profile becomes parabolic and $\mathrm{Nu} = \mathrm{Nu_{st}}$.

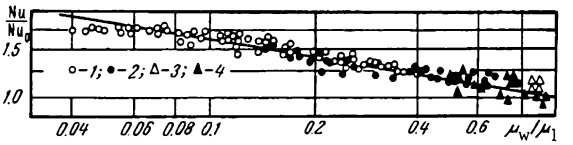


FIGURE 3. Relationship between $\frac{\mathrm{Nu}}{\mathrm{Nu_0}}$ and $\frac{\mu_1}{\mu_w}$ for oil VM-4 (1, 2) and water (3, 4):

1 — in the developed flow region; 2 — in the hydrodynamic entry section.

The value of $Nu_{st}$ may be calculated by the equation presented in /7/ or with the aid of an interpolation equation:

$$Nu_{st} = 1.31\left(\frac{1}{Pe}\frac{x}{d}\right)^{-1/3}\left(1+2\frac{1}{Pe}\frac{x}{d}\right). \qquad (17)$$

Equation (17) describes the results of our calculations for a parabolic velocity profile with an accuracy of ±4% and is valid in the range of $\frac{1}{Pe}\frac{x}{d} \leqslant 0.038$.

In order to account for the effect of the variable viscosity on the heat transfer during the flow of dropping liquids at high temperature gradients, we used experimental data /10-11/ for water and VM-4 oil, which were obtained in the hydrodynamic entry section and in the region of developed flow (Figure 3). These data are satisfactorily described by the equation

$$\frac{Nu}{Nu_0} = \left(\frac{\mu_w}{\mu_l}\right)^{-1/6}, \qquad (18)$$

where Nu and $Nu_0$ are the Nusselt numbers determined in the experiment and calculated from equation (16) (assuming that the physical properties are constant); $\mu_w$ and $\mu_l$ are the values of the viscosity coefficient at the wall temperature and at the mean calorimetric temperature of the liquid in the given section. The physical properties of the liquid and the expressions for the Nu, Pe, and Re numbers were taken to correspond to a temperature $t = \frac{1}{2}(t_w + \bar{t})$.

Equation (17) is valid for the case of heating of a liquid at $0.04 \leqslant \frac{\mu_w}{\mu_x} \leqslant 1$.

## Symbols

$r_0$ — tube radius; $t_0$ — liquid temperature at the inlet; $q_w$ — heat flux density on the wall; $\lambda$ — thermal conductivity coefficient of the liquid; $\Delta$ and $\delta$ — thicknesses of the thermal and hydrodynamic boundary layers; $w_0$ — liquid velocity at the inlet; $w_1$ — velocity in the stream core or on the outer boundary of the boundary layer; $t_0'$ — temperature at the tube axis.

## Bibliography


1. Knudsen, J.G. and D.L. Katz. Fluid Dynamics and Heat Transfer. 1958.
2. Stephan, K.—Ingenieur Archiv. Vol. 29, No. 3. 1960.
3. Siegel, R. and E.M. Sparrow.—I. Ch. E. Journal, Vol. 5, No. 1. 1959.
4. Kays, W.M.—Trans. ASME, Vol. 77. 1955.
5. Schiller L. The Motion of Fluids in Pipes [Russian translation. 1936.]
6. Landhaar, H.L. — Trans. ASME, 64. 1942.

7. Siegel, R., E.M. Sparrow, and T.M. Hollman. — Appl. Sci. Res., Sect. A, Vol. 7, No. 5. 1958.
8. Sellers, J., M. Tribus, and J. Klein. — Trans. ASME, Vol. 78, No. 2. 1956.
9. Tribus, M. and J. Klein. Heat Transfer Symposium, University of Michigan. 1953.
10. Mikheev, M.A., S.S. Filimonov, and B.A. Khrustalev. In sbornik: Konvektivnyi i luchistyi teploobmen (Convective and Radiant Heat Transfer). — Izd. AN SSSR. 1960.
11. Ma Tung-Tse. Razvitie protsessa teplootdachi v trubakh pri laminarnom rezhime (Development of the Heat Transfer in Tubes During Laminar Flow). In sbornik: "Teploperedacha". — Izd. AN SSSR. 1962.

The Moscow Power Institute

A. A. Zhukauskas and I. I. Zhyugzhda

# EXPERIMENTAL STUDY OF THE HEAT TRANSFER AND HYDRAULIC RESISTANCE IN THE ENTRY SECTION OF A FLAT CHANNEL DURING LAMINAR FLOW OF A VISCOUS LIQUID

The fact that laminar flow obeys certain strict laws makes possible the use of the exact and approximate boundary layer methods /1-6/ (based on the Navier-Stokes, continuity, impulse, heat flux, and Bernoulli equations) for the determination of the various hydrodynamic and heat transfer characteristics of the entry section. However, all analytical studies have been based on a number of simplifying assumptions, while only a few experimental studies did not use these assumptions. Most of these studies were carried out in air streams /5, 7/. Very little experimental data have been collected on the local heat transfer, although such data may be used for the more exact determination of the nature of the physical phenomena. Hence, the main purpose of this work was to study the local heat transfer and resistance in various streams of a dropping liquid, within a wide range of variation of its physical properties.

Our experiments were carried out in two hydrodynamic loops, in air, water, and transformer oil streams. The experimental section ( a rectangular channel with a cross section of $0.2 \times 0.1$ m) contained parallel plates assembled in a block, which simulated the investigated channel (Figure 1). The whole channel cross section was uniformly packed with the plates. However, only three plates at the channel center were heated directly by d.c. from a homopolar generator or from rectifiers. The measurements were made only on the middle plate, while the two outer plates served only for modeling. The required distances between the plates (or the heights of the flat channels) were adjusted with the aid of lateral "getinaks"* strips. The heated surface of the plates was made of manganin alloy strips 0.00018 m thick (the thickness was uniform over the whole cross section). Thus, we were able to obtain a constant heat flux density on the surface ($q_w \cong$ const.). The manganin alloy strips were glued onto the "getinaks" frame. Copper-constantan thermocouples used to measure the surface temperature were fitted underneath the alloy strips. Only the 0.04 m wide middle region of the plate was used in the measurements. The thermocouple emf and the potential drop on the measuring section of the plate and in the shunts were measured by compensation. The flow velocity was determined from the amount of liquid, measured with a normal or duplex diaphragm.

The studies were carried out at four different heights ($s$ = 0.004; 0.01; 0.02; and 0.05 m) of the 0.002 m thick plates forming the channel. The velocity was varied between 1.5 and 10.5 m/sec for the air stream, and

* [Paper laminated with resin.]

between 0.1 and 0.4 m/sec for water and transformer oil streams. The local temperature gradient was varied between 274 and 313°K, the stream temperature between 286 and 333°K, and the values of $Pr_f$ from 0.7 to 580. The hydrodynamic resistance was determined from the static pressure drop $\Delta P = P_0 - P_1$ (Figure 1).

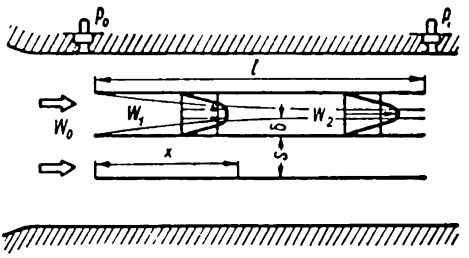


FIGURE 1. Schematic view of the experimental section and the development of the hydrodynamic process.

Over the length of the entry section (Figure 1), a region not affected by the viscosity forces (i. e., a potential flow region) was created in the channel center. In view of the growth of the boundary layers and the constant flow rate of the liquid in each channel section, there should be an increase in the potential flow velocity. This creates a pressure gradient. The pressure gradient and the increase in velocity are the main factors causing various phenonema in the entry section of the channel and accounting for the difference between the phenomena on a plate and in an infinite stream. The pressure gradient distorts the velocity and temperature profiles within the boundary layer, reduces the boundary layer thickness, and thus increases the heat transfer rate (as compared with a plate). The potential flow velocity increases in the same direction. An analysis of our experimental data obtained at different $s$ in various liquid streams confirms this assumption, since our data lie above the straight line describing the heat transfer on a plate /8/. The data in Figure 2 show that the heat transfer rate in the entry section depends on the geometric characteristics of the channel, and that the increase in the rate (as compared with the heat transfer on a plate) may be accounted for by the introduction of an additional parameter $\frac{x}{s\mathrm{Re}_{fs}}$. In that case, the heat transfer in the entry section of a flat channel could be expressed by the following dimensionless equation (taking into account the effect of the temperature factor):

$$\mathrm{Nu}_{fx} = c\,\mathrm{Re}_{fx}^{m}\,\mathrm{Pr}_f^{n}\left[\frac{x}{s\,\mathrm{Re}_{fs}}\right]^{r}[\mathrm{Pr}_f/\mathrm{Pr}_w]^{0.25}. \qquad (1)$$

The values of the exponents of $\mathrm{Re}_{fx}$ and $\mathrm{Pr}_f$ in equation (1) remain the same as in the case of a plate: $m = 0.5$ and $n = 0.33$. Subsequently, by plotting the function $\mathrm{Nu}_{fx}\mathrm{Re}_{fx}^{-0.5} \times \mathrm{Pr}_f^{-0.33}[\mathrm{Pr}_f/\mathrm{Pr}_w]^{-0.25} = f\left(\frac{x}{s\,\mathrm{Re}_{fs}}\right)$ it is possible to determine the value of the exponent $r = 0.1$ (Figure 3). The same figure contains data on the local heat transfer on a plate /8/. As is evident from

Figure 3, the experimental data for the heat transfer in the entry section approach asymptotically the data for heat transfer on a plate. Thus, on the basis of the data in the figure, we can derive a general equation for the local heat transfer in the entry section of a flat channel:

$$\mathrm{Nu}_{fx} = \left[0.43 + c_1\left(\frac{x}{s\,\mathrm{Re}_{fs}}\right)^{0.1}\right] \mathrm{Re}_{fx}^{0.5}\,\mathrm{Pr}_f^{0.33}[\mathrm{Pr}_f/\mathrm{Pr}_w]^{0.25} \qquad (2)$$

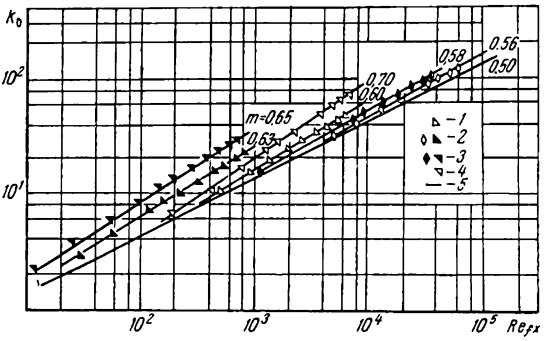


FIGURE 2. The relationship $K_0 = \mathrm{Nu}_{fx}\,\mathrm{Pr}_f^{-0.33}(\mathrm{Pr}_f/\mathrm{Pr}_w)^{-0.25} = f(\mathrm{Re}_{fx})$.

1, 4 — with transformer oil at $s$ = 0.05 and 0.004 m respectively; 2, 3 — with air, water and transformer oil at $s$ = 0.02 m and 0.01 m respectively; 5 — experimental data for a plate /8/.

The experimental data are shown in Figure 3; the same data were used to derive equation (2). The data were obtained with the aid of the same plate-type calorimeter in the cases of both the plate and the channel.

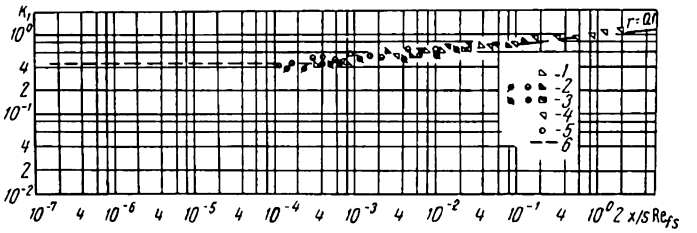


FIGURE 3. The function $K_1 = \mathrm{Nu}_{fx}\,\mathrm{Re}_{fx}^{-0.5}\mathrm{Pr}_f^{-0.33}\,[\mathrm{Pr}_f/\mathrm{Pr}_w]^{-0.25} = f\left(\frac{x}{s\mathrm{Re}_{fs}}\right)$

(the symbols used are the same as in Figure 2).

5, 6 — experimental data from /5/ and /8/.

Using the data in Figure 3, let us determine the constant $c_1$; it is expressed by the equation

$$c_1 = 0.55\left(\frac{x}{s\,\mathrm{Re}_{fs}}\right)^{0.15} \qquad (3)$$

In order to make equation (2) more general, it is necessary to introduce a coefficient $\varkappa$ for the nonisothermal conditions on the channel surface /8/. In our investigation (as in the case of /8/) the temperature gradient changed

in accordance with the equation $\Delta t_x = t_{wx} - t_f = Ax^{\vartheta}$, where $\vartheta \cong 0.4$. Thus, the local heat transfer in the entry section of a flat channel is expressed by the equation

$$\mathrm{Nu}_{fx} = \left[0.33 + 0.42\left(\frac{x}{s\,\mathrm{Re}_{fs}}\right)^{0.25}\right] \times \mathrm{Re}_{fx}^{0.5}\,\mathrm{Pr}_f^{0.33}\,[\mathrm{Pr}_f/\mathrm{Pr}_w]^{0.25}. \qquad (4)$$

The mean heat transfer may be determined by integration of the local heat transfer coefficient (calculated from equation (4)) over the given channel length.

The hydraulic resistance is a parameter of great practical importance. In our investigation, its value was determined by measuring the static pressure drop in front of and behind the channel, with subsequent processing of the collected data by using the equation

$$\mathrm{Eu} = c_0\left(\frac{l}{2s\,\mathrm{Re}_{2s}}\right)^{\kappa}, \qquad (5)$$

where

$$\mathrm{Eu} = \frac{\Delta P}{\rho w_0^2}; \quad \mathrm{Re}_{2s} = \frac{w_0 2s}{\nu_f}.$$

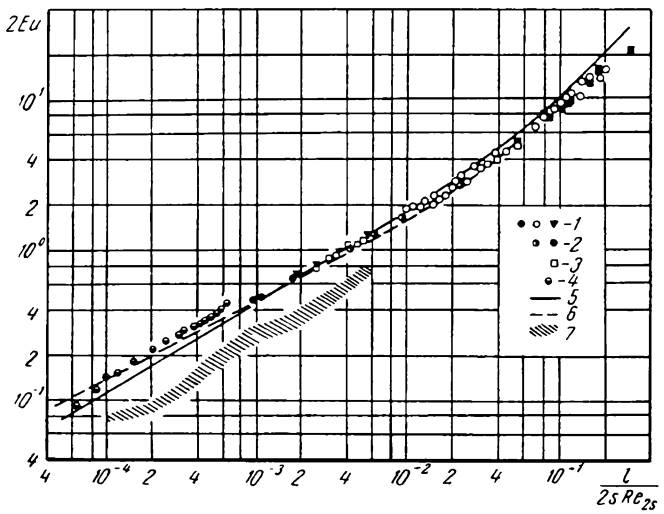


FIGURE 4. Hydrodynamic resistance in the entry section of a flat channel.

1 — with air, transformer oil, and water at $s = 0.01$ m; 2 — with air and transformer oil at $s = 0.004$ m; 3 — with transformer oil at $s = 0.02$ m; 4, 7 — experimental data from /5/ and /7/ respectively; 5, 6 — results obtained by theoretical [analytical] calculations in /4/ and /1/ respectively.

The nature of the hydrodynamic process in the entry section of the channel shows that in it the energy is expended for overcoming the friction forces and for accelerating the potential flow. A very small fraction of

the energy is lost as a result of velocity redistribution at the channel inlet and outlet.

By generalizing the experimental data in logarithmic coordinates with the aid of equation (5), we determined the values of the constant $c_0$ and the exponent $\kappa$. We found that the hydrodynamic resistance in the entry section at $\frac{x}{2s\,\mathrm{Re}_{2s}}$ values between $2\cdot 10^{-2}$ and $9\cdot 10^{-4}$ is expressed by the equation

$$\mathrm{Eu} = 11.0\left(\frac{l}{2s\,\mathrm{Re}_{2s}}\right)^{0.56}. \qquad (6)$$

As is evident from Figure 4, at high values of the above parameter $[\frac{x}{2s\,\mathrm{Re}_{2s}}]$, the resistance in the entry section approaches asymptotically the steady-flow resistance law, while at low values of the above parameter, it approaches the law describing the resistance on a plate.

The data of other investigators, which are shown in Figures 3 and 4, are in good agreement with our experimental data.

Bibliography


1. Schlichting, H. — ZAMM, 14(6):364. 1934.
2. Leibenzon, L.S. Rukovodstvo po neftepromyslovoi mekhanike, part 1. Gidravlika (Manual of Petroleum Technology, Part 1, Hydraulics). — GNTTs. 1931.
3. Targ, S.M. Osnovnye zadachi teorii laminarnykh techenii (Main Problems of the Theory of Laminar Flows). — Moskva-Leningrad, GITTL. 1951.
4. Stephan, K. — Chemie-Ingenieur Technik, Vol. 31, No. 12. 1959.
5. Sugawara, T. and S. Sato. — Mem. Fac. Engng. Kyoto Univ., Vol. 16, No. 3. 1954.
6. Knudsen, J. and D. Katz. — Fluid Dynamics and Heat Transfer, New-York — Toronto — London. 1958.
7. Raesfeld, A. — Chemie-Ingenieur Technik, Vol. 25, No. 5. 1953.
8. Zhyugzhda, I.I. and A.A. Zhukauskas. — Trudy Akademii Nauk Litovskoi SSR, 4(31):117. 1962.



The Power and Electrical Engineering Institute of the Academy of Sciences of the Latvian SSSR

E.E. Solodkin and A.S. Ginevskii

# TURBULENT NONISOTHERMAL FLOW OF A VISCOUS COMPRESSIBLE GAS IN THE ENTRY SECTIONS OF AXISYMMETRICAL AND FLAT WIDENING CHANNELS WITH ZERO PRESSURE GRADIENT

The flow of viscous incompressible fluids in the entry sections of flat and axisymmetrical channels with fully turbulent boundary layers has been studied in /1, 2/. In particular, these studies were concerned with the flow in the entry section of an axisymmetrical slightly expanding channel with zero pressure gradient and in the entry sections of flat, round, and annular tubes.

As indicated in /1/, in addition to their theoretical value, the results of such studies may be used also for the investigation of flow in the entry sections of corresponding cylindrical tubes.

It is of interest to investigate such flows in the case of a viscous compressible gas, both with and without heat transfer in the entry sections of axisymmetrical and flat channels at subsonic stream velocities.

It could be assumed that the compressibility of the gas, and in particular the heat transfer, would have a marked influence on the aerodynamic characteristics of the channel — the Pitot loss coefficient, the length of the entry sections, etc.

In this paper we report the study of the nonisothermal flow of a viscous compressible gas in the entry sections of axisymmetrical and flat channels with zero pressure gradient at subsonic flow velocities, and within a wide range of values of the temperature factor.

We now analyze the nonisothermal flow of a viscous compressible gas within the entry sections of expanding round and flat channels with a zero pressure gradient. The following schematic presentation of the flow would serve as a basis of the above analysis.

In the entry section of the channel, the velocity, temperature, Mach number, and other flow parameters are uniformly distributed across the channel. As the distance from the entry section of the channel increases, the effect of viscosity forces on the channel walls causes an increase in the boundary layer thickness while an isoentropic flow core is created within the remaining part of the channel cross section, nearer the axis. If heat transfer takes place, the last assumption implies also that it affects the velocity and temperature distributions only within the boundary layer. The static pressure across the boundary layer remains constant. The last two assumptions lead to the conclusion that the velocity, temperature, Mach number, and other flow parameters remain constant across the channel within the flow core. It is assumed that the flow in the boundary layer is turbulent. In order to confirm this assumption, we shall analyze the

nonisothermal flow of a viscous compressible gas in an expanding round channel with a zero pressure gradient at a constant wall temperature.

The problem will be solved by taking into account the effect of the lateral surface curvature on the characteristics of the axisymmetrical turbulent boundary layer. A general solution to the problem of the effect of lateral surface curvature on the characteristics of an axisymmetrical turbulent layer of compressible gas has been presented in /3/.

The above method is applied below to the particular case analyzed by us, using the following approach.

The velocity profile in an axisymmetrical turbulent boundary layer is determined with the aid of the Prandtl equation

$$\tau = \rho l^2 (\partial u/\partial y)^2, \tag{1}$$

relating the frictional stress to the averaged velocity gradient ($l$ is the mixing path length).

On the basis of the motion equations and the boundary conditions on the walls for the longitudinal and lateral velocity components, we can represent with an accuracy down to the third decimal point) the frictional stress near the surface by an equation of the type

$$r\tau = \text{const} = r_w \tau_w. \tag{2}$$

Here and below we shall assume that for any section of the channel, the tangent to its generatrix forms a very small angle $\Theta$ with the channel axis; this assumption is supported by the calculation results. Hence, it may be assumed with great accuracy that

$$\cos\Theta = 1 \quad \text{and} \quad r_w - y\cos\Theta = r_w - y. \tag{3}$$

In the vicinity of the surface (where condition (2) is obeyed), it may be assumed that the mixing path length is proportional to the distance from the wall

$$l = ky,$$

where $k$ is an empirical constant ($k$ = 0.392).

In order to establish a relationship between the temperature and the velocity, the energy equation (with the respective boundary conditions) is written in terms of Crocco variables and is integrated for condition (2).

As a result we obtain

$$T = T_w + (T_r - T_w)\bar{u} - r_* \alpha_\delta^2 \bar{u}^2, \tag{4}$$

where

$$\bar{T} = \frac{T}{T_0}; \quad \bar{u} = \frac{u}{u_\delta}; \quad \alpha_\delta^2 = \frac{\frac{\varkappa - 1}{2} M_\delta^2}{1 + \frac{\varkappa - 1}{2} M_\delta^2};$$

$r_*$ is the temperature recovery coefficient ($r_*=0.88$); the subscript $w$ refers to the conditions on the wall, $\delta$ to the conditions on the outer boundary of the boundary layer, 0 to the stagnation in the outer flow, and $r$ to the conditions on the thermally insulated surface.

By using the phase equation and the condition of constant pressure in the boundary layer, we obtain an equation for the relationship between the density and velocity in the boundary layer:

$$\rho = \frac{\rho_w}{1 + 2Bu - A^2\bar{u}^2}, \tag{5}$$

where

$$2B = \frac{T_\delta}{T_w}\frac{1-(1-r_*)\alpha_\delta^2}{1-\alpha_\delta^2}; \quad A^2 = \frac{T_\delta}{T_w}\frac{r_*\alpha_\delta^2}{1-\alpha_\delta^2}.$$

By substituting (2), (3), and (5) in (1) and integrating across the boundary layer, we obtain the final equation for the velocity profile

$$\bar{u} = \frac{B}{A^2} - \frac{B-A^2}{A^2}\cos q + \frac{\sqrt{1+2B-A^2}}{A}\sin q, \tag{6}$$

where

$$q = \frac{A}{z}\ln\frac{\left(\sqrt{1-\bar{\delta}\,y}-1\right)\left(\sqrt{1-\bar{\delta}}+1\right)}{\left(\sqrt{1-\bar{\delta}\,y}+1\right)\left(\sqrt{1-\bar{\delta}}-1\right)};$$

$$\bar{\delta} = \frac{\delta}{r_w}; \quad \bar{y} = \frac{y}{\delta};$$

$$z = \frac{ku_\delta}{v_*}; \quad v_* = \sqrt{\frac{\tau_w}{\rho_w}}.$$

In order to derive the law of resistance, we introduce into our analysis the laminar sublayer. It is assumed that the thickness of the laminar sublayer depends on the frictional stress on the wall, on the values of the density and viscosity over the laminar layer thickness and on the radius of the channel cross section, i. e.,

$$\delta_L = \delta_L(\tau_w, \rho_{av}, \mu_{av}, r_w).$$

Then, on the basis of the II theorem of the theory of dimensionality, we obtain

$$\frac{\delta_L\sqrt{\tau_w\rho_{av}}}{\mu_{av}} = \alpha(\eta_w),$$

where

$$\eta_w = \frac{r_w\sqrt{\tau_w/\rho_{av}}}{\mu_{av}/\rho_{av}}. \tag{7}$$

The value of the term $\sqrt{\rho_{av}}/\mu_{av}$ in equation (7) is determined as follows:

$$\frac{\sqrt{\rho_{av}}}{\mu_{av}} = \int_0^{\delta_L} \frac{r_w}{r} \frac{\sqrt{\rho}}{\mu} dy \Big/ \int_0^{\delta_L} \frac{r_w}{r} dy. \tag{8}$$

By using the Newton equation for the frictional stress $\tau = \mu \frac{\partial u}{\partial y}$ under condition (2), we obtain the following equation (valid within the laminar sublayer):

$$dy = \frac{r\mu}{r_w \tau_w} du.$$

By substituting the expression for $dy$ in (7) and (8), and by assuming that the viscosity coefficient $\mu \sim T^n$, we obtain equations for $\eta_w$ and $u_L$

$$\eta_w = \mathrm{Re}_r \frac{k^2 \alpha}{z^2} \frac{(1 + 2B\bar{u}_L - A^2\bar{u}_L^2)^{1-n}(1 + 2B - A^2)^{1+n}}{\bar{u}_L\left(1 + B\bar{u}_L - \frac{1}{3}A^2\bar{u}_L^2\right)}; \tag{9}$$

$$\bar{u}_L = \frac{B}{A^2} - \frac{1}{A^2}\left\{B\cos\left[A\frac{k\eta_w}{z}\ln\left(1 - \frac{\alpha}{\eta_w}\right)\right] - A\sin\left[A\frac{k\eta_w}{z}\ln\left(1 - \frac{\alpha}{\eta_w}\right)\right]\right\}, \tag{10}$$

where $\mathrm{Re}_r = u_1 r_1 \rho_1/\mu_1$; $n = 0.76$, and the subscript 1 refers to the values in the entry section of the channel.

The values of $\bar{u}_L$ and $\eta_w$ may be determined by simultaneous solution of equations (9) and (10). Because of the small thickness of the laminar sublayer with respect to the channel cross-section radius, we have $\frac{\alpha}{\eta_w} \ll 1$, and hence equation (10) may be greatly simplified yielding

$$\bar{u}_L = \frac{1}{A^2}\left[B - B\cos\left(A\frac{k\alpha}{z}\right) + A\sin\left(A\frac{k\alpha}{z}\right)\right]. \tag{11}$$

Equation (11) coincides with the equation for $\bar{u}_L$ in the case of a flat plate, and hence we shall assume below that $\alpha$ is constant and has a value of 12.5.

By equating expressions (10) and (6) for $y = \delta_L$, we derive the law of resistance, which may be presented in the following form:

$$\frac{\delta}{r_w} = \frac{4Ce^{\Phi}}{(1 + Ce^{\Phi})^2}, \tag{12}$$

where

$$C = \frac{1 - \sqrt{1 - \alpha/\eta_w}}{1 + \sqrt{1 - \alpha/\eta_w}}\left(1 - \frac{\alpha}{\eta_w}\right)^{k\eta_w}, \quad \Phi = \frac{z}{A}\arcsin\left[\frac{AB}{A^2 - B^2} \times \left(\sqrt{1 + 2B - A^2} - 1 + \frac{A^2}{B}\right)\right].$$

In the case of $M_1 = 0$ but $\frac{T_w}{T_\delta} \neq 1$ $\left(A^2 = 0.2B = \frac{T_\delta}{T_w} - 1\right)$, the preceding equations assume the forms:

$$\bar{u} = 1 + \frac{1}{z}\sqrt{1+2B}\,\ln\frac{z}{A}q + \frac{B}{2}\frac{1}{z^2}\ln\left(\frac{z}{A}q\right); \tag{6a}$$

$$\bar{u}_L = \frac{k\alpha}{z}\left(1 + \frac{B}{2}\frac{k\alpha}{z}\right); \tag{10a}$$

$$\tau_{lw} = \mathrm{Re}_r\,\frac{k^2\alpha}{z^2}\,\frac{(1+2B\bar{u}_L)^{1-n}(1+2B)^{1+n}}{\bar{u}_L(1+B\bar{u}_L)}; \tag{9a}$$

$$\frac{\delta}{r_w} = \frac{4Ce^{\Phi}}{(1+Ce^{\Phi})^2}; \tag{12a}$$

where

$$C = \frac{1-\sqrt{1-\alpha/\eta_w}}{1+\sqrt{1+\alpha/\eta_w}}\left(1-\frac{\alpha}{\eta_w}\right)^{k\eta_w};\quad \Phi = \frac{\sqrt{1+2B}-1}{B}.$$

In the case of $M_1 = 0$ and $T_w/T_\delta = 1$ $(A^2 = 0,\ B = 0)$, the above equations become even simpler:

$$\bar{u} = 1 + \frac{1}{z}\ln\left(\frac{z}{A}q\right); \tag{6b}$$

$$\eta_w = \frac{k}{z}\,\mathrm{Re}_r; \tag{9b}$$

$$\bar{u}_L = \frac{k\alpha}{z}; \tag{10b}$$

$$\frac{\delta}{r_w} = \frac{4Ce^{\Phi}}{(1+Ce^{\Phi})^2},$$

where

$$C = \frac{1-\sqrt{1-\alpha/\eta_w}}{1+\sqrt{1-\alpha/\eta_w}}. \tag{12b}$$

The impulse equation for a round expanding channel with zero pressure gradient has the form

$$\frac{\partial \vartheta^{**}}{dx} = r_w\frac{\tau_w}{\rho_\delta u_\delta^2} = (1+2B-A^2)\,r_w\frac{k^2}{z^2}$$

or

$$\frac{d}{dx}\left(\frac{\vartheta^{**}}{r_1^2}\right) = (1+2B-A^2)\,\frac{r_w}{r_1}\,\frac{k^2}{z^2}, \tag{13}$$

where

$$\vartheta^{**} = \int_0^\delta \bar{\rho}\bar{u}(1-\bar{u})(r_w - y)\,dy =$$

$$= (1+2B-A^2) r_w^2 \frac{\delta}{r} \int_0^1 \frac{\bar{u}(1-\bar{u})}{1+2B\bar{u}-A^2\bar{u}^2} \left(1-\frac{\delta}{r_w}\bar{y}\right) d\bar{y};$$

$$\bar{r}_w = \frac{r_w}{r_1}; \quad \bar{\rho} = \frac{\rho}{\rho_0}; \quad \bar{y} = \frac{y}{\delta}.$$

The physical meaning of $\vartheta^{**}$ is the momentum area. The value of may be calculated by using the flow rate equation. In the case of a round expanding channel with zero pressure gradient, the flow rate equation is

$$Q = \pi r_1^2 \rho_1 u_1 = \pi (r_w - \delta) \rho_\delta u_\delta + 2\pi \int_{r_w-\delta}^{r_w} \rho u r dr \tag{14}$$

or, in a dimensionless form

$$\bar{r}_w^2 = \frac{1}{1-2\dfrac{\vartheta^*}{r^2}}, \tag{15}$$

where

$$\vartheta^* = \int_0^\delta (1-\overline{\rho u})(r_w - y)\, dy = r_w^2 \frac{\delta}{r_w} \int_0^1 \sigma \left(1-\frac{\delta}{r_w}\bar{y}\right) d\bar{y},$$
$$\sigma = 1 - \frac{1+2B-A^2}{1+2B\bar{u}-A^2\bar{u}^2}\bar{u}. \tag{16}$$

In the expression above, $v^*$ is the displacement area.

Thus, the three unknowns $z$, $\bar{r}_w$, and $\vartheta^{**}/r_1^2$ can be determined for given values of the parameters $M_1$, $T_w/T_\delta$ and $\mathrm{Re}_r$ by using the differential equation (13) and equations (14), (15), and (16).

In equation (13), we may leave the value of $z$ as the unkown. A function $z = z(x/r_1)$ may be derived by substituting in equation (13) the values $\bar{r}_w(z)$ and $\frac{\vartheta^{**}}{r_1^2}(z)$ for given values of the parameters $M_1$, $T_w/T_\delta$ and $\mathrm{Re}_r$, and by integrating (taking into account the fact that at $x=0$ we have $z=z_0$). However, since the functions $r_w(z)$ and $\frac{\vartheta^{**}}{r_1^2}(z)$ are complicated and hence may be expressed only by graphs, and the determination of the derivative $\frac{d}{dz}\left(\frac{\vartheta^{**}}{r_1^2}\right)$ involves graphical differentiation, it is more convenient to use the value of $\frac{\vartheta^{**}}{r_1^2}$ as the independent variable.

By integrating (13) over $\vartheta^{**}/r_1^2$ (bearing in mind the condition that at $x=0$ $\frac{\vartheta^{**}}{r_1^2}=0$), we obtain

$$\frac{1}{1+2B-A^2} \int_0^{\frac{\vartheta^{**}}{r_1^2}} \frac{1}{\bar{r}_w} \frac{z^2}{k^2}\, d\left(\frac{\vartheta^{**}}{r_1^2}\right) = \frac{x}{r_1}. \tag{17}$$

From the values of $\frac{\vartheta^{**}}{r_1^2}\left(\frac{x}{r_1}\right)$ derived in this way, we may obtain the distribution of the remaining parameters along the channel axis, namely: $\frac{\delta}{r_w}\left(\frac{x}{r_1}\right)$ from equation (2), $\frac{\vartheta^{**}}{r_1^2}\left(\frac{x}{r_1}\right)$ from equation (16), and $\bar{r}_w\left(\frac{x}{r_1}\right)$ from equation (15).

It is possible to determine also the values of $\frac{\vartheta^*}{r_w^2} = \frac{1}{\bar{r}_w^2}\frac{\vartheta^*}{r_1^2}$, $\frac{\vartheta^{**}}{r_w^2} = \frac{1}{\bar{r}_w^2}\frac{\vartheta^{**}}{r_1^2}$, the local coefficient of friction

$$c_f = \frac{\tau_w}{\frac{1}{2}\rho_\delta u_\delta^2} = 2(1+2B-A^2)\frac{k^2}{z^2}, \tag{18}$$

and the local heat transfer coefficient

$$c_h = \frac{q_w}{\rho_\delta u_\delta c_p (T_r - T_w)} = \frac{c_f}{2s}, \tag{19}$$

where $s$ is the Reynolds analogy coefficient equal to /3/:

$$s = 0.858 - 0.058\bar{u}_\perp. \tag{20}$$

The determination of the Pitot loss coefficient is of great importance in the investigation of flows in channels. We shall derive below equations for the calculation of the Pitot loss coefficients for the flow of a viscous compressible gas in the entry sections of flat and axisymmetrical channels both with and without heat transfer, provided that the Prandtl number for turbulent mixing is other than unity.

Since the total head is substantially nonuniform across the channel, some averaging law must be used for the determination of the Pitot loss coefficient. As in the case of an incompressible fluid /1/, we shall average the total head on the basis of the mass flow rate.

In accordance with the above, we shall define the Pitot loss coefficient as the ratio of the total head differences between the entry and the given channel section (averaged on the basis of the mass flow rate) to the velocity head in the entry section

$$\xi = \frac{P_{01} - P_{02}}{Q\frac{1}{2}\rho_1 u_1^2}, \tag{21}$$

where

$$P_{01} = \pi r_1^2 \rho_1 u_1 p_{01}, \tag{22}$$

$$P_{02} = \pi(r_w - \delta)^2 \rho_\delta u_\delta p_{01} - 2\pi \int_{r_w-\delta}^{r_w} p_0 \rho u r dr. \tag{23}$$

By substituting (22) and (23) in (21) and using the flow rate equation we obtain the following expression for $\xi$:

$$\xi = \frac{\varkappa+1}{\varkappa} \frac{1}{\lambda_1^2 \rho(\lambda_1)} \frac{2\frac{\delta}{r_w}}{1+2\frac{\vartheta^*}{r_w^2}} \int_0^1 \left(1-\frac{p_0}{p_{01}}\right) \bar{\rho}\,\bar{u} \left(1-\frac{\delta}{r_w}\bar{y}\right) d\bar{y}. \tag{24}$$

On the basis of the above assumptions concerning the constancy of the static pressure across the boundary layer, and in the presence of an isoentropic flow core, the $p_0/p_{01}$ ratio may be presented as follows:

$$\frac{p_0}{p_{01}} = \left(\frac{T_\delta}{T}\frac{T_0}{T_{01}}\right)^{\frac{\varkappa}{\varkappa-1}}, \tag{25}$$

where

$$\frac{T_\delta}{T}\frac{T_0}{T_{01}} = 1-\frac{\varkappa-1}{\varkappa+1}\lambda_\delta^2(1-\bar{\rho}\,\bar{u}^2).$$

Using the above equation for $p_0/p_{01}$, we obtain the final equation for the calculation of $\xi$:

$$\xi = \frac{\varkappa+1}{\varkappa} \frac{1}{\lambda_1^2 \rho(\lambda_1)} \frac{2\delta/r_w}{1-2\vartheta^*/r_w^2} \int_0^1 \left\{1- \right.$$
$$\left. -\left[1-\frac{\varkappa-1}{\varkappa+1}\lambda_\delta^2(1-\bar{\rho}\,\bar{u}^2)\right]^{\frac{\varkappa}{\varkappa-1}}\right\} \bar{\rho}\,\bar{u}\left(1-\frac{\delta}{r_w}\bar{y}\right) d\bar{y}. \tag{26}$$

In some cases, equation (26) may be somewhat simplified. For instance, at subsonic velocities in the presence of heat transfer, it assumes the form

$$\xi = \frac{1}{\rho(\lambda_1)} \frac{2\delta/r_w}{1-2\vartheta^*/r_w^2} \int_0^1 \bar{\rho}\,\bar{u}\,(1-\rho u^2)\left(1-\frac{\delta}{r_w}\bar{y}\right) d\bar{y} \tag{27}$$

Equation (27) may be simplified even further in the case of $M=0$. In this case:

$$\xi = \frac{2\delta/r_w}{1-2\vartheta^*/r_w^2} \int_0^1 \bar{\rho}\,\bar{u}(1-\bar{\rho}\,\bar{u}^2)\left(1-\frac{\delta}{r_w}\bar{y}\right) d\bar{y}. \tag{28}$$

Equation (26) is greatly simplified also in the absence of heat transfer, assuming that $\mathrm{Pr} = \mathrm{Pr}_t = 1$ (when $T_0 = T_{01}$). For subsonic velocities it assumes the form

$$\xi = \frac{1}{\rho(\lambda_1)} \frac{2\vartheta^{***}/r_w^2}{1-2\vartheta^*/r_w^2}, \tag{29}$$

where $\vartheta^{***} = \int_0^1 \bar{\rho}\,\bar{u}(1-\bar{u}_2)(r_w-y)\,dy$ is the energy loss area.

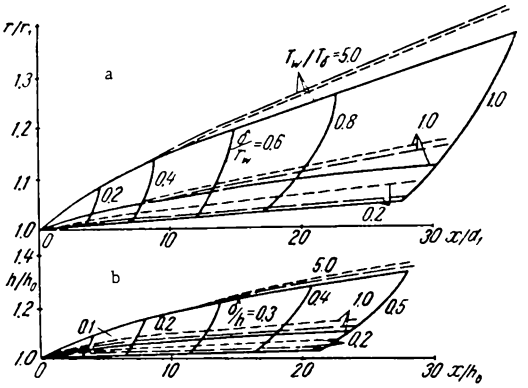


FIGURE 1. Changes in $r_w/r_1$ along the axis.

a — axisymmetrical expanding channel with a zero pressure gradient at $Re_r = 10^5$ and Mach numbers 0; 0.5; and 1.0: ——— 0; — — — 0.5; - - - - - 1.0; b — flat channel at $Re_h = 10^5$ and the same Mach numbers.

In the case of an incompressible fluid, equation (29) assumes an even simpler form /1/

$$\xi = \frac{2\vartheta^{***}/r_w^2}{1-2\vartheta^{*}/r_w^2}. \qquad (30)$$

The above equations were used to calculate the characteristics of an axisymmetrical expanding channel with zero pressure gradient, for the following values of the flow parameters: $M_1 = 0$; 0.5; 1.0; $T_w/T_\delta = 0.2$; 1.0; 5.0; and $Re_r = 10^5$. The results are tabulated in Tables 1-5. In all cases $d_1 = 2r_1$.

In analyzing the calculation results, we notice that for the above values of $Re_r$ and the temperature factor $T_w/T_\delta$, all characteristics except the Pitot loss coefficient $\xi$ are virtually independent of the value of M (within the range of Mach numbers studied), but are strongly affected by the temperature factor $T_w/T_\delta$. Within the above range of Mach numbers, the value of $\xi$ changes as a function of M according to the $\rho(\lambda_1)$ law. Thus, the value of $\xi/\rho(\lambda_1)$ is also virtually independent of the Mach number (see Figure 5).

Check calculations made by us show that the effect of the Mach number and the temperature factor also remain the same at other values of $Re_r$.

The above result enables us to suggest a method for the determination of the various characteristics of a round expanding channel, within the above range of Mach numbers and at different values of the temperature factor.

For given values of $Re_r$ and the relative distance from the channel inlet $x/r_1$, we determine the respective characteristics for an incompressible fluid using the graphs from /1/. From there we take the values of $\delta/r_w$ (the lines showing the values of $\delta_{r_w}$ are plotted on all the graphs).

Since for the above values of $Re_r$ and the temperature factor $T_w/T_\delta$ the curves showing $\delta/r_w$ as a function of $x/r_1$ are virtually independent of the

Mach number (in other words, the maximum length of the entry section $(x/r_1)_{max}$ is independent of M at the given $Re_r$ and $T_w/T_\delta$), the effect of the temperature factor on the respective characteristics could be determined with great accuracy by linear interpolation between the values of the said characteristics for various values of $T_w/T_\delta$ along the line $\delta/r_w$ = const.

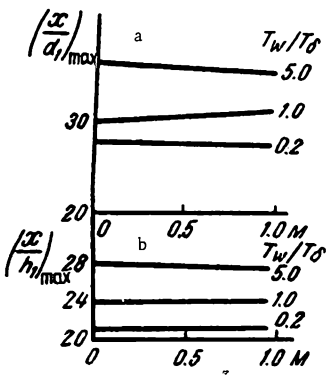


FIGURE 2. Calculation of the entry section length for:

a — an axisymmetrical channel at $T_w/T_\delta$ $Re_r = 10^5$ and a temperature factor of 5.0, 1.0, 0.2; b — flat channel at $Re_h = 10^5$ and the same values of $T_w/T_\delta$

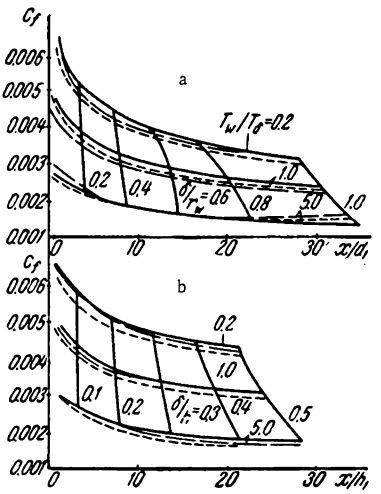


FIGURE 3. Changes in the local friction resistance coefficient along the axis.

a — axisymmetrical channel at $Re_r = 10^5$ and temperature factor $T_w/T_\delta$ values of 0.2, 1.0, and 5.0; b — flat channel at $Re_h = 10^5$ and the same values of $T_w/T_\delta$.

The velocity and temperature profiles, as well as other boundary layer characteristics of a nonisothermal flow of a viscous compressible gas in the entry section of a flat expanding channel with zero pressure gradient may be calculated using the equation derived by finite transition of the respective equations for the axisymmetrical case at $r_w \to \infty$.

The equations thus derived for a flat expanding channel were also used for the calculation of the characteristics of such a channel.

It is of interest to mention that also in the case of a flat channel, all characteristics except $\xi$ are practically independent of the Mach number (within the Mach range studied) but are strongly affected by the temperature factor. Also, within the Mach range studied, the value of $\xi$ changes with M according to the $\rho(\lambda_1)$ law, i.e., $\xi/\rho(\lambda_1)$ is virtually independent of the Mach number (see Figure 5).

On the basis of the above statements, we can suggest a method for the determination of the characteristics of a flat expanding channel for different values of the temperature factor; the method is analogous to the one outlined for the case of an axisymmetrical expanding channel.

The above results for axisymmetrical and flat expanding channels with zero pressure gradient make it possible to determine also the

characteristics of annular expanding channels with zero pressure gradient (except for the entry section length, which is determined on the basis of the condition that the combined thickness of the boundary layers on the convex and concave surfaces must equal its doubled hydraulic radius $h=r_1-r_2$).

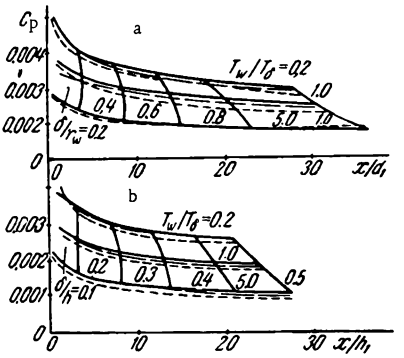


FIGURE 4. Changes in the local heat transfer coefficient along the axis.

a — axisymmetrical channel at $Re_r = 10^5$ and temperature factor $T_w/T_\delta = 0.2, 1.0, 5.0$; b — flat channel at $Re_h = 10^5$ and the same values of $T_w/T_\delta$.

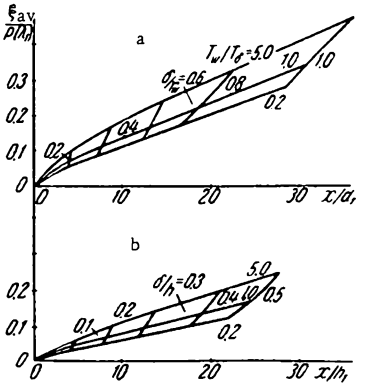


FIGURE 5. Changes in $\xi/\rho(\lambda_1)$ along the axis.

a — axisymmetrical channel at $Re_r = 10^5$ and temperature factor $T_w/T_\delta = 0.2, 1.0, 5.0$; b — flat channel at the same values of $T_w/T_\delta$.

If the doubled hydraulic radius is taken as the characteristic linear dimension of the annular channel, this would be equal to the radius $r_w$ in the case of a round channel, and to the channel height $h$ in the case of a flat channel. Curves for the function $\xi=\zeta\left(\frac{x}{h}\right)$ at $Re_h = 10^5$ are shown in Figure 6 for axisymmetrical and flat channels.

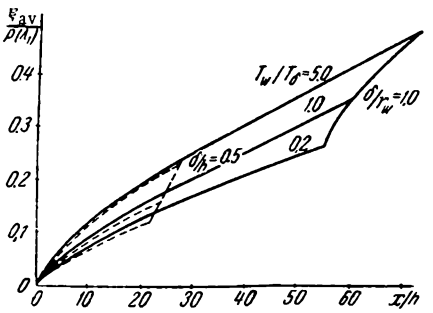


FIGURE 6. Plots of $\frac{\xi}{\rho(\lambda_1)}$ against $\left(\frac{x}{h}\right)$ for axisymmetrical and flat channels at $Re_h = 10^5$.

As is evident from the figure, the curves for the round and flat channels lie close to each other. A similar agreement is also observed for the other channel characteristics.

However, it should be noted that the problem of a slightly expanding annular channel with zero pressure gradient is not unambiguous, since the cross section may be expanded either by increasing the radius of the outer concave surface, by reducing the radius of the inner convex surface, or by the combined effect of both the above factors.

Bibliography

1. Solodkin, E.E. and A.S. Ginevskii. Turbulentnoe techenie vyazkoi zhidkosti v nachal'nykh uchastkakh osesimmetrichnykh i ploskikh kanalov (Turbulent Flow of a Viscous Fluid in the Entry Sections of Axisymmetrical and Flat Channels). — Trudy TsAGI, No. 701. 1957.
2. Ginevskii, A.S. and E.E. Solodkin. Aerodinamicheskie kharakteristiki nachal'nogo uchastka truby kol'tsevogo secheniya pri turbulentnom techenii v pogranichnom sloe (Aerodynamic Characteristics of the Entry Section in Annular Tubes During Turbulent Flow in the Boundary Layer). — Promyshlennaya Aerodinamika, Oborongiz, No. 12. 1959.
3. Ginevskii, A.S. and E.E. Solodkin. Vliyanie poperechnoi krivizny poverkhnosti na kharakteristiki neizotermicheskogo osesimmetrichnogo turbulentnogo pogranichnogo sloya szhimaemogo gaza (Effect of Lateral Surface Curvature on the Characteristics of a Nonisothermal Axisymmetrical Turbulent Boundary Layer of Compressible Gas). — Izv. AN SSSR, OTN. Mekhanika i Mashinostroenie, No. 1. 1963.

Moscow

P.N. Romanenko and N.V. Krylova

# EFFECT OF THE ENTRY CONDITIONS ON THE HEAT TRANSFER IN THE ENTRY SECTION OF A TUBE WITH TURBULENT AIR FLOW

The knowledge of averaged (over the surface) values of the heat transfer coefficient alone is insufficient for the effective use of heat transfer surfaces for the determination of the maximum temperature points, and for solving the problem of the reliability of heat transfer equipment with relatively short tubes; all these require the availability of data on the distribution of local heat transfer coefficients over the surface.

In the case of a laminar boundary layer in the entry section of a tube, the heat transfer problem may be solved by known analytical methods. The extremely complex nature of the mechanism of turbulent flow makes it impossible to obtain reliable heat transfer data on the basis of a theoretical analysis in the case of a turbulent boundary layer.

Local values of the heat transfer coefficient in the entry section of a tube are determined by the development of the thermal and dynamic boundary layers. For given values of the flow parameters at the inlet of the tube, the development of the boundary layers in the entry section depends on the boundary conditions on the tube wall and on the outer boundary of the boundary layer. The conditions on the wall are determined by the law of wall temperature changes and by the heat load distribution. The conditions on the outer boundary of the boundary layer depend mainly on the pattern of change of the potential flow velocity over the longitudinal coordinate, which is determined by the boundary conditions on the wall and by the intensity of the heat load.

In many cases, the flow at the tube inlet is either disturbed by the inlet edge of the tube, or else it has a definite velocity profile, this depending on the conditions at the tube inlet. These peculiarities in the development of the heat transfer process at the entry section of a tube give rise to the difficulties encountered in attempting to derive general rules for local heat transfer coefficients. The dimensionless equations derived through generalization of experimental data by the conventional methods of the theory of similarity have limited application, since for flow similarity in the entry section, it is necessary to have both similar boundary conditions at the tube inlet and similar values of an additional dimensionless number characterizing the heat flux intensity. The need to account for the simultaneous effect of several dimensionless numbers on the heat transfer causes technical difficulties in the dimensionless processing of experimental data for the entry section. In some cases, adequate selection of exponents for the dimensionless similarity numbers makes it possible to group the experimental data around a single curve. However, it is never certain

whether the effect of each separate number has been accounted for, and whether mutual compensation of the effects of several dimensionless numbers has been eliminated.

Experimental studies of the effect of entry conditions on the heat transfer in the entry section of a tube, with generalization of the experimental data in the form of dimensionless equations, have been carried out in /1-3/. The authors of the above papers have discussed the heat transfer and friction in the flow of a heated fluid in a straight tube with a smooth, tapered-edge inlet, as well as with a smooth deflection at an angle of 90° /1/; experimental data are provided on the heat transfer in the entry section of a tube with smooth inlet, sharp edge, and a hydrodynamic stabilization section, in the case of turbulent water flow /2/; the investigation of the heat transfer in the entry section of a tube with air flow and under two inlet conditions (contraction, and a preliminary hydraulic stabilization section) is described /3/. The measured data for the contraction inlet were insufficient for the establishment of any general laws.

All the above papers are characterized by a common flaw, namely, the narrow range of values of the Reynolds number ($Re_D \leqslant 6 \cdot 10^4$) encompassed by the experiments. Developed turbulent flow in the entry section could hardly be expected at low $Re_D$. The authors of /2/ note that in the entry section of a tube with smooth inlet, a laminar boundary layer was observed at $Re_D$ values up to $5 \cdot 10^4$. Transitional flow conditions were observed simultaneously with the laminar flow. Because of the difficulties in the dimensionless processing of experimental data by the conventional methods of the theory of similarity, the authors of the above papers were unable to derive general laws taking into account the effect of the entry condition on the heat transfer in the entry section. Some data on the above problem may be found in /4-7/. Our investigation was based on the fact that virtually no studies have been made on the effect of entry conditions on the heat transfer in the entry section, while the available dimensionless equations generalizing the experimental data for separate entry conditions are very scarce. The investigation procedure was based on the theory of local modeling, the basic principles of which have been established by Ievlev /9, 10/, and developed by Leont'ev /11, 12/. According to the above theory, the heat transfer and friction coefficients may be determined from the integral equations for motion and energy, provided that the generalization of the experimental data has established the general laws for the friction and heat transfer in the turbulent boundary layer. The general laws for heat transfer and friction in the boundary layer are described by empirical equations showing the relationship between the local values of the friction coefficient and the Reynolds number for the momentum thickness $Re_\varphi$ on the one hand, and the heat transfer coefficient and Reynolds number for the energy loss thickness $Re_\varphi$ on the other hand. At supersonic flow velocities, in the case of fluid flow under injection or evacuation of the mass, and in the presence of other disturbing factors, the friction and heat transfer equations comprise additional terms accounting for the effect of these factors on the friction and heat transfer.

The integral energy equation for the boundary layer may be written as

$$\frac{d\,\mathrm{Re}_\varphi}{d\bar{x}} + \frac{\mathrm{Re}_\varphi}{T_e - T_w}\,\frac{d(T_e - T_w)}{d\bar{x}} = \mathrm{St}\,\mathrm{Re}_D; \qquad (1)$$

$$\mathrm{Re}_{\varphi} = \frac{u_1 \varphi}{\nu_1} ; \quad \frac{\varphi}{R} = \int_0^1 \frac{\rho u}{\rho_1 u_1} \frac{T_1 - T}{T_1 - T_w} \frac{r}{R} \, d\left(\frac{r}{R}\right) ; \tag{2}$$

$$\mathrm{Re}_D = \frac{u_1 D}{\nu_1} ; \quad \bar{x} = \frac{x}{D} ; \quad \mathrm{St} = \frac{q_w}{\rho_1 u_1 c_{p_1} (T_e - T_w)} . \tag{3}$$

Equation (1) yields the following equation for the determination of the Reynolds number for the range of subsonic gas-flow velocities:

$$\mathrm{Re}_{\varphi} = \frac{\int_0^x q_w \, dx}{\mu_1 c_{p_1} (T_e - T_w)} . \tag{4}$$

Within the entry section of the tube, the temperature in the potential-flow core remains constant and is equal to the temperature of the fluid at the tube inlet. Hence, the measured heat fluxes on the walls $q_w$ may be used to calculate the values of $\mathrm{Re}_{\varphi}$ at any control cross section of the entry section, and from there to determine the distribution of $\mathrm{Re}_{\varphi}$ over the entry section length. In addition to the heat flux, it is necessary to determine the wall temperature. The gas parameters within the flow core (which must be known in order to calculate the local St numbers) may be determined by using gas-dynamics functions, and the data obtained in measuring the flow braking parameters and the static pressure distribution over the tube length.

The experimental setup used to study the effect of entry conditions on the heat transfer in the entry section of the tube consisted of an aerodynamic tube (for intermittent action) with detachable nozzles and experimental sections. The setup comprised, in addition, an air compressor (2R-4/220) with an output of 0.5 $nm^3$/sec, a receiver with 120 oxygen cylinders of the A-40 type, a 300 kw electric heater, an ejector, an oil separator, filters for the removal of oil and dust from the air, and measuring instruments. An 1100 kg reserve of air could be accumulated using the receiver, and thus, at a flow rate of 0.5 kg/sec the experimental time was about 35 min.

The experimental section was made of a copper tube 15 m long and 0.047/0.05 m in diameter. The experimental section was surrounded by a jacket, and cooling water from a pressure vessel was passed through the space between the tube wall and this jacket. The jacket was divided into 15 compartments over the section length with independent coolant supply to each compartment. The flow rate of water through the section was constant. The heating of the water in the compartments was measured with differential thermocouples.

The following parameters were measured during the experiment: the distribution of the static pressure and the wall temperature over the tube length, the flow rate of the cooling water and the temperature gradient between the water in each compartment, the airstream braking parameters at the entry of the working section, the temperature and dynamic head distribution in the potential flow core, and in the boundary layer, the pressure drop in the measuring diaphragm. The dynamic head was measured using pneumometric microtubes connected to differential manometers filled with ethanol or mercury. The static pressure was measured with extraction tubes, which were introduced into the experimental tube through the wall. In those compartments in which we measured the dynamic head distribution, the extraction tubes were placed on the planes of the Pitot tube tips. The other ends of the static-pressure

measuring tubes were connected to differential manometers, which had their second tubes open to the atmosphere. The barometric pressure was measured with aneroid barometers.

The stream temperature in the control cross sections of the experimental section was measured with movable chromel-alumel thermocouples which (like the Pitot tubes) were positioned within the stream by means of a coordinating device. The construction of the experimental setup and the working section have been described in more detail in /13, 14/.

On the basis of the measured static pressure, wall temperature, and temperature increase of the cooling water in the compartments, we plotted graphs for the changes in the static pressure $p$, the wall temperature $T_w$, and the temperature of the coolant in the compartments over the tube length. The graphs were then used to calculate the local values of the heat flux $q_w$, the St number, and the $Re_\varphi$ number. The thermodynamic air temperature was calculated using aerodynamic functions, with the aid of the equation

$$T = \frac{T_{meas}}{1 + \dfrac{0.04055\lambda^2 r}{c_p(1 - 0.1667\lambda^2)}}, \qquad (5)$$

where $r$ is the temperature recovery coefficient (its value was assumed to be 0.88), and $\lambda$ is the velocity coefficient.

The heat flux on the wall $q_w$ was determined from the heat balance for the cooling water in each compartment

$$q_w = \frac{c_p G \Delta t}{F}, \qquad (6)$$

where $G$ is the flow rate of the cooling water, kg/hr; $\Delta t$ is the increase in the water temperature, deg; $F$ is the heat-transfer area, $m^2$; and $c_p$ is the isobaric heat capacity of the water at its mean temperature in the section, j/kg deg.

We carried out 80 experiments and processed the data obtained in 56 of them. The experiments were carried out with entry elements of the following types: nozzle section with tapers of 30, 45, and 60°; sudden contraction (sharp edge) at $D_{inlet}/D = 4.3$ (where $D_{inlet}$ and $D$ are the inner diameters of the tube before the section and in the working section); smooth entry; preliminary hydrodynamic stabilization section with a length of 40 diameters; sudden expansion with $D_{inlet}/D = 0.5$. The experiments extended over a $Re_\varphi$ range of from $5 \cdot 10^4$ to $8.7 \cdot 10^5$ with air temperatures from 470 to 650°K. The flow velocity of the air at the entry to the working section ranged from 30 to 300 m/sec, and the wall temperature in the different experiments ranged from 300 to 335°K. A constant wall temperature was maintained throughout each experiment corresponding to a given set of conditions.

The experimental section was heated before the start of the experiment. It was assumed that steady-state conditions had been established when the fluctuations in the flow stagnation temperature did not exceed ±0.5°.

The experimental data for the different entry condition to the tube were processed in terms of the St number as a function of $Re_\varphi$. The values of these numbers were determined by means of equations (3) and (4), after the determination of the heat flux $q_w$ from equation (6).

The results obtained in the processing of the experimental data are shown in Figure 1, on which there are straight lines approximating the positions of the experimental points. The points lie round the respective lines with a dispersion of ±10%.

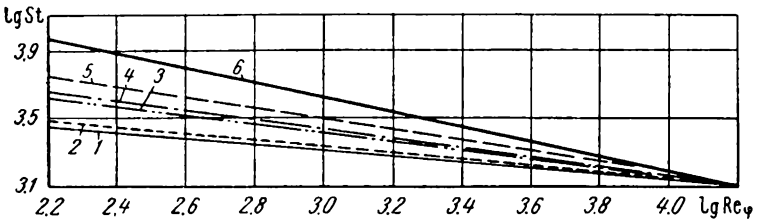


FIGURE 1. Dependence of the local Stanton number (St) on the local Reynolds number ($Re_\varphi$).

1 — smooth entry; 2 — preliminary hydrodynamic stabilization section; 3, 4, 5 — nozzle entry sections with tapers of 30, 45, and 60°, respectively; 6 — sharp edge.

Figure 1 shows that the smooth entry affects the heat transfer least. The heat transfer pattern in the entry section of the tube with preliminary hydrodynamic stabilization section is almost identical with the heat transfer pattern in the case of a smooth entry, i. e., in the case of simultaneous growth of the thermal and dynamic boundary layers. Evidently, this could be attributed to the high degree of filling of the velocity and temperature profiles in the last case.

The contraction angle of contracted entry sections also affects the heat transfer in the entry section of the tube. The heat transfer increases with increasing taper, and reaches a maximum in the case of a sharp edge. As the taper is reduced, the heat transfer rate approaches that in the case of a smooth entry. Approximate equations describing the heat transfer in the cases shown in Figure 1 are presented below.

In the case of a smooth entry $St = 0.009\ Re_\varphi^{-0.2}$; in the presence of a hydrodynamic stabilization section $St = 0.01\ Re_\varphi^{-0.21}$.

In the case of a nozzle entry with a taper $\alpha = 30°$, $St = 0.0153\ Re_\varphi^{-0.263}$; $\alpha = 45°$, $St = 0.0198\ Re_\varphi^{-0.285}$; $\alpha = 60°$, $St = 0.0252\ Re_\varphi^{-0.306}$. In the case of a sudden contraction (sharp edge) $\alpha = 180°$, $St = 0.116\ Re_\varphi^{-0.479}$.

The data in Figure 1 show also that at Reynolds numbers of the order of $Re_{\varphi_1} \approx 10^4$, the curves showing St as a function of $Re_\varphi$ for any entry condition coincide with the respective curve for a smooth entry. In view of the above experimental observation, the effect of the taper (in the nozzle entry) on the heat transfer in the entry section of the tube could be described by the equation

$$St = St' \frac{Re_{\varphi_1}^m}{Re_\varphi^m}, \qquad (7)$$

where St′ and $Re_{\varphi_1}$ are the Stanton and Reynolds numbers for which the curves $St = f(Re_\varphi)$ for the different entry conditions intersect with the respective curve for a smooth entry.

The dependence of $m$ on the taper $\alpha$ is shown in Figure 2. It is evident that the experimental points lie on a straight line described by the equation

$$m = 0.22 + 0.00144\alpha. \tag{8}$$

In experiments with a sudden expansion of the flow at the entry to the tube, there was a certain decrease in the heat flux near the entry cross section, but an increase in the heat transfer rate was observed afterward. This may be attributed to the fact that an eddying zone with a small, low-velocity reverse flow of air is created in the immediate vicinity of the entry to the tube in the case of a sudden expansion of the flow. The problem of heat transfer calculations for the region where macroscopic eddies prevail should be the subject of a separate study.

Using equations (7) and (8), it is possible to determine the length of the thermal stabilization section, i.e., the distance between the entry cross section and the cross section at which the thermal boundary layer reaches the axis of the tube. The values of $Re_{\varphi}$ at the end of the entry section, calculated from the flow conditions for thermal stabilization and from the steady-state flow, must coincide.

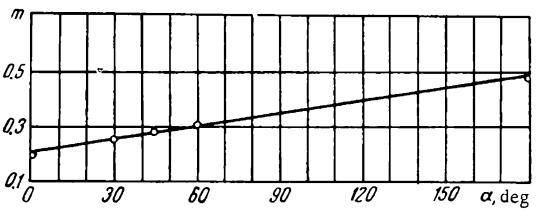


FIGURE 2. Dependence of the exponent of the Reynolds number for the energy loss thickness (in the case of heat transfer in the entry section of a tube) on the taper of the nozzle entry.

The empirical equations describing the relationship between St and $Re_{\varphi}$ for different entry conditions (of the flow into the tube) and the integral energy equation for the boundary layer may be used to derive a calculation method for the heat transfer in the entry section. In view of the fact that the changes in the potential flow velocity over the longitudinal coordinate are unknown (for the internal problem), it is necessary to use an additional equation for the total flow rate of the gas in the tube cross sections. This means that the calculations of the thermal boundary layer should be made in conjunction with calculations of the dynamic boundary layer.

We write the continuity equation in the following form:

$$G = \int_0^R 2\pi r \rho u dr \tag{9}$$

or

$$\rho_1 u_1 = \rho u \left(1 - 2\frac{\delta^*}{R}\right). \tag{10}$$

where $u_1$ and $\rho_1$ are the velocity and density of the flow at the tube entry;

$\delta^* = \int_0^{\delta} \left(1 - \frac{\rho u}{\rho_1 u_1}\right)\left(1 - \frac{y}{R}\right) dy$ is the dynamic displacement thickness.

It has been shown /11/ that at subsonic flow velocities, the continuity equation may be presented in the following form:

$$\mathrm{Re}_D = \mathrm{Re}_{D_1} + 5.2\,\bar{T}_w\,\mathrm{Re}_\varphi, \tag{11}$$

where

$$\mathrm{Re}_{D_1} = \frac{u_1 D_1}{\nu}; \quad \bar{T}_w = \frac{T_w}{T_1}.$$

Equation (11) describes the relationship between the thermal and geometric effects in the entry section of the tube.

The calculation of the heat transfer in the entry section of the tube is thus reduced to the solution of the system of three equations (1), (7), and (11). Taking into account equations (7) and (11), equation (1) takes another form:

$$\frac{d\,\mathrm{Re}_\varphi}{d\bar{x}} + \mathrm{Re}_\varphi \frac{d(T_e - T_w)}{(T_e - T_w)\,d\bar{x}} = (\mathrm{Re}_{D_1} + 5.2\,\bar{T}_w\,\mathrm{Re}_\varphi)\,\mathrm{St}'\,\frac{\mathrm{Re}_{\varphi_1}^m}{\mathrm{Re}_\varphi^m}. \tag{12}$$

When the temperature factor $\bar{T}_w$ remains constant over the tube length, we obtain

$$\frac{\mathrm{Re}_\varphi^m\,d\,\mathrm{Re}_\varphi}{\mathrm{St}'\,\mathrm{Re}_{\varphi_1}^m(\mathrm{Re}_{D_1} + 5.2\bar{T}_w\,\mathrm{Re}_\varphi)} = d\bar{x}. \tag{13}$$

Integration of equation (13) yields

$$\bar{x} = \frac{1}{\mathrm{St}'\,\mathrm{Re}_{\varphi_1}^m} \int_0^{\mathrm{Re}_\varphi} \frac{\mathrm{Re}_\varphi^m\,d\,\mathrm{Re}_\varphi}{\mathrm{Re}_{D_1} + 5.2\,\bar{T}_w\,\mathrm{Re}_\varphi}. \tag{14}$$

An expression for the integral in equation (14) for the case of a smooth entry of the gas into the tube has been given in the literature /11/.

Using equation (14), it is possible to calculate the changes in the local values of $\mathrm{Re}_\varphi$ over the length of the entry section of the tube. From these values of $\mathrm{Re}_\varphi$, it is possible to calculate the respective values of the Stanton number, by using equation (7).

The general solution of the energy equation (1) may be presented as a series.

Taking into account equations (7) and (11), we can write equation (1) in the following form:

$$\frac{d\,\mathrm{Re}_\varphi}{d\bar{x}} = A\,\mathrm{Re}_\varphi^{-m} + B\,\mathrm{Re}_\varphi^{1-m}, \tag{15}$$

where

$$A = \mathrm{St}'\mathrm{Re}_{\varphi_1}^m\,\mathrm{Re}_{D_1}; \quad B = 5.2\bar{T}_w\,\mathrm{St}_1\mathrm{Re}_{\varphi_1}^m.$$

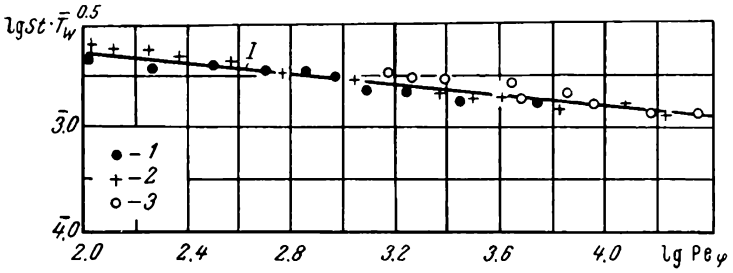


FIGURE 3. Dependence of St $\bar{T}_w^{0.5}$ on Re$_\varphi$ for the entry section of the tube.

1 and 2 — data of the authors for a nozzle entry with $\alpha = 60°$ and for a sharp edge; 3 — data of Lel'chuk and Dedyakin /5/; I — heat transfer law for a turbulent boundary layer /12/.

From equation (15) we obtain

$$\bar{x} = \int_0^{\mathrm{Re}_\varphi} \frac{\mathrm{Re}_\varphi^m d\,\mathrm{Re}_\varphi}{A + B\,\mathrm{Re}_\varphi} . \tag{16}$$

The integral in equation (16) is expressed by the series

$$\int_0^{\mathrm{Re}_\varphi} \frac{\mathrm{Re}_\varphi^m d\,\mathrm{Re}_\varphi}{A + B\,\mathrm{Re}_\varphi} = \frac{1}{A}\sum_{i=0}^{\infty}\int_0^{\mathrm{Re}_\varphi} (-1)^i \left(\frac{B}{A}\right)^i \mathrm{Re}_\varphi^{i+m} d\mathrm{Re}_\varphi = \frac{1}{A}\sum_{i=0}^{\infty} (-1)^i \left(\frac{B}{A}\right)^i \frac{\mathrm{Re}_\varphi^{i+m+1}}{i+m+1} . \tag{17}$$

The series (17) converges rapidly at $\mathrm{Re}_\varphi < \frac{A}{B}$.

Our experimental data on the heat transfer in the entry section of a tube (for various entry conditions) are compared in Figure 3 with the experimental data of /5/ and the theoretical curve of /12/; a satisfactory agreement is observed.

## Conclusions

1) New experimental data have been collected on the effect of the entry conditions on the heat transfer in the entry section of a cooled tube during turbulent flow of hot air.

2) Generalization of the experimental data on the basis of the local modeling theory makes it possible to suggest a method for the calculation of the local heat transfer coefficients in the entry section, taking into account the entry conditions.

3) The data required for heat transfer calculations by the above method have been collected.

4) Our experimental data are in good agreement with the data of other investigators.

Bibliography


1. Gutarev, V.V. Candidate's Thesis, MIKhM. 1954.
2. Filimonov, S.S. and B.A. Khrustalev. Teplo- i massoperenos (Heat and Mass Transfer) Vol. 3. — Moskva-Leningrad, Gosenergoizdat. 1963.
3. Rubinshtein, Ya.M. Issledovanie protsessov obratnogo okhlazhdeniya (Investigation of Reverse Cooling Processes). — GONTI. 1938.
4. Alad'ev, I.I. Candidate's Thesis; ENIIN, AN SSSR. 1949.
5. Dedyakin, B.V. and V.L. Lel'chuk. Voprosy teploobmena (Problems of Heat Transfer). — Izd. AN SSSR. 1959.
6. Mikheev, M.A. Konvektivnyi i luchistyi teploobmen (Convective and Radiant Heat Transfer). — Izd. AN SSSR. 1959.
7. Petukhov, B.S. and V.V. Kirillov. — Teploenergetika, No. 5. 1960.
8. Kutateladze, S.S. and A.I. Leont'ev. Turbulentnyi pogranichnyi sloi szhimaemogo gaza (Turbulent Boundary Layer of a Compressible Gas). — Izd. Sib. Otd. AN SSSR. 1962.
9. Ievlev, V.M. — DAN SSSR, Vol. 86, No. 1. 1952.
10. Ievlev, V.M. — DAN SSSR, Vol. 87, No. 6. 1952.
11. Leont'ev, A.I. and V.K. Fedorov. — IFZh, No. 8. 1961.
12. Kosterin, S.I., A.I. Leont'ev, and V.K. Fedorov. — Teploenergetika, No. 5. 1962.
13. Romanenko, P.N. and A.I. Leont'ev. — Trudy MIIT, No. 139. 1961.
14. Krylova, N.V. Tezisy dokladov nauchno-tekhnicheskoi konferentsii (Abstracts of Reports presented at the Scientific Technological Conference). — MLTI. 1963.


Moscow

## *IV. STUDIES OF THE INTENSIFICATION OF CONVECTIVE HEAT TRANSFER PROCESSES*

A. V. Ivanova

### INTENSIFICATION OF THE HEAT TRANSFER IN AN AIR-COOLED ROUND TUBE

The simplest and most effective method of increasing the heat transfer rate is by increasing the velocity of the stream in contact with the convective heating surface. In small-diameter tubes, such an increase in velocity may be achieved by imparting a spiral movement to the stream.

In the investigation reported here, the stream was swirled by means of blade swirlers, which were mounted directly at the inlet to the tube. Since an increase in the heat transfer rate requires power not only for the pumping of the heat transfer medium through the tube but also for overcoming the resistance of the swirlers, we determined the most advantageous profile and number of blades for each given swirling angle.*

In this paper, we present the results of experiments using four swirlers, with angles $\psi$ = 20, 35, 65, and 75°.

The experimental setup used in the investigations is shown in Figure 1.

The main part in the setup was a steel (1Kh18N9T) tube with a constant heat supply over its length (this was accomplished by changing the external diameter while the internal diameter remained constant). The tube was heated by passing an alternating current from a low-voltage power transformer (OSU-80/05).

Heat outflow at the ends and heat losses to the surrounding medium were eliminated by using inlet and outlet sleeves of a special design, and a compensating thermal jacket surrounding the tube. Hence, all the heat evolved from the tube was transferred to the air flowing within the tube. In nearly all experiments, losses not accounted for did not exceed 1%.

The tube wall temperature was measured with chromel-alumel thermocouples ($d$ = 0.5 mm) with the aid of a PP-type potentiometer. The inlet and outlet air temperatures were taken as the average of five measurements made with thermocouples fitted in the inlet and outlet sleeves respectively. The emf was measured with a PPTV-1 potentiometer.

The static pressure was measured with a standard manometer, while the pressure drop over the tube length was measured with a differential manometer filled with tetrabromoethane or mercury.

All experiments were carried out under the same conditions: air temperature at the inlet $t_{in} \approx 283\text{-}293$°K and temperature of the inner tube surface $t_{c_{max}} = 973$°K.

* The swirlers were computed and designed by V. F. Naryshkin and A. D. Goflin, assistants at the TsKTI Laboratory of Turbine Compressors.

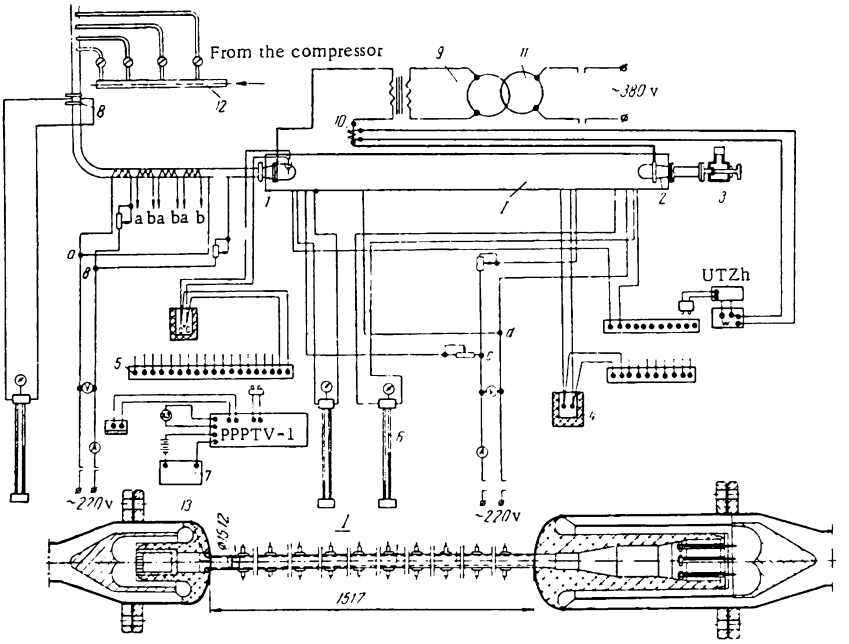


FIGURE 1. Schematic circuit of the experimental setup.

1 — inlet sleeve; 2 — outlet sleeve; 3 — shut-off valve; 4 — thermostats; 5 — thermocouple switches; 6 — differential manometers; 7 — resistance box; 8 — measuring diaphragm; 9 — power transformer OSU-80/5; 10 — current transformer UTT-6; 11 — autotransformer AOMK-100/05; 12 — reduction valves for air; 13 — blade-type swirler.

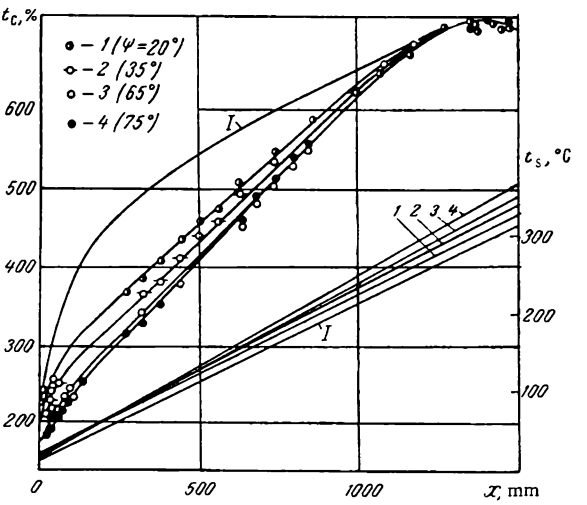


FIGURE 2. Distribution of the wall and stream temperatures over the tube length.

I — without swirling of the flow.

The experimental data on the local heat transfer and resistance coefficients were processed in the form of the functions

$$Nu_f = f(Re_{in}),$$
$$\zeta = f(Re_{in})$$

and are plotted as graphs. In addition, empirical equations are given for calculating the local heat transfer coefficients over the tube length.

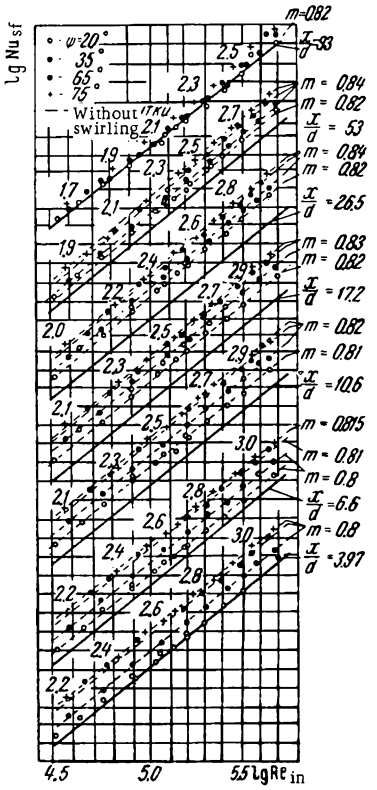


FIGURE 3. The function $Nu_{sf} = f(Re_{in})$ for different inlet swirlers at $t_{c\,max} \approx 700°C$ and $t_{in} \approx 20°C$.

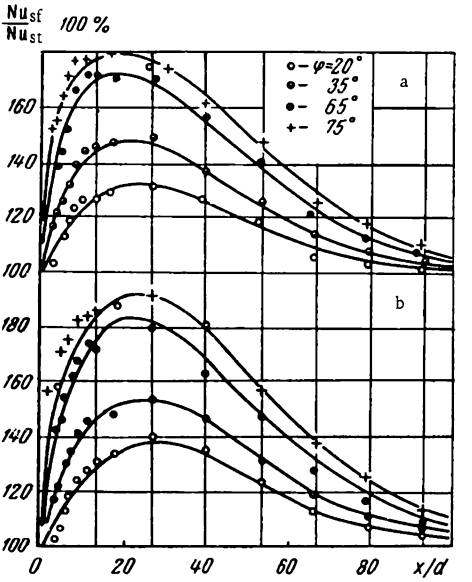


FIGURE 4. Attenuation of the heat transfer over the [tube] length with different swirlers.

a — $Re_{in}$ = 100,000; b — 300,000; the continuous line represents data calculated with the aid of equations.

In view of the fact that it is almost impossible to determine the actual speed of the swirled stream washing the heat transfer surface, the Reynolds number was calculated from the flow rate (weight units) and the air temperature at the tube inlet, using the equation

$$Re_{in} = \frac{wd}{\nu} = \frac{4G_A}{3600\,\pi\, dg\,\mu_{in}}.$$

The values of the physical constants in the $Po_f$ and $Nu_f$ numbers were determined from the stream temperature.

The changes in the temperature of the inner wall surface and in the stream temperature over the tube length are shown in Figure 2. As is evident from the figure, the increase in the velocity of the air in contact with the wall (caused by the helical motion of the stream) reduces the wall temperature and increases the stream temperature; these effects become more pronounced as the stream swirling angle is increased, and this causes a proportional increase in the heat transfer coefficient at a constant air flow rate.

The function $Nu_{sf} = f(Re_{in})$ for several values of $\frac{x}{d}$ is shown in Figure 3, using translated ordinates. For the purpose of comparison, the figure also shows curves corresponding to the heat transfer in a smooth tube with sharp entry. Since the experimental $Pr_s$ number remained nearly constant, the numerical value of $Pr_s^{0.4}$ is comprised in the term for the proportionality coefficient.

As regards the intensification of the heat transfer, the effectiveness of the swirlers may be judged from Figure 4, which is a graphical presentation of the function

$$\frac{Nu_{sf}}{Nu_{st}} = f\left(\frac{x}{d}\right)$$

for different swirling angles and two values of $Re_{in}$.

As is evident from the curves in Figures 3 and 4, the increase in the heat transfer rate caused by the helical motion is maintained and even increases with increasing $Re_{in}$, i.e., during developed turbulent flow. The same results were reported by other authors /1-2/, who found that the increase in the heat transfer rate becomes more pronounced as the Reynolds number is increased.

By processing a large amount of graphical material, we derived equations for the determination of the local heat transfer in the case of a swirling flow created by blade-type swirlers:

$$\frac{Nu_{sf}}{Nu_{st}} = 1 + Axe^{-(x-1)+a\left(\sqrt{(x-1)^2+1}-1\right)}$$

Here $A = 0.043\,(Re_{in} \cdot 10^{-5})^{0.126}\,\psi^{0.68}$ characterizes the maximum value of $\frac{Nu_{sf}}{Nu_{st}}$ for the given swirling angle $\psi$ and flow rate $Re_{in}$, while

$$x = \frac{x/d}{\left(\frac{x}{d}\right)_{max}},$$

where $x$ is the distance from the entry to the tube and $\left(\frac{x}{d}\right)_{max}$ is the relative distance from the entry for which the local heat transfer (at given $\psi$ and $Re_{in}$) has a maximum

$$\left(\frac{x}{d}\right)_{max} = 42.7\,(Re_{in} \cdot 10^{-5})^{0.17}\,\psi^{-0.21}.$$

The absolute value of the term $a$ in the exponent of $e$ depends on $Re_{in}$, $\psi$, and $\frac{x}{d}$ and may be determined by using the equation

$$a = -0.21 - 0.09 \cdot 10^{-5} Re_{in} - 0.075\dot{x} + 0.011\psi.$$

The data on the local heat transfer calculated by means of the above equations are in good agreement with the experimental data.

For the maximum in heat transfer, the discrepancy between experimental and calculated values did not exceed 2%. The discrepancy between $Nu_{s.ex}$ and calculated Nu for any other $\frac{x}{d}$ was within ± 5%, which corresponds to the accuracy of the experiments.

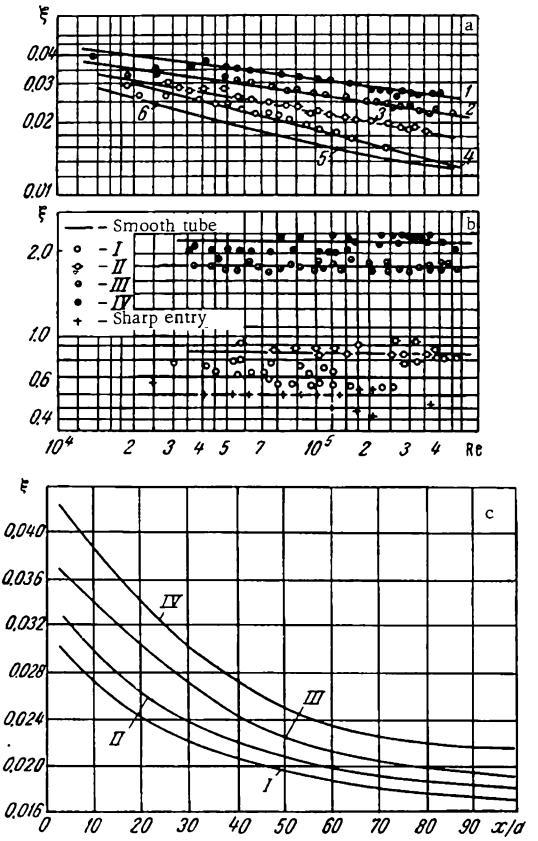


FIGURE 5. Local resistance coefficients.

a — resistance coefficients of the swirling flow (1 — $\xi = 0.156\ Re_s^{-0.134}$; 2 — $\xi = 0.153\ Re_s^{-0.146}$; 3 — $\xi = 0.189\ Re_s^{-0.18}$; 4 — $\xi = 0.347\ Re_s^{-0.246}$; 5 — $\xi = 0.0032 + 0.221\ Re_s^{-0.237}$; 6 — $\xi = 0.316\ Re_s^{-0.25}$); b — resistance of a sharp entry and swirlers (I, II, III, IV — $\psi$ = 20, 35, 65, 75°, respectively); c — changes in the local resistance coefficients over the tube length ($\xi = f(x/d)$; $Re_{in}$ = 100,000).

The creation of a swirling flow is associated with a noticeable increase in the hydraulic resistance. Figure 5 shows the curves for the hydraulic resistance coefficient (of the tube) during adiabatic discharge at different swirling angles of the stream, as well as the resistance coefficients of the swirlers.

The resistance coefficients for the flow in the presence of heat transfer are in good agreement with the above equations, after introduction of a temperature factor in the form $\left(\frac{T_w}{T_s}\right)^{-0.55}$.

The local resistance coefficients plotted in Figure 5 show that both the resistance coefficients and the heat transfer coefficients decrease as the swirling is ceased, and at a distance of $\frac{x}{d} \approx 100$, their values coincide (within 10%) with the values of $\zeta$ and $\alpha$ for a smooth tube.

In order to establish the optimum swirling angle, we compared the effectiveness of swirlers at different angles. As a measure of the effectiveness, we used the energy coefficient of Kirpichev as modified by Antuf'ev:

$$E = \frac{\alpha}{\text{ANo}},$$

where ANo is the energy needed to overcome the resistance (per hour) in terms of thermal units. The power needed was determined by taking into account the resistance of the blade swirlers.

The average values of the heat transfer coefficient $\alpha$ obtained at a given power consumption for the pumping of the heat transfer fluid (at a relative tube length $\frac{x}{d} \approx 100$) are as follows: at $\psi$ = 0, 20, 35, 65, and 75°, $\alpha$ = 325, 334, 353, 379, and 394 $w/m^2 \cdot deg$, respectively.

The above data show that for a given power consumption, an increase in the swirling angle (within the range given above) improves the economic performance of the setup.

Thus, it may be seen from the above that a swirling flow causes a noticeable increase in the heat transfer rate due to the increased velocity of the stream in contact with the heat transfer surface, and that swirlers of the above type can be used successfully in the case of small-diameter tubes or a close packing of the tubes in a system. Their chief advantage is that they fit within the tube diameter.

Bibliography

1. Alimov, R.Z. Intensifikatsiya konvektivnogo teplo- i massoobmena v trubakh s pomoshch'yu zavikhrennogo dvukhfaznogo potoka (Increase in the Heat- and Mass-Transfer Rates in Tubes by Means of Swirling Two-Phase Streams). — Izv. AN SSSR, OTN Energetika i avtomatika, No. 2. 1962.
2. Referativnyi zhurnal "Mekhanika", No. 16293. 1960, and No. 16546. 1961.

The Central Boiler and Turbine Institute
im. I.I. Polzunov

E.K. Karasev

# INVESTIGATION OF THE HYDRODYNAMICS AND HEAT TRANSFER IN A CHANNEL WITH TURBULIZERS ON THE HEAT TRANSFER SURFACE

Recent studies in the USSR and abroad have shown that turbulizers (in the form of protuberances or pits) may be used to increase the heat transfer rate.

However, the published papers deal mainly with the mean values of the heat transfer and hydraulic resistance. This is attributed to the fact that small-size models (which do not allow for an accurate investigation of the local structures of the stream and the temperature field) were used in the experiments.

In addition, our investigations have shown that the local conditions in the heat transfer on the surface between the fins is a function of the coordinates. Hence, as a result of heat flow along the wall, the heat transfer coefficient depends on the wall material, wall thickness, and the nature of the heating (for instance, Grass /1/ has found that the heat transfer from copper and aluminum surfaces is higher by 30% than from a steel surface). At the same time, a knowledge of the local heat transfer conditions is required for equipment operating at high heat loads.

Most authors did not take into account the effect of the fin width on the hydrodynamics and heat transfer, and the main studies were carried out with fin width-to-height ratios in the range $0<b/h\leqslant 1$.

Wieghardt's data /2/ for a single fin indicate that the hydraulic resistance remains constant for $0<b/h\leqslant 1$, while it decreases by a factor of 1.5-2 when $b/h$ changes in the range between 1 and 4. The effect of the above factor on the heat transfer has not been the subject of special study.

We studied in our investigation the effect of rectangular turbulizers with different $b/h$ and $s/h$ ratios on the hydraulic resistance, the flow pattern, and the local heat transfer.

The experiments were carried out on a tube with square cross section ($0.12 \times 0.12\ m^2$) and a total length of 6 m (Figure 1). Air at normal pressure was pumped through a honeycomb (with square cells, $0.01 \times 0.01\ m^2$) and a filter screen into a double Vitoshinskii nozzle. The end of the nozzle was fitted with a flow-rate measuring section ($0.120 \times 0.120\ m^2$) where the required air flow rate was determined by measuring the drop on a calibrated Pitot-Prandtl tube. The first 5 m of the tube served as a stabilizer section.

All basic measurements were made on a working section 1 m long made of Plexiglas and fitted with removable lids.

One of the walls over the whole tube length was fitted with an electric heater made of stainless steel foil ($\delta = 0.0001$ m) ribbon pasted onto

paronit ($\delta$ = 0.004 m). Asbestos sheet (with a total thickness of 0.020 m) was fitted beneath the working heater, and below this was placed a compensating heater (made of Mn — Ni — Co alloy wire) which was also covered with an asbestos heat insulator. The heat load on the compensating heater was controlled by means of three thermocouples placed between the working and the compensating heater.

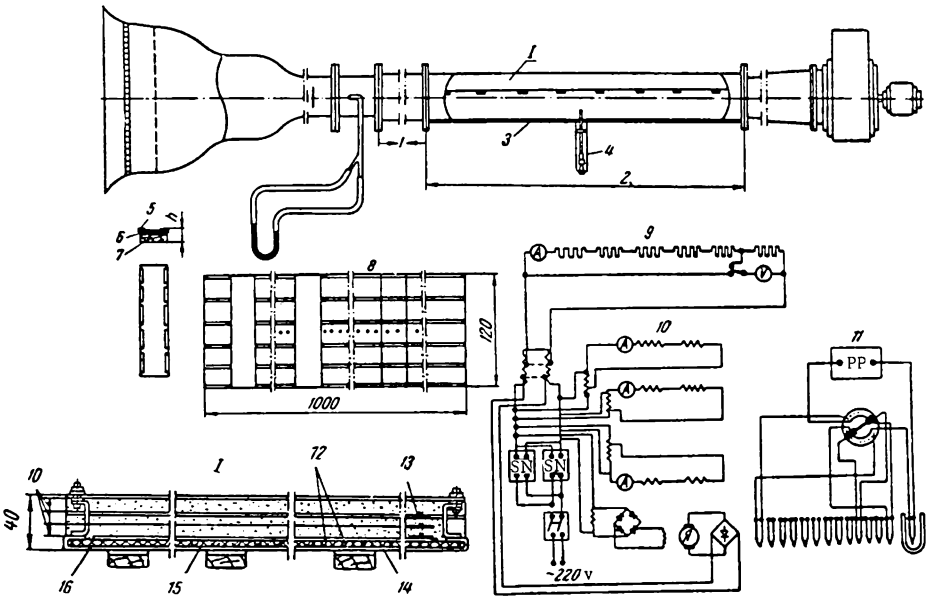


FIGURE 1. Schematic view of the setup.

1 — flow stabilizer section (5000); 2 — working section (1000); 3 — removable lid; 4 — leveling device; 5 — shunt; 6 — rubber pad; 7 — fin; 8 — heater; 9 — working heaters; 10 — compensating heaters; 11 — thermocouple (30 pieces) connection circuit; 12 — thermocouples; 13 — copper foil; 14 — 1Kh18N9T steel foil, $\delta$ = 0.1; 15 — paronit [insulating material] $\delta$ = 4; 16 — 1Kh18N9T steel sheet, $\delta$ = 2.

Thirty chromel-kopel thermocouples (0.00015 m thick) were welded 0.01 m apart on the reverse side of the working heater in the center portion of the working section. The thermocouples were welded without beads, the contact being made through the metal of the wall. The emf of the thermocouples was recorded with a PP-type potentiometer, with a common cold junction.

The experimental tube fins were of two types: Plexiglas fins of $h$ = = 0.014 m and $b$ = 0.012 m and wooden fins of $h$ = 0.010 m and $b$ = 0.010, 0.020, and 0.040 m, with a brass foil ($\delta$ = 0.0001 m) electric shunt. In order to measure the temperature field on the fin surface, one fin of $h$ = 0.040 m was fitted with a separate electric heater and 5 thermocouples were welded to its inner surface. The power of the working heater was checked by taking ammeter and voltmeter readings. The velocity field and the degree of turbulence of the flow were recorded with an ETAM-3A electric thermoanemometer, fitted with the ESU stabilized electronic amplifier and using a milliammeter with the T-13 thermal converter.

The pressure field on a smooth wall, and the hydraulic resistance coefficient were measured through holes bored in the wall facing the wall fitted with the turbulizers. The temperature field in the stream was studied by means of chromel-kopel thermocouples (diameter 0.00015 m) connected to the PPTN-1 potentiometer. The measuring techniques were worked out and the apparatus was adjusted using a similar tube without turbulizers.

The experimental data show that the hydraulic resistance coefficient has a value close to the value calculated using the Blasius equation $\lambda = \frac{0.3164}{Re^{0.25}}$, while the value of the Nusselt number Nu was close to the value calculated using equation $Nu = 0.018\ Re^{0.8}$.

The flow pattern was studied in a channel fitted with fins of $h = 0.014$ m and $b = 0.012$ m, the distance between the fins being $s = 0.077$, 0.155, and 0.255 m at $Re = 4.4 \cdot 10^4$. All the fins were placed on the same side.

The experiments showed that the flow between the fins may be divided arbitrarily into three main zones. The eddying zone, the length of which, depending on the distance between the fins, was either $3h$ (for a distance of 0.155 m or $s/h = 11.1$) or $2.5 - 3.5\,h$ (for a distance of 0.255 m or $s/h = 18.2$), was immediately behind the fins. The eddying zone contained two connected eddies. Their height was greater (by about $1/3$-$1/4\,h$) than the height of the upper edge of the fin. A diffuser zone (which at $s/h = 11.1$-$18.2$ extended to $x/h = 8.5$-$10.0$) lay behind the eddying zone. The flow zone, lying behind the diffuser zone, was parallel to the side wall, while the contraction zone started at a distance of $3h$ from the beginning of the next fin.

The flow of the turbulent core was also noticeably deformed in comparison with the flow in a smooth channel. Thus, a turbulent wake with its pole on the front edge of the fin was created behind the fin and extended toward both the periphery and the center of the flow. The zero velocity gradient line shifted toward the smooth wall. However, the flow pattern of the flow core depended to a large extent on the $s/h$ ratio. For instance, while at $s/h = 5.5$ ($s = 0.077$ m) the flow in the turbulent core remained practically constant, and the $du/dy$ line was at a distance of 0.65a from the wall fitted with the turbulizers, at $s/h = 18.2$ the velocity profile showed marked changes over the whole cross section, but the zero gradient line was not parallel to the wall and was at a distance of 0.55-0.65a from the wall fitted with the turbulizers.

The pressure field on a smooth wall was investigated on a channel with turbulizers having the following dimensions: $h = 0.01$ m; $b/h = 1$, 2, 3, and 4 for $s/h$ ratios between 7 and 40.

The experimental results confirmed the results of previous studies of flow kinematics. The investigations showed that at large $s/h$ ratios (higher than 15), all three flow zones may be observed immediately behind the fin: the stream after passing above the eddying zone was slightly accelerated and the resulting static pressure losses were negligible; however, because of the braking of the whole stream in the diffuser zone, there occurred a certain increase in the static pressure which afterward remained virtually constant until the contraction zone; the whole stream was accelerated, and the main losses of static pressure as well as dissipation occurred in the contraction zone.

The experiments showed that at relatively small distances between the fins ($s/h = 7$-$11$), no increase in pressure was observed in the diffuser zone, while the static pressure decreased gradually over the stream path. The main decrease in pressure occurred again in the contraction zone (Figure 2).

The investigation of the turbulence field $\varepsilon = \frac{\sqrt{\overline{u'^2}}}{\bar{u}}$ showed that the turbulent structure of the stream underwent marked changes as compared with the flow in a smooth channel.

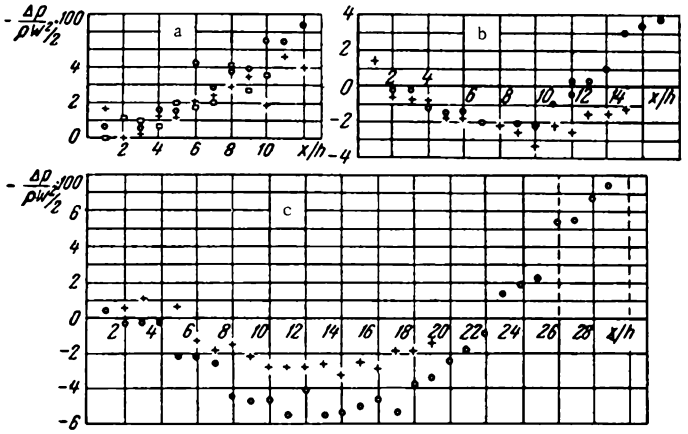


FIGURE 2. Relative pressure drop on the smooth wall of a channel with turbulizers at Re = $1.6 \cdot 10^5$, $b$ = 0.04 m, and $h$ = 0.01 m (the total cross-section plane passing through the back edge of the fin was taken as the reference plane).

a, b, and c refer to $s$ = 0.07, 0.18, and 0.26 m, respectively.

Thus, during the flow in a channel with turbulizers of $h$ = 14 mm ($h/a$ = 0.117) and $b/h$ = 0.86, the stream passing through the cross section plane on the back edge of the fin had a much higher degree of turbulence than the stream adjacent to the smooth wall (Figure 3). At the same time, the streams at $s/h$ = 11.1 and $s/h$ = 18.2 showed only slight difference in the degree of turbulence; on the other hand, at $s/h$ = 5.5, the degree of turbulence of the core was high.

The stream passing between the smooth wall and the zero gradient line had the same turbulent structure as in the case of a smooth channel, while the values of $\varepsilon$ were in agreement with the corresponding values reported by Minskii /3/ and Laufer /4/.

As the distance from the fin increased, there was an increase in the width of the turbulent wake, and near the wall the degree of turbulence reached a value of 0.4. However, starting at $x$ = 10-12, the stream became less turbulent because of turbulent diffusion and dissipation, while at the same time, the production of turbulent energy decreased because of the drop in the absolute value of $\frac{du}{dy}$ along the stream path (leveling of the stream). The greatest dissipation of turbulent energy occurred in the contraction zone, where the fact that $\frac{du}{dy} > 0$ caused a decrease in the turbulent energy and, hence, an increase in the energy dissipation (see Figure 3).

In addition, the experiments showed that in the contraction zone, the dissipation of turbulent energy occurs mainly in the turbulent wake adjacent

to the main flow core, and not in the region adjacent to the wall. This phenomenon may serve as a partial explanation of the rapid increase in the hydraulic resistance as a function of increasing relative fin height.

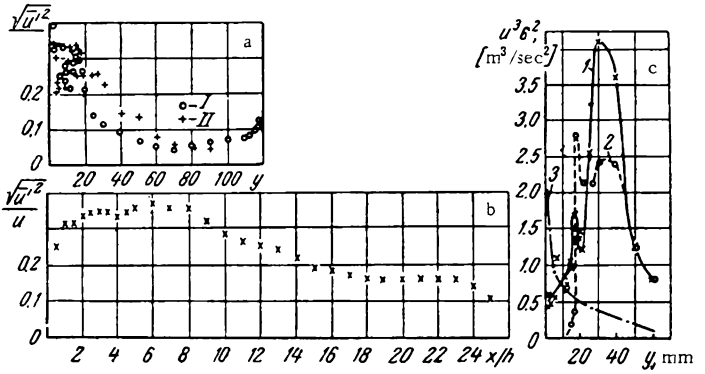


FIGURE 3. Degree of turbulization at $h$ = 0.014 m, $b$ = 0.012 m, Re = $4.4 \cdot 10^4$.

a — $x/h$ = 1.13 (I — $s/h$ = 11.2; II — $s/h$ = 5); b — $s/h$ = 18.2; $v$ = 14; c — $s/h$ = 11.2; 1 — $x/h$ = 8.6; 2 — $x/h$ = 11.2; 3 — smooth channel, calculated from the data of Laufer.

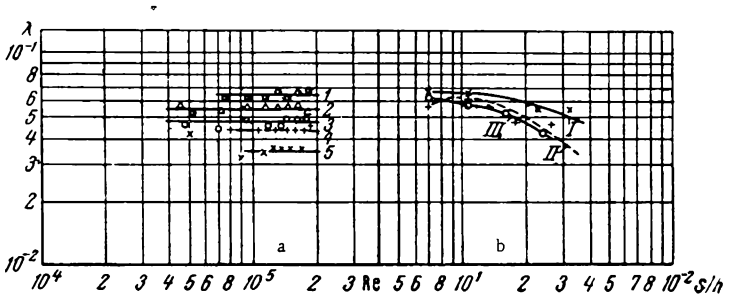


FIGURE 4. Dependence of the hydraulic resistance coefficient in a channel on the Reynolds number.

a — $\lambda = f$ (Re); $b/h = 4$; 1, 2, 3, 4, 5 — refer to $s/h$ = 11, 7, 18, 26, 40, respectively; b — $\lambda = f$ ($s/h$); I, II, III — refer to $b/h$ = 1, 4, 2, respectively.

The results of our study of the hydraulic resistance (Figure 4) follow the same pattern with respect to Re at Re > $5 \cdot 10^4$. The hydraulic resistance of channels with turbulizers with $b/h$ = 1 was about 10% higher than in the case of $b/h$ = 2-4. When plotted as a function of $s/h$, the hydraulic resistance had a maximum at $s/h$ = 11 and decreased gradually with increasing $s/h$.

The local and average heat transfers were studied with turbulizers of $h$ = 0.010 m ($h/a$ = 0.0835) and $b/h$ = 1.2 and 4, in the $s/h$ range of 7-30.

The experiments with turbulizers of $b/h$ = 1 and 2 were carried out at $q$ = 1.4 kw/m$^2$ in the Re range of $4 \cdot 10^4 - 8 \cdot 10^4$. However, the experimental accuracy was not high enough. By using a different fan we were able to increase the heat load to 3.3 kw/m$^2$ and the velocity to Re = $8 \cdot 10^4 - 1.6 \cdot 10^5$.

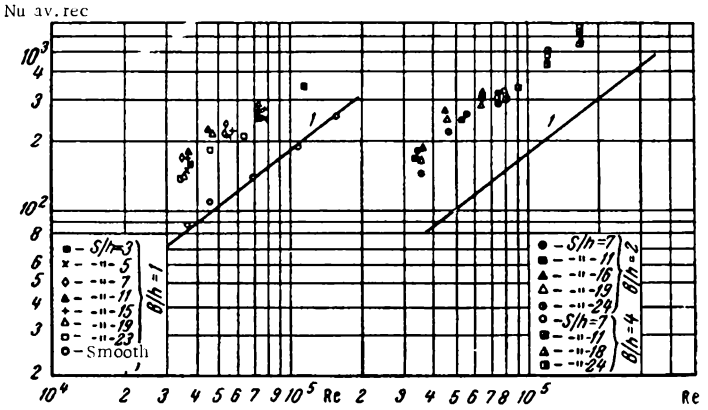


FIGURE 5. Dependence of $Nu_{av.rec}$ on the Reynolds number (1 — calculated from equation $Nu = 0.018\ Re^{0.8}$).

The experiments with turbulizers of $b/h = 4$ were carried out under the same conditions.

Heat losses into the surrounding medium were taken into account in calculating the heat loads and temperatures.

The values of $Nu_{av}$ were calculated only for the spaces between the fins. In order to account for heat transfer on the fins, we intend carrying out a special experiment. The values of $Nu_{loc}$ were calculated from the measured temperature fields on the walls.

Our processing of the experimental data showed that the value of $Nu_{av.rec}$ for $b/h = 1$ and $s/h = 5$-7 is higher (by a factor of 1.8-1.9) than in the case of a smooth channel, while at $s/h = 23$, it is higher by a factor of 1.5-1.6 (Figure 5).

Enlargement of the fin to $b/h = 2$ causes a 10% increase in $Nu_{av.rec}$ (Figure 5).

In the case of turbulizers of $b/h = 4$, we observed a well-defined relationship described by the equation $Nu_{av.rec} = C\,Re^{0.8}$, where $C = 0.04$ for $7 \leqslant s/h \leqslant 15$; at higher $s/h$ there was a decrease in $Nu_{av.rec}$, and its value for $15 \leqslant s/h \leqslant 26$ could be calculated from $C = 0.085\,(s/h)^{-0.28}$.

The study of the local heat transfer showed that the value of $\frac{Nu_{loc}}{Nu_{av.rec}}$ is independent of Re at $Re > 4 \cdot 10^4$.

A typical distribution pattern of the values of $\frac{Nu_{loc}}{Nu_{av.rec}}$ is shown in Figure 6. In this case, the minimum value of $\frac{Nu_{loc}}{Nu_{av.rec}}$ for $b/h = 1$ was 0.75-0.8, and it decreased to 0.65 as $b/h$ increased to 4. However, it should be noted that the above minimum occupies a small area of about $(1\text{-}1.5)\,h$ and lies immediately behind the fin; this is followed by a sharp increase in the heat transfer to a maximum (with a small area, of about $(3\text{-}4)h$), which is followed by a gradual decrease in $Nu_{loc}$ (for $s/h > 11$).

For instance, in the case of $b/h = 2$, $s/h = 24$ $\frac{Nu_{loc}}{Nu_{av.rec}} = 1.2\text{-}0.025\ (x/h - 5)$,

where $x$ is the distance from the back edge of the turbulizer measured in the direction of the flow. A slight increase in the heat transfer occurs in front of the next fin.

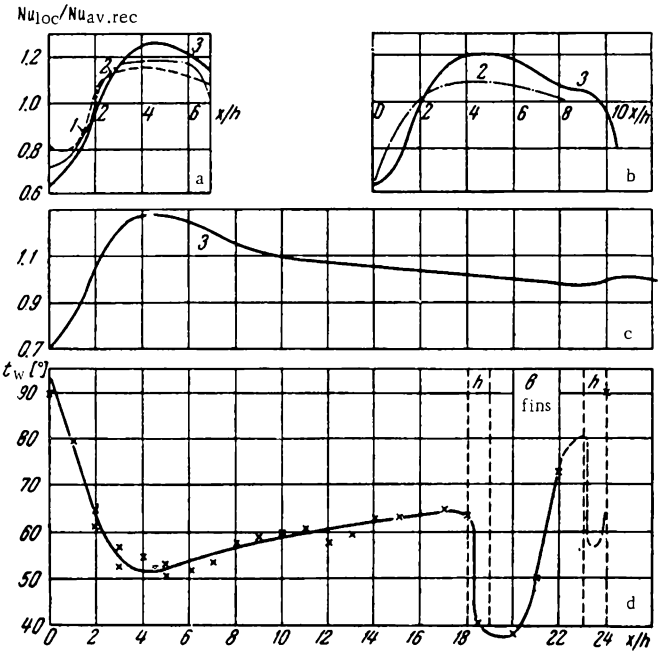


FIGURE 6. $Nu_{loc}/Nu_{av.rec}$ ratio as a function of $x/h$.

a, b, c — $Re = 8 \cdot 10^4$, $h = 10$ mm, $s/h = 7, 11, 26$, respectively (1 — $b/h = 1$; 2 — 2; 3 — 4); d — temperature distribution on the heat transfer surface: $h = 0.01$; $s/h = 18$; $Re = 1.6 \cdot 10^5$; $q = 3.3$ kw/m$^2$; $t_{air} = 300.7°$ K.

Heat transfer on the fin was studied only for the case of $b/h = 4$, $s/h = 18$. The experimental results are shown in Figure 6. As is evident from the results, heat transfer on the fin is on the average somewhat higher than heat transfer between the fins. At the same time, starting with the second half of the fin, there is a sharp decrease in heat transfer which is explained by the deterioration of the heat transfer conditions due to the braking and heating of the stream adjacent to the wall (as shown by the temperature field studies). The same phenomenon accounts for the poor heat transfer in the eddying zone immediately behind the fin.

The relatively slight decrease in the heat transfer rate in the diffuser zone is attributed to the good turbulent mixing of the flow in the wake, and the slow growth of the laminar sublayer, the thickness of which could probably be calculated from the experimental data obtained.

Symbols

$h$ — fin height, m; $b$ — fin width, m; $s$ — distance between the fins, m; $a$ — channel size (square cross section), m; $Nu_{av.rec}$ — average Nusselt number for the recess between the fins— $Nu_{loc}$ — local Nusselt number; $\varepsilon = \frac{\sqrt{\overline{u^2}}}{\bar{u}}$ — degree of turbulence; $\lambda$ — hydraulic resistance coefficient.

Bibliography


1. Grass. Increasing the Rate of Heat Transfer to Water by Artificially Roughening the Heat Transfer Surfaces of Reactors or Heat Exchangers. [Russian translation. 1959.]
2. Schlichting, H. Theory of the Boundary Layer. — New York, McGraw-Hill. 1955.
3. Minskii, E.M. Turbulentnost' ruslovogo potoka (Turbulence of Stream in Channels). — Gidrometeoizdat. 1952.
4. Khintse, I.O. Turbulentnost' (Turbulence). — Gosudarstvennoe Izdatel'stvo Fiziko-matematicheskoi Literatury, Moskva. 1963.

A.S. Nevskii, A.V. Arseev, L.A. Chukanova,
A.I. Malysheva, and T. V. Sharova

# CONVECTIVE HEAT TRANSFER IN CYLINDRICAL CHAMBERS WITH RECIRCULATION

When a gas is discharged into a cylindrical chamber through a nozzle or small-diameter hole placed at the chamber end, the stream formed entrains the surrounding medium, and thus creates a vacuum near the walls at the entry to the chamber. When the stream fills the chamber, a fraction of its kinetic energy is transformed into potential energy, and the pressure in the chamber cross section and on the walls increases. In this way, a pressure gradient is created along the chamber walls near the entry, together with a flow of gas in a direction opposed to the main stream (i. e., gas circulation in the dead corners near the entry to the chamber).

The phenomenon of gas recirculation creates peculiar conditions for the convective heat transfer between the gas and the chamber walls. Hence, the conventional equations for the determination of the magnitude of convective heat transfer cannot be applied to the above case.

Our experiments were carried out with chambers 0.300 and 0.180 m in diameter. Each chamber was surrounded with a water jacket divided into calorimeter sections. The basic data concerning the chamber dimensions are tabulated in Table 1. Each calorimetric section had a separate water supply. The heat transferred to each calorimeter was calculated on the basis of the water flow rate through the calorimeter and the increase in its temperature. The air was heated to 973°K in electric heaters before introducing it into the chamber. The air was discharged into the chamber through a central nozzle and an annular external nozzle, the dimensions of which are given in Table 2.

TABLE 1. Experimental chambers

| Chamber parameters | Chamber diameter, m | |
|---|---|---|
| | 0.300 | 0.180 |
| Length, m | | |
| total | 1.880 | 2.437 |
| used in the data processing | 1.650 | 1.910 |
| Number of calorimeters | | |
| total | 13 | 16 |
| used in the data processing | 11 | 14 |
| Heating area of the calorimeters, as used in the data processing, $m^2$ | 1.555 | 1.080 |

Note. In the chamber with a diameter of 0.180 m, the first calorimeter (0.185 m long) was disconnected in all experiments except in experiments 28 and 29, where it was used as a working calorimeter in addition to the 14 calorimeters listed in the table.

TABLE 2. Main nozzle parameters

| Inner diameter of the external nozzle, m | Diameter of the central nozzle, m | | Cross-section area of the nozzle at the outlet [discharge area], $m^2$ | |
|---|---|---|---|---|
| | inner | outer | central | external |
| 0.04983 | 0.03276 | 0.03503 | 0.000843 | 0.000986 |
| 0.04983 | 0.03608 | 0.03834 | 0.001023 | 0.000796 |
| 0.02940 | 0.02168 | 0.02302 | 0.000369 | 0.000263 |

In the experiments we varied the total amount of air supplied to the chamber, the velocity ratio of the air supplied through the central and external nozzles, and the nozzle dimensions. We carried out some experiments in which air was supplied only through one of the nozzles and other experiments in which hot air was supplied through one nozzle and cold air through the other. In addition, a swirled air stream was introduced in one experiment, while in two experiments, the air flow was constant over the chamber cross section. There were 29 experiments in all (Table 3).

TABLE 3. Main experimental parameters

| Experiment No. | Diameter, m | | | Air flow rate ($10^3 nm^3$*/sec) through | | Outflow velocity ratio of central to external streams | Stream temperature, °K | | Average heat transfer coefficient w/$m^2$ deg | φ | | l/D corresponding to max φ |
|---|---|---|---|---|---|---|---|---|---|---|---|---|
| | chamber | external nozzle $D_0$ | central nozzle | central nozzle | external nozzle | | central nozzle | external nozzle | | average up to $l/D = 5.5$ | maximum | |
| 1 | 0.300 | 0.0498 | 0.0328 | 1.040 | 1.19 | 1.02 | 973 | 973 | 17.0 | 7.6 | 11.6 | 2.7 |
| 2 | " | " | " | 2.270 | 2.36 | 1.12 | " | " | 26.8 | 6.6 | 9.8 | 2.6 |
| 3 | " | " | " | 2.260 | 2.36 | 1.12 | " | " | 29.4 | 7.3 | 11.0 | 2.7 |
| 4 | " | " | 0.0361 | 2.020 | 2.09 | 0.75 | " | " | 25.6 | 7.0 | 10.5 | 2.7 |
| 5 | " | " | " | 1.265 | 1.44 | 0.68 | " | " | 19.8 | 7.5 | 11.4 | 2.5 |
| 6 | " | " | " | 2.030 | 2.15 | 0.74 | " | " | 25.3 | 6.8 | 10.1 | 2.4 |
| 7 | " | " | " | 0 | 1.31 | — | — | 987 | 9.55 | 6.6 | 9.4 | 2.5 |
| 8 | " | " | " | 0 | 1.88 | — | — | 980 | 14.9 | 7.4 | 11.3 | 2.2 |
| 9 | " | " | " | 0 | 2.34 | — | — | 974 | 15.8 | 6.7 | 10.7 | 2.6 |
| 10 | 0.180 | " | " | 2.030 | 2.02 | 0.79 | 975 | 965 | 45.7 | 5.0 | 7.3 | 2.2 |
| 11 | " | " | " | 2.250 | 2.24 | 0.79 | 975 | 968 | 48.2 | 4.8 | 6.8 | 2.7 |
| 12 | " | " | " | 1.270 | 1.27 | 0.78 | 976 | 970 | 33.3 | 5.3 | 7.5 | 2.5 |
| 13 | " | " | " | 2.170 | 0 | — | 968 | — | 35.2 | 6.4 | 9.8 | 2.8 |
| 14 | " | " | " | 0 | 2.25 | — | — | 969 | 33.1 | 6.1 | 9.1 | 2.2 |
| 15 | " | " | " | 2.200 | 2.24 | 0.23 | 295 | 969 | 44.2 | 4.8 | 6.5 | 2.2 |
| 16 | " | " | " | 2.250 | 2.20 | 2.60 | 972 | 297 | 42.2 | 4.5 | 6.8 | 2.8 |
| 17 | " | " | " | 1.645 | 1.64 | 0.78 | 965 | 967 | 39.3 | 5.0 | 7.0 | 2.5 |
| 18 | " | " | " | 2.580 | 1.00 | 2.00 | 970 | 974 | 37.9 | 4.5 | 6.1 | 2.1 |
| 19 | " | " | " | 1.970 | 1.55 | 0.99 | 972 | 971 | 34.4 | 4.1 | 5.8 | 1.6 |
| 20 | " | " | " | 1.465 | 1.99 | 0.57 | 972 | 968 | 35.0 | 4.3 | 6.4 | 1.5 |
| 21 | " | 0.0294 | 0.0217 | 1.140 | 1.00 | 0.82 | 979 | 965 | 38.4 | 7.0 | 9.7 | 2.6 |
| 22 | " | " | " | 1.710 | 0.97 | 1.25 | 966 | 973 | 44.3 | 6.7 | 9.6 | 2.7 |
| 23 | " | " | " | 1.385 | 1.43 | 0.25 | 348 | 972 | 25.6 | 3.9 | 5.8 | 2.1 |
| 24 | " | " | " | 0 | 1.47 | — | — | 966 | 19.8 | 4.8 | 7.3 | 2.3 |
| 25 | " | " | " | 1.400 | 1.41 | 1.70 | 979 | 410 | 45.4 | 6.9 | 10.2 | 2.9 |
| 26 | " | " | " | 1.410 | 0 | — | 971 | — | 31.6 | 8.2 | 11.6 | 2.9 |
| 27 | " | 0.0500 | 0.0500 | 3.77 | | — | 967 | | 49.2 | 5.7 | 10.1 | 0.9 |
| 28 | " | 0.1800 | 0.1800 | 4.70 | | — | 965 | | 17.0 | — | — | — |
| 29 | " | " | " | 5.62 | | — | 969 | | 18.4 | — | — | — |

* [$nm^3$ denotes a cubic meter of gas at 15°C and 760 mmHg.]

The air temperature in the chamber sections between the calorimeters was determined from the heat balance between the starting and the investigated sections. The heat transfer coefficient for each calorimeter was determined by the equation

$$k = \frac{Q_i}{F_i(t_{av.a} - t_{0.i})}. \quad (1)$$

In the chamber with a diameter of 0.180 m, the wall temperature was measured at six points by means of thermocouples. The measurements showed that the thermal resistance in the case of heat transfer from the wall to the water is small. It is easily shown by calculation that the resistance to heat transfer through the wall is negligible. Thus, it may be assumed that the heat transfer coefficient sought is equal to the coefficient of heat transfer from the air to the chamber walls. The small error (not exceeding 4%) resulting from this assumption is partially compensated by the fact that in determining the heat transfer coefficient we also took into account the heat transferred by radiation from the water vapor entering with atmospheric air.

We determined the experimental values of the Nusselt number $Nu_{exp}$ from the measured values of $\alpha_i$ and from the values of the Reynolds number (calculated on the basis of the average air velocity in the chamber) we calculated the values of the Nusselt number for the heat transfer in the case of a uniform gas flow in the tube by using the equation $Nu = 0.018\ Re^{0.8}$. In the above calculations, the values of the thermal conductivity and viscosity coefficients were taken on the basis of the average air temperature for the given calorimeter.

In all experiments, we calculated for each calorimeter the ratio

$$\varphi = \frac{Nu_{exp}}{Nu}, \quad (2)$$

which shows to what extent the actual heat transfer in any cross section is greater than the heat transfer in the tube calculated for an established turbulent flow.

The values of $\varphi$ over the chamber length obtained in the experiments are shown in Figures 1-4. The figures show that noticeable changes in $\varphi$ are observed over the chamber length, and that the value of $\varphi$ depends on the method by which air is supplied to the chamber. However, the general nature of the changes in $\varphi$ over the length of the chamber is approximately the same. At the entry to the chamber (i.e., first calorimeter) $\varphi$ = 1.9-4.3. The value of $\varphi$ increased with increasing distance from the entry and reached a maximum at a distance $l = (1.5\text{-}2.9)D$; after the maximum, $\varphi$ decreased, rapidly at first and then more slowly. The maximum values of $\varphi$ ranged from 5.8 to 11.6. At very great distances from the entry to the chamber, the value of $\varphi$ approaches unity.

We calculated the average values of $\varphi$ and the average heat transfer coefficients (Table 3) for each experiment in the section from the entry of the chamber to a distance $l = 5.5D$. We determined the Nusselt and Reynolds numbers for these sections. In this case, the average heat

transfer coefficients were calculated using the equation

$$k_{av} = \frac{\Sigma k_i F_i}{\Sigma F_i} . \quad (3)$$

The Reynolds number was calculated using the equation

$$Re = \frac{G_a}{900 \pi D \mu g} . \quad (4)$$

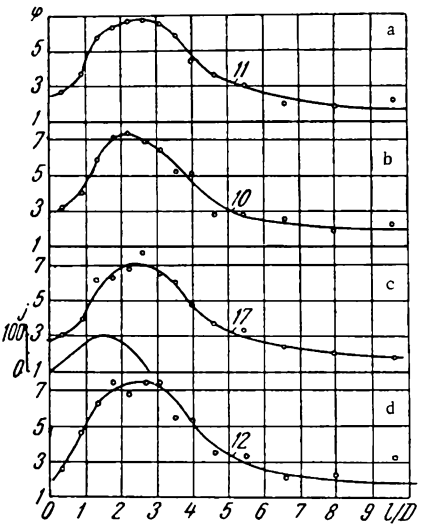


FIGURE 1. Variation of φ over the length of a chamber with $D = 0.180$ m and $m = 3.6$, for different air supply and recirculation ($j$) rates; here and below the numbers adjacent to the curves indicate the number of the experiment in Table 3.

a — air flow rate 0.045; b — 0.0406; c — 0.0329; d — 0.0254 nm$^3$/sec.

The values of the thermal conductivity coefficient and the viscosity of air were taken on the basis of the mean arithmetic temperature for the beginning and the end of the section under consideration.

Logarithms of the Nusselt number are shown in Figure 5 as functions of logarithms of the Reynolds number. Only those experiments in which the air was supplied through the two nozzles at equal stream temperatures, and those experiments in which the air was supplied through the central nozzle are included. We did not include experiments 18, 19, and 20, which were performed in order to study the effect of the air-velocity ratio (from the two nozzles) on the heat transfer.

Figure 5 shows clearly the relationship between the two similarity numbers, which is described by the equation

$$Nu = C Re^{0.67} . \quad (5)$$

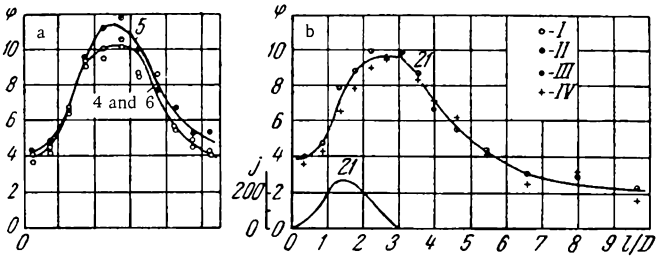


FIGURE 2. Variation of $\varphi$ over the length of the chamber, and the recirculation $j$ at $m = 6.0$.

a — for a chamber with $D = 0.300$ m; I — at an air flow rate of 0.0412-0.0418 nm$^3$/sec; II — 0.0271 nm$^3$/sec; b — for a chamber with $D = 0.180$ m; III — at a velocity ratio $w_{cen}/w_{ext} = 0.82$ (experiment 21); IV — 1.25 (experiment 22).

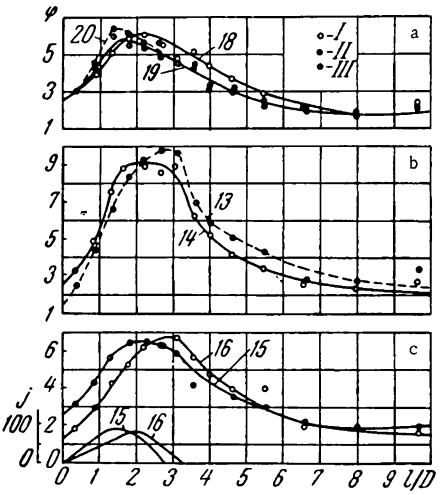


FIGURE 3. Variation of $\varphi$ (continuous lines) and the recirculation (curves 15 and 16 on the bottom) over the length of a chamber with $D = 0.180$ m, for different methods of supplying air to the chamber.

a — I — experiment 18, velocity ratio $w_{cen}/w_{ext} = 2.00$; II — experiment 20, $w_{cen}/w_{ext} = 0.99$; III — experiment 20, $w_{cen}/w_{ext} = 0.57$; b — with air supplied only through the central nozzle (experiment 13) or only through the external nozzle (experiment 14); c — with hot air supplied only through the external nozzle (experiment 15) or only through the central nozzle (experiment 16).

The series of experiments (10, 11, 12, and 17) in which the chamber diameter to stream diameter ratio at the gas entry to the chamber was $m = 3.6$, was carried out in order to elucidate the effect of the air flow rate on the heat transfer. In all experiments, the ratio of the air velocities

from the central and the external nozzles was the same (0.78). In Figure 5, the relationship between the dimensionless numbers for these experiments is represented by the lower straight line, for which the value of the coefficient $C$ in equation (5) is 0.29. The curves for $\varphi$ in the above experiments are shown in Figure 1, which shows that changes in the air flow rate have little effect on the nature of the curves for $\varphi$. The curves for $\varphi$ plotted at different air flow rates are compared also in Figure 2,a, where a slightly better defined maximum in heat transfer was obtained at lower flow rates. This is, apparently, a general observation which can be attributed to the fact that $Nu_{exp}$ is proportional to the velocity to the power 0.67, while the calculated Nu is proportional to the velocity to the power 0.80.

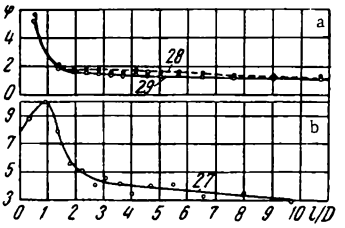


FIGURE 4. Variation of $\varphi$ over the length of a chamber with $D$ = 0.180 m.

a — with air supplied through 55 holes uniformly distributed over the bottom of the chamber; b — in the case of a swirling air stream blown into the chamber.

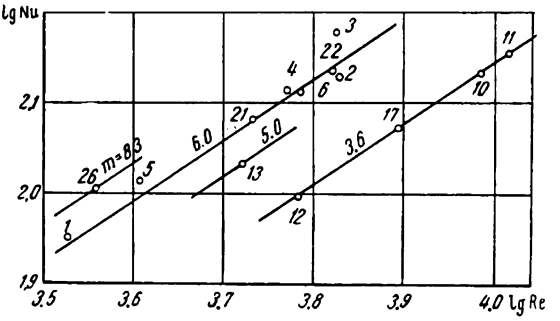


FIGURE 5. Relationship between Nu and Re for a chamber of length $l = 5.5D$.

For experiments 1-6, which were carried out using a chamber of $D$ = 0.300 m, and for experiments 21 and 22, using a chamber of $D$ = 0.180 m, the value of $m$ was 6. On Figure 5, the respective points lie above the line for $m$ = 3.6. It is significant that the points obtained in experiments on different chambers lie on the same lines. In these experiments, the velocity ratio for air supplied through the central and the [external] annular nozzles was not maintained strictly constant, but (as we shall see below) this inaccuracy in the velocity distribution has little effect on the average heat transfer rate.

A comparison of the curves in Figure 2,a,b shows that the nature of the changes in $\varphi$ over the length of the chambers is the same for both chambers.

In experiments 13 and 26, the air was supplied only through the central nozzle, at $m$ = 5.0 and 8.3. The points corresponding to these experiments lie on the lines corresponding to their respective values of $m$ (see Figure 5). Straight lines parallel to the line for $m$ = 3.6 were drawn through the group of points with $m$ = 6.0 and the experimental points from experiments 13 and 26. We obtained the following values for the coefficient $C$ in equation (5): $m$ = 3.6, 5.0, 6.0, 8.3; $C$ = 0.290, 0.345, 0.378, 0.418.

Thus, it is evident that a decrease in the ratio of the stream diameter at the entry of the chamber to the chamber diameter causes an increase in the heat transfer from the air to the walls of the chamber. As is seen from Table 3, there is a simultaneous increase in $\varphi_{max}$, i.e., in the degree of nonuniformity of the heat transfer over the length of the chamber.

The effect of the initial velocity field on heat transfer is shown in Figure 3,a. The air is supplied from both nozzles, but at different ratios.

When the air throughput from the central nozzle is increased, the maximum in heat transfer shifts toward the end of the chamber. The smallest value of the maximum in heat transfer is obtained in the case of equal velocities of air outflow from the two nozzles, and it becomes greater as this equality is disturbed.

The results of experiments in which the air was supplied only through the central nozzle or only through the annular nozzle (Figure 3,b) may be regarded as the limiting cases for the series of experiments shown in Figure 3,a.

All statements concerning the changes in the nature of distribution of the heat transfer over the length of the chamber are confirmed by the results of the above experiments, although the maximum $\varphi$ in the experiment in which air was supplied only through the external nozzle was shifted to the right-hand side somewhat more than might be expected on the basis of the above conclusions.

The results of two experiments at different ratios of air outflow velocities are shown in Figure 2,b.

The points (on the figure) corresponding to experiment 22 (i. e., at a high air throughput through the central nozzle) lie at a slightly greater distance from the entry to the chamber than do the points corresponding to experiment 21; this is in agreement with the above conclusion. It should be noted, however, that changes in the ratio of the throughputs from the two nozzles up to 2:1 have little effect on the velocity distribution and the average heat transfer coefficients.

The effect of the method of introduction of hot air on the shape of the curves for $\varphi$ is shown in Figure 3,c. In experiment 16 we heated only the air from the central nozzle and the air from the external nozzle was supplied cold, while in experiment 15, we heated only the air from the external nozzle. It can be seen that in the first case the maximum heat transfer is shifted (as compared with the second case) toward the end of the chamber. This is caused by the fact that when hot air is supplied through the central nozzle alone, the cold air stream from the external nozzle serves as a shield between the hot central stream and the chamber walls, thus reducing the heat transfer rate near the entry to the chamber.

In experiments 23 and 24, the hot air was supplied through an annular aperture 0.00319 m wide. In these experiments, the heat transfer was lower than in other experiments with the same diameter of the external nozzle, as is evident from the low values of $\varphi_{max}$ and $\varphi_{av}$. This may be caused by the small aperture of the nozzle used for the air supply, which leads to disturbance of the structure of the discharged stream.

In experiments 28 and 29, the air was supplied through 55 round holes 0.012 m in diameter, uniformly spaced on the bottom of the chamber. The curves for $\varphi$ in the above case are shown in Figure 4,a. The high values of $\varphi$ at the entry to the chamber drop rapidly, and at $\frac{l}{D} > 1.5$, the measured values of the heat transfer coefficient are in satisfactory agreement with the known data for heat transfer in the entry sections of tubes.

The high values of the heat transfer coefficient at the entry to the chamber are attributed to the effect of the method of air supply into the chamber through holes of small diameter.

Because the air is discharged in numerous narrow streams uniformly distributed over the chamber cross section, the chamber is filled with the discharged streams over a short length, and the gas recirculation zone (and hence, the increase in heat transfer) is much smaller up to $l = 1.5\,D$.

Experiment 27 was carried out with a swirling air stream. Eight blades 0.05 m long, with screw-shaped ends, were placed in a nozzle 0.05 m in diameter. As seen from Figure 4,b, the heat transfer coefficient in this experiment had a high value at the immediate entry to the chamber; the maximum $\varphi$ was at $\frac{l}{D} = 1.8$, and the curve for $\varphi$ had a smooth downward slope toward the end of the chamber.

In addition to the curves for $\varphi$, Figures 1-3 contain also the values of the air recirculation $j = \frac{G_{rec}}{G_a}$.

The recirculation was noticeable in the experiments at high $m$, for which the heat transfer was also high. The maximum heat transfer was observed at the end of the recirculation zone. The value of $\varphi$ decreased rapidly in subsequent cross sections where there was no recirculation, although its value for a large section over the length of the tube remained much higher than in the case of stabilized flow in a tube.

We did not investigate the physical nature of the process, but it is possible to explain the high experimental values of the heat transfer coefficients. In cross sections near the end of the recirculation zone, high values of $\varphi$ are obtained as a result of the impact on the chamber walls of that part of the stream which branches out to create the recirculation, and the consequent decrease in the thickness of the boundary layer. The high values of $\varphi$ in the recirculation zone and at the end of the chamber may be attributed to the formation of annular eddies near the entry to the chamber as a result of the interaction between two opposite air streams — forward and reverse. As they move along the chambers, the eddies gradually attenuate although they persist for a considerable distance behind the recirculation zone.

The higher values of the heat transfer coefficient in the experiments with a low nozzle-to-chamber diameter ratio are obtained as a result of the formation of stronger recirculation streams and the creation of a more turbulent air flow in the chamber.

## Symbols

$Q_i$ — amount of heat supplied to each calorimeter, $F_i$ — heating area of the calorimeters, $m^2$; $t_{av.a}$ — mean air temperature (arithmetic mean of the temperatures at the cross sections in front of and behind the calorimeter, °K; $t_{0.i}$ — average temperature of water in calorimeter, °K; $G_a$ — flow rate of the air, kg/sec; $g$ — gravity acceleration, m/sec$^2$; $\mu$ — viscosity of air, kg · sec/m$^2$; $G_{rec}$ — amount of air moving in a direction contrary to the main stream.

The All-Union Scientific Research Institute of Thermal Metallurgy, Sverdlovsk

K. Rybáček

# CERTAIN CHARACTERISTICS OF HEAT TRANSFER AND FRICTION IN THE CASE OF LONGITUDINAL FLOW AROUND [FUEL] ELEMENTS

Many experimental studies have dealt with the problem of the heat transfer during longitudinal flow parallel to [fuel] elements and its intensification, in particular with respect to the design of efficient fuel elements for nuclear reactors. The greatest attention has been given to bundles of smooth tubes /6/ or smooth annular channels /1, 14, 25/ while comparatively few papers deal with fuel elements fitted with longitudinal or transverse fins /7, 9, 10/.

As yet, there is no general agreement on the effect of additional geometric factors on the heat transfer in channels of more complicated cross sections, and the results of various experimental studies may sometimes differ by several percent. In most cases, such differences can be attributed to the use of different measurement and evaluation methods, different working media, and the use of the test elements under different conditions. Some of the papers do not present data on the frictional coefficient under experimental conditions. This leads to considerable difficulty in evaluating the various heat-transfer surface elements for practical use.

The design of a test setup is based on the need to reduce the effect of the Prandtl number on the experimental results, and to enable the determination of the overall heat transfer coefficients during turbulent flow round channels of different geometric shapes without measuring the wall temperature.

The working medium used was air at 1-5 atm, which transferred heat to water-cooled tubes with a nearly constant wall temperature maintained over the length of the element. The test setup comprised an open air-circulation loop and a closed cooling-water loop; the latter could be divided (by means of branching pipes) into two separate loops (Figure 1). The compressed air from the compressor plant was treated to remove moisture, heated by electric heaters to 353-433°K, and passed first through the test channel, which was placed between two coaxial settling chambers, and then through a diaphragm and a throttle valve. Mixing cells were built in front of all thermocouple (Ni-CrNi, diameter $0.5 \cdot 10^{-3}$ m) groups mounted on the chambers.

A constant mean temperature (~ 298°K) was maintained in the water loop, which was equipped with a bypass, an open tank (with overflow), and a diaphragm.

The water temperature at the two ends of the measuring section was measured with calorimetric thermometers (1/100°C graduation) placed in countercurrent sockets.

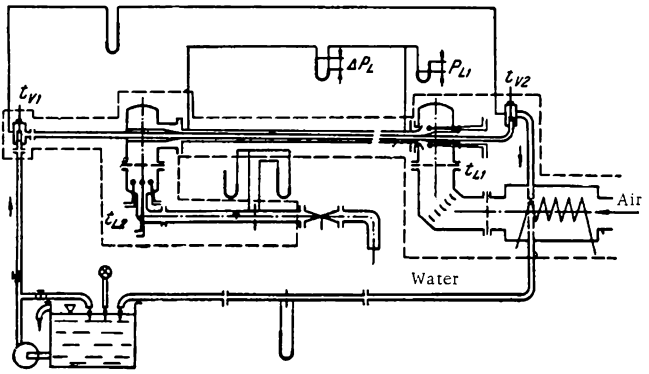


FIGURE 1. Schematic view of the experimental setup with an annular channel fitted with a cooled inner tube.

The whole setup, beginning at the electric heater, was insulated thoroughly.

Extruded copper or brass tubes (variants 10–15) were used as the test elements (Table 1). In the case of variants 5-9 and 16, longitudinal copper fins were inserted in grooves and soldered with tin onto the tube. In the case of the elements with transverse fins (variants 10-15), the fins were machined from a thick-walled tube. The tube bundles were arranged in the form of equilateral triangles. In the case of variant 16, six cooled tubes fitted with fins formed a model bundle for the central measuring element.

Uniform entry conditions were provided for the cylindrical channels in variants 1-14, their entrances being fitted with a quarter-circle suction opening The static air pressure in the channels was measured through apertures 0.0008 m in diameter.

In order to eliminate parasitic effects, the parts of test elements (in variants 1-14) that passed through the settlers were insulated. The tubular channels were fixed in coaxial position by means of spacers.

Since we established only the overall air temperature using the equation

$$T_{Lc} = T_{LSt} + \frac{A\omega_L^2}{2gc_{pL}} [^\circ K], \tag{1}$$

the static temperatures determining the flow conditions and the temperature conditions in the test elements were determined using the equation

$$T_{Lc} - \frac{A}{2gc_p}\left(\frac{R_L G_L}{3600 f_L p_{LSt}}\right)^2 T_{LSt}^2 - T_{LSt} = 0 \tag{2}$$

for higher flow velocities; the effective air temperatures were calculated using the equation

$$T_{Lc} = T_{Lc} - (1-\sigma)\frac{A\omega_L^2}{2gc_{pL}} [^\circ K], \quad \sigma = 0.84. \tag{3}$$

The heat transfer coefficient was

$$k = \frac{Q_v}{\Theta_s F_L} \text{ w/m}^2 \cdot \text{deg}, \tag{4}$$

TABLE 1. Technical details of the tested elements

| Variant | Channel | $D_2$, mm | $D_1$, ($D_z$), mm | $d_h$, m | $\frac{L}{d_h}$ | $n_z$ | $h_z$, mm | $s_z$, mm | $\delta_z$, mm | $\frac{D_2}{D_1}\left(\frac{D_2}{D_z}\right)$ |
|---|---|---|---|---|---|---|---|---|---|---|
| 1 | Cylindrical | 38.0 | — | $D_2 = 0.038$ | 52 | — | — | — | — | — |
| 2 | Annular | 38.0 | 16 | $D_2 - D_1 = 0.022$ | 91 | — | — | — | — | 2.376 |
| 3 | Annular, smooth inner tube | 38.0 | 25 | $D_2 = 0.013$ | 154 | — | — | — | — | 1.52 |
| 4 | " " " " | 38.0 | 32 | $D_2 = 0.006$ | 333 | — | — | — | — | 1.188 |
| 5 | Annular, inner tube fitted with longitudinal fins | 45.8 | 16 | $4f_L / O_h = 0.01658$ | 120 | 12 | 6.22 | — | 1.26 | 2.86 |
| 6 | " | 45.8 | 25 | $4f_L / O_h = 0.01205$ | 166 | 12 | 5.73 | — | 1.05 | 1.832 |
| 7 | " | 38.0 | 16 | $4f_L / O_h = 0.01052$ | 190 | 12 | 6.22 | — | 1.26 | 2.376 |
| 8 | " | 38.0 | 25 | $4f_L / O_h = 0.00681$ | 293 | 12 | 5.73 | — | 1.05 | 1.52 |
| 9 | " | 32.0 | 16 | $4f_L / O_h = 0.00737$ | 271 | 12 | 6.22 | — | 1.26 | 2.0 |
| 10 | Annular channel, fitted with transverse fins | 45.8 | 18(26) | $D_2 - D_z = 0.0198$ | 51 | 434 | 3.99 | 1.43 | 0.88 | (1.76) |
| 11 | " | 38.0 | 18(26) | $D_2 - D_z = 0.012$ | 83 | 434 | 3.99 | 1.43 | 0.88 | (1.46) |
| 12 | Annular, with circular fins | 32.0 | 18(26) | $D_2 - D_z = 0.006$ | 166 | 434 | 3.99 | 1.43 | 0.38 | (1.23) |
| 13 | " | 38.0 | 18.1(26) | $D_2 - D_z = 0.012$ | 166 | 869 | 3.97 | 1.48 | 0.80 | (1.46) |
| 14 | Annular, with helical fins | 38.0 | 18.3(25.5) | $D_2 - D_z = 0.0125$ | 79 | 428 | 3.61 | 1.48 | 0.82 | (1.41) |
| 15 | Bundle of 7 tubes with transverse fins | 112.0 | 18(26.1) | $4f_L / O_h = 0.0265$ | 76 | 869* | 4.05* | 1.41* | 0.8* | — |
| 16 | Bundle of tubes with longitudinal fins | — | 25 | $4f_L / O_h = 0.01369$ | 146 | 12 | 5.73 | — | 1.05 | — |

Note. Variant 1 — cooling to $O_h$; variant 2 — $L = 2$ m, cooled inner tube; variants 5-9 — $L = 2$ m, cooled inner tube; variants 10, 11, 12, 14 — $L = 1$ m; variant 13 — $L = 2$ m, cooled inner tube; variants 15* — continuation of the middle tube, separatory circle with a diameter of 0.074 m; variant 16 — separatory circle of 0.075 m, all tubes cooled.

where

$$\Theta_s = \frac{(t_{Le1} - t_{v2})(t_{Le2} - t_{v1})}{\ln\left(\frac{t_{Le1} - t_{v2}}{t_{Le2} - t_{v1}}\right)};$$

$$k = \frac{1}{\frac{F_L}{\alpha_L F_{L\,red}} + \frac{F_L}{F_v \alpha_v} + R_t} \text{ w/m}^2 \cdot \text{deg}.$$

For finned tubes, $F_{Lred} = F_t + \eta_z F_z$; for smooth elements $F_{L\,red} = F_L$ was determined from the amount of heat $Q_v$ removed by the water.

In the case of two separate water loops (variants 15 and 16), the establishment of identical water-heating conditions in the two branches made it possible to use common values of the temperature differences, taking into account the flow rates.

The heat transfer coefficient for the air was determined by the well-known Wilson method (which was used also in /9/), based on the extrapolation of the function

$$\frac{1}{k_L} - R_t = \frac{1}{\alpha F} + \frac{1}{w_v^{0.8}}, \qquad (5)$$

(measured at constant air parameters and variable water flow rate) to a value of $w_v \to \infty$. The obtained value of $\alpha_L$ may be used to determine (by a reversed procedure) the function $\alpha_v = f(w_v)$. In processing the obtained heat transfer functions in dimensionless terms, we used the main air flow temperature to determine the properties of the substance. In all variants, the equivalent hydraulic diameter was taken as the decisive criterion. The heat transfer coefficient was assumed to have a constant value over the whole expanded surface. In order to reduce the errors caused by the above assumption, the fins were designed in such a way that their efficiency $\eta_z \geq 0.85$ (variant 12).

The frictional coefficient $\xi$, which was determined from the static pressure gradient over the channel length $L$, was calculated by the equation

$$\xi = \frac{\Delta p_L - \frac{G_L}{3600 f_L g}(w_{L2} - w_{L1})}{\frac{L}{d_h}\frac{w_{LS}}{2g}\gamma_{Ls}}, \qquad (6)$$

(where $w_{Ls} = \frac{w_{L1} + w_{L2}}{2}$), taking into account the impulse gradient between the inlet and outlet.

In processing the experimental results, we neglected the effect of radiation (from the noncooled surface) on the heat transfer, which in the least favorable cases (variants 2-4) could be from 0.4 to 2.4%, assuming that the emissivity coefficient $\varepsilon$ has a value of about 0.6. The accuracy of the obtained values of Nu (including parasitic effects) ranged from 3.5 to 5%, while in the case of $\xi$ it was from 2.7 to 4.4%. In most measurements, the discrepancy between the thermal balances for air and water did not exceed 2-4%.

The results of the tests, together with some of the experimental conditions, are listed in Table 2 and Figure 2. In Table 2, the values of Nu are shown as $Nu/Pr^{0.4}$ (assuming that $Pr_L = 0.7 = \text{const.}$).

TABLE 2. Results of the measurements and test conditions

| Variant | $Nu/Pr^{0.4}$ | $10^{-3}$ Re | $\Theta_s$ [°C] | $\xi$ | $10^{-3}$ Re |
|---|---|---|---|---|---|
| 1 | $0.0235\ Re^{0.8}$ (7) | 102—600 | 40.2—48.1 | $0.03537\ Re^{-0.06}$ (7′) | 102—600 |
| 2 | $0.0242\ Re^{0.8}$ (8) | 38—216 | 47.5—112 | $0.335\ Re^{-0.24}$ (8′) | 19.2—100 |
| | | | | $0.12\ Re^{-0.15}$ | 100—333 |
| 3 | $0.0214\ Re^{0.8}$ (9) | 28—189 | 40.4—103 | $0.326\ Re^{-0.24}$ (9′) | 8.4—100 |
| | | | | $0.1156\ Re^{-0.15}$ | 100—282 |
| 4 | $0.0201\ Re^{0.8}$ (10) | 25—124 | 29.3—62.1 | $0.317\ Re^{-0.24}$ (10′) | 7.1—100 |
| | | | | $0.1121\ Re^{-0.15}$ | 100—139 |
| 5 | $0.0167\ Re^{0.8}$ (11) | 40—213 | 38—44.9 | $0.221\ Re^{-0.21}$ (11′) | 10.7—234 |
| 6 | $0.01968\ Re^{0.8}$ (12) | 34—163 | 31.8—39.2 | $0.228\ Re^{-0.21}$ (12′) | 34—189 |
| 7 | $0.18\ Re^{0.8}$ (13) | 44—119 | 35—66.6 | $0.327\ Re^{-0.246}$ (13′) | 6.8—100 |
| | | | | $0.0664\ Re^{-0.108}$ | 100—196 |
| 8 | $0.02023\ Re^{0.8}$ (14) | 54—105 | 36.8—42.9 | $0.27\ Re^{-0.23}$ (14′) | 6.2—171 |
| 9 | $0.0187\ Re^{0.8}$ (15) | 47—157 | 24.5—31.5 | $0.22\ Re^{-0.21}$ (15′) | 11.5—100 |
| | | | | $0.0871\ Re^{-0.13}$ | 100—179 |
| 10 | $0.026\ Re^{0.70}$ (16) | 43—228 | 40—46.8 | $\xi$ in Figure 2 | |
| 11 | $0.01034\ Re^{0.85}$ (17) | 27—100 | 29.7—42.3 | | |
| 12 | $0.00678\ Re^{0.88}$ (18) | 24—81 | 19.4—27.6 | | |
| 13 | $0.01034\ Re^{0.85}$ (19) | 56—100 | 23.5—37.6 | | |
| 14 | $0.0277\ Re^{0.76}$ (20) | 32—160 | 30—42.8 | | |
| 15 | $0.006455\ Re^{0.89}$ (21) | 16—82 | 26.3—32.5 | | |
| 16 | $0.02195\ Re^{0.8}$ (22) | 24—157 | 21.6—33.1 | $0.1766\ Re^{-0.18}$ (22′) | 10—160 |

Control measurements in a channel $38 \cdot 10^{-3}$ m in diameter (variant 1) yielded results that were in good agreement with the conventional relationships as far as Nu is concerned, but the values of $\xi$ corresponded to tubes with a relative roughness of $2 \cdot 10^{4}$ (according to Colebrook).

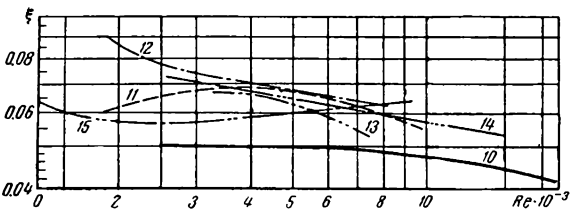


FIGURE 2. Test results under certain test conditions. The numbers next to the curves correspond to the numbers of the variants in Table 1.

In the case of smooth annular channels with $\frac{D_2}{D_1}$ ratios within the range studied (from 1.188 to 2.376), the function $Nu = f(Re_1 D_2/D_1)$ could be described by a general formula

$$Nu = 0.0191\, Re^{0.8}\, Pr^{0.4} \left(\frac{D_2}{D_1}\right)^{0.2715}, \qquad (7)$$

which yields the same dispersion of points (± 5%) for variants 8-10 in Table 2.

The data obtained using equation (7) are in good agreement with the results of /2/ and /11/, and differ from the results of /1/ by no more than 14%. The greatest discrepancy is observed with respect to Quirrenbach's results /14/. In the Re range from $2 \cdot 10^4$ to $10^5$, the discrepancy between calculations by the Roizen /13/ equation and equation (23) reaches 10%.

According to /8/-/10/, the frictional coefficients in smooth annular channels satisfy the equations

$$\xi = 0.312\,\mathrm{Re}^{-0.24}\left(\frac{D_2}{D_1}\right)^{0.09} \quad \text{for } \mathrm{Re} < 10^5,$$
$$\xi = 0.111\,\mathrm{Re}^{-0.15}\left(\frac{D_2}{D_1}\right)^{0.09} \quad \text{for } \mathrm{Re} > 10^5, \tag{7'}$$

which yield values of $\xi$ that are slightly higher (no more than 7.5%) than the values reported in /15/.

For the given number and height of the fins, the simplest equation for the heat transfer on elements with longitudinal fins is

$$\mathrm{Nu} = 0.0226\,\mathrm{Re}^{0.8}\,\mathrm{Pr}^{0.4}\left(\frac{D_2}{D_1}\right)^{-0.261} \tag{8}$$

In more general terms, however, the $D_2/D_1$ ratio is not the decisive parameter. The effect of the distortion of the velocity profile (caused by the channel outside the fins), and the effect of the imperfect radial-flow mixing, are most satisfactorily described by the parameter proposed in /10/:

$$\Phi = \frac{d_{h2}}{d_{h1} + d_{h2}},$$

where $d_{h1}$ or $d_{h2}$ are the hydraulic diameters of the channels formed between the inner tube and the fins, or between the fin edges and the outer channel diameter (the limits of the two cross sections create a circle with a diameter of $D_1 + 2h_z$).

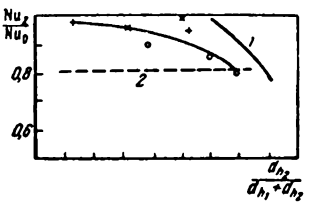


FIGURE 3. Dependence of $\mathrm{Nu}_z/\mathrm{Nu}_0$ on $\frac{d_{h_2}}{d_{h_1} + d_{h_2}}$ according to /10/ and /7/. 1 — according to /10/; 2 — according to /7/.

The relative values of $\mathrm{Nu}/\mathrm{Nu}_0$ for the investigated variants 5-9 (Table 3), where $\mathrm{Nu}_0$ is the actual value for a smooth channel (according to /10/), are shown in Figure 3 as a function of $\Phi$. For the sake of comparison, the same figure contains also the value of $\mathrm{Nu}/\mathrm{Nu}_0$ for a number of fins, given by Fortescue and Hall in /7/. The higher relative values of $\mathrm{Nu}/\mathrm{Nu}_0$ obtained in /10/ may be attributed to the shape and the rounding of the fins at their roots and tips, which caused greater deterioration of the channel flow conditions than occurred in our experiments. On the other hand, the values from /7/, which were based on a larger number of variants, but without more detailed specifications, were somewhat lower.

Good correlation, with maximum deviations of ± 3% , is obtained for the coefficient ξ in the case of variants 5-9. The equation

$$\xi = 0.244\,\mathrm{Re}^{-0.2175} \qquad (8')$$

yields values lower by 16-22% than those given in /7/ for the same cases.

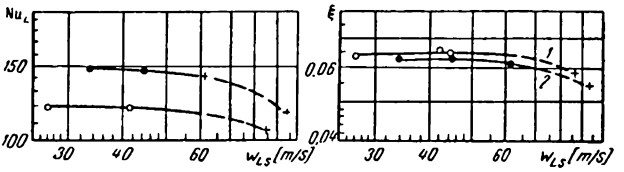


FIGURE 4. Anomalies in the functions Nu = f(Re) and ξ = φ(Re) at:
1 — Re = $7.9 \cdot 10^4$; 2 — Re = $10^5$.

Measurements made on narrower annular channels with longitudinal fins on the inner tube showed anomalies in the functions Nu = f (Re) and ξ=φ (Re) at flow velocities of about 60 m/sec when a certain decrease in Nu and ξ occurred for Re = const. (Figure 4), while no change occurred in the nature of the $\alpha/\xi$ ratio. No such anomaly was observed in variant 10 (Table 3), and the flow peculiarities, which could be attributed to the dynamic effect of the mainstream on the shedding of eddies from the space between the fins, depend also on the proximity of the outer channel wall. A more detailed explanation would require direct optical observation of the flow. The results for tubes with transverse fins shown in Table 3 and Figure 2 are valid at velocities lower than 60 m/sec.

Despite the fact that the values of the exponents of the Reynolds number have a marked dispersion, the experimental points can be described with a maximum dispersion of 15% by using averaging equation

$$\mathrm{Nu} = 0.00628\,\mathrm{Re}^{0.89}\,\mathrm{Pr}^{0.4} \qquad (9)$$

in the range Re = $2 \cdot 10^4$-$10^5$. Equation (9) differs only slightly from equation (5) for a bundle of elements with transverse fins. The fact that equation (9) may be applied to various cases of longitudinal flow around [fuel] elements with such transverse fins (circular and helical) is a justification of the selection of $d_h = 4f/O_h$ as the decisive criterion, assuming that the envelope of the fin edges ($\Phi D_z$) is the basic dimension of finned tubes. For variants 11 and 13, which differ in their channel lengths, the Nusselt number is described by the same equation, while the shapes of the curves describing the changes in ξ differ to a certain extent (Figure 2).

Compared with other published data, our results agree relatively well (deviations of 13-21%) with the relationships reported by Petrovskii et al. /13/, while extrapolation of the well-known Knudsen and Katz equation /9/ yield much (about 140%) higher values of Nu.

The separate equations describing the frictional coefficient ξ in the case of variants 10-15 (Table 1) cannot be combined into a single equation. The reported values are, however, in qualitative agreement with the graphical data of Braun and Knudsen /3/.

It was found that the heat transfer in a bundle of tubes with longitudinal fins is slightly lower than in the case of flow in channels, while the measured resistances are 10-30% higher than the respective values for a smooth channel.

## Symbols

$A$ — the mechanical equivalent of heat; $c_p$ — specific heat at constant pressure, j/kg. deg; $D_1$ — diameter of the tested element, m; $D_2$ — inner diameter of the channel, m; $d_h$ — hydraulic diameter, m; $F$ — surface area, $m^2$; $f$ — flow cross section, $m^2$; $G$ — flow rate, kg/sec; $g$ — acceleration by gravity, $m^2$/sec; $h_z$ — fin height, m; $k$ — heat transfer coefficient, $w/m^2$.deg; $L$ — channel length, m; $n_z$ — number of fins; $O_h$ — channel parameter in contact with the flow, m; $\Delta p$ — static pressure gradient, $n/m^2$; $R$ — thermal resistance, $m^2$.deg/w; $s_z$ — distance between the fins, m; $T$ — absolute temperature, °K; $t$ — temperature, °C; $w$ — flow velocity, m/sec; $\alpha$ — heat transfer coefficient (overall), $w/m^2$.deg; $\gamma$ — specific gravity, $kg/m^3$; $\sigma_z$ — fin thickness, m; $\eta_{iz}$ — thermal efficiency of the fin; $\Theta_s$ — mean logarithmic temperature gradient, deg; $\xi$ — frictional coefficient; $\sigma$ — recovery coefficient.

Subscripts: $c$ — total or overall; $e$ — effective; $L$ — air; red — reduced; $s$ — mean or average; St — static; $t$ — tube; $v$ — water; $z$ — fin; 1, 2 — inlet, outlet, (internal or external).

## Bibliography


1. Averin et al. Teplootdacha pri dvizhenii zhidkosti v kol'tsevykh i shchelevykh kanalakh (Heat Transfer During Fluid Flow in Annular and Slit Channels). — In sbornik: Teploperedacha i teplovoe modelirovanie, Izd. AN SSSR. 1959.
2. Cordier, Bory. Contribution a l'étude de la convection forcée de la chaleur dans les espaces annulaires en vue de l'application au refroidissement des canaux des réacteurs. — Proceedings of the International Conference on the Peaceful Uses of Atomic Energy, Geneva, A. Conf. (15P), 1149. 1956.
3. Braun and Knudsen. Pressure Drop in Annuli-Containing Transverse Fin Tubes. — Chem. Eng. Progress. 1952.
4. Danilov, I.D. and V.E. Keilin. — IFZh, Vol.V, No.9. 1962.
5. Davis. Heat Transfer and Pressure Drop in Annuli. — TASME. 1943.
6. Dingee Chastain. Heat Transfer Parallel Rods in Axial Flow. Reactor Heat Transfer Conference, 1956, N.Y. Viscardi Comp. 1957.
7. Fortescue and Hall. Heat Transfer Experiments on the Fuel Elements. — Journ. Brit. Energy Conf. April, 1957.
8. Inayatov, A.Ya. and M.A. Mikheev. — Teploenergetika, No. 3. 1957.
9. Knudsen and Katz. Heat Transfer and Pressure Drop in Annuli. — Chem. Eng. Progress, No. 10. 1961.

10. Le Foll Gelin, Robert. Échanges thermiques dans les piles à gaz. — Proceedings of the International Conference on the Peaceful Uses of Atomic Energy, A. Conference (15P), 1145. 1958.
11. McAdams, Kennel, and Addoms. Heat Transfer to Superheated Steam at High Pressure. — TASME. May, 1950.
12. Melese. Efficacité d'une silette longitudinale avec variation du coefficient d'échange de couleur lelong de l'ailette. — J. Nuclear Energy 5, 3/4. 1957.
13. Petrovskii, Yu. L., V. G. Fastovskii, and L. I. Roizen. — Khimicheskaya Promyshlennost', No. 6. 1962.
14. Quirrenbach. Wärmeübergang bei turbulenter Strömung in Ringspalten. — Allg. Wärmetechnik, Vol. 9, No. 13. 1961.
15. Rothfus, Monrad, and Senecal. Velocity Distribution and Fluid Friction in Smooth Concentric Annuli. — Ind. Eng. Chemistry. December, 1950.
16. Rothfus, Monrad, and Sikni. Isothermal Skin Friction in Flow through Annular Sections. — Ind. Eng. Chem, No. 5. 1955.

The State Research Institute of Heat Engineering, Prague

V.F. Yudin and L.S. Tokhtarova

# INVESTIGATION ON THE HEAT TRANSFER AND RESISTANCE OF FINNED, STAGGERED BANKS WITH FINS OF DIFFERENT SHAPES

Finned tubes of many different fin shapes are extensively used in gas-liquid heat exchangers. In addition to tubes with wire fins, tubes with stud and disk fins have also been used recently.

In designing new heat exchangers, difficulties arise in connection with the selection of the most effective type of fins and with the adequate arrangement of the tubes in the bank.

Comparative studies on the heat transfer and resistance of finned, staggered banks were carried out at the Central Boiler and Turbine Institute im. I.I. Polzunov in order to determine which type of fin was most efficient; the banks studied were made of tubes with cylindrical studs, flat fins, disk fins, wire fins, and disk fins with zigzag surface roughness imparted by tooth-shaped protuberances.

A detailed study of the effect of the geometric parameters of staggered and in-line finned banks on heat transfer and resistance is reported in /1/. The banks consisted of tubes (Table 1). The range of variation of the relative pitch was

$$S_1/d = 1.7 - 3 \text{ and } S_2/d = 1.2 - 3.$$

Of the 17 bundles studied, the best power-consumption characteristics were obtained in the case of staggered banks having $S_1/d=3$ and $S_2/d = 1.2$. Hence, we studied only staggered banks with relative pitches close to the optimum values.

The experimental setup and procedure are described in detail in /1/.

The heat transfer studies were carried out in an open-type aerodynamic tube by the method of local thermal similarity. Electric heating was used in the measuring tube-calorimeter. The heat flux was in the "wall-to-gas" direction. All the banks investigated consisted of seven rows of tubes.

The temperature of the outer surface of the measuring tube-calorimeter was measured at the roots of the fins, using chromel-alumel thermocouples; this made it possible to calculate the values of the reduced heat transfer coefficient $\alpha_{red}$).

The temperature of the air entering and leaving the bank was measured with a laboratory mercury thermometer with 0.1° scale divisions. The wall temperature ($t_w$) in the different experiments ranged from 358 to 383°K, and the air temperature ($t_a$), from 288 to 298°K.

The heat transfer coefficients were evaluated from the heat load, which was determined from the electrical power consumed to heat the calorimeter.

TABLE 1. Geometric characteristics of the finned surfaces

| Characteristics of finned surface | No. of finned surface | | | | | | | | | | | | | | |
|---|---|---|---|---|---|---|---|---|---|---|---|---|---|---|---|
| | 1 | 2 | 3 | 4 | 5 | 6 | 7 | 8 | 9 | 10 | 11 | 12 | 13 | 14 | 15 |
| Diameter of the basic surface $d$, m | 0.032 | 0.032 | 0.032 | 0.032 | 0.032 | 0.032 | 0.032 | 0.032 | 0.032 | 0.019 | 0.019 | 0.023 | 0.023 | 0.023 | 0.050 |
| Type of fins | trapezoid screw thread $D_н = 50$ $\delta_f = 1.3$ | trapezoid screw thread $D_н = 50$ $\delta_{f.av} = 2.25$ | trapezoid screw thread, with zigzag roughness $D_н = 50$ $\delta_{f.av} = 2$ | trapezoid straight $D_н = 72$ $\delta_{f.av} = 2.25$ | round studs $D_н = 72$ $d_s = 10$ | plate studs $D_н = 72$ $e = 27$ $\delta_{pl} = 2.5$ | round studs $D_н = 50$ $d_s = 5$ | round studs $D_н = 72$ $d_s = 5$ | plate studs $D_н = 72$ $e = 16$ $\delta_{pl} = 2.5$ | wire $D_н = 72$ $d_w = 0.76$ $z = 60$ | cylindrical with screw thread $D_н = 43$ $\delta_f = 1.2$ | $D_н = 47$ $\delta_f = 1.2$ | $D_н = 63$ $\delta_f = 1.2$ | $D_н = 43$ $\delta_{f.av} = 1.7$ VNII-MET-MASH* | smooth tube with diameter 50×3 |
| Method of attaching or producing the fins | Machining | | | Welding | | | Soldering | | | | Machining | | | Rolling | |
| Longitudinal pitch between the fins $t$, m | 0.006 | 0.006 | 0.006 | 0.006 | 0.015 | 0.012 | 0.015 | 0.015 | 0.012 | 0.0075 | 0.005 | 0.005 | 0.005 | 0.0065 | |
| Height of fins $h$, m | 0.009 | 0.009 | 0.009 | 0.020 | 0.020 | 0.020 | 0.009 | 0.020 | 0.020 | 0.0165 | 0.012 | 0.012 | 0.020 | 0.010 | |
| Density of fins $\varphi$ | 5.1 | 5.4 | 5.9 | 12.2 | 5.46 | 6.78 | 2.46 | 4.3 | 7.68 | 11.3 | 9.32 | 8.73 | 16.4 | 5.47 | 1 |

Symbols: $D_н$ — finned surface diameter; $\delta_f$ — fin thickness; $d_s$ — stud diameter; $e$ — plate width; $\delta_{pl}$ — plate thickness; $d_w$ — wire diameter; $z$ — number of loops on the circumference.

* [All-Union Research Institute for the Design of Metallurgical Machines.]

The main tube diameter was taken as the determining linear dimension. The air velocity was determined in the cross section of the contracted bank. The physical characteristics of the air refer to the average air temperature in the bank /2/.

The shapes and geometrical dimensions of the finned tubes studied are listed in Table 1*. The fins were either machined from solid, or attached by welding, soldering, or rolling; there was no thermal resistance between the fin and the tube base.

All tubes and fins were made of plain carbon steel, except tube 10 which was made of brass, with soldered copper wires.

TABLE 2. Characteristics of the investigated staggered banks

| Bank No. | Type of surface and its No. as listed in Table 1 | Relative pitch | | Compactness coefficient $\pi$, $m^2/m^3$ | Ratio of compressed to running cross section $F_{com}/F_r$ |
|---|---|---|---|---|---|
| | | $S_1/d$ | $S_2/d$ | | |
| 1 | Bank with screw-thread disk fins, 1 | 2 | 2 | 122 | 0.434 |
| 2 | Bank with screw-thread trapezoid fins, with toothed surface roughness, 3 | 2 | 2 | 144 | 0.434 |
| 3 | Bank with straight trapezoid disk fins, 4 | 3 | 2 | 188 | 0.505 |
| 4 | Bank with round studs, 5 | 3 | 2 | 84 | 0.383 |
| 5 | Bank with wire fins, 10 | 3 | 2.6 | 223 | 0.593 |
| 6 | Bank with seamless screw-thread disk fins (VNIIMETMASH), 14 | 3.13 | 1.78 | 128 | 0.634 |
| 7 | Bank with plate-shaped fins, 6 | 3 | 2 | 104 | 0.914 |

We studied the heat transfer and drag in seven staggered banks assembled from tubes with various types of fins. The geometric characteristics of the banks are listed in Table 2. For the above seven banks, the calorimeter surface calculations were based on the diameter of the main (supporting) tube.

In addition, we studied the heat transfer in 14 staggered banks assembled from finned tubes (Table 1) with relative pitches $S_1/d = S_2/d = 2$, in which the calorimeters were of variable surface from 2 to 15. The calorimeter was placed in the center of the fifth row. In this case, the calculations were based on the total surface (the surfaces both of the fins and of the supporting tube not occupied by the fins).

Apparently such an investigation could not establish the true value of the heat transfer from every type of surface in the case of banks of tubes with a certain type of fin, but it did yield data on the relative heat transfer rates from the different surfaces.

True values of the heat transfer and drag in the banks could be collected by using banks assembled solely of tubes with the given type of fin, but the production of such tubes is laborious and expensive, and we adopted the above method for the determination of the relative magnitudes of the heat transfer from different surfaces. The tube bank (1) served as a turbulizer grid for the investigated surface (calorimeter).

* The heat transfer and resistance experiments were carried out by E. K. Osipova.

The experimental data on the heat transfer and drag were processed in terms of dimensionless similarity numbers, as the functions:

$$Nu = f(Re) \text{ and } Eu = f(Re).$$

The experimental results of the heat transfer in fourteen staggered banks of finned tubes are shown in Figure 1 (the heat transfer calculations being based on the total surface of the finned tube). For the sake of comparison, the same figure also contains experimental data on a smooth-tube calorimeter (15).

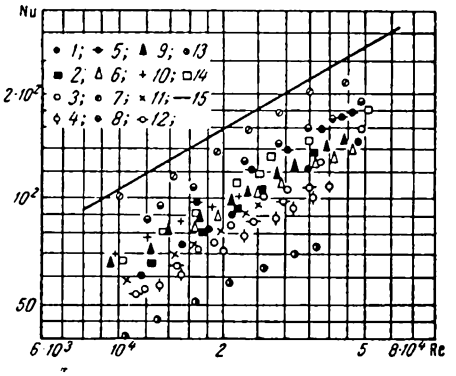


FIGURE 1. Heat transfer from different surfaces.

1-15 — the numbers of finned surfaces as listed in Table 1.

The data in Figure 1 show that higher thermal efficiency was obtained with the smooth tube.

Data on the heat transfer and drag in the seven staggered banks investigated (Table 2) are shown in Figures 2 and 3.

The data in Figure 2 show that the most satisfactory heat transfer was obtained with banks 3 and 5. The heat transfer in bank 5 was 20-25% more intensive than in bank 3. This may be attributed to the effective performance of the wire fins which (in contrast to the other fins) were made of copper, whose thermal conductivity coefficient is 8.5 times that of steel, and also to the smaller diameter of the main supporting tube ($d$ = 0.019 m).

It should be mentioned that the heat transfer in bank 2, where the fin surface was roughened by tooth-shaped protuberances, increased more rapidly than in the remaining banks — the curve was steeper.

The data in Figure 3 show that the greatest drag was observed in bank 5 (made of tubes with wire fins), where the drag was 2.2 times that in bank 3. The lowest drag was observed in bundles 1 and 6, made of tubes with disk fins (VNIIMETMASH).

The comparative evaluation of the thermal characteristics of the different banks was based on the Kirpichev /3/ power coefficient for the evaluation of heat exchangers. In the case of convective surface investigations /4/,

$$E = \frac{\alpha_{red}}{2.69\sigma_1 Eu_0 \rho_s w_f^3}. \qquad (1)$$

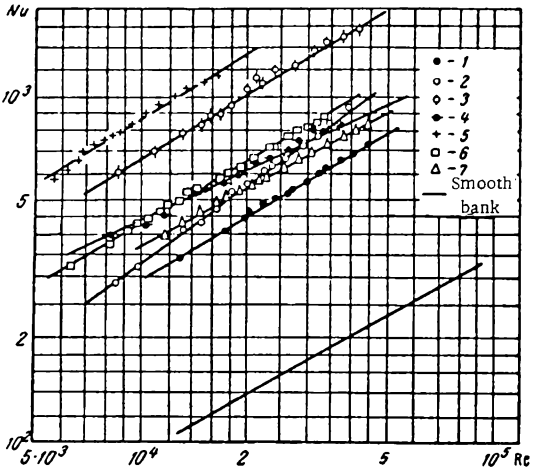


FIGURE 2. Heat transfer in different banks (see Table 2).

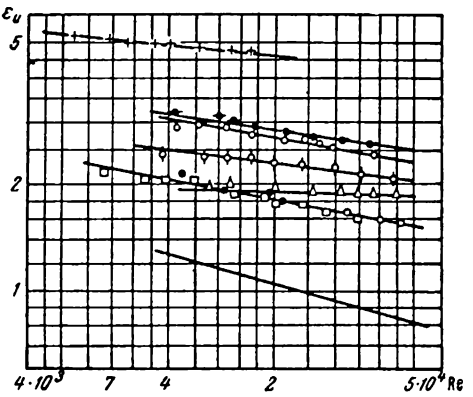


FIGURE 3. Drag in different banks (the symbols used are as in Figure 2).

The power consumption for the pumping of the heat exchange medium (per hour and unit heat transfer surface) was calculated in thermal units, using the equation

$$AN_0 = 2.69\sigma_1 Eu_0 \rho_s w_f^3. \qquad (2)$$

Since the heat transfer coefficients were calculated on the basis of a round tube with a diameter equal to the diameter of the main tube, the power consumption for the pumping of the heat transfer medium was also referred to the total surface of all tubes in the bank, the calculation being based on round tubes of the same diameter.

Graphs for the function $E = f(AN_0)$ were plotted for the different banks on the basis of calculations made using equations (1) and (2).

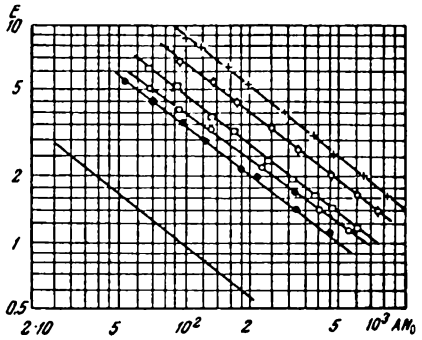


FIGURE 4. Comparison of the thermal characteristics of different banks (the symbols used are as in Figure 2).

The effectiveness coefficient of the $i$-th bank was

$$\psi_i = \frac{E_i}{E_{\text{std}}} = \frac{\alpha_{\text{red}\,i}}{\alpha_{\text{red. std}}}. \tag{3}$$

Bank 1 was taken as the standard.

For instance, at $AN_0^{\circ} = 300$, the effectiveness coefficient of the fifth bank $\psi_5 = \frac{3.7}{1.45} = 2.55$, and of the sixth bank, $\psi_6 = \frac{2}{1.45} = 1.38$.

A graphical presentation of the volume characteristics of seven investigated banks is shown in Figure 5, as the function

$$E_{\text{std}} = \frac{E_i}{\psi_i} = f\left(\frac{AN_0}{\Pi_i \psi_i}\right). \tag{4}$$

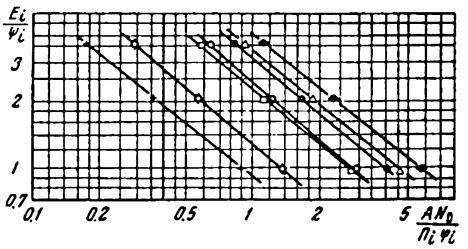


FIGURE 5. Comparison of the volume characteristics of the banks (symbols as in Figure 2).

The intersection of the straight line for $E_{\text{std}}$ = idem with these curves in Figure 5 formed on the abscissa segments with length characterizing the size of the banks for a given (equal) heat transfer and an equal power consumption for the pumping of the heat transfer medium.

The data in the figure show that bank 5 is the smallest and bank 4, the largest.

Of the seven investigated banks, the optimum performance was obtained with bank No. 5, fitted with copper wire fins. Bank No. 3 (VNIITMETMASH-fins), was the best among the banks made of steel. It is known, however, that the thermal characteristics and the size of the banks are determined by the tube diameter, the geometric dimensions of the fins, the material they are made of, and the relative spacing of the tubes in the bank; hence, any of the finned surfaces could be adapted to yield the same performance.

The data in Figure 1 show that the efficiency of all finned tubes (with various types of fins) was lower than that of the smooth tube. The layer-by-layer separation of experimental points was caused, firstly, by differences in the fin height and thickness, and secondly, by differences in the influences of fin performance on the total surface effectiveness due to differences in the fin density and, in the case of the surface with copper wire fins (No. 10), to differences in the thermal conductivity of the fins.

The tube having round studs (No. 7) of $d_s = 0.005$ m and $h = 0.009$ m was the most effective of the finned tubes investigated. The same surface had the lowest fin density, $\varphi = 2.46$. In the range of Re numbers investigated, the surface fins performed very efficiently and since their density coefficient was small, their performance had little effect on the performance of the surface as a whole, the experimental points lying close to those for a smooth tube.

The lowest thermal efficiency was observed in the case of surface No. 13, with screw-thread cylindrical fins with $\delta_f = 1.2$ mm, $h = 0.020$ m, and $\varphi = 16.4$. The thin high fins on that surface were not very efficient, and since the fin density coefficient was large ($\varphi = 16.4$), their performance had a strong effect on the overall performance of the whole surface.

We should mention the efficiency of surface No. 10, which had wire fins of $d_{red} = 0.00076$ m, $h = 0.0165$ m, and $\varphi = 11.3$. In spite of the high density coefficient and the considerable height of the fins, the efficiency of the surface was relatively high. This should be attributed mostly to the small diameter of the tube ($d = 0.019$ m). Unlike all the other fins, those on surface No. 10 were made of copper (having a thermal conductivity coefficient $\lambda = 330$ w/m.deg), and as a result, they were very efficient in spite of their considerable height ($h = 0.0165$ m).

In order to determine the effect of the fin shape on heat transfer, it is necessary to carry out experiments with calorimeters having fins of different shapes. The calorimeters must have fins of the same density, $\varphi$, thickness, and height, and must be made of the same material on tubes of the same diameter.

The production of such calorimeters is quite complicated. Hence we studied heat transfer in calorimeters with surfaces Nos. 1-14 (Table 1). In order to establish the effect of the fin shape on heat transfer, we introduced a correction for the efficiency of the fin. The efficiency of different fins $E$ was determined as a function of the parameters $\beta h$ and $\frac{D}{d}$ using a nomograph for round fins on a cylindrical base, which at first approximation gives satisfactory accuracy. Here

$$\beta = \sqrt{\frac{2\alpha_c \psi}{\delta_f \lambda_{..}}}. \qquad (5)$$

In order to eliminate the need for calculations by the method of successive approximations, we plotted an auxiliary graph for the function

$\alpha_{red}=f(\alpha_c)$, for all finned surfaces with different values of $\alpha_c$. The values of the reduced heat transfer coefficients were calculated by the equation

$$\alpha_{red}=0.85\alpha_c\left(\frac{H_f}{H}E+\frac{H_{bt}}{H}\right). \quad (6)$$

Using the auxiliary graph and the experimental values of $\alpha_{red}$ for all surfaces, we found the corresponding values of $\alpha_c$, and using equation (5), we calculated the values of $\beta$. The efficiency of the fins was then determined with the aid of the nomograph, as described above.

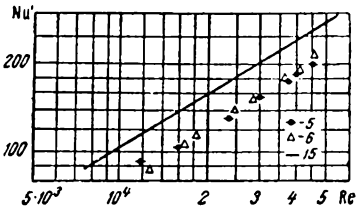


FIGURE 6. Effect of the fin shape on heat transfer.

By correcting the experimental values of Nu for the fin efficiency, it was possible to eliminate (to first approximation) the effects of the different fin heights, thicknesses, and metals of which they were made, i.e., to establish the effect of fin shape on the heat transfer ($Nu = f(Re)$).

It was impossible to eliminate completely the layer-by-layer separation of experimental points for the different surfaces because of the great differences in the fin density ($\varphi = 2.46$-$12.2$) and the heights ($h = 0.009$-$0.020$ m) of the investigated calorimeters. The correction for fin efficiency was introduced into the overall value of the reduced heat transfer coefficient, which refers both to the fin performances and to the performance of the bearing-tube areas not occupied by fins. Using the corrected values of Nu', we plotted a graph for the function $Nu' = f(Re)$ (Figure 6) for two surfaces (Nos. 5 and 6) with close finning parameters; in the case of surface No. 5, $h = 0.020$ m and $\varphi = 5.46$, and in the case of surface No. 6, $h = 0.020$ m and $\varphi = 6.78$. Surface No. 5 was fitted with round stud fins, while surface No. 6 was fitted with plate studs.

Despite the considerable differences in the shapes of the fins (and thus, in the nature of flow around them), the heat transfer on these surfaces was virtually the same. This leads to the conclusion that the fin shape has no substantial effect on the heat transfer process. Thus, the selection of the type of surface for a heat exchanger should be based on the facilities for production of finned tubes and the reliability of the heat exchanger.

The production of tubes with round and plate studs and with wire fins is rather complex and expensive. Hence, it is worthwhile to base the design of heat exchangers on tubes with seamless disk fins (VNIIMETMASH), since they are produced by rolling smooth tubes. The same conclusion was reached also by V. M. Antuf'ev /4/.

## Symbols

$\alpha_{red}$ – reduced heat transfer coefficient calculated on the basis of a smooth tube of diameter equal to that of the main (bearing) tube; $\sigma_1=\frac{S_1}{d}$ relative pitch in the transverse direction; $S_1$ — transverse pitch of

the tubes in the bank; $d$ — diameter of the main bearing tube; $\mathrm{Eu}_0 = \frac{\mathrm{Eu}}{m}$ — Euler number calculated for the flowing stream and referred to one row in the bank (in the direction of flow) $m$; $\rho_s$ — stream density; $w_f$ — flow velocity; $\Pi_i$ — compactness coefficient of the $i$-th bank; $\alpha_c$ — convective heat transfer coefficient; $\psi$ — constant accounting for the nonuniform distribution of $\alpha_c$ over the fin surface (it is assumed that it has a value of 0.85 for all fins); $\delta_f$ — mean fin thickness; $\lambda$ — thermal conductivity coefficient of the structural metal of the fins; $H_f$ — fin surface area; $H_{bt}$ — surface area of the bearing tube sections not occupied by fins; $H = H_p + H_{bt}$ — total exterior surface of the tubes with the fins.

Bibliography


1. Yudin, V.F. and L.S. Tokhtarova. — Energomashinostroenie, No. 1. 1964.
2. Vargaftik, N.B. Spravochnik "Teplofizicheskie Svoistva Veshchestva" (Handbook of the Thermal-Physical Properties of Materials). — Gosenergoizdat. 1956.
3. Kirpichev, M.V. O naivygodneshei forme poverkhnosti nagreva (Optimal Shape of Heating Surfaces). — Izv. ENINa im. Krzhizhanovskii, Vol. 12. 1944.
4. Antuf'ev, V.M. — Energomashinostroenie, No. 2. 1961.



The Central Boiler and Turbine Inst.
im. I.I. Polzunov

I. Vampola

# GENERALIZATION OF THE LAWS GOVERNING HEAT TRANSFER AND PRESSURE DROP DURING TRANSVERSE FLOW OF GASES IN FINNED TUBE BANKS

The derivation of general laws for the heat transfer coefficients during flow in contact with devices such as finned tube banks is outside the scope of theoretical analyses based on physical calculations. Hence, it is necessary to base the derivation of such laws strictly on experimental data.

In spite of the fact that finned tubes are widely used in technology, the published data are insufficient for the determination of the heat transfer and drag coefficients for arbitrary distribution of the transfer surface. This is due to the large number of variable parameters which complicate the solution of the problem. Thus, every design of a new type of finned tube requires rather extensive measurements involving large expenditure, especially for the determination of the optimum dimensions and distribution of the fins.

A series of measurements, the interpretation of which made it possible to derive some fairly accurate general laws, were carried out at the State Research Institute of Heat Engineering (SVUTT). The results make it possible to determine the optimum fin dimensions for various applications.

When a gas flows in contact with a bank of tubes, the total amount of heat transferred is equal to the sum of the heat transferred by radiation and convection. In the case of fins spaced at a small pitch, the complex radiation pattern may be replaced by the radiation from the exterior surface of the heat exchanger to the surrounding channel walls. Since the ratio of exterior surface to total transfer surface is negligibly small, it is possible to ignore the contribution of radiation to the heat flux; at gas temperatures up to 100°C, the error caused by this simplification does not usually exceed 1%. In the case of thin-walled tubes, the main equation for the amount of transferred heat is as follows:

$$Q = \frac{1}{\frac{1}{\alpha_L} + \frac{F_L}{F_v}\left(\frac{1}{\alpha_v} + \frac{\alpha_t}{\lambda_t}\right)} F_L \vartheta_s, \qquad (1)$$

where $\alpha_L$ is the apparent coefficient of heat transfer related to the total outer transfer surface of the heat exchanger and comprises also the effect of the fin material. In order to determine its value, it would be advantageous to carry out a more detailed analysis of the heat transfer conditions on the finned tube.

The amount of heat transferred (in the heat exchanger) by convection equals the sum of the amounts of heat transferred by the fins and the tube surfaces together:

$$Q = \alpha_z F_z \vartheta_z + \alpha_t F_t \vartheta. \tag{2}$$

In practice, it is impossible to determine the partial heat transfer coefficients on the basis of thermal measurements with the heat exchanger. However, analyses of the experimental results indicate that the difference between $\alpha_t$ and $\alpha_z$ usually does not exceed 20%. In view of the small value of $F_t/F_z$, it can be assumed that $\alpha_t = \alpha_z$ and the resulting error in the determination of $\alpha_z$ would not exceed 2%.

If $\frac{\vartheta_z}{\vartheta_t} = \eta_z$, we obtain from equation (2):

$$Q = \alpha_z F_z \vartheta_z \left(\eta_z + \frac{F_t}{F_z}\right) = \alpha_z F_z \vartheta_t (\eta_z + \varkappa), \tag{3}$$

where $\varkappa$ is a constant depending solely on the transfer surface ratio. Since the heat transferred may be written also as

$$Q = \alpha_L F_L \vartheta_t, \tag{4}$$

we obtain from (3) and (4) the following equation for the apparent heat transfer coefficient

$$\alpha_L = \alpha_z \frac{F_z}{F_L} (\eta_z + \varkappa). \tag{5}$$

The $\vartheta_z/\vartheta_t$ ratio is determined from the fin efficiency, which for fins other than round or flat may be calculated using the approximate equations proposed by Schmidt /9/.

According to Barker /1/, the efficiency of thin multilayer fins may be calculated using the same equations, assuming that the mean thermal conductivity is

$$\lambda = \frac{\sum_{i=1}^{i=n} \lambda_i \delta_i}{\delta_z}, \tag{6}$$

where the subscript $i$ refers to the separate layers in the fin.

In designing heat exchangers, it is important to know not only the heat transfer coefficient but also the drag coefficient. Since the results of experimental studies show that in the case of heat exchangers comprising more than two rows of finned tubes, the drag coefficient is virtually independent of the number of rows, the total pressure drop may be described by the equation

$$\Delta p_L = \xi n_t \frac{w_L^2}{2g} \gamma_L + 2\left[\frac{w_{L2}^2}{2g} \gamma_{L2} - \frac{w_{L1}^2}{2g} \gamma_{L1}\right], \tag{7}$$

where $w_L$ and $\gamma_L$ are determined at the mean temperature and the mean gas pressure in the heat exchanger.

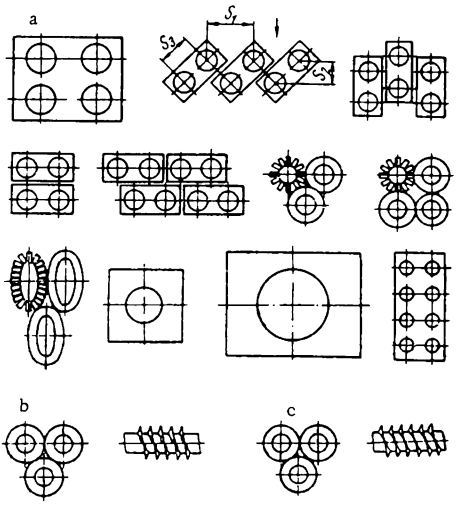


Types of investigated finned tubes.

a — smooth soldered fins; b — fiber-reinforced fins; c — knurled fins.

In order to determine the thermal and drag characteristics, we studied about 30 different finned-tube distribution patterns in the form of experimental banks with a face cross section of 0.320 × 0.320 m. Three types of finned tubes were used: in the first type the main tube was fitted with soldered square and rectangular fins; in the second type the fins were formed by a helical corrugated strip; and in the third case the fins were knurled from a thick-walled tube. A schematic view of the distribution pattern of the finned tubes for which we varied the geometrical dimensions is presented in the figure, and details of the dimensions are reported in /11/. Most measurements were carried out with air pressure close to atmospheric, but in some cases, the finned tubes designated for synchronous hydrogen turbogenerators were tested in media with various hydrogen contents. The tests were carried out with air heated or cooled by water. The maximum temperature of the air was 393°K, and that of water was 353°K. The discrepancies in the thermal balance were within ±2%.

The heat transfer coefficient inside a tube during turbulent flow was determined by calculation, since the heat transfer coefficient on the fins could be calculated by using equations (1) and (5). The drag coefficient was calculated using equation (7) on the basis of the measured pressure drop.

The experimental results were processed in the form of dimensionless functions.

$$\mathrm{Nu} = \frac{\alpha_2 d_e}{\lambda} = m\,\mathrm{Re}^n \text{ and } \xi = p\,\mathrm{Re}^q.$$

We neglected the effect of the Prandtl number, which is approximately constant for gases of the same atomic weight. The boundary layer temperature was taken as the decisive criterion for the thermal conductivity and the kinematic viscosity. Its value was determined from the equation

$$t_a = t_{Ls} \pm \frac{\Theta_z}{2}, \tag{8}$$

where, for slight cooling with water,

$$t_{Ls} = \frac{t_{v1} + t_{v2}}{2} \mp \Theta_s. \tag{9}$$

The gas velocity was determined by taking into account the minimum flow cross section in the exchanger, the arithmetic mean temperatures, and the mean pressure. The equivalent diameter (according to Harrison)

$$d_e = \frac{F_t' d_t + F_z' \sqrt{\frac{F_z'}{2n_z}}}{F_z' + F_t'}, \tag{10}$$

where the transfer surfaces $F_z'$ and $F_t'$ are the surfaces of the respective single tubes and $n_z$ is the number of fins, was taken as the decisive criterion.

The experimental results, supplemented by some data from the literature /2, 7/ (which could be processed by the above method), showed large deviations with respect to the Nusselt number and especially with respect to the drag coefficient. In order to present the results in the form of a single function, we analyzed the effect of the geometric dimensions of the finned tubes, thus deriving equations for a dense distribution with an ideal metallic bond between the fins and the main tube and for banks with more than two finned tubes.

In the case of finned tubes in a staggered bank:

for $\frac{s_1 - d_t}{s_3 - d_t} > 1$

$$\mathrm{Nu} = 0.251\,\mathrm{Re}^{0.67} \left(\frac{s_1 - d_t}{d_t}\right)^{-0.2} \left(\frac{s_1 - d_t}{u}\right)^{-0.2} \left(\frac{s_1 - d_t}{s_3 - d_t}\right)^{0.4}, \tag{11}$$

for $\frac{s_1 - d_t}{s_3 - d_t} \leq 1$

$$\mathrm{Nu} = 0.251\,\mathrm{Re}^{0.67} \left(\frac{s_1 - d_t}{d_t}\right)^{-0.2} \left(\frac{s_1 - d_t}{u} + 1\right)^{-0.2}. \tag{12}$$

The above equations are valid with an accuracy of ±20% for all investigated types of finned tubes over the following ranges: $\mathrm{Re} = 1 \cdot 10^3 - 1 \cdot 10^5$; $d_e = 0.01617 - 0.0341$ m; $\frac{s_1 - d_t}{d_t} = 0.48 - 1.64$; $\frac{s_1 - d_t}{u} + 1 = 1.34 - 25.2$; $\frac{s_1 - d_t}{s_3 - d_t} = 0.45 - 2.53$.

In order to check the observed effect of the geometric dimensions in the case of fins of markedly different shape, the above method was used to process the experimental results of Tulin /10/ for tubes with copper wire fins. The results satisfied (with an accuracy of ±10%) the equation

$$\mathrm{Nu} = 2.147\,\mathrm{Re}^{0.46}\left(\frac{s_1 - d_t}{d_t}\right)^{-0.2}\left(\frac{s_1 - d_t}{u} + 1\right)^{-0.2} \qquad (13)$$

The dimensionless equations derived above, which are valid for heat transfer in turbulent flow regions, are virtually independent of the shape of flat fins, all other conditions being equal. In order to determine the drag coefficient, it is necessary to classify the finned tubes into groups according to the fin shape: smooth fins, parallel fins, and knurled helical fins, helical corrugated fins, and finally, wire fins. The drag coefficients can be calculated with an accuracy of ±20% by the following equations:

smooth fins

$$\xi = 1.463\,\mathrm{Re}^{-0.245}\left(\frac{s_1 - d_t}{u} + 1\right)^{0.7}\left(\frac{s_1 - d_t}{d_t}\right)^{-0.9}\left(\frac{d_e}{d_t}\right)^{0.9}; \qquad (14)$$

corrugated fins formed by deformation of a wound wire

$$\xi = 1.075\mathrm{Re}^{-0.112}\left(\frac{s_1 - d_t}{u} + 1\right)^{0.7}\left(\frac{s_1 - d_t}{d_t}\right)^{-0.9}\left(\frac{d_e}{d_t}\right)^{0.9}; \qquad (15)$$

wire fins

$$\xi = 1.33\mathrm{Re}^{-0.175}\left(\frac{s_1 - d_t}{u} + 1\right)^{0.7}\left(\frac{s_1 - d_t}{d_t}\right)^{-0.9}\left(\frac{d_e}{d_t}\right)^{0.9}. \qquad (16)$$

Tubes with smooth (square or rectangular) fins were tested in banks arrayed in-line, a staggered array being more suitable for tubes with round fins. Despite the rather extensive range of variation of the parameters ($d_e$ = 0.02235 — 0.1612 m, $\frac{s_1 - d_t}{d_t}$ = 0.72 — 1.86, $\frac{s_1 - d_t}{d_t}$ + 1 = = 2.1 — 29.2), we were unable to establish the exact effect of the geometric dimensions on the heat transfer. However, satisfactory agreement between the experimental results could be obtained by employing the equivalent diameter, since the heat transfer satisfies the following equation (with an accuracy of ±20%):

$$\mathrm{Nu} = 0.183\,\mathrm{Re}^{0.63}. \qquad (17)$$

The drag coefficient obeys the following equation

$$\xi = 0.72\,\mathrm{Re}^{-0.245}\left(\frac{s_1 - d_t}{u} + 2\right)^{0.9}\left(\frac{s_1 - d_t}{d_t}\right)^{-0.9}\left(\frac{d_e}{d_t}\right)^{0.9}\left(\frac{s_1 - d_t}{s_2 - d_t}\right)^{-0.1}. \qquad (18)$$

The general equations for the heat transfer and drag coefficient, which are valid over a wide range of values of the variable parameters (and which take into account the effect of those parameters) are a fairly satisfactory expression of the laws governing the phenomena occurring on various types

of fins during turbulent gas flow. The equivalent diameter calculated by means of equation (10) gives good correlation between values, but is not the main factor determining the boundary between turbulent and laminar flows. This is determined by the hydraulic diameter $d_h = 4f/O$ for the narrowest cross section between the tubes. For different finned tubes, the transition flow region fluctuates between $Re^*$ values ($Re^* = \frac{w_L d_h}{\nu}$) of from 500 to 1500. It is obvious that when the equivalent diameter is used (from (10)) it is necessary to state the range of application of the derived equations for each type of finned tube. Thus, it is recommended to limit that range to $Re^* > 1000$. The upper limit of Reynolds numbers could not be attained with the setup we used. It could, however, be assumed that by analogy with smooth tube banks, a similarity region (with constant drag coefficient and a sharper dependence of Nu on Re) would be established at $Re < 1 \cdot 10^5 - 3 \cdot 10^5$.

Since in the equations derived above, the effect of geometric dimensions on the heat transfer does not exceed ±10%, the above equations may be used also to determine the optimum fin dimensions for the specific case under consideration. To this end, it is necessary to compare different heat exchanger designs under similar conditions. Assuming that the front cross section of the heat exchanger and the amount of heat transferred are constant, we should have equal mass flow rates (of the gas) for equal inlet and outlet gas temperatures, so that for an equal tube wall temperature, the evaluation criteria should be based on the power consumed to pump the gas, the heat exchanger volume and weight, and the amount of heat per unit $\frac{Q}{AN}, \frac{Q}{v}, \frac{Q}{G}$.

For the selected tube diameter, the above criteria are functions of the pitch of the fins, the fin thickness, and the fin diameter:

$$\frac{Q}{AN} = f\left(\frac{R}{r_t}, \frac{u}{d_t}, \frac{\delta_z}{d_t}\right); \quad \frac{Q}{v} = \varphi\left(\frac{R}{r_t}, \frac{u}{d_t}, \frac{\delta_z}{d_t}\right);$$

$$\frac{Q}{G} = \Psi\left(\frac{R}{r_t}, \frac{u}{d_t}, \frac{\delta_z}{d_t}\right).$$

At maximum $Q/AN$, the optimum fin dimensions may be determined by solving the system of equations

$$\frac{\partial f}{\partial \frac{R}{r_t}} = \Phi; \quad \frac{\partial f}{\partial \frac{u}{d_t}} = \Phi; \quad \frac{\partial f}{\partial \frac{\delta_z}{\delta_t}} = \Phi,$$

for which the function may have an extremum. The optimum of the function $\Phi$ may be determined in a similar way.

The above method of solution is cumbersome (due to the complexity of the functions) and requires a knowledge of the exact nature of the changes near the extremum; hence, the problem was solved graphically. As a working example, we selected a finned tube with parallel round steel fins mounted in a staggered array on steel tubes having a constant wall thickness of 0.001 m. The calculation was carried out for air at a pressure of $9.8 \cdot 10^4$ n/m$^2$ and 50°C, assuming that the heat transfer coefficient within

the tube was infinitely large. The values of the variable parameters ranged within the following limits: $d_t$ from 0.010 to 0.030 m; $u/d_t$ from 0.1 to 0.4; $\delta_z/d_t$ from 0.005 to 0.05; $R/r_t$ from 1-3; the air velocity before the heat exchanger ranged from 1 to 20 m/sec. The shape of the curves describing the function showed that at the maximum $Q/AN$ the value of $R/r_t$ ranged from 1.6 to 2.2; considering the amount of material used and the small volume of the heat exchangers, it would be advantageous to use smaller values of $R/r_t$ and the value of $R/r_t = 1.8$ may be regarded as the optimum. The distance between the fins should be small, but not smaller than $u/d_t = 0.05$, since a sharp decrease in $Q/AN$ takes place at smaller values. From the standpoint of power consumption, a somewhat higher value of is better at high air velocities, $u/d_t = 0.1$ being regarded as satisfactory.

At maximum $Q/AN$, the optimum fin thickness corresponds to $\delta_z/d_t = 0.02$, while for $Q/G$ , $\delta_z/d_t = 0.005$. Since the changes in $Q/v$ are little affected by $\delta_z/d_t$ at $\delta_z/d_t > 0.01$, we may assume that the optimum value is $\delta_z/d_t = 0.01$. The tube diameter should be as small as possible. Reducing the diameter from 0.020 to 0.010 m causes an ~ 16% decrease in the drag, a 63% decrease in the volume of the heat exchanger, and a 50% decrease in the weight of the finned tubes.

In order to explain the effect of the thermal conductivity of the fins on their optimum dimensions, we carried out analogous calculations for copper fins. The results show that at maximum $Q/AN$ the optimum relative fin dimensions are somewhat higher than in the case of steel fins ($R/r_t = 2-2.5$). In order to simplify the production of finned tubes from different materials we may assume, however, that the above value of $R/r_t$ is satisfactory in the case of copper fins as well, since the decrease in $Q/AN$ is compensated for by an increase in $Q/G$ and a much greater increase in $Q/v$. The optimum fin thickness corresponds to $\delta_z/d_t = 0.005$, and the distance between the fins should be small, but not smaller than $u/d_t = 0.05$.

In order to compare the effect of the arrangement of finned tubes on the main heat exchanger properties we carried out calculations for two heat exchangers made of identical finned tubes with round fins at the optimum $R/r_t = 1.8$, the only difference being the tube arrangement (staggered or in-line). An analysis of the results shows that the [hydraulic] resistance of the heat exchangers was roughly the same, but the volume of the heat exchanger with the in-line tube arrangement was about 43% greater, while the weight of the finned tubes was 25% greater. The difference between the two types of heat exchangers disappears only at higher values of $R/r_t$.

In order to elucidate the effect of square fins on the heat exchanger size we compared two heat exchangers made of finned tubes with round and square fins; the tubes were mounted in an in-line arrangement since a staggered array would lead to differences in the diagonal pitch. The use of square fins is more advantageous since in that case, the heat exchanger resistance is 25% lower, the volume is 1.5% smaller, and the weight is 9% less.

## Symbols

$A$ — the mechanical equivalent of heat; $d$ — diameter; $F$ — heat-transfer surface; $G$ — weight; $k$ — heat-transfer coefficient; $N$ — power consumed

to pump the gas through the heat exchanger; $n$ — number of elements; $\Delta_p$ — pressure difference; $Q$ — amount of heat transferred; $R$ — fin radius; $r$ — radius; $s_1$, $s_2$, $s_3$ — transverse, longitudinal, and diagonal pitch of the finned tubes; $t$ — temperature; $u$ — distance between fins; $v$ — volume; $w$ — velocity; $\alpha$ — heat transfer coefficient (overall); $\gamma$ — specific gravity; $\delta$ — thickness; $\xi$ — drag coefficient; $\eta_z$ — fin efficiency; $\Theta$ — temperature difference; $\lambda$ — thermal conductivity coefficient; $\nu$ — kinematic viscosity.

Subscripts: $e$ — equivalent; $L$ — gas, total surface in contact with the gas; $s$ — mean; $t$ — tube, outer tube surface; $v$ — water, inner tube surface; $z$ — fin.

Bibliography


1. Barker, J.—Nuclear Science and Engineering. No. 3, pp. 300-312. 1958.
2. Dehn, K.—VDI Forschungsheft, No. 342. Ausgabe B. 1931.
3. Gardner, K.A.—TASME, pp. 612-631. November, 1945.
4. Gunter, A.Y. and W.A. Schow.—TASME, pp. 643-660. November, 1945.
5. Harrison, E.—Mechanical World, pp. 33-39, 62-66. January, 1948.
6. Jameson, S.L.—TASME, pp. 633-642. November, 1945.
7. Kays, W.M. and A.L. London. Compact Heat Exchangers.—McGraw-Hill, New York. 1958.
8. Krischer, O.—VDI-Forschungheft 474, Ausgabe B. 1959.
9. Schmidt, Th.E.—Die Wärmeleistung von berippten Oberflächen. C.F. Miller Verlag, Karlsruhe. 1950.
10. Tulin, Ts.N.—Teploenergetika, No. 3, pp. 67-72. 1958.
11. Vampola, J.— Zobecnění závislosti pro určení součinitele přestupu tepla a součinitele odporu při proudění plynu svazkem žebrovaných trubek s příčnými žebry. Výzkumná zpráva SVUTT 61-05002. 1961.
12. VDI Wärmeatlas, Düsseldorf. 1954, 1957.



The State Research Institute of Heat Engineering, Prague

A. I. Mitskevich

# EFFICIENCY OF HEAT TRANSFER SURFACES

Much attention has recently been given to the intensification of heat transfer processes. The extremely large amount of experimental data accumulated necessitates a standardized and well-based generalization. A method for evaluation of the efficiency in convective heat transfer, which can be applied to different surfaces, is proposed in this paper.

In this method, a standard heat transfer surface to which all other surfaces are compared and the heat transfer surface under consideration, both occupying the same construction volumes, are studied at equal power consumptions (for the pumping of the heat transfer medium); the ratio of the amounts of heat transferred at equal temperature gradients (between the heat transfer surface and the medium) is then determined. This ratio will be known below as the efficiency coefficient.

This method is a further development of an idea proposed by Kirpichev /1/, from which it differs only in the introduction of a standard surface for comparison purposes, since the ratio of the amount of heat transferred to the power consumed to pump the heat transfer medium is by itself arbitrary, and being most favorable in the case of large heat exchangers, it does not favor the use of more compact heat exchange equipment despite the modern trend toward such compact units.

An important feature of the method is the fact that the heat transfer surfaces are compared on the basis of equal construction volumes rather than equal surface areas, which eliminates the ambiguity in the interpretation of the experimental results observed when other methods are used /2/.

The efficiency may be determined by analytical calculations if we know the heat transfer and hydraulic resistance functions for the surfaces to be compared.

Thus, if we know the following functions for the given surface:

$$\xi = a_1 \mathrm{Re}^{m_1}, \tag{1}$$

$$\mathrm{St} = \frac{\Delta t_\tau F}{\Delta t_w hL} = a_2 \mathrm{Re}^{m_2} \mathrm{Pr}^{m_3}, \tag{2}$$

the amount of thermal energy transferred per unit construction volume comprising the heat transfer surface would be

$$E_t = \frac{\Delta t_\tau G c_p}{Lf} = \frac{\mathrm{St}\, h}{fF} G c_p \Delta t_w. \tag{3}$$

By writing the flow rate in terms of the Reynolds number

$$G = \mathrm{Re}\,\frac{\mu s}{4}, \tag{4}$$

we obtain from (2), (3), and (4)

$$E_t = \frac{\mathrm{sh}}{4fF}\,\lambda_t a_2\,\mathrm{Re}^{m_t+1}\,\mathrm{Pr}^{m_t+1}\,\Delta, t_w. \tag{5}$$

The power needed to overcome the hydraulic resistance in a unit construction volume occupied by the channel of the heat transfer surface can be represented by the equation

$$E_{\mathrm{fr}} = \frac{G\,\Delta P}{\gamma L f}. \tag{6}$$

which does not take into account the compressibility of the heat transfer medium. Since

$$\Delta P = \xi\,\frac{w^2\gamma}{2}\,\frac{L}{d_h} = \xi\,\frac{w^2\gamma\,sL}{8F} = \xi G^2\,\frac{sL}{8\gamma F^3}, \tag{7}$$

we obtain from (1), (6), and (7)

$$E_{\mathrm{fr}} = \frac{1}{2^9}\,\frac{s^4}{fF^3}\,\frac{\mu^3}{\gamma^2}\,a_1\mathrm{Re}^{m_t+3}. \tag{8}$$

In agreement with the above statement concerning the possibility of comparing different channels from the standpoint of heat transfer efficiency, we use one such channel as a standard. Using the subscript "0" to denote the constants referring to the standard, we obtain from (5) and (8)

$$E_{t0} = \frac{s_0 h_0}{4f_0F_0}\,\lambda_{T0}\,a_{20}\,\mathrm{Re}_0^{m_{t0}+1}\,\mathrm{Pr}_0^{m_{t0}+1}\,\Delta t_{w_0}, \tag{9}$$

$$E_{\mathrm{fr}_0} = \frac{1}{2^9}\,\frac{s_0^4}{f_0F_0^3}\,\frac{\mu_0^3}{\gamma_0^2}\,a_{10}\,\mathrm{Re}^{m_{t0}+3}. \tag{10}$$

From (8) and (10), we determine the relationship between Re and $\mathrm{Re}_0$ for which we would have the same power consumption in pumping the heat transfer medium through a unit volume occupied by the channels in the standard and in the sample to be compared with it:

$$\mathrm{Re} = \left[\frac{s_0^4 fF^3}{s^4 f_0F_0^3}\,\frac{\mu_0^3\gamma^2}{\mu^3\gamma_0^2}\,\frac{a_{10}}{a_1}\right]^{\frac{1}{m_t+3}}\mathrm{Re}^{\frac{m_{t0}+3}{m_t+3}}. \tag{11}$$

By substituting equation (11) in (5), we obtain an expression for the amount of thermal energy withdrawn from a unit construction volume of the sample in the case of equal power consumption in pumping the medium through the

sample and through the standard:

$$E_t = \frac{sh}{4fF}\lambda_\tau a_2\left[\frac{s_0^4 f F^3}{s^4 f_0 F_0^3}\,\frac{\mu_0^3\gamma^2}{\mu^3\gamma_0^2}\,\frac{a_{10}}{a_1}\right]^{\frac{m_2+1}{m_1+3}}\times \\ \times \mathrm{Re}_0^{\frac{m_2+1}{m_1+3}(m_{10}+3)}\,\mathrm{Pr}^{m_3+1}\Delta t_w. \tag{12}$$

The surface efficiency coefficient determines the ratio of the thermal energies transferred to the sample and to the standard at equal power consumptions in pumping the heat transfer medium:

$$\eta = \frac{E_t}{E_{t_0}}. \tag{13}$$

Combining (9), (12), and (13), we obtain

$$\eta = \frac{shf_0F_0}{s_0h_0fF}\,\frac{\lambda_\tau a_2}{\lambda_{\tau_0} a_{20}}\left[\frac{s_0^4 f F^3}{s^4 f_0 F_0^3}\,\frac{\mu_0^3\gamma^2}{\mu^3\gamma_0^2}\,\frac{a_{10}}{a_1}\right]^{\frac{m_2+1}{m_1+3}}\times \\ \times \mathrm{Re}_0^{\frac{(m_2+1)(m_{10}+3)}{m_1+3}-m_{20}-1}\,\frac{\mathrm{Pr}^{m_3+1}}{\mathrm{Pr}_0^{m_{30}+1}}\left[\frac{\Delta t_w}{\Delta t_{w_0}}\right]. \tag{14}$$

Equation (14) may be written in terms of cofactors:

$$\eta = \eta_1\eta_2\eta_3\,\frac{\Delta t_w}{\Delta t_{w_0}}. \tag{15}$$

In the above equation,

$$\eta_1 = \frac{shf_0F_0}{s_0h_0fF}\left[\frac{s_0^4 f F^3}{s^4 f_0 F_0^3}\right]^{\frac{m_2+1}{m_1+3}} \tag{16}$$

is a coefficient accounting primarily for the effect of the geometric parameters of the standard and the sample;

$$\eta_2 = \frac{a_2}{a_{20}}\left(\frac{a_{10}}{a_1}\right)^{\frac{m_2+1}{m_1+3}}\mathrm{Re}_0^{\frac{(m_2+1)(m_{10}+3)}{m_1+3}-m_{20}-1} \tag{17}$$

is a coefficient accounting for the effect of the stream turbulizing;

$$\eta_3 = \frac{\lambda_\tau}{\lambda_{\tau_0}}\left[\frac{\mu_0^3\gamma^2}{\mu^3\gamma_0^2}\right]^{\frac{m_2+1}{m_1+3}}\frac{\mathrm{Pr}^{m_3+1}}{\mathrm{Pr}_0^{m_{30}+1}} \tag{18}$$

is a coefficient accounting for the thermal properties of the heat transfer medium.

Equation (11) established the relationship between the Re numbers at which we need the same power to pump the heat transfer medium through

equal volumes of the standard surface and the compared surface. The ratio of the amounts of heat transferred under these conditions is determined using equation (14).

We should mention that in the case of heat transfer of a complex nature, i. e., when the purely convective heat transfer also involves thermal conductivity, the experimental data on heat transfer should be expressed (according to (3) and (4)) as follows:

$$St = f(Re_{obs}, Pr_{obs}), \tag{19}$$

where

$$Re_{obs} = Re\left(\frac{\lambda_T}{\lambda_W}\right)^{n_1},$$

$$Pr_{obs} = Re\left(\frac{\lambda_T}{\lambda_W}\right)^{n_2}.$$

The values of the exponents $n_1$ and $n_2$ are determined from

$$n_1 = \frac{1-n}{m-n},$$

$$n_2 = \frac{m-1}{m-n},$$

where $m$ and $n$ correspond to the exponents in the equation for a "pure" heat transfer, i. e., for fins with infinitely large thermal conductivity ($St - aRe^m Pr^n$).

If the previous calculations are carried out for the above most general case, we find that equations (11), (16), and (17) remain unchanged, while equation (18) assumes the form

$$\eta_3 = \frac{\lambda_T}{\lambda_{T_0}}\left[\frac{\mu_0^3\gamma^2}{\mu^3\gamma_0^2}\right]^{\frac{m_3+1}{m_1+3}} \frac{Pr^{m_3+1}}{Pr_0^{m_{30}+1}} \frac{\left(\frac{\lambda_T}{\lambda_W}\right)^{n_1m_2+n_2m_3}}{\left(\frac{\lambda_{T_0}}{\lambda_{W_0}}\right)^{n_{10}m_{20}+n_{20}m_{30}}}. \tag{20}$$

Equations (11), (16)-(18), or (11), (16), (17), and (20) make it possible to compare the efficiency of different surfaces tested with different heat transfer media under different flow conditions (longitudinal, transverse, internal, external), with smooth and finned tubes. In all cases, the surface to be compared was characterized by a value of $\eta$, which was a function of the $Re_0$ number of the standard surface. The efficiency coefficient assumes a very simple form in cases in which the compared surfaces are in contact with the same heat exchange medium under the same conditions. In such a case, $\eta$ is a measure of the inherent thermal efficiency of the surfaces.

Another limiting case involves identical surfaces in contact with different heat exchange media. In such a case, the coefficient $\eta$ reveals the effect of the heat exchange medium on the efficiency of heat transfer. Examples of the changes in $\eta$ in such cases are shown in Figures 1 and 2.

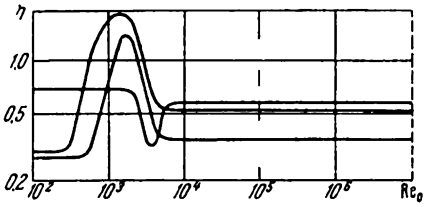


FIGURE 1. Effect of heat exchange media on the efficiency of heat transfer.

For the turbulent region: upper line — helium, middle line — carbon dioxide, and lower line — nitrogen. It is assumed that $\eta = 1$ for hydrogen.

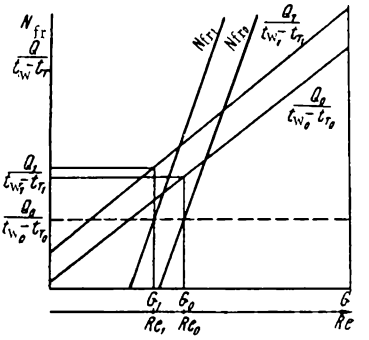


FIGURE 2. Comparison of heating surfaces having the same volumes and working with the same heat transfer medium under the same physical conditions.

The method is extremely simple to apply in cases in which it is necessary to compare the efficiency of surfaces already having the same construction volume (e. g., investigation of the effect of different turbulizer baffles in the same tube), when they are tested with the same heat transfer medium under equal conditions.* In such a case, from the available experimental data in the form of functions $\Delta P = f_1(G)$ and $\frac{Q}{t_w - t_r} = f_2(G)$, we calculate the values of $N_{fr} = \frac{\Delta P G}{\gamma}$ for the compared surfaces and plot a graph for the Reynolds number as a function of the flow rate $G$ (Figure 2).

Afterward, by assigning some value to $N_{fr_0}$ (to which there is a corresponding value of $G_0$ and hence of $Re_0$), we obtain the corresponding values of $\frac{Q}{t_w - t_r}$ for the compared surfaces. The ratio of the last values gives the efficiency coefficient

$$\eta = \frac{Q}{Q_0} \frac{t_{w_0} - t_{r_0}}{t_w - t_r} = f(Re_0). \qquad (21)$$

The above method is very convenient in experiments to find effective surfaces, since a comparison may be made on the basis of four tests (two sets of conditions for each surface).

As a rule, heat exchangers consist of a row of identical elementary channels operating in parallel. The unit volume of such a heat exchanger may be selected by assuming an arbitrary channel length. However, if the heat transfer channel lengths for unit volumes in the compared heat exchangers are assigned arbitrary values, the degree of heating of the heat transfer medium in the channels may be different even at equal temperature gradients between the heat transfer surface and the medium and equal power consumptions for the pumping of the heat transfer medium.

It is common practice to limit the upper or lower temperatures (or both temperatures) of the heat transfer medium. Thus, for a complete

* [The physical conditions with respect to the medium, i.e., pressure, temperature, etc.]

evaluation of different heat transfer surfaces, let us compare the channel lengths required to obtain an equal degree of heating of the heat exchange medium.

The channel length required to obtain a temperature gradient $\Delta t_т$ in the heat transfer medium can be calculated from the equation

$$L = \frac{F}{ha_2} \mathrm{Re}^{-m_2} \mathrm{Pr}^{-m_3} \frac{\Delta t_т}{\Delta t_w} \left(\frac{\lambda_т}{\lambda_w}\right)^{-n_1 m_2 - n_2 m_3} \tag{22}$$

(the above equation is derived by substituting (19) and (2) in (5)). By writing equation (22) for the standard, we obtain the required coefficient in the form

$$\delta = \frac{L}{L} = \delta_1 \delta_2 \delta_3 \frac{\Delta t_т \Delta t_{w_0}}{\Delta t_{т_0} \Delta t_w} = f(\mathrm{Re}_0), \tag{23}$$

where

$$\delta_1 = \frac{Fh_0}{F_0 h} \left[\frac{s_0^4 f F^3}{s^4 f_0 F_0^3}\right]^{-\frac{m_2}{m_1+3}}; \tag{24}$$

$$\delta_2 = \frac{a_{20}}{a_2} \left(\frac{a_{10}}{a_1}\right)^{-\frac{m_2}{m_1+3}} \mathrm{Re}_0^{-m_2 \frac{m_{10}+3}{m_1+3} + n_{20}}; \tag{25}$$

$$\delta_3 = \left(\frac{\mu_0^3 \gamma^2}{\mu^3 \gamma_0^2}\right)^{-\frac{m_2}{m_1+3}} \frac{\mathrm{Pr}^{-m_3}}{\mathrm{Pr}_0^{-m_{30}}} \frac{\left(\frac{\lambda_т}{\lambda_w}\right)^{-n_1 m_2 - n_2 m_3}}{\left(\frac{\lambda_{т_0}}{\lambda_w}\right)^{-n_{10} m_{20} - n_{30} m_{30}}}. \tag{26}$$

If the heat transfer is of a simple nature and does not involve thermal conductivity, we should assume in equations (22) and (26) that $n_1 = n_2 = 0$. If the heat transfer in the standard is also simple, we have $n_{10} = n_{20} = 0$.

In practice, it is convenient to use as the standard a circular tube with internal flow of the heat transfer medium.

## Symbols

$\xi$ — resistance coefficient; $a_1$, $a_2$, $m_1$, $m_2$, $m_3$, $n_1$, $n_2$ — dimensionless coefficients; $\Delta t_т$ — temperature gradient in the heat transfer medium; $\Delta t_w$ — temperature gradient between the heat transfer surface and medium; $F$ — flow cross section, $m^2$; $h$ — perimeter of heat evolution, m; $L$ — length of the heat exchanger, m; $G$ — flow rate of the heat transfer medium, kg/sec; $f$ — structural cross section of the heat exchanger, $m^2$; $\mu$ — dynamic viscosity of the heat transfer medium, sec/$m^2$; $s$ — wetted perimeter, m; $\lambda_т$ — thermal conductivity of the heat transfer medium, w/m°K; $\lambda_w$ — thermal conductivity of the wall material; $d_э$ — hydraulic diameter, m; $\gamma$ — density of the heat transfer medium, kg/$m^3$; $E_{fr}$, $E_f$ friction energy and transferred thermal energy, respectively, w/$m^3$; $\Delta P$ — pressure drop, n/$m^2$; $\eta$ — efficiency coefficient; $N_{fr}$ — power needed to overcome the friction, w; $Q$ — amount of heat, w; $\delta$ — length ratio coefficient.

Bibliography

1. Kirpichev, M.V. — Izv. ENINa, No. 12. 1944.
2. Antuf'ev, V.M. Energomashinostroenie, No. 2. 1961.
3. Fortescue. — Voprosy Yadernoi Energetiki, No. 6. 1957.
4. Borishanskii, V.M. and A.I. Mitskevich. — Energomashinostroenie, No. 8. 1962.

The Central Boiler and Turbine Institute
im. I.I. Polzunov, Leningrad

## *V. CONVECTIVE HEAT TRANSFER UNDER UNSTEADY-STATE CONDITIONS*

Yu. L. Rozenshtok

### THE UNSTEADY LAMINAR THERMAL BOUNDARY LAYER ON A SEMI-INFINITE PLATE IN A VISCOUS LIQUID FLOW

The investigation of unsteady-state effects in the dynamic, thermal, and diffusion laminar boundary layers under forced convection conditions is of ever increasing importance because of their extensive practical application. The usual methods for the approximate solution of the unsteady-state problem (based on the presentation of the velocity and temperature fields as series converging over short or long time periods, as well as on inertia methods) are very cumbersome and do not always yield the correct physical representation of the investigated process in the transition region. Hence, use of the integral method of Karman-Pohlhausen in solving the problem of formation of the boundary layer appears very promising. In many cases, the use of this method to solve dynamic and thermal boundary layer problems yields results with an accuracy sufficient for practical purposes. Thus, a solution of the steady-state problem for heat transfer on an isothermal plate under forced convection conditions /1, 2/, with proper approximation of the velocity and temperature profiles, yields results that are in good agreement with those obtained by an exact solution /3/.

By neglecting the viscous dissipation and the changes in the viscosity and in the thermal characteristics of the fluid (as a function of temperature), we obtain, for a plane unsteady laminar boundary layer for homogeneous flow of the flowing fluid, equations in the following forms:

$$\frac{\partial u}{\partial t} + u\frac{\partial u}{\partial x} + v\frac{\partial u}{\partial y} = \nu\frac{\partial^2 u}{\partial y^2}, \tag{1}$$

$$\frac{\partial T}{\partial t} + u\frac{\partial T}{\partial x} + v\frac{\partial T}{\partial y} = \frac{\nu}{\sigma}\frac{\partial^2 T}{\partial y^2}, \tag{2}$$

$$\frac{\partial u}{\partial x} + \frac{\partial v}{\partial y} = 0, \tag{3}$$

where $\sigma$ is the Prandtl number (the remaining symbols having the conventional meaning). By integration of equations (1) and (3) over the thickness of the dynamic boundary layer $\delta$, and equation (2) over the thickness of the thermal boundary layer $\delta_T$, the Prandtl equation is converted into the Karman integral equations for dimensionless variables $\varphi = u/u_0$ and $\vartheta = \frac{T_w - T}{T_w - T_0}$:

$$\frac{\partial}{\partial t}\int_0^{\delta}(1-\varphi)\,dy + u_0\frac{\partial}{\partial x}\int_0^{\delta}\varphi(1-\varphi)\,dy = \nu\left.\frac{\partial\varphi}{\partial y}\right|_{y=0}, \tag{4}$$

$$\frac{\partial}{\partial t}\int_0^{\delta_T}(1-\vartheta)\,dy + u_0\frac{\partial}{\partial x}\int_0^{\delta_T}\varphi(1-\vartheta)\,dy = \frac{\nu}{\sigma}\left.\frac{\partial\vartheta}{\partial y}\right|_{y=0}, \tag{5}$$

where $u_0$ and $T_0$ are the free flow velocity and temperature and $T_w$ is the wall temperature.

In the case of an isothermal plate in a uniform motion started by impulse from a state of rest, the boundary and initial conditions have the form:

$$\varphi = 0,\ \vartheta = 0 \text{ at } t = 0, \tag{6}$$

$$\varphi = 0,\ \vartheta = 0 \text{ at } x = 0, \tag{7}$$

$$\varphi = 0,\ \vartheta = 0 \text{ at } y = 0, \tag{8}$$

$$\varphi = 1 \text{ at } y = \delta;\ \vartheta = 1 \text{ at } y = \delta_T. \tag{9}$$

We approximate the velocity and temperature fields in the boundary layer by parabolas of the fourth degree:

$$\varphi = 2\eta - 2\eta^3 + \eta^4 \quad (\eta = y/\delta), \tag{10}$$

$$\vartheta = 2\eta_T - 2\eta_T^3 + \eta_T^4 \quad (\eta_T = y/\delta_T). \tag{11}$$

We shall now examine consecutively the cases of $\sigma = 1$, $\sigma > 1$ and $\sigma < 1$.

Prandtl number equal to unity

By substituting (10) in (4), we obtain a differential equation in terms of partial derivatives of the first order:

$$\frac{3}{40\nu}\frac{\partial\psi}{\partial t} + \frac{37u_0}{1260\nu}\frac{\partial\psi}{\partial x} = 1 \quad (\psi = \delta^2). \tag{12}$$

Equation (12) may be solved by various methods (Laplace transforms for one or two variables, the similarity method, but in order to maintain uniformity in subsequent presentation, we shall solve it by the classical method of characteristics /4/. The system of equations for the characteristics of (12) may be written as follows:

$$\frac{1260\nu\,dx}{37u_0} = \frac{40\nu\,dt}{3} = \frac{d\psi}{1}. \tag{13}$$

Taking into account the zero initial conditions, we obtain the following solution of the system (13):

$$\delta = 5.83\sqrt{\frac{\nu x}{u_0}} \quad (x < x_H), \tag{14}$$

$$\delta = 3.65\sqrt{\nu t} \quad (x > x_H). \tag{15}$$

The value of $x_H$ determining the boundary of the dynamic wave is found from the first equation in (13):

$$x_H = 0.392 u_0 t. \tag{16}$$

Thus, as has been mentioned in the analysis of the unsteady dynamic boundary layer /5, 6/ equation (12) characterizes the propagation of the steady state in the velocity profiles.

When $x < x_H$, equation (14) coincides with the solution of the steady-state problem, while for $x > x_H$, equation (15) yields the solution of the Rayleigh problem obtained as a result of omitting the convective term in (1) (at small $t$).

The velocity of the uniform motion of the dynamic wave is

$$W_H = 0.392 u_0. \tag{17}$$

Thus, a steady-velocity profile is established at the point with coordinate $x$ after a time $t$ equal to

$$t = 2.55 \frac{x}{u_0}. \tag{18}$$

Since at $\sigma = 1$ the equations describing the dynamic and thermal boundary layers are equivalent, the above conclusions are also valid for the formation of the thermal boundary layer at $\sigma = 1$. In this particular case, the hydrodynamic wave boundary $x_H$ (which characterizes the rate of stabilization of the hydrodynamic boundary layer) coincides with the thermal wave boundary $x_T$ (which characterizes the rate of stabilization of the thermal boundary layer), i.e., $(x_H = x_T)$. In general, at $\sigma \neq 1$, the rates of establishment of steady temperature and velocity are different. Thus, at $\sigma < 1$, the heat advances with respect to the dynamic wave, while at $\sigma > 1$ the heat wave falls behind the dynamic wave. Thus, in general, there are four different velocity and temperature distribution zones (Figure 1): zone I with steady velocity and temperature profiles; zone II with unsteady velocity and temperature profiles; zone III with a steady velocity profile but fairly unsteady temperature profile; and zone IV with unsteady velocity profile and almost steady temperature profile. It is evident that zones I, II, and III exist at $\sigma > 1$ $(x_H > x_T)$, while zones I, II, and IV exist at $\sigma < 1$ $(x_H < x_T)$. Zones III and IV do not exist at $\sigma = 1$.

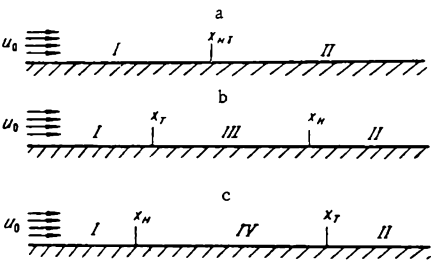


FIGURE 1. Schematic view of the formation of the dynamic and thermal boundary layers at $\sigma = 1$ (a); $\sigma > 1$ (b); and $\sigma < 1$ (c).

Prandtl number greater than unity

In the case of Prandtl numbers greater than unity, the integral condition for a local thermal balance assumes the form

$$\frac{3\delta_T\sigma}{20\nu}\frac{\partial\delta_T}{\partial t}+\frac{u_0\delta_T\sigma}{2\nu}\frac{\partial}{\partial x}\times$$

$$\times\left\{\delta_T\varepsilon\left(\frac{2}{15}-\frac{3}{140}\varepsilon^2+\frac{1}{180}\varepsilon^3\right)\right\}=1\quad\left(\varepsilon=\frac{\delta_T}{\delta}\right). \tag{19}$$

In view of the small changes in the term in parentheses at $0\leqslant\varepsilon\leqslant 1$, it may be replaced by its average values in the above range (which is equal to 1/8),

$$\frac{3\sigma}{40}\frac{\partial\psi_T}{\partial t}+\frac{u_0\sigma\varepsilon}{32\nu}\frac{\partial\psi_T}{\partial x}+\frac{u_0\sigma\psi_T}{16\nu}\frac{\partial\varepsilon}{\partial x}=1\quad(\psi_T=\delta_T^2). \tag{20}$$

The system of characteristics for equation (20) is written in the form

$$\frac{32\nu\,dx}{u_0\sigma\varepsilon}=\frac{40\nu\,dt}{3\sigma}=\frac{d\psi_T}{1-\dfrac{u_0\sigma\psi_T}{16\nu}\dfrac{\partial\varepsilon}{\partial x}}. \tag{21}$$

The system (21) is decomposed into three equations:

$$\frac{dx_T}{dt}=0.416u_0\varepsilon, \tag{22}$$

$$\frac{d\psi_T}{dx}+2\psi_T\frac{\partial}{\partial x}\ln\varepsilon=\frac{32\nu}{u_0\sigma\varepsilon}\quad(x<x_T), \tag{23}$$

$$\frac{d\psi_T}{dt}+\frac{5}{6}u_0\psi_T\frac{\partial\varepsilon}{\partial x}=\frac{40\nu}{3\sigma}\quad(x>x_T). \tag{24}$$

The initial conditions for equations (22)-(24) have the form $x_T(0)=0$; $\psi_T(0,\ t)=0$; $\psi_T(x,\ 0)=0$. Equation (22) is analogous with the corresponding equation (17) and determines (as we shall show below) the velocity of the heat wave front that causes the establishment of a steady, or almost steady, temperature profile at $x<x_T$, while an unsteady temperature profile persists at $x>x_T$. Since for $\sigma>1$ we have $\varepsilon<1$, the velocity of the heat wave front is smaller than the velocity of the dynamic wave front, which is in agreement with the above assumptions. At $\sigma=1$, equations (22) and (17) yield almost identical results. The $\sim 6\%$ difference in the multiplier constants is attributed to the approximations made in the transition from equation (19) to equation (20). In the case discussed here, zone I is defined by the condition $0\leqslant x<x_T$, zone II by the condition $x>x_H$, and zone III by $x_T<x<x_H$. We now analyze the effects in each of the zones separately.

Zone I.

Since a steady velocity profile exists in zone I, in accordance with (14) we have

$$\psi_T=\psi\varepsilon^2=\frac{1260}{37}\frac{\nu x}{u_0}\varepsilon^2. \tag{25}$$

The simultaneous solution of (25) and the differential equation (23), taking into account the zero initial condition, satisfies the expression

$$\epsilon = 0.980\sigma^{-1/3}, \tag{26}$$

which indicates a steady temperature profile in zone I:

$$\delta_T = 5.72 \sqrt{\frac{\nu x}{u_0}}\, \sigma^{-1/3}, \tag{27}$$

and which is in agreement with the known solution of the steady-state problem /2/.

Zone II

In zone II we have an unsteady velocity profile, and from (15) we obtain

$$\psi_T = \frac{40}{3}\, \nu t\, \epsilon^2. \tag{28}$$

The simultaneous solution of (28) and the differential equation (24) is:

$$\epsilon = \sigma^{-1/2}. \tag{29}$$

Thus, a strictly unsteady temperature profile exists in zone II:

$$\delta_T = 3.65 \sqrt{\nu t}\, \sigma^{-1/2}. \tag{30}$$

Zone III

Zone III is the transition zone between I and II. By introducing a new variable $\xi = 0.392\, \frac{u_0 t}{x}$, we obtain from (14) and (24),

$$\epsilon\epsilon'_\xi (1 - 1.063\epsilon\xi) = \frac{1}{2\sigma}. \tag{31}$$

Equation (31) is linear with respect to the independent variable $\xi$. The integral of the above equation for the zero initial conditions is determined by

$$\xi = 2\sigma \exp\{-0.708\sigma\epsilon^3\} \int_0^\epsilon \epsilon \exp\{0.708\sigma\epsilon^3\}\, d\epsilon. \tag{32}$$

At small $\epsilon$ an approximate solution may be obtained by expanding the integral (32) into a series:

$$\xi = \sigma\epsilon^2 - 0.426\sigma^2\epsilon^5 + 0.113\sigma^3\epsilon^8 - \ldots, \tag{33}$$

which at sufficiently small $\epsilon$ yields

$$\epsilon = \sqrt{\frac{\xi}{\sigma}} \tag{34}$$

or

$$\delta_T = 3.65 \sqrt{\frac{\nu t}{\sigma}} . \tag{35}$$

Equation (35) corresponds to the unsteady part of the problem.

We shall now determine the heat transfer in zones I, II, and II:

$$\mathrm{Nu}_x^{(1)} = 0.35 \mathrm{Re}_x^{1/2} \sigma^{1/3}, \tag{36}$$

$$\mathrm{Nu}_x^{(11)} = 0.55 \mathrm{Fo}_x^{-1/2}, \tag{37}$$

$$\mathrm{Nu}_x^{(111)} = 0.55 \mathrm{Fo}_x^{-1/2} \left[ 1 - 0.052 \left( \frac{u_0 t}{x} \right)^{3/2} \sigma^{-1/2} + \ldots \right] . \tag{38}$$

In the above equations $\mathrm{Nu}_x = \frac{\alpha x}{\lambda}$, $\mathrm{Re}_x = \frac{u_0 x}{\nu}$ and $\mathrm{Fo}_x = \frac{\nu t}{\sigma x^2}$ are the local Nusselt, Reynolds, and Fourier numbers, $\alpha$ is the overall heat transfer coefficient, and $\lambda$ is the thermal conductivity coefficient of the fluid.

We now determine the velocity of the heat wave front. At the side of the steady wave end, the expression for $\varepsilon$ would be determined by equation (27). By substituting it in (32) we obtain

$$w_T = 0.407 u_0 \sigma^{-1/3} \tag{39}$$

or

$$t = 2.46 \frac{x}{u_0} \sigma^{1/3} . \tag{40}$$

If the solution of equation (19) is not based on simplifying assumptions, we obtain (by analogy with the above)

$$w_T = \frac{4}{9} \varepsilon u_0 \left( 1 - \frac{9}{56} \varepsilon^2 + \frac{1}{54} \varepsilon^3 \right) . \tag{41}$$

Since an exact solution of the steady-state problem indicates that

$$\varepsilon = \sigma^{-1/3} , \tag{42}$$

we obtain

$$w_T = \frac{4}{9} \sigma^{-1/3} u_0 \left( 1 - \frac{9}{56} \sigma^{-2/3} + \frac{1}{54} \sigma^{-1} \right) . \tag{43}$$

It is obvious that at $\sigma = 1$, equation (43) is transformed into (17).

Equation (40) for the transition time to a steady state is in fairly good agreement with a similar equation derived by Cess /7/, who used a method based on finding an asymptotic solution for short and long periods and the combination of the obtained solutions in a Laplace transform plane. Cess obtained the following expression for the transition time:

$$t = 2.88 \frac{x}{u_0} \sigma^{1/3} . \tag{44}$$

The Goodman /8/ equation for the transition time differs from equations (40) and (44); the numerical value of the constant is about half the value of that in (40). We are of the opinion that the Goodman equation is inaccurate, since it does not yield the true boundary transition at $\sigma = 1$ in accordance with (17). It can be shown that this is caused by the fact that the processes leading to the establishment of a dynamic boundary layer are neglected (in /8/) in solving the problem. Indeed, if we assume at the very beginning that the velocity profile in (20) is steady, we find that the time needed for the establishment of a steady-state temperature field in accordance with the derived system of characteristics would be half the time in (40), i. e., the results would be the same as those of Goodman.

Prandtl number smaller than unity

By taking into account the penetration of the thermal boundary layer into the region of a hydrodynamically unperturbed flow, we obtain

$$\frac{3\delta_T\sigma}{20\nu}\frac{\partial\delta_T}{\partial t}+\frac{3u_0\sigma\delta_T}{20\nu}\frac{\partial}{\partial x}\left\{\delta_T\left(1-\frac{1}{\varepsilon}+\frac{4}{9\varepsilon^2}-\frac{1}{14\varepsilon^4}+\frac{1}{54\varepsilon^5}\right)\right\}=1. \qquad (45)$$

By neglecting the terms in (45) containing $1/\varepsilon$ with an exponent greater than unity, which is valid for sufficiently small Prandtl numbers, we obtain

$$\frac{3\sigma}{40\nu}\frac{\partial\psi_T}{\partial t}+\frac{3u_0\sigma(\varepsilon-1)}{40\nu\varepsilon}\frac{\partial\psi_T}{\partial x}+\frac{3u_0\sigma\psi_T}{20\nu\varepsilon^2}\frac{\partial\varepsilon}{\partial x}=1. \qquad (46)$$

The system of characteristic equations for (46)

$$\frac{40\nu\varepsilon\,dx}{3u_0\sigma(\varepsilon-1)}=\frac{40\nu\,dt}{3\sigma}=\frac{d\psi_T}{1-\frac{3u_0\sigma\psi_T}{20\nu\varepsilon^2}\frac{\partial\varepsilon}{\partial x}}, \qquad (47)$$

is reduced to three ordinary differential equations:

$$\frac{dx_T}{dt}=u_0(1-1/\varepsilon), \qquad (48)$$

$$\frac{d\psi_T}{dx}+\frac{2\psi_T}{\varepsilon(\varepsilon-1)}\frac{\partial\varepsilon}{\partial x}=\frac{40\nu\varepsilon}{3u_0\sigma(\varepsilon-1)}\quad(x<x_T), \qquad (49)$$

$$\frac{d\psi_T}{dt}+\frac{2u_0\psi_T}{\varepsilon^2}\frac{\partial\varepsilon}{\partial x}=\frac{40\nu}{\sigma}\quad(x>x_T). \qquad (50)$$

The initial conditions for equations (48)-(50) are the same as for equations (22)-(24). Since at $\sigma<1$ we have $\varepsilon>1$, equation (48), which determines the velocity of the heat wave front, shows that the heat wave moves in front of the dynamic wave, at least if $\varepsilon>1.7$. We shall show below that a more detailed analysis leads to the conclusion that the above statement is valid for all values of the Prandtl number smaller than unity.

As in the case of $\sigma>1$, let us analyze the dynamic and thermal boundary layers at each of their zones.

Zone I ($0 \leqslant x < x_H$)

From (47) and (14) we obtain for $\sigma \ll 1$ ($\varepsilon \gg 1$)

$$\varepsilon^2 = 0.392\sigma^{-1}, \tag{51}$$

and from there

$$\delta_T = 3.65 \sqrt{\frac{\nu x}{u_0}}\, \sigma^{-1/2}. \tag{52}$$

Equation (52) refers to the steady part of the problem and coincides with the solution of the steady-state problem at small Prandtl numbers /9/.

Zone II ($x > x_T$)

By introducing the variable $\beta = \frac{x}{u_0 t}$, we obtain from (50) and (15) the following expression for zone II (with an unsteady velocity profile), for zero initial conditions:

$$\varepsilon = \sigma^{-1/2}; \tag{53}$$

the above expression yields for the thickness of the thermal boundary layer $\delta_T$ another expression that corresponds to equation (35) and characterizes the unsteady temperature profile.

Zone IV ($x_H < x < x_T$)

Taking into account equations (49) and (14) and condition I, we obtain for zone IV:

$$\varepsilon = \sqrt{\frac{x}{u_0 t \sigma}}, \tag{54}$$

which yields an expression identical to (52) for the value of $\delta_T$. When the higher powers of $\sigma$ in (54) are taken into account, there appear additional terms that characterize the transition processes in the transition zone IV from a strictly unsteady state described by equation (35) to a steady state defined by equation (52).

The heat transfer at $\sigma < 1$ is described by the following functions

$$\mathrm{Nu}_x^{(I)} = 0.55\mathrm{Re}_x^{1/2}\sigma^{1/2}, \tag{55}$$

$$\mathrm{Nu}_x^{(II)} = 0.55\mathrm{Fo}_x^{-1/2}. \tag{56}$$

By calculating the value of $\varepsilon$ from (53) for the unsteady part of the heat wave, we obtain the following approximate equation (in accordance with (48)) for the propagation velocity of the heat wave:

$$W_T = u_0(1 - \sigma^{1/2}). \tag{57}$$

A more accurate analysis of the initial equation (45) yields

$$W_T = u_0\left(1 - \frac{1}{\varepsilon} + \frac{4}{9\varepsilon^2} - \frac{1}{14\varepsilon^4} + \frac{1}{54\varepsilon^5}\right) \tag{58}$$

or, by taking into account equation (53)

$$W_T = u_0 \left(1 - \sigma^{1/2} + \frac{4}{9}\sigma - \frac{1}{14}\sigma^2 + \frac{1}{54}\sigma^{5/2}\right). \qquad (59)$$

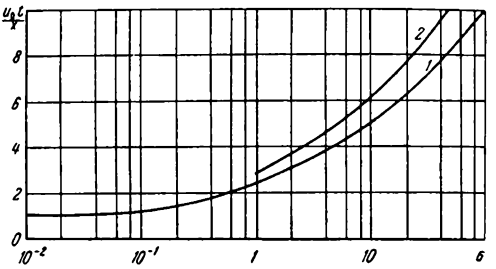


FIGURE 2. Graphical presentation of $\frac{u_0 t}{x}$ as a function of the Prandtl number $\sigma$.

1 — calculated by equations (43) and (59); 2 — according to /7/.

In the case of $\sigma = 1$, equation (59) is transformed into (17). Figure 2 shows values of $\frac{u_0 t}{x}$ calculated by equations (43) and (59) (curve 1), and for the sake of comparison, values of the same parameter calculated by the Cess equation (44).

The conclusion reached on the basis of the above statements is that an a priori assumption of a steady velocity profile during the solution of the problem of the unsteady thermal boundary layer is justified only if $\sigma > 1$, since at $\sigma < 1$ it produces only the steady part of the problem (zone I), the solution of which has been studied to a satisfactory extent. At the same time, as we mentioned above, the integral method yields transition times from an unsteady to a steady state reduced to half their actual value. Hence, the extrapolation of data obtained by the analysis of the unsteady-state problem in (7) and (8) (based on a steady velocity profile at $\sigma < 1$, according to Blasius and Pohlhausen) is not valid. We should mention that an extension of the application of equations of the tyoe of (44) to the case of small $\sigma$ could confirm the statement that at sufficiently small Prandtl numbers, the propagation velocity of the heat wave may be greater than the free stream velocity $u_0$. Moreover, the extension of the longitudinal velocity components into a Blasius series and the use of the first few terms of the series alone (the method used in /7/) can be applied only if $\sigma \gg 1$.

In the case of flow around a plate whose temperature changes with time, a solution may be obtained by using the Duhamel integral, and the solutions derived above may be used as the transition functions.

Bibliography

1. Kruzhilin, G.N. — ZhTF, Vol. 6, No. 3, 1936.
2. Schlichting, H. Theory of the Boundary Layer [Russian translation. 1956].
3. Pohlhausen, E. — ZAMM, Vol. 1:115. 1921.
4. Courant, R. and D. Hilbert. — Methods of Mathematical Physics [Russian translation. 1951.]
5. Targ, S.M. Osnovnye zadachi teorii laminarnykh techenii (Fundamental Problems of the Theory of Laminar Flow). — Gostekhteorizdat. 1951.
6. Dobryshman, E.M. — PMM, Vol. 20, No. 3. 1936.
7. Cess, R.D. — Trans. ASME, Vol. 83, No. 3. 1961.
8. Goodman, T.R. — Trans. ASME, Vol. 84, No. 4. 1962.
9. Kutateladze, S.S. — Osnovy teorii teploobmena (Principles of the Theory of Heat Transfer). — Mashgiz. 1956.

The Leningrad Agrophysical Institute

E.K. Kalinin

# DETERMINATION OF THE STREAM TEMPERATURE AND FRICTION COEFFICIENT IN CHANNELS DURING UNSTEADY NONISOTHERMAL FLOW OF A HEAT-TRANSFER MEDIUM

The energy equation referred to unit volume for one-dimensional unsteady flow in a channel with heat supply may be written as:

$$\rho c_p \frac{\partial T}{\partial t} + \rho c_p u \frac{\partial T}{\partial x} = q_{av}, \tag{1}$$

where $\rho$ is the density; $c_p$ is the specific heat; $t$ is the time; $x$ is a coordinate; $T = T(x, t)$ is the mean temperature in a given cross section; $u = u(x, t)$ is the mean flow rate through the given cross section; and $q_{av}$ is the heat flux referred to unit volume of the flowing heat transfer medium.

The heat generated by dissipation and gas compression work is neglected since it is small in comparison to $q_{av}$ for all heat exchangers. In the case of the flow of gaseous heat transfer media at Mach numbers greater than 0.6-0.7, the thermodynamic temperature in (1) should be replaced by the impact temperature.

By applying (1) to a channel volume element (for a tube with $dv = \frac{\pi d^2}{4} dx$)

$$dv = F dx$$

and introducing the mass flow rate $G = \rho u F$, we obtain

$$G \frac{c_p}{u} \frac{\partial T}{\partial t} + G c_p \frac{\partial T}{\partial x} = U q. \tag{2}$$

In the above equation, $U$ is the heated channel (or tube) perimeter (i.e., $U = \pi d$) and $q$ is the specific heat flux on unit surface, while $q = q(x, t)$ is a known function.

By substituting the variables $X = \frac{x}{d}$; $H_0 = \int_0^t \frac{\bar{u}(t)\, dt}{d}$

and

$$\vartheta = \frac{T}{T_0} \tag{3}$$

we transform equation (2) into

$$\frac{\bar{u}}{u} \frac{\partial \vartheta}{\partial H_0} + \frac{\partial \vartheta}{\partial X} = 4\,\mathrm{St}_0. \tag{4}$$

where $d$ is the characteristic dimension (i. e., the diameter in the case of a tube); $T_0$ is the characteristic temperature ($T_0$ = const.); for a gas [$\rho = \rho(x, t) = \text{var}$].

The average velocity over the channel length is

$$\bar{u}(t) = \frac{1}{l}\int_0^l u(x, t)\, dx.$$

For an incompressible medium (or $\rho = \rho(t)$) with a constant velocity over the channel length, $\bar{u}(t)$ equals the true velocity in the channel at the given moment $u(t)$,

$$\mathrm{St}_0 = f(H_0, X) = \frac{U dq(H_0, X)}{4 T_0 c_p G(H_0)} = \frac{\mathrm{Nu}_0}{\mathrm{Re\,Pr}},$$

where $\mathrm{Nu}_0 = \frac{qd}{\lambda T_0}$ and $\mathrm{Re} = \frac{4G}{\mu U} = \frac{\rho u d_{\mathrm{equ}}}{\mu}$.

Assumptions.

1) $c_p$ = const.

2) For gases, we assume in (4) that $\bar{u}/u \approx 1$. When the velocity over the length changes by a factor of 2, the linear rule gives $\frac{3}{u} \leqslant \frac{\bar{u}}{u} \leqslant \frac{3}{2}$. In the case of heating within the coordinates $\vartheta$, $H_0$, $X$, the above assumption leads to an overestimate of the temperature in the entry section of the channel, and a certain underestimate in the outlet section. However, the reverse transition to $T$, $t$, $x$ coordinates largely compensates for this error. In the case of relatively slow processes, the above assumption is not of importance since for such processes it does not affect $\frac{\partial \vartheta}{\partial H_0} \ll \frac{\partial \vartheta}{\partial X}$ and hence the transition to a steady state.

Applying assumption 2 to gases, and not applying it to those cases in which the velocity does not depend on $X$, we obtain equation (4) in the form

$$\frac{\partial \vartheta}{\partial H_0} + \frac{\partial \vartheta}{\partial X} = 4\,\mathrm{St}_0(H_0, X). \tag{5}$$

Its general solution, derived by the method of characteristics using a system of ordinary equations is

$$\vartheta(H_0, X) = 4\int \mathrm{St}_0(X + a, X)\, dX + f(H_0 - X) \tag{6}$$

or

$$\vartheta(H_0, X) = 4\int \mathrm{St}_0(H_0, H_0 - a)\, dH_0 + f_1(H_0 - X), \tag{7}$$

where $a = H_0 - X$.

The solution of the Cauchy problem for the region $X \leqslant H_0 < \infty$ (at $X = 0$; $\vartheta = \psi(H_0)$ being a prescribed function) is

$$\vartheta(H_0, X) = 4\int_{X - H_0}^{X} \mathrm{St}_0(y + H_0 - X, y)\, dy + \varphi(X - H_0) \tag{8}$$

or

$$\vartheta(H_0, X) = 4\int_0^{H_0} \mathrm{St}_0(y, y - H_0 + X)\,dy + \varphi(X - H_0). \tag{8a}$$

The solution of the Cauchy problem for the region $H_0 \leqslant X \leqslant X_k$ (at $H_0=0$; $\vartheta=\varphi(X)$ being a prescribed function) is

$$\vartheta(H_0, X) = 4\int_0^{X} \mathrm{St}_0(y + H_0 - X, y)\,dy + \psi(H_0 - X) \tag{9}$$

or

$$\vartheta(H_0, X) = 4\int_{H_0 - X}^{H_0} \mathrm{St}_0(y, y - H_0 + X)\,dy + \psi(H_0 - X). \tag{9a}$$

Equations (8), (8a), (9), and (9a) give the solution of the problem.

Example

Let us assume:

1) flow rate $G = G_0 e^{-bt}$; 2) velocity $\bar{u} = u_0 e^{-bt}$; 3) heat flux $q = q_0 e^{-at} \sin \pi \frac{x}{e} =$ $= q_0 e^{-at} \sin \pi \frac{X}{X_k}$; 4) stream temperature at the entrance $\vartheta_0 = A - Be^{-ct}$. In the above equations $G_0$, $u_0$, $q_0 \sin \pi \frac{X}{X_k}$, and $A - B$ are, respectively, the steady values of the flow rate, the velocity, the heat flux, and the temperature at the entry to the channel, at the moment $t = 0 (H_0 = 0)$. It is evident that the temperature distribution over the length of the channel at the moment $H_0 = 0 (t = 0)$ (for a steady flow) would be

$$\vartheta = \varphi(X) = 4\int_0^X \mathrm{St}_1\,dx + (A - B) = 4\int_0^X \frac{U dq_0}{4 T_0 c_p G_0} \sin \pi \frac{X}{X_k}\,dX + A - B$$

or

$$\vartheta = \varphi(x) = 4 c_1 \frac{X_k}{\pi}\left(1 - \cos \pi \frac{X}{X_k}\right) + (A - B), \tag{10}$$

where

$$c_1 = \frac{U dq_0}{4 T_0 c_p G_0}.$$

We have

$$\mathrm{St}_0 = \frac{Ud}{4} \frac{q_0 e^{-at} \sin \pi \frac{X}{X_k}}{T_0 c_p G_0 e^{-bt}} = c_1 e^{(b-a)t} \sin \pi \frac{X}{X_k},$$

but

$$H_0 = \int_0^t \frac{u_0 e^{-bt} dt}{d} = \frac{u_0}{bd}(1 - e^{-bt})$$

and

$$t = -\ln\left|1 - \frac{H_0 bd}{u_0}\right|^{\frac{1}{b}}. \tag{11}$$

From here

$$\mathrm{St}_0 = c_1\left(1 - \frac{H_0 bd}{u_0}\right)^{\frac{a-b}{b}} \sin \pi \frac{X}{X_k}. \tag{12}$$

A solution of the Cauchy problem, yielding the stream temperature profile in the region $H_0 \leqslant X \leqslant X_k$, is obtained by substituting (12) and (10) in (8a):

$$\vartheta(H_0, X) = 4\int_0^{H_0} c_1\left(1 - \frac{y\,bd}{u_0}\right)^{\frac{a-b}{b}} \sin \pi \frac{y - H_0 + X}{X_k}\, dy +$$

$$+ 4c_1 \frac{X_k}{\pi}\left(1 - \cos \pi \frac{X - H_0}{X_k}\right) + (A - B). \tag{13}$$

Since at $X = 0$ (in view of (11)) we have

$$\vartheta = \psi(H_0) = A - Be^{-ct} = A - B\left(1 - \frac{H_0 bd}{u_0}\right)^{\frac{c}{b}},$$

by substituting (12) in (9) we obtain the following expression for the region $X \leqslant H_0 < \infty$:

$$\vartheta = (H_0, X) = 4c_1 \int_0^X \left[1 - \frac{(y + H_0 - X)\, bd}{u_0}\right]^{\frac{a-b}{b}} \sin \pi \frac{y}{X_k}\, dy +$$

$$+ A - B\left[1 - \frac{(H_0 - X)\, bd}{u_0}\right]^{\frac{c}{b}}. \tag{14}$$

We shall see below that a relatively simple solution exists even in the case of simultaneous change in several of the parameters.

The Navier-Stokes equation

$$\rho \frac{d\vec{w}}{dt} = \vec{F} - \operatorname{grad} P + \frac{2}{3} \operatorname{grad} \mu \operatorname{div} \vec{w} + 2 \operatorname{div} \mu \operatorname{def} \vec{w},$$

(where $\vec{F}$ are the mass forces and def $\vec{w}$ is the deformation velocities tensor) may, by neglecting the mass forces, be written in the following form:

$$\rho \frac{d\vec{w}}{dt} = -(1 - \delta) \operatorname{grad} P. \tag{15}$$

From there

$$\delta \operatorname{grad} P = \frac{2}{3} \operatorname{grad} \mu \operatorname{div} \vec{w} + 2 \operatorname{div} \mu \operatorname{def} \vec{w}.$$

Thus, $\delta = \delta(x, y, z, t)$ is that part of the pressure gradient that is consumed as work against the viscosity force, while $(1 - \delta)$ is the part (of the pressure gradient) determined by the unsteady and the nonisothermal state of the flow of heat-transfer medium.

In the case of one-dimensional flow in a channel along the axis, equation (15) assumes the form

$$\rho \frac{\partial u}{\partial t} + u \rho \frac{\partial u}{\partial x} = -(1 - \delta) \frac{\partial P}{\partial x}, \tag{15a}$$

where $\delta = \delta(x, t)$.

By applying (15a) to a channel volume element $dv = Fdx$

$$\frac{G}{u} \frac{\partial u}{\partial t} + G \frac{\partial u}{\partial x} = (1 - \delta) \frac{\partial P}{\partial x} F. \tag{15b}$$

Substitution of the values of

$$X = \frac{x}{d}, \quad H_0 = \int_0^t \frac{\bar{u}(t)\, dt}{d},$$

where

$$\bar{u}(t) = \frac{1}{l} \int_0^l u(x, t)\, dx,$$

transforms (15b) into

$$\frac{\bar{u}}{u} \frac{\partial u}{\partial H_0} + \frac{\partial u}{\partial X} = -(1 - \delta) \frac{\partial P}{\partial X} \frac{F}{G}.$$

In the case of a heat transfer medium with $\rho = \rho(t)$, we always have $u(x, t) = u(t) = \bar{u}(t)$; for gases this will be accepted as an assumption. Then

$$\frac{\partial u}{\partial H_0} + \frac{\partial u}{\partial x} = -(1 - \delta) \frac{\partial P}{\partial x} \frac{F}{G}. \tag{16}$$

By definition, the drag coefficient is

$$\xi(x, t) = -\frac{\delta(x, t) \dfrac{\partial P}{\partial x}}{\rho u^2 / 2 d} \tag{17}$$

so since

$$\frac{\partial P}{\partial x} = \frac{1}{d} \frac{\partial P}{\partial X},$$

we obtain

$$\xi(H_0, X) = -\frac{\delta \dfrac{\partial P}{\partial X}}{\rho u^2 / 2}. \tag{17a}$$

In the above equation, $\delta$, $P$, $\rho$ and $u$ are functions of $H_0$ and $X$. Substituting

the value of $\delta \frac{\partial P}{\partial X}$ from (17a) in (16) we obtain

$$\frac{\partial u}{\partial H_0} + \frac{\partial u}{\partial X} = -\frac{\partial P}{\partial X}\frac{F}{G} - \frac{u}{2}\xi. \tag{18}$$

The solution of (18) is analogous to that of (5). For the region $H_0 \leqslant X \leqslant X_k$, the Cauchy problem $[H_0 = 0;\ u = \varphi_1(x)]$ is

$$u(H_0, X) = -\int_0^{H_0} \frac{\partial P(y, y-a)}{\partial y}\frac{F}{G(y)}\,dy - \int_0^{H_0} \frac{u(y, y-a)}{2} \times$$
$$\times\, \xi(y, y-a)\,dy + \varphi_1(X - H_0). \tag{19}$$

By analogy, for the region $X \leqslant H_0 < \infty$, the Cauchy problem $[X = 0;\ u = \psi_1(H_0)]$ is

$$u(H_0, X) = -\int_0^{X} \frac{\partial P(y+a, y)}{\partial y}\frac{F\,dy}{G(y+a)} - \int_0^{X} \frac{u(y+a, y)}{2} \times$$
$$\times\, \xi(y+a, y)\,dy + \psi_1(H_0 - X). \tag{20}$$

In (19) and (20), $a = H_0 - X$.

From (20), by applying the generalized theorem on the mean value and by integrating from 0 to $X = X_k = l/d$, we obtain

$$u(H_0, X_k) - \psi_1(H_0 - X_k) = -\frac{F}{G(H_0)}[P(H_0, X_k) - P(H_0 - X_k, 0)] -$$
$$-\,\bar{u}(H_0)\frac{X_k}{2}\bar{\xi}(H_0), \tag{21}$$

where $\psi_1(H_0 - X_k) = u(H_0 - X_k, 0)$ is the entry velocity at the moment $H_0 - X_k$; $P(H_0, X_k)$ is the pressure at the channel end at the moment $H_0$; $P(H_0 - X_k, 0)$ is the pressure at the entry, at the moment $H_0 - X_k$ ($X_k$ being the time of passage of a particle through the whole channel); $\bar{G}(H_0) = G(\bar{X} + H_0 - X_k)$ is the mean flow rate during a time interval $[H_0 - X_k, H_0]$; $\bar{u}(H_0) = u(\bar{X} + H_0 - X_k, \bar{X})$ is the mean integral velocity over the length $[0, X_k]$ averaged over the time interval $[H_0 - X_k, H_0]$, since $0 \leqslant \bar{X} \leqslant X$.

From equation (21), we derive an expression for the mean (over the length) drag coefficient $\bar{\xi}(H_0) = \xi(\bar{X} + H_0 - X_k, \bar{X})$ averaged over the time interval $[H_0 - X_k, H_0]$:

$$\bar{\xi}(H_0) = \frac{P(H_0 - X_k, 0) - P(H_0, X_k)}{\bar{G}(H_0)\,\bar{u}(H_0)}\frac{2F}{X_k} + \frac{u(H_0 - X_k, 0) - u(H_0, X_k)}{\bar{u}(H_0)}\frac{2}{X_k}. \tag{21a}$$

For steady flow at $\frac{\partial u}{\partial H_0} = 0$, we obtain from (18)

$$\bar{\xi} = \frac{P(0) - P(X_k)}{G\bar{u}}\frac{2F}{X_k} + \frac{u(0) - u(X_k)}{\bar{u}}\frac{2}{X_k}. \tag{21b}$$

We shall show below that (21a) is transformed into (21b) if all the terms in (21a) are time independent. Equation (21a) shows that the drag coefficient for the unsteady flow region $X \leqslant H_0 < \infty$ may be calculated relatively easily from the experimental data. The difference between the experiment and the steady-state case is that the same terms must be recorded as a function of time.

For the region of unsteady flow $H_0 \leqslant X \leqslant X_k$, i. e., for the channel cross section $X < X_k$ not yet reached by the particles which at the moment $H_0 = 0$ are at the cross section $X = 0$, we may use the mean steady value of $\bar{\xi}$ for the section $[X - H_0, X_k]$, and equation (21a) for $[0, X - H_0]$.

It is true that by analogy with (21a), we may derive from (19) the following expression for $H_0 \leqslant X \leqslant X_k$:

$$\xi(\tilde{H}_0, \tilde{H}_0 - H_0 + X) = \frac{P(0, X - H_0) - P(H_0, X)}{G(\tilde{H}_0)\, u(\tilde{H}_0, \tilde{H}_0 - H_0 + X)} \frac{2F}{H_0} + \\ + \frac{u(X - H_0, 0) - u(H_0, X)}{u(\tilde{H}_0, \tilde{H}_0 - H_0 + X)} \frac{2}{H_0}, \qquad (19a)$$

where $0 \leqslant \tilde{H}_0 \leqslant H_0$. This is the value of the drag coefficient averaged over the time $[0, H_0]$ and the length $[X - H_0, X]$: it is, however, practically impossible to determine its value from experimental data.

Let us mention that at high flow velocities, the conditions corresponding to $H_0 \leqslant X \leqslant X_k$ change very quickly, and conditions corresponding to $X \leqslant H_0 \leqslant \infty$ are established. Under the conditions of $H_0 \leqslant X \leqslant X_k$, the term $\partial P/\partial y$ (and hence $\xi$) may change its sign, and the use of the generalized theorem of the mean value in deriving (19a) and (19) is not valid.

In the case of unsteady flow of an incompressible liquid ($\rho$ = const.), the solution of (18) becomes much simpler as the flow velocity depends only on the time, and is constant over the channel length; hence $\partial u/\partial x = 0$. In this case for instance, equation (18) is valid and, without assuming $u(x, t) = u(t) = \bar{u}(t)$, it takes the form

$$\frac{du(H_0)}{dH_0} = -\frac{dP(H_0, X)}{dX} \frac{F}{G(H_0)} - \frac{u(H_0)}{2} \xi(H_0, X). \qquad (18a)$$

Integrating the above equation over the channel length from 0 to $X = X_k = \frac{l}{d}$, we obtain

$$\frac{du(H_0)}{dH_0} X_k = -\frac{F}{G(H_0)} [P(H_0, X_k) - P(H_0, 0)] - \frac{u(H_0)}{2} \int_0^{X_k} \xi(H_0, X)\, dX. \qquad (18b)$$

However, since the mean (over the length) coefficient of friction is

$$\bar{\xi}(H_0) = \frac{1}{X_k} \int_0^{X_k} \xi(H_0, X)\, dX,$$

we obtain from (18b)

$$\bar{\xi}(H_0) = \frac{[P(H_0, 0) - P(H_0, X_k)}{G(H_0)u(H_0)} \frac{2F}{X_k} - \frac{du(H_0)}{dH_0} \frac{2}{u(H_0)} . \qquad (21c)$$

If the velocity changes linearly with time, or if the change is fairly slow with respect to the time taken by a particle to pass through the channel, we have

$$-\frac{du(H_0)}{dH_0} \approx \frac{u(H_0 - X_k) - u(H_0)}{X_k}$$

in which case equation (21c) assumes the form

$$\bar{\xi}(H_0) = \frac{P(H_0, 0) - P(H_0, X_k)}{G(H_0)u(H_0)} \frac{2F}{X_k} + \frac{u(H_0 - X_k) - u(H_0)}{u(H_0)} \frac{2}{X_k} . \qquad (21d)$$

It is easy to see that the above is the particular form of equation (21a) for the case of an incompressible liquid.

Let us write (21c) in terms of the variables $t, x$. Since $H_0 = \int_0^t \frac{u(t)}{d} dt$, $X = \frac{x}{d}$, and $\frac{du(H_0)}{dH_0} = \frac{\frac{du(t)}{dt}}{\frac{dH_0(t)}{dt}} = \frac{du(t)}{dt} \frac{d}{u(t)}$, we obtain

$$\bar{\xi}(t) = \frac{P(t, 0) - P(t, L)}{G(t)u(t)} \frac{2Fd}{L} - \frac{du(t)}{dt} \frac{2d\rho F}{u^2(t)} , \qquad (21e)$$

or, since $G = \rho u F$ and $\rho$ and $F$ are constants, we have

$$\bar{\xi}(t) = \frac{P(t, 0) - P(t, L)}{G^2(t)} \frac{2\rho F^2 d}{4} - \frac{dG(t)}{dt} \frac{2d\rho F}{G^2(t)} . \qquad (21f)$$

If $\bar{\xi}(t)$ is known, the hydraulic pressure losses are determined from (21f):

$$P(t, 0) - P(t, L) = \bar{\xi}(t) \frac{G^2(t)}{2\rho F^2} \frac{L}{d} + \frac{dG(t)}{dt} \frac{L}{F} . \qquad (21g)$$

In cases where mass forces have a marked effect on the hydraulic losses, these may be taken into account in the solution without much difficulty.

In these cases, the right-hand term in equation (18) should be complemented by the term $\vec{F}_x \frac{Fd}{G}$, where $\vec{F}_x$ is the projection of the mass forces vector $\vec{F}$ on the $X$ axis. The solution of (18) with consideration of the above term gives rise to additional terms, namely $\frac{\vec{F}_{x_{av}}(H_0) 2Fd}{G(H_0)\bar{u}(H_0)}$ in equations (21a), (21c), and (21d); $\frac{\vec{F}_{x_{av}} 2Fd}{Gu}$ in (21b); $\frac{\vec{F}_{x_{av}}(t) 2Fd}{G(t)u(t)}$ in (21e); and $[-\vec{F}_{x_{av}}(t)L]$ in (21g). In these terms, $\vec{F}_{x_{av}} = \frac{1}{X} \int_0^X \vec{F}_x dX$.

Bibliography

1. Seigel, R. Heat Transfer for Laminar Flow in Ducts with Arbitrary Time Variations in Wall Temperature. — Trans. ASME, Paper No. 59, ARMW-2.
2. Seigel, R. Transient Heat Transfer for Laminar Slug Flow in Ducts. — Trans. ASME J. of Appl. Mech. March, 1959.
3. Sparrow, E.M. and R. Seigel. Unsteady Turbulent Heat Transfer in Tubes. — Trans. ASME, Paper No. 59, HT-16, pp. 1-9.
4. Bonilla, C.F., J.S. Busch, H.G. Landau, and L.L. Lynn. Formal Heat Transfer Solutions. — Nuclear Science and Engineering, No. 9, pp. 323-331. 1961.

The Moscow Aviation Institute
im. Ordzhonikidze

L. I. Kudryashev and A. A. Smirnov

# ACCOUNTING FOR THE EFFECT OF THERMAL UNSTEADY STATE ON THE COEFFICIENT OF CONVECTIVE HEAT TRANSFER DURING FLOW ROUND SPHERICAL BODIES AT SMALL REYNOLDS NUMBERS

Nusselt /1/ showed that in the case of very small Reynolds numbers, the heat transfer problem could be transformed into a problem of the steady-state thermal conductivity through a sphere of infinite radius, i. e., the problem is reduced to the solution of the following differential equation:

$$\frac{\partial^2 \vartheta}{\partial r_1^2} + \frac{2}{r_1} \frac{\partial \vartheta}{\partial r_1} = 0, \tag{1}$$

where

$$\vartheta = \frac{t - t_\infty}{t_W - t_\infty}; \quad r_1 = \frac{r}{r_0}.$$

In the above equations, $t_W$ is the maximum temperature considered in the problem, $t_\infty$ is the temperature of the surrounding medium, and $r_0$ is the radius of the sphere.

Under boundary conditions

$$r_1 = 1, \quad \vartheta_W = \frac{t - t_\infty}{t_W - t_\infty} = 1, \tag{2}$$

$$r_1 = \infty, \quad \vartheta_W = 0 \tag{2a}$$

the solution of equation (1) is

$$\vartheta = \frac{1}{r_1}. \tag{3}$$

The heat transfer coefficient is determined from the condition

$$-\left(\frac{\partial \vartheta}{\partial r_1}\right)_{r_1=1} = \mathrm{Nu}_{r_0} \vartheta_{r_1=1}, \tag{4}$$

where

$$\mathrm{Nu}_{r_0} = \frac{r_0 \alpha}{\lambda}.$$

From equations (3) and (4), we obtain

$$Nu_{r_0} = 1. \tag{5}$$

Kudryashev /2/ has derived the following solution for the case of heat transfer on a sphere, at small Reynolds numbers:

$$Nu = 2 + 0.388 (Re\, Pr)^{0.5}, \tag{6}$$

in which the diameter of the sphere is taken as the decisive criterion.

In this paper, we shall present a general method for the solution of the prescribed problem, which was used to derive equations for the determination of the coefficient of convective heat transfer, taking into account the effect of the thermal unsteady state. Equations (1) and (2) are particular cases of these general equations.

Under the conditions of rapid unsteady heat transfer processes, solutions (1) and (2) are only approximate, since they do not take into account the effect of the thermal unsteady state on the heat transfer coefficient.

The boundary problem of the heat transfer on a spherical body, taking into account the thermal unsteady state is reduced to the solution of the following differential equation:

$$\frac{\partial \vartheta}{\partial F_0} = \frac{\partial^2 \vartheta}{\partial r_1^2} + \frac{2}{r_1} \frac{\partial \vartheta}{\partial r_1} \tag{7}$$

for the boundary conditions

$$r_1 = 1, \quad \vartheta = \vartheta_w (Fo), \tag{8}$$

$$r_1 = \infty, \quad \vartheta = 0. \tag{8a}$$

The solution of (7) for a simplified boundary condition (8), namely $r_1 = 1$, $\vartheta = \vartheta_w = 1$, is easily obtained by classical methods, and has the form

$$\vartheta = \frac{1}{r_1} \left( 1 - \frac{2}{\sqrt{\pi}} \int_0^{\frac{r_1 - 1}{2\sqrt{Fo}}} e^{-\xi} d\xi \right). \tag{9}$$

By differentiating (9) with respect to $r_1$, and assuming that $r_1 = 1$, we obtain

$$\left( \frac{\partial \vartheta}{\partial r_1} \right)_{r_1 = 1} = -\left( 1 + \frac{1}{\sqrt{\pi Fo}} \right). \tag{10}$$

Substitution of (10) in (4) yields

$$Nu_{r_0} = 1 + \frac{1}{\sqrt{\pi Fo}}. \tag{11}$$

The above solution indicates that even in the most simple case (constant wall temperature), the thermal unsteady state has a marked effect, and solution (11) approximates the classical solution of Nusselt (1) only at very large values of Fo.

It should be mentioned that it is difficult to solve the problem if boundary condition (8a) is retained in the general form.

Hence, we shall suggest here a simplified approach to an approximate solution of sufficient accuracy. The approach is based on the use of integral relations (of the Karman type) for the solution of the problem.

Indeed, by assuming $\vartheta r_1 = u$, equation (7) would be transformed to

$$\frac{\partial u}{\partial \mathrm{Fo}} = \frac{\partial^2 u}{\partial r_1^2}. \tag{12}$$

By introducing the variable $y_1 = r_1 - 1$ we transform equation (12) to

$$\frac{\partial u}{\partial \mathrm{Fo}} = \frac{\partial^2 u}{\partial y_1^2}. \tag{13}$$

By multiplying the two terms of (13) by $dy$ and integrating from 0 to $\delta$, we obtain the integral relation

$$\frac{\partial}{\partial \mathrm{Fo}}\left(\delta_1 \int_0^1 u\, d\eta_1\right) = -a\left(\frac{\partial u}{\partial \eta_1}\right)_{\eta_1=0}, \tag{14}$$

where

$$\delta_1 = \frac{\delta}{r_0}; \quad \eta_1 = \frac{y_1}{\delta_1}.$$

The unknown temperature profile is represented by a polynomial

$$\frac{u}{u_w} = A_0 + A_1\left(\frac{y_1}{\delta_1}\right) + A_2\left(\frac{y_1}{\delta_2}\right)^2. \tag{15}$$

In order to determine the coefficients in the polynomial, we shall use the following apparent conditions:

$$\begin{aligned} &\eta_1 = 0,\ u = u_w(\mathrm{Fo}), \\ &\eta_1 = 1,\ u = 0,\ \frac{\partial u}{\partial \eta_1} = 0. \end{aligned} \tag{16}$$

By satisfying conditions (16), we obtain from (15)

$$\frac{u}{u_w} = 1 - 2\left(\frac{y_1}{\delta_1}\right) + \left(\frac{y_1}{\delta_1}\right)^2. \tag{17}$$

By substituting (17) in (14), we obtain the following differential equation with respect to $\delta_1$:

$$\frac{\partial}{\partial \mathrm{Fo}}(\delta_1 u_w) = \frac{6u_w}{\delta_1}. \tag{18}$$

Integrating the above equation, and taking into account the fact that at Fo = 0 we have $\delta_1 = 0$, we obtain

$$\delta_1 = \sqrt{12\,\mathrm{Fo}}\,\frac{\bar{\vartheta}_w}{\vartheta_w}, \tag{19}$$

where

$$\bar{\vartheta}_w = \left(\frac{\int_0^{\mathrm{Fo}} \vartheta_w^2\, d\,\mathrm{Fo}}{\mathrm{Fo}}\right)^{\frac{1}{2}}; \tag{20}$$

and from (17) we obtain

$$\frac{\vartheta}{\vartheta_w} = \frac{1}{r_1}\left[1 - 2\left(\frac{y_1}{\delta_1}\right) + \left(\frac{y_1}{\delta_1}\right)^2\right]. \tag{21}$$

Equation (21) together with (19) gives an approximate solution of the problem.

By differentiating (21) with respect to $y$ and assuming that $r_1 = 1$, we obtain

$$\left(\frac{\partial \vartheta}{\partial y_1}\right)_{y_1=0} = -\left(\frac{2}{\delta_1} + 1\right)\vartheta_w. \tag{22}$$

By substituting (22) in (4) and taking into account (19), we find that

$$\mathrm{Nu}_{r_0} = 1 + \frac{1}{\sqrt{3\,\mathrm{Fo}}}\,\frac{\vartheta_w}{\vartheta_w}. \tag{23}$$

In the particular case of $\vartheta_w = 1$, equation (23) assumes the form

$$\mathrm{Nu}_{r_0} = 1 + \frac{1}{\sqrt{3\,\mathrm{Fo}}}. \tag{24}$$

A comparison of (24) with (11) indicates a satisfactory agreement between the exact and approximate solutions.

We now analyze the more general problem of the effect of the thermal unsteady state when convective heat transfer takes place; this is defined approximately by the following differential equation:

$$\frac{\partial \vartheta}{\partial\,\mathrm{Fo}} + \mathrm{Pe}_\infty \bar{W}_{1s}\frac{\partial \vartheta}{\partial s_1} = \frac{\partial^2 \vartheta}{\partial r_1^2} + \frac{2}{r_1}\,\frac{\partial \vartheta}{\partial r_1}, \tag{25}$$

where

$$\mathrm{Pe}_\infty = \frac{w_\infty r_0}{\nu};\quad s_1 = \frac{s}{r_0};\quad \bar{W}_{1s} = \frac{\bar{W}_s}{W_\infty},$$

In the above equation

$$\frac{\bar{W}_s}{W_\infty} = \int_0^1 \frac{W_s}{W_\infty}\, d\,\eta_1. \tag{26}$$

The velocity profile would be represented by

$$\frac{W_s}{W_\infty} = \frac{3}{2} \sin\psi\,(2\eta_1 - \eta_1^2). \tag{27}$$

Substitution of (27) in (26) gives

$$\frac{\overline{W}_s}{W_\infty} = \sin\psi. \tag{28}$$

The equation

$$\frac{d\vartheta_w}{d\,\mathrm{Fo}} = -3\,\mathrm{Bi}\,\mathrm{Fo}$$

may be written as

$$\frac{\partial u}{\partial\,\mathrm{Fo}} + \mathrm{Pe}_\infty \overline{W}_{1s} \frac{\partial u}{\partial s_1} = \frac{\partial^2 u}{\partial y_1^2}. \tag{29}$$

The solution of (29) is to be found in the form of a sum

$$u = u_1 + u_2, \tag{30}$$

where

$$u_1 = u_1(\mathrm{Fo},\ y_1); \tag{31}$$

$$u_2 = u_2(s_1,\ y_1). \tag{31a}$$

In this case, equation (29) is divided into two equations:

$$\frac{\partial u_1}{\partial\,\mathrm{Fo}} = \frac{\partial^2 u_1}{\partial y_1}, \tag{32}$$

$$\mathrm{Pe}_\infty W_{1s} \frac{\partial u_2}{\partial s_1} = \frac{\partial^2 u}{\partial y_1^2}. \tag{33}$$

An approximate solution of equation (32) is given by (23).

The differential equation (33) may be replaced by the following integral relation:

$$\frac{\partial}{\partial\psi}\left(\delta_1 \int_0^1 \frac{\overline{W}_{1s} u_2}{1+\eta_1}\, d\eta_1\right) = -\frac{1}{\mathrm{Pe}_\infty}\frac{1}{\delta_1}\left(\frac{\partial u_2}{\partial \eta_1}\right)_{\eta_1=0}. \tag{34}$$

The unknown temperature profile is presented in the form of a polynomial,

$$\frac{u_2}{u_{w2}} = B_0 + B_1\left(\frac{y_1}{\delta_1'}\right) + B_2\left(\frac{y_1}{\delta_1'}\right)^2 + B_3\left(\frac{y_1}{\delta_1'}\right)^3 + B_4\left(\frac{y_1}{\delta_1'}\right)^4. \tag{35}$$

The coefficients in the above polynomial are determined from the following conditions:

$$\eta_1 = 0,\ u_2 = 1,\ \frac{\partial^2 u}{\partial \eta_1^2} = 0, \tag{36}$$

$$\eta_1 = 1,\ u_2 = 0. \tag{36a}$$

By satisfying the above conditions, we obtain

$$\vartheta_2 = \frac{u_2}{1+\eta_1} = \frac{1 - 2\eta_1 + 2\eta_1^3 - \eta_1^4}{1+\eta_1} = 1 - 3\eta_1 + 3\eta_1^2 - \eta_1^3. \tag{37}$$

Substitution of (37) and (28) in (34) yields the following differential equation

$$\frac{d}{d\psi}(\delta_1' \sin\psi) = \frac{8}{3}\,\frac{1}{\mathrm{Pe}_\infty}\,\frac{1}{\delta_1'}. \tag{38}$$

Integration yields

$$\delta_1' = \frac{1{,}64}{\sqrt{\mathrm{Pe}_\infty}} \frac{\sqrt{1-\cos\psi}}{\sin\psi}. \tag{39}$$

Hence, an approximate solution of equation (33) would be

$$\vartheta_2 = 1 - 3\left(\frac{y_1}{\delta_1'}\right) + 3\left(\frac{y_1}{\delta_1'}\right)^3 - \left(\frac{y_1}{\delta_1'}\right)^4, \tag{40}$$

where $\delta_1'$ is determined from equation (39).

Thus, the general solution of equation (25) could be written as

$$\vartheta = \frac{\vartheta_w}{r_1}\left[1 - 2\left(\frac{y_1}{\delta_1}\right) + \left(\frac{y_1}{\delta_1}\right)^2\right] + \\ + 1 - 3\left(\frac{y_1}{\delta_1'}\right) + 3\left(\frac{y_1}{\delta_1'}\right)^3 - \left(\frac{y_1}{\delta_1'}\right)^4. \tag{41}$$

By differentiating equation (41) with respect to $y_1$ and assuming $r_1 = 1$, we obtain

$$\left(\frac{\partial \vartheta}{\partial y_1}\right)_{y_1=0} = -\left(1 + \frac{2}{\delta_1}\right)\vartheta_w - \frac{3}{\delta_1'}. \tag{42}$$

By substituting (42) in (4) and taking into account (19) and (39), we obtain

$$\mathrm{Nu}_{r_0} = 1 + \frac{1}{\sqrt{3\,\mathrm{Fo}}}\,\frac{\vartheta_w}{\vartheta_w} + \frac{1.1\sqrt{\mathrm{Pe}_\infty}}{\vartheta_w}\,\frac{\sin\psi}{\sqrt{1-\cos\psi}}. \tag{43}$$

The average value of $\bar{N}u_{r_0}$ over the whole surface of the sphere is determined from the expression

$$\bar{N}u_{r_0} = \frac{\int_0^{\pi} Nu_{r_0} r_1 d\psi}{\int_0^{\pi} r_1 d\psi} = \frac{\int_0^{\pi} Nu_{r_0} \sin\psi \, d\psi}{\int_0^{\pi} \sin\psi \, d\psi},$$

where

$$r_1 = l \sin\psi.$$

By substituting the value of (43) in the above expression, and making the necessary calculations, we obtain

$$\bar{N}u_{r_0} = 1 + \frac{1}{\sqrt{3\,Fo}} \frac{\vartheta_w}{\bar{\vartheta}_w} + \frac{0.304\sqrt{Pe_\infty}}{\bar{\vartheta}_w}. \tag{44}$$

By using the notation

$$(Nu_{r_0})_{av} = 1 + 0.304\sqrt{Pe_\infty}, \tag{45}$$

we may write equation (44) as

$$\frac{\bar{N}u_{r_0}}{(Nu_{r_0})_{av}} = \frac{1}{\bar{\vartheta}_w}\left[1 + \frac{\vartheta_w\left(1 + \frac{1}{\sqrt{3\,Fo}} \frac{\vartheta_w}{\bar{\vartheta}_w}\right) - 1}{1 + 0.304\sqrt{Pe_\infty}}\right]. \tag{46}$$

For the most simple case of a constant wall temperature equation, (46) is transformed into

$$\frac{\bar{N}u_{r_0}}{(Nu_{r_0})_{av}} = 1 + \frac{0.578}{\sqrt{Fo}(1 + 0.304\sqrt{Pe_\infty})}. \tag{47}$$

By taking the diameter of the sphere as the determining parameter in equation (45), we obtain

$$(Nu_{r_0})_{av} = 2 + 0.43(Re\,Pr)^{0.5}. \tag{48}$$

A comparison of equations (48) and (2) shows that the solution method used in this paper leads to a scatter of the results not exceeding 10%.

## Conclusions

1) Our investigation shows that thermal unsteady state is of great importance in determining the coefficient of convective heat transfer under the conditions of the prescribed problem.

2) Equation (47) gives in an explicit form the effect of changes in the Fo number during the process on the heat transfer coefficient. The solutions of Nusselt and Kudryashev are particular cases of equation (47).

Bibliography

1. Zeitschrift des Vereines deutscher Ingenieure. Vol. 68, No. 6. 1924.
2. Izv. AN SSSR, OTN, No. 11. 1949.
3. Trudy Kuibyshevskogo Aviatsionnogo Instituta, No. XV, Part II. 1963.

The Kuibyshev Aviation Institute

I. S. Kochenov and Yu. N. Kuznetsov

# UNSTEADY FLOW IN TUBES

At present it is a common assumption that during unsteady flow in tubes and various channels, the changes in the frictional coefficient are quasi-steady, i. e., that the well-known Poiseuille, Blasius, and other laws are valid /1-3/. All practical calculations of unsteady flows are based on the above assumption.

Attempts have been made to check this assumption experimentally /4-6/. Because of the great scatter of experimental points (apparently due to errors in the experimental technique and in the analysis of the experimental data), and the small flow accelerations achieved (low degree of "unsteady state"), it was impossible to derive any definite relationships; however, it may be stated that differences probably do exist between the frictional coefficient in unsteady and quasisteady processes.

Since 1960, we have carried out experimental and theoretical investigations on unsteady flow in tubes in order to derive equations for the frictional coefficient under conditions of unsteady flow /7/.

We now analyze the unsteady flow of a fluid in a rigid tube of constant cross section. The flow equation for the above case

$$\int_F \frac{\partial u}{\partial t} dF = -\frac{1}{\rho}\int_F \frac{\partial p}{\partial x} - \frac{1}{\rho}\int_\chi \tau_{av} d\chi - \int_F \frac{\partial u^2}{\partial x} dF, \qquad (1)$$

is transformed into a form containing values averaged over the channel cross section:

$$-\frac{\partial \bar{p}}{\partial x} = \rho \frac{\partial w}{\partial t} + \frac{1}{F}\int \tau_{av} d\chi + \rho w^2 \frac{\partial \beta}{\partial x}. \qquad (2)$$

In the above equation,

$$\bar{p} = \frac{1}{F}\int_F p dF, \qquad w(t) = \frac{Q}{F} = \frac{1}{F}\int_F u dF,$$

$$\beta w^2 F = \int_F u^2 dF,$$

and $\chi$ is the perimeter.

As is evident from equation (2), the pressure drop $\left(\Delta p = -\int_{x_1}^{x_2} \frac{\partial p}{\partial x} dx\right)$ consists of three components which are known (according to their physical meaning)

as the inertial drop $\Delta p_{in}$, the friction drop $\Delta p_{fr}$, and the drop caused by the rearrangement of the velocity profile $\Delta p_{pr}$:

$$\Delta p = \Delta p_{in} + \Delta p_{fr} + \Delta p_{pr}. \tag{3}$$

The inertial pressure drop $\Delta p_{in} = \rho \frac{\partial w}{\partial t} \Delta x$ can be calculated accurately if the flow rate $Q(t)$, i.e., the mean flow velocity, is known. It is important to note that this term contains no averaging coefficient. In the case of flows under acceleration, the inertia term $\Delta p_{in}$ increases the total pressure drop, while in the case of decelerating flows (when $\Delta p_{in} < 0$), the inertial term reduces the total drop. Cases are possible of inertial flow with a constant and increasing pressure $\Delta p \leqslant 0$ over the length. In such cases

$$-\Delta p_{in} \geqslant \Delta p_{fr} + \Delta p_{pr}.$$

It is convenient to present the pressure drop caused by friction on the channel walls $\left(\Delta p_{fr} = \frac{1}{F} \int_{x_1}^{x_2} \int_{\chi} \tau_w \, d\chi \, dx\right)$ in the Darcy form, as used in engineering practice in the case of steady flows:

$$\frac{1}{F} \int_{\chi} \tau_{av} d\chi = \lambda \frac{\rho w^2}{2D}, \tag{4}$$

$$\Delta p_{fr} = \frac{\rho w^2}{2D} \int_{x_1}^{x_2} \lambda(x, t) dx. \tag{5}$$

For tubes of circular cross section, condition (4) is simplified to

$$\lambda = \frac{8\tau_{av}}{\rho w^2}. \tag{6}$$

The coefficient of unsteady friction resistance $\lambda$, defined by (4) and (6), is identical with the frictional coefficient under steady-state conditions. In the case of unsteady flow, it depends also on the time and on the various dimensionless numbers describing the flow as a function of time.

We shall show below that the unsteady frictional coefficient may at certain moments assume a value of zero or even negative values over given time intervals.

This leads to the conclusion that the unsteady friction resistance coefficient is not directly related to the dissipation (the dissipation always being positive).

In steady flow at $w = 0$, the stress on the walls also equals zero. In unsteady flows changing their direction, the fact that the mean flow velocity $w = 0$ does not indicate that local velocities also equal zero. A tangential frictional stress may thus exist on the wall ($\tau_w \neq 0$) at $w = 0$. In that case, according to definition (from (4) and (6)), the frictional coefficient becomes infinite.* A discontinuity in $\lambda$ occurs when $w$ passes through zero. In this

* Indeed, the friction resistance coefficient $\lambda = \frac{64\nu}{wD}$ approaches infinity even in the case of steady flow when the velocity $w$ approaches zero.

particular case, the use of $\lambda$ as determined from (4) has some formal inadequacies. In general, however, the presentation of $\lambda$ in the Darcy form is fairly convenient.

A pressure drop caused by the rearrangement of the velocity profile $\Delta p_{pr} = \rho w^2 \int_{x_1}^{x_2} \frac{\partial \beta}{\partial x} dx = \rho w^2 [\beta_1(t) - \beta_2(t)]$, occurs in both unsteady and steady flows, but only at the entrance of the channel. In the section with steady flow over the length, we have $\frac{\partial \beta}{\partial x} = 0$ and $\Delta p_{pr}$ assumes a value of zero, although a rearrangement of the profile occurs with time.

Thus, in the case of unsteady flow of an incompressible liquid in a stabilized section (the entry section has different lengths for steady and unsteady flows), we obtain

$$\Delta p = \left(\frac{dw}{dt} + \lambda \frac{w^2}{2D}\right) \rho l. \tag{7}$$

The unsteady friction resistance coefficient $\lambda$ in the case of laminar flow may be determined from the analytical solution for the velocity profile:

$$\lambda = -\frac{8\nu}{w^2} \frac{\partial u}{\partial r}\Big|_{r=r_{av}} \tag{8}$$

For the experimental determination of $\lambda$ in unsteady turbulent flows over the stabilized section (and for the experimental checking of the theoretical values of $\lambda$ in laminar flow), it is sufficient to know (i. e., to measure experimentally) the flow rate $Q(t)$ and the pressure drop $\Delta p(t)$ as functions of time. Then, from (7),

$$\lambda(t) = \frac{2D}{w^2}\left(\frac{\Delta p}{\rho l} - \frac{dw}{dt}\right). \tag{9}$$

The determination of the pressure drop in the entry section in the cases of both steady and unsteady flows requires a knowledge of the coefficients $\lambda$ and $\beta$. For their experimental determination, it is not enough to measure the pressure drop alone, but in addition, either the velocity profile or the frictional stress on the wall $\tau_w(x, t)$ must be measured, which involves considerable technical difficulty.

Moreover, in engineering practice, it is inconvenient to use two variable coefficients. Thus, we suggest, rather than distinguishing between $\Delta p_{fr}$ and $\Delta p_{pr}$, making use of their sum by introducing a local overall coefficient for the friction resistance and the rearrangement of the velocity profile $\lambda_\Sigma$:

$$\Delta p_{fr} + \Delta p_{pr} = \frac{\rho w^2}{2D} \int_{x_1}^{x_2} \lambda_\Sigma(x, t) dx. \tag{10}$$

An analysis of the flow equation (2) and equations (7) and (10) shows that

$$\lambda_\Sigma(x, t) = \lambda(x, t) + 2\frac{\partial \beta}{\partial x}. \tag{11}$$

The hydraulic resistance in the entry section is expressed by the above equations, by analogy with (7).

It is evident that for the experimental determination of $\lambda_\Sigma$, it is not necessary to measure the velocity field and the frictional stress on the wall. It is enough to measure the pressure gradient $\frac{\partial p}{\partial x}(x,t)$ at a known (measured) flow rate. It is evident that the local overall coefficient depends on the entry conditions.

For each given entry, we may find the mean overall coefficient $\bar{\lambda}_\Sigma$:

$$\bar{\lambda}_\Sigma = \frac{1}{x}\int_0^x \lambda_\Sigma \, dx. \tag{12}$$

The equation for the calculation of the pressure drop $\Delta p$ is in this case in its simplest form, analogous with equation (7).

The laws governing the changes in the friction resistance coefficient $\lambda$ for steady flow must, naturally, comprise as a particular case the laws of steady flow. Thus, we shall describe the unsteady friction resistance coefficient $\lambda$ as a product:

$$\lambda = \Lambda \lambda_*, \tag{13}$$

where $\lambda_*$ is the resistance coefficient under quasisteady conditions for the same value of the Reynolds number that characterizes the unsteady flow at a given moment (for a laminar stabilized stream in a circular tube, we have $\lambda = 64/\mathrm{Re}$), and $\Lambda$ is the equivalent unsteady friction resistance coefficient, which is to be investigated.

It is essential to note that the thus-defined equivalent coefficient $\Lambda$ is independent of the Reynolds number.

This shall be proved by using laminar flow within the stabilized section of a circular tube as an example. In that case the exact Navier-Stokes equation is

$$\frac{\partial u}{\partial t} = -\frac{1}{\rho}\frac{\partial p}{\partial x} + \nu\left(\frac{\partial^2 u}{\partial r^2} + \frac{1}{r}\frac{\partial u}{\partial r}\right), \tag{14}$$

and in a case in which the law of changes $\frac{\partial p}{\partial x}$ is prescribed while the flow rate $Q(t)$ is to be determined, this equation is conveniently written in terms of dimensionless numbers

$$\frac{\partial U}{\partial \mathrm{Fo}} + \mathrm{K_p} U = 8 + \frac{\partial^2 U}{\partial R^2} + \frac{1}{R}\frac{\partial U}{\partial R}, \tag{15}$$

where

$$U = \frac{u(r,\, t)}{w_k(t)}; \quad w_k(t) = \frac{r_0^2}{8\mu}\left(-\frac{\partial p}{\partial x}\right);$$

$$\mathrm{Fo} = \frac{\nu}{r_0^2} t \text{ is the dimensioness time;} \tag{16}$$

$$K_p = \frac{1}{\frac{\partial p}{\partial x}} \frac{\partial \left(\frac{\partial p}{\partial x}\right)}{\partial \mathrm{Fo}} \text{ is a criterion of the unsteady state (dimensionless variable).} \tag{17}$$

By introducing $u$ instead of $U$ in equation (8), we derive an expression for the equivalent unsteady friction resistance coefficient:

$$\Lambda = -\frac{\left.\frac{\partial U}{\partial R}\right|_{R=1}}{4\,\overline{U}}, \tag{18}$$

where

$$\overline{U} = 2\int_0^1 URdR. \tag{19}$$

Equations (15), (18), and (19) show that $\Lambda$ depends only on Kp and Fo and, in particular, that it is independent of the Reynolds number. In cases in which we prescribe a certain definite mode of variation of $\frac{\partial p}{\partial x}$ with time, i. e., if we prescribe

$$K_p = cf(\mathrm{Fo}), \tag{20}$$

then $\Lambda$ would depend on a function of one variable alone, $\Lambda = \varphi(\mathrm{Fo})$. It is interesting to note that the above function is not affected by the constant $c$ in (20).

In cases in which the flow rate $Q(t)$ rather than the pressure drop is prescribed in place of $K_p$, we similarly introduce a criterion for the unsteady state with respect to the relative changes in the flow rate (or the Reynolds number):

$$K_Q = \frac{1}{\mathrm{Re}} \frac{\partial \mathrm{Re}}{\partial \mathrm{Fo}} = \frac{\partial \ln \mathrm{Re}}{\partial \mathrm{Fo}}. \tag{21}$$

We shall show that in some cases, the equivalent unsteady friction resistance coefficient may markedly differ from unity.

The simplest (and apparently the most convincing) proof is to use as an example the case of laminar flow with a numerical or analytical solution of the Navier-Stokes equation. Gromeka /8/ solved the above equation (i. e., determined $u = u(r, t)$) for a case in which the pressure gradient is an arbitrary but prescribed function of time. Unfortunately, these solutions have not been extended to the calculation and analysis of the unsteady friction resistance coefficient.

We have derived a solution for the case of prescribed flow rate $Q = Q(t)$ and unknown pressure drop.

The two solutions (for prescribed $\frac{dp}{dx}$ and prescribed $Q$) have been written in terms of dimensionless numbers and worked out into equations

for the calculation and the digital computation of the referred coefficient of friction.

The dependence of the referred coefficient $\Lambda$ on $K_Q$ at various parameters of dimensionless time Fo is shown in the figure for the case of a linear increase in the flow rate with time. As is evident from the figure, in the considered range of variation (of the variables) the value of $\Lambda$ may reach several tens or even hundreds.

For some flows, we obtained regions with negative or zero values of the equivalent coefficient $\Lambda$. For $\Lambda$ with a value of zero at a given moment, the velocity profile is such that $\left.\frac{\partial u}{\partial r}\right|_{r=r_w}=0$; in the case of negative values of $\Lambda$, the above derivative is positive (usually $\frac{\partial u}{\partial r}<0$) since there exists a stream near the wall in a direction opposite to the main flow (near the wall $u<0$). In such a case, the friction on the wall does not retard the main-stream, but favors its motion in the direction of the main flow.

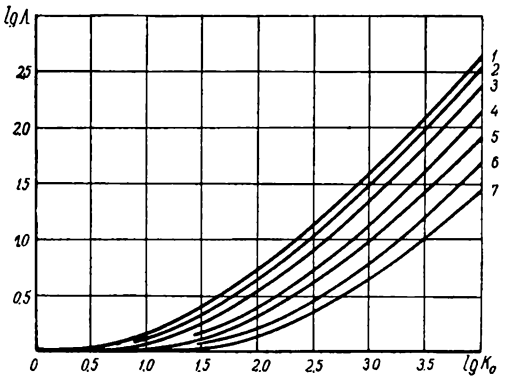


Dependence of the equivalent coefficient $\Lambda$ on $K_Q$, at different Fo

1– $Fo \geqslant 10^{-1}$; 2–$3.16 \cdot 10^{-2}$; 3–$10^{-2}$; 4–$3.16 \cdot 10^{-3}$; 5–$10^{-3}$; 6–$3.16 \cdot 10^{-4}$; 7–$10^{-4}$.

According to the results of theoretical calculations of laminar flows, the equivalent coefficient $\Lambda$ is larger than unity in accelerating, and smaller than unity in decelerating flows. However, the experimental data below show that the above conclusion is valid only in the case of flows with a small or monotonously changing (with time) second derivative of the flow rate.

The experimental study of the equivalent unsteady friction resistance coefficient $\Lambda$ involves considerable difficulties, since the measuring devices and instruments used must have virtually no lag. Moreover, the selected method of processing the experimental data demands a high degree of experimental accuracy: firstly, because the investigation is based on only a fraction (which as a rule does not exceed 50%) of the measured total pressure drop, and the entire experimental error is comprised in it; and secondly, because the processing of the data for the calculation $\Delta p_{in}$ requires use of the derivative $dw/dt$, and the error of differentiation is thus comprised in the result.

The experiments were carried out on two experimental setups, using water and oil as the working media. A certain reproducible mode of variation of the flow rate with time ($Q=f(t)$) was obtained with the aid of special flow-rate governors. The flow rates were measured with an electromagnetic flowmeter, based on the ERI-25 flowmeter.

The pressure gradients (drops) were measured at three consecutive sections of a circular tube 0.007 m in diameter, in the region of stabilized flow (this is confirmed by the fact that the measured pressure drops had the same value with an accuracy of ±3%).

The measurements were made with the DIF 1-M induction sensor and the ID-2I auxiliary apparatus, with which it was possible to measure pressure drops of 20,000 n/m$^2$ with an accuracy of up to 0.5%.

The data from the pressure drop sensors and the electromagnetic flowmeter were recorded with a loop oscillograph. The duration of each experiment was about one second. Before each series of experiments under unsteady-flow conditions, we calibrated the equipment and recorded the steady hydraulic characteristics of the sections, which roughly satisfied the Blasius law (on the average, the measured resistance was 3% higher than the value corresponding to the Blasius law). The experiments were carried out at Reynolds numbers from $10^4$ to $10^5$. The values of $K_Q$ ranged from 5 to 100 (corresponding to flow accelerations up to 200 m/sec$^2$).

In the experiments, we obtained values of $\Lambda$ that differed markedly from unity (by several units), as well as negative values of $\Lambda$.

Experiments with turbulent flows, as well as special calculations of laminar flows, showed that $\Lambda$ depends both on the first and the second logarithmic derivatives of the flow rate with respect to time.

In addition to the above experiments on the unsteady friction coefficient, we also carried out experiments on the local resistance to unsteady flow; in these experiments, we also obtained values of the equivalent unsteady friction resistance coefficient which differed markedly from unity.

Thus, the theoretical and experimental studies show that the value of the hydraulic friction resistance coefficient under well-defined unsteady-flow conditions differs markedly from the quasisteady value, and that this difference must be accounted for in the calculation processes which change rapidly with time.

Bibliography


1. Charnyi, I.A. Neustanovivsheesya dvizhenie real'noi zhidkosti v trubakh (Unsteady Flow of a Real Fluid in Tubes). Moskva-Leningrad. 1951.
2. Ginzburg, I.P. Prikladnaya gidrogazodinamika (Applied Hydrogasodynamics). — Izd. Leningradskogo Universiteta. 1958.
3. Yablonskii, V.S. Kratkii kurs tekhnicheskoi gidromekhaniki (Short Course in Technical Hydromechanics). — Fizmatgiz, Moskva. 1961.
4. Panchurin, N.A. Gidravlicheskoe soprotivlenie pri nestatsionarnykh techeniyakh (Hydraulic Resistance in Unsteady Flows). — Trudy Leningradskogo Instituta Vodnogo Transporta, No. 13. 1961.

5. Daily, W, W. Haukey, R. Olive, and H. Yordaan. Resistance Coefficients for Accelerated and Decelerated Flow-Transactions of the ASME, Vol. 78, No. 5. 1956.
6. Cartens, M.R. and E. Roller. Boundary-shear Stress in Unsteady Turbulent Pipe "Flow". — Journal of the Hydraulics Division HY. r. February, 1959.
7. Vilenskii, V.D., I.S. Kochenov, and Yu.N. Kuznetsov. K voprosu o gidravlicheskikh soprotivleniyakh pri nestatsionarnykh rezhimakh (On the Problem of the Hydraulic Resistance under Unsteady-State Conditions). — Pnevmo- i gidroavtomatika, Izd. AN SSSR. 1963.
8. Gromeka, I.S. K teorii dvizheniya zhidkosti v uzkikh tsilindricheskikh trubkakh (Contribution to the Theory of Fluid Flow in Narrow Cylindrical Tubes). — Kazan'. 1882.

Moscow

## EXPLANATORY LIST OF ABBREVIATED NAMES OF USSR INSTITUTIONS, ORGANIZATIONS, AND JOURNALS APPEARING IN THIS TEXT

| Abbreviation | Full name (transliterated) | Translation |
|---|---|---|
| AN SSSR | Akademiya Nauk SSSR | Academy of Sciences of the USSR |
| DAN SSSR | Doklady Akademii Nauk SSSR | Reports of the Academy of Sciences of the USSR |
| IFZh | Inzhenerno-Fizicheskii Zhurnal | Engineering-Physics Journal |
| Izv. ENINa | Izvestiya Energeticheskogo Instituta (im. G.M. Krzhizhanovskogo) | Bulletin of the Power Institute im. G.M. Krzhizhanovskii |
| MIIT | Moskovskii Institut Inzhenerov Zheleznodorozhnogo Transporta (im. I.V. Stalina) | Moscow Institute of Railroad Engineering (im. I.V. Stalin) |
| MIKhM | Moskovskii Institut Khimicheskogo Mashinostroeniya | The Institute of Chemical Equipment Design, Moscow |
| MLTI | Moskovskii Lesotekhnicheskii Institut | Moscow Forest Engineering Institute |
| NTO | Nauchno-Tekhnicheskii Otdel | Scientific and Technical Division |
| OTN AN SSSR | Otdelenie Tekhnicheskikh Nauk (Akademiya Nauk SSSR) | Department of Technical Sciences (of the Academy of Sciences of the USSR) |
| TsAGI | Tsentral'nyi Aero-Gidrodinamicheskii Institut (im. N.E. Zhukovskogo) | Central Aero-Hydrodynamical Institute (im. N.E. Zhukovskii) |
| TsKTI | Tsentral'nyi Nauchno-Issledovatel'skii Kotloturbinnyi Institut | The Central Boiler and Turbines Institute |
| VTI | Vsesoyuznyi Teplotekhnicheskii Institut (im. F. Dzerzhinskogo) | All-Union Heat Engineering Institute (im. F. Dzerzhinskii) |
| ZhTF | Zhurnal Tekhnicheskoi Fiziki | Journal of Technical Physics |

NASA TT F-431
[1842] Cover printed in Jerusalem, Israel TT 67-51367